PL-TR--95-1023

PL-TR--
95-1023

PARAMETRIC STUDIES ON A SHORT PULSED KrF PUMPED ATOMIC IODINE LASER

B. Scott Hunt

April 1995

Final Report

PHILLIPS LABORATORY
Lasers and Imaging Directorate
AIR FORCE MATERIEL COMMAND
KIRTLAND AIR FORCE BASE, NM 87117-5776

PL-TR--95-1023

This final report was prepared by the Phillips Laboratory, Kirtland Air Force Base, New Mexico, under Job Order 3326LA02. The Laboratory Project Officer-in-Charge was Capt B. Scott Hunt (LIDB).

When Government drawings, specifications, or other data are used for any purpose other than in connection with a definitely Government-related procurement, the United States Government incurs no responsibility or any obligation whatsoever. The fact that the Government may have formulated or in any way supplied the said drawings, specifications, or other data, is not to be regarded by implication, or otherwise in any manner construed, as licensing the holder, or any other person or corporation; or as conveying any rights or permission to manufacture, use, or sell any patented invention that may in any way be related thereto.

This report has been authored by an employee of the United States Government. Accordingly, the United States Government retains a nonexclusive royalty-free license to publish or reproduce the material contained herein, or allow others to do so, for the United States Government purposes.

This report has been reviewed by the Public Affairs Office and is releasable to the National Technical Information Service (NTIS). At NTIS, it will be available to the general public, including foreign nationals.

If your address has changed, if you wish to be removed from the mailing list, or if your organization no longer employs the addressee, please notify PL/LIDB, 3550 Aberdeen Ave SE, Kirtland AFB, NM 87117-5776, to help maintain a current mailing list.

This report has been reviewed and is approved for publication.

B. SCOTT HUNT, CAPT
Laser Systems Engineer
Project Officer

FOR THE COMMANDER

CHRISTOPHER COULS, LT COL
Chief, Laser Systems Division

LANNY I. LARSON, COL
Director, Lasers and Imaging Directorate

DO NOT RETURN COPIES OF THIS REPORT UNLESS CONTRACTUAL OBLIGATIONS OR NOTICE ON A SPECIFIC DOCUMENT REQUIRES THAT IT BE RETURNED.

REPORT DOCUMENTATION PAGE

Form Approved
OMB No. 0704-0188

1. AGENCY USE ONLY *(Leave blank)*	2. REPORT DATE	3. REPORT TYPE AND DATES COVERED
	April 1995	Final; Aug 1993

4. TITLE AND SUBTITLE
PARAMETRIC STUDIES ON A SHORT PULSED KrF PUMPED ATOMIC IODINE LASER

5. FUNDING NUMBERS
PE: 62601F
PR: 3326
TA: LA
WU: 02

6. AUTHOR(S)
B. Scott Hunt

7. PERFORMING ORGANIZATION NAME(S) AND ADDRESS(ES)
Phillips Laboratory
3550 Aberdeen Avenue, SE
Kirtland AFB, 87117-5776

8. PERFORMING ORGANIZATION REPORT NUMBER
PL-TR--95-1023

9. SPONSORING / MONITORING AGENCY NAME(S) AND ADDRESS(ES)

10. SPONSORING / MONITORING AGENCY REPORT NUMBER

11. SUPPLEMENTARY NOTES

12a. DISTRIBUTION / AVAILABILITY STATEMENT
Approved for public release; distribution is unlimited.

12b. DISTRIBUTION CODE

13. ABSTRACT *(Maximum 200 words)*

This paper describes parametric studies performed on a short pulsed KrF excimer pumped atomic Iodine laser. Three different approaches were used to determine the gain in the laser cell. The first technique uses a tunable diode laser to directly measure the transient gain. The second method involves measuring the energy extracted from the laser for various outcoupling mirrors and applying the threshold gain condition to determine the small signal gain of the dominant 3-4 laser transition. The final measurement is of the amount of UV energy deposited in the CF_3I extraction volume. A maximum theoretical value for the gain can be calculated from this energy and previously measured parameters of CF_3I. Both experimental gain measurements compare favorably to the theoretically calculated value. A theoretical rate equation model involving all of the relevant kinetic processes of the hyperfine structure associated with the laser was developed and tested. Experimental laser intensity and cavity buildup time were compared to the theoretical model in both a qualitative and quantitative sense. With minor adjustment to the model, agreement was reached between theory and experiment.

14. SUBJECT TERMS	15. NUMBER OF PAGES
Iodine, laser, hyperfine, excimer, short pulsed, CF_3I, diode laser, photodissociation, parametric studies	244
	16. PRICE CODE

17. SECURITY CLASSIFICATION OF REPORT	18. SECURITY CLASSIFICATION OF THIS PAGE	19. SECURITY CLASSIFICATION OF ABSTRACT	20. LIMITATION OF ABSTRACT
Unclassified	Unclassified	Unclassified	UL

This thesis is dedicated to my father,

Brian R. Hunt, Major (retired) USAF,

who introduced me to problem solving at an early age,

and whom is also responsible for my great interest in electronics.

ACKNOWLEDGMENTS

This work was funded by the United States Air Force and performed at the Chemical Laser Facility located at the Air Force Phillips Laboratory, Kirtland Air Force Base, New Mexico. Funding was provided through the Air Force Office for Scientific Research (AFOSR).

Dr. Gordon Hager of the Phillips Laboratory has been the technical director of the project from the very beginning. He has always been willing to help answer the many questions which I have had, and has spent quite a few weekends with me explaining the theoretical issues behind the project. Thank you for your dedication and support.

Dr. Jack McIver, who has a joint appointment to the Department of Physics and Astronomy and the Department of Electrical and Computer Engineering at the University of New Mexico, has been my academic advisor for the research project. It has been a great benefit to have him working out at the Chemical Laser Facility during the summers to answer questions and discuss my work. Thank you for being involved in the LBARS contract, which has brought the Phillips Laboratory in contact with the University of New Mexico, and which has allowed you to be close to the experiment on an everyday basis.

I would like to thank the other two members of my thesis committee:

Dr. Bob McNiel of the Department of Electrical and Computer Engineering at the University of New Mexico, who is responsible for a large portion of my education in Optics, and has answered many questions (both directly and indirectly) about the project.

Dr. David Wolf, head of the Department of Physics and Astronomy at the University of New Mexico: thank you for agreeing on such short notice to serve on my committee, and also for expressing an interest in the relationship between the Phillips

Laboratory and the University of New Mexico.

I would like to thank everyone at the Chemical Laser Facility:

Dr. Helms, Dr. Machara, and Dr. Miller were there to answer questions about theory and experiment

Brian Anderson and Lt. Kopf helped with the diode laser setup.

Marty Vallez and Stuart Hidalgo helped around the laboratory and put in purchases for equipment. Thank you Stuart for maintaining the Iris workstations and taking that responsibility off my hands, allowing me to have time to pursue this work.

Ralph Tate and Captain Ken Gurley. Though they both arrived just recently, it feels like Ralph has been there all the time. Ken has spent much time discussing the laser system with me in preparation for his own work.

Carrie Lopez. Though she no longer works at the Chemical Laser Facility, she helped a great deal with the initial typing. I hope I wasn't responsible for her departure.

Dr. Truesdell and Major Scott. Thank you for allowing me to spend a great deal of my time out at the Chemical Laser Facility working on my thesis.

I would like to thank Dr. Wodkiewicz for his rigorous class on laser theory.

Finally, I would like to thank my fiance, Dena Lewis, for her endless support, and helping me maintain my sanity throughout this project.

PARAMETRIC STUDIES ON A SHORT PULSED KrF PUMPED ATOMIC IODINE LASER

BY

BRIAN SCOTT HUNT

ABSTRACT OF THESIS

Submitted in Partial Fulfillment of the
Requirements for the Degree of

Master of Science in Electrical and Computer Engineering

The University of New Mexico
Albuquerque, New Mexico
August, 1993

PARAMETRIC STUDIES ON A SHORT PULSED KrF PUMPED ATOMIC IODINE LASER

BRIAN SCOTT HUNT

B.S.E.E., United States Air Force Academy, 1990

This paper describes parametric studies performed on a short pulsed KrF excimer pumped atomic Iodine laser. Three different approaches were used to determine the gain in the laser cell. The first technique uses a tunable diode laser to directly measure the transient gain. The second method involves measuring the energy extracted from the laser for various outcoupling mirrors and applying the threshold gain condition to determine the small signal gain of the dominant 3-4 laser transition. The final measurement is of the amount of UV energy deposited in the CF_3I extraction volume. A maximum theoretical value for the gain can be calculated from this energy and previously measured parameters of CF_3I. Both experimental gain measurements compare favorably to the theoretically calculated value. A theoretical rate equation model involving all of the relevant kinetic processes of the hyperfine structure associated with the laser was developed and tested. Experimental laser intensity and cavity buildup time were compared to the theoretical model in both a qualitative and quantitative sense. With minor adjustment to the model, agreement was reached between theory and experiment.

CONTENTS

LIST OF FIGURES

LIST OF TABLES

PREFACE ON NOTATION

The symbol I is used to represent several different types of quantities in this paper. The manner in which is written clarifies its use:

When talking about quantum mechanics, I is used as the nuclear spin quantum number. $\hat{I}_z$, $\hat{I}_+$, and $\hat{I}_-$ are all operators associated with this qunatum number. This definition of I is used exclusively in Section 2.1.

Section 2.2 introduces I^*, I, and I_2 as individual iodine atoms or molecules. I^* represents the excited state iodine atom, while I represents the ground state atom. I_2 is molecular iodine.

Brackets [] are used to signify number density of a species. For example, $[I_2]$ is used to describe number density of molecular iodine. To specify number density of atomic iodine within a particular hyperfine state, the notation is: $[I^*_3]$ for the excited F=3 hyperfine state or $[I^g_4]$ for the F=4 hyperfine ground state. To describe the more general case of population in an upper or lower energy level $[N_U]$ or $[N_L]$ are used respectively. The general case of excited state or ground state iodine population densities are $[I^*]$ or $[I^g]$ respectively.

Intensity is another case where I is used. Intensity traveling right within a laser cavity, or in the positive z direction is specified by I^+. Intensity traveling left within a laser cavity, or in the negative z (positive s) direction is specified by I^-. Two way circulating intesity and intensity outside a resonator is written with a bar over it. The general case of intensity caused by atoms transitioning from some upper energy level to a lower level is given by $\bar{I}_{U\text{-}L}$. The more specific case of a transition from the F=3 exited hyperfine state to the F=4 hyperfine ground state is written similarly: $\bar{I}_{34}$. The hyphen between the states is dropped for brevity.

Hyperfine relaxation occurs only between the exited states or between the ground states. In general terms the rate constants are written k_U for the upper states and k_L for the lower states. In more specific terms the rate constants are written $k^*_{i\text{-}j}$ for the excited

states and k_{i-j} for the ground states. The rate constant between the upper F=3 and F=2 hyperfine states is written k^*_{32}. The rate constant between the lower F=4 and F=1 hyperfine states is written k_{41}.

A-coefficients for particular transitions are written A_{34}. The more general form is A_{U-L}. This is not to be confused with the emperical constants $A_{U,L}$. A_U and A_L are only seen in Section 2.2.

1. INTRODUCTION

The laser system being studied uses a KrF excimer at 248 nm to photodissociate CF_3I. The excimer laser transversely pumps a well defined volume of CF_3I producing CF_3 radicals and excited iodine atoms. Nearly 100% of the iodine produced is initially found in one of the two excited levels of the hyperfine structure [1]. The hyperfine structure of atomic iodine results from the splitting of the fine structure components due to interactions between the nucleus and the angular momentum of the electrons [2]. This splitting leads to six hyperfine energy states, two upper ($^2P_{1/2}$) and four lower ($^2P_{3/2}$). Absorption and emission which occurs between the upper and lower hyperfine levels is caused by a magnetic dipole interaction. The selection rule specifying which magnetic dipole transitions may occur is $\Delta F = 0, \pm 1$ [3]. This gives six transitions: 3-4, 3-3, 3-2, 2-3, 2-2, and 2-1. The relative strengths of these six transitions and the frequencies at which they occur can be determined by a detailed quantum mechanical calculation involving both the nuclear magnetic dipole moment and the electric quadrupole moment. A fairly detailed description of this quantum mechanical vector model is outlined in Section 2.1. The strongest of these transitions is the 3-4, which is the predominant line in most atomic iodine lasers and produces infrared light at 1.315 μm.

There are numerous processes, some radiative and some nonradiative which shift population around between the hyperfine energy states [4]. The radiative processes, or magnetic dipole processes as mentioned above, include stimulated emission and absorption and spontaneous emission. Nonradiative processes include relaxation or mixing between hyperfine energy levels and quenching of exited iodine by constituents in the gas mixture. Other important processes include photodissociation and recombination. All of the processes listed above are combined into a set of nine rate equations to describe population in each of the hyperfine energy states. A set of six intensity rate equations which describe two way circulating flux within the laser cavity

are coupled to the population rate equations to form a sixteen equation model which describes the laser action in an excimer pumped CF_3I photodissociation laser. A detailed description of this rate equation model is developed in the second part of Chapter 2.

Chapter 3 of the thesis introduces the set of experiments performed on the iodine photodissociation laser. One set of experimental measurements involves obtaining gain using a diode probe laser which can be tuned to any of the six radiative transitions in the hyperfine structure. The CF_3I laser resonator mirrors are removed and transient gain plus loss along a given hyperfine transition as the excimer photodissociates the CF_3I is found by measuring amplification of the diode laser as it passes through the cell of CF_3I. The gain along the 3-4 transition is checked by another experiment which involves a study of the energy extracted from the CF_3I laser. This study is accomplished by varying the outcoupling mirror reflectivity and measuring the amount of energy extracted from the laser. By determining the highest outcoupler transmission which still allowed lasing to occur and applying the threshold gain condition, the small signal gain plus the loss is determined. Under the assumption that the losses in the system are small, both gain measurements are compared to a theoretical maximum value found by knowing the amount of excimer energy deposited in the CF_3I. Knowing the amount of energy deposited in the gas, and that the photon yield is 100%, the total number of I^* produced is found, and from this a maximum small signal gain is calculated for the 3-4 hyperfine transition.

Chapter 4 uses basic laser principles and the detailed rate equation model to analyze experimental data. A set of three comparisons are made. First is a detailed analysis of the gain comparison made above. Second is a qualitative comparison between laser intensity measurements and the rate equation model, and finally an error analysis is made and modification of the rate equation model to describe the laser is discussed. Conclusions about these comparisons are drawn in Chapter 5.

2. THEORY

2.1 Energy Structure of Atomic Iodine

Modeling of the 1.315 μm atomic iodine laser system requires a knowledge of the hyperfine energy level structure of atomic iodine. This structure can be described with a quantum mechanical vector model in which the electronic angular momentum of the system is coupled to the nuclear angular momentum. The electronic state of the iodine atom is defined by the electron configuration of the valence shell. Iodine ^{157}I, as it occurs in nature, has 53 protons and 74 neutrons [5]. The ground state electron configuration follows from that of krypton (Kr): (Kr) $5s^2 4d^{10} 5p^5$. The 5s and 4d subshells are completely filled and the 5p subshell is short of being filled by one electron. By performing a vector sum of the wave functions of the individual electrons in the valence shell, the electronic state of the system is determined. The Russell-Saunder's coupling assumption determines the order in which the basis vectors are summed: The vectors that are strongly coupled with one another must always be added together first [6]. The total electronic angular momentum of an atom is determined by first summing the individual orbital angular momenta of the electrons in unfilled subshells. The individual orbital angular momenta of the 5 electrons in the p shell sum to give the atom a total orbital angular momentum quantum number of L = 1. Next, the total spin angular momentum is determined by first summing the electron spins in the p shell. Due to the single unpaired electron, the total spin angular momentum quantum number of the iodine atom is S = 1/2. Using Dirac notation, the eigenvectors for the electronic orbital angular momentum and the spin angular momentum can be written as $| L M_L \rangle$ and $| S M_S \rangle$ respectively, where M_L and M_S are the magnetic quantum numbers associated with L and S which take on the values: M_L = L, L-1, ..., -L and M_S = S, S-1, ..., -S. This gives the eigenvectors listed in Table 2-1.

The resultant quantum numbers, L and S, according to Russell-Saunder's coupling, are less strongly coupled with one another, and their vector sum leads to a total electronic angular momentum quantum number J. The vector summation scheme is often times referred to as LS-coupling [7]. By LS-coupling, the total electronic angular

$\|\ L\ M_L\ \rangle$	$\|\ S\ M_S\ \rangle$
$\|\ 1\ \ 1\ \rangle$	$\|\ 1/2\ \ 1/2\ \rangle$
$\|\ 1\ \ 0\ \rangle$	$\|\ 1/2\ -1/2\ \rangle$
$\|\ 1\ -1\ \rangle$	

Table 2-1 Eigenvectors for the electronic orbital angular momentum and spin angular momentum

momentum has the possible values $J = \{\ |\ L+S\ |\ ,\ |\ L+S-1\ |\ ,\ \ldots,\ |\ L-S\ |\ \}$. For LS-coupling, the general expression for a term describing the fine structure energy states is denoted by $^{2S+1}P_J$. Thus iodine has two energy levels in the fine structure: $^2P_{1/2}$ and $^2P_{3/2}$. From Hund's second rule [8] (more than half full, invert order) the $J = 1/2$ is the higher energy state, and the $J = 3/2$ is the lower energy state. Additionally, the magnetic quantum number for the total angular momentum can be defined by $M_J = J, J-1, \ldots, -J$. Using Dirac notation, the resulting basis vectors are labeled $|\ J\ M_J\ \rangle$. The electronic state of the system can be summarized in Figure 2-1.

The complete Hamiltonian (or energy operator) for the system may be written as:

$$\hat{H} = \hat{H}_0 + \hat{H}_{so} \qquad \textbf{(2.1-1)}$$

where $\hat{H}_0$ is the initial energy operator and $\hat{H}_{so}$ is the perturbation due to the spin-orbit interaction. If we define a spin-orbit interaction constant ξ_0, we can write the spin-orbit interaction Hamiltonian as:

$$\hat{H}_{so} = \xi\ \hat{L}\cdot\hat{S} \qquad \textbf{(2.1-2)}$$

$\hat{H}_{so}$ is also referred to as the fine structure Hamiltonian [9]. The next step is to find the energy states which result from this splitting.

The procedure for determining the energies of the states in the fine structure is standard. The first step is to expand the Hamiltonian $\hat{H}$ in the M_L, M_S basis. The result is a 6 X 6 matrix with elements $\langle M_L\, M_S \mid \hat{H}_{so} \mid M_L\, M_S \rangle$. In order to operate easily

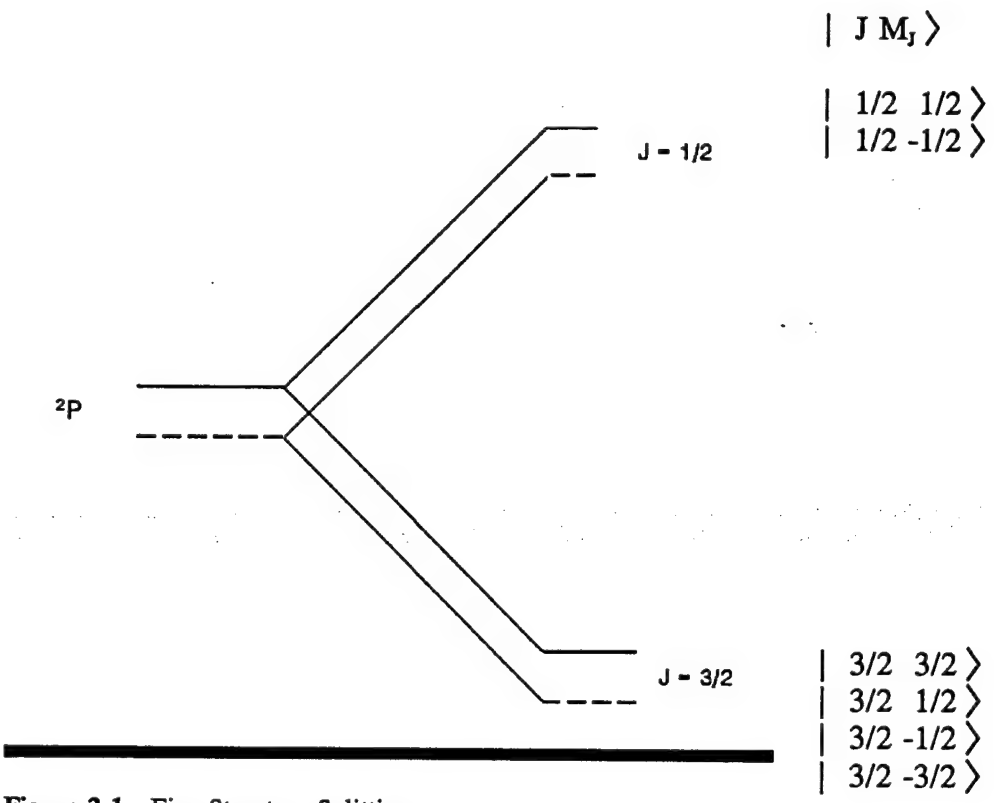

Figure 2-1 Fine Structure Splitting

on the basis vectors, the Hamiltonian operator $\hat{H}_{so}$ is expanded using a standard algebraic technique into operators which follow a set of general rules. First we know:

$$\hat{L}\cdot\hat{S} = \hat{L}_X\hat{S}_X + \hat{L}_Y\hat{S}_Y + \hat{L}_Z\hat{S}_Z \qquad \textbf{(2.1-3)}$$

If we define:

$$\hat{K}_+ = \hat{K}_X + i\,\hat{K}_Y \text{ and } \hat{K}_- = \hat{K}_X - i\,\hat{K}_Y \qquad \textbf{(2.1-4)}$$

where $\hat{K}$ is an operator such as $\hat{L}$ or $\hat{S}$, and make the substitution into Equation 2.5 we get the expression:

$$\hat{L}\cdot\hat{S} = \hat{L}_Z\hat{S}_Z + (1/2)(\hat{L}_+\hat{S}_- + \hat{L}_-\hat{S}_+) \qquad (2.1\text{-}5)$$

$\hat{L}_Z,\hat{S}_Z,\hat{L}_+,\hat{S}_+,\hat{L}_-$ and $\hat{S}_-$ are all operators which follow the general rules:

$$\hat{K}_Z \mid K\,M_K\rangle = \hbar\, M_K \mid K\,M_K\rangle \qquad (2.1\text{-}6)$$

$$\hat{K}_\pm \mid K\,M_K\rangle = \hbar\,[\,K\,(K+1) - M_K\,(M_K \pm 1)\,]^{1/2} \mid K\,M_K \pm 1\rangle \qquad (2.1\text{-}7)$$

$\hat{K}_Z$ is an operator which returns an eigenvalue of the wave function which it is operating on. $\hat{K}_+$ steps up a state when it operates on a basis vector and $\hat{K}_-$ steps down a state. $\hat{K}_+$ and $\hat{K}_-$ are often referred to as step operators or ladder operators. Another useful property used in analyzing quantum mechanical angular momentum is:

$$\hat{K}^2 \mid K\,M_K\rangle = \hbar^2\,K(K+1) \mid K\,M_K\rangle \qquad (2.1\text{-}8)$$

Using these properties, the matrix elements $\langle M_L\ M_S \mid \hat{H}_{so} \mid M_L\ M_S\rangle$ are determined.

Arranging the basis vectors $\mid M_L\ M_S\rangle$ in the following order,

1.	$\mid 1\ \ 1/2\rangle$	4.	$\mid -1\ \ 1/2\rangle$
2.	$\mid 0\ \ 1/2\rangle$	5.	$\mid 0\ -1/2\rangle$
3.	$\mid 1\ -1/2\rangle$	6.	$\mid -1\ -1/2\rangle$

Table 2-2 Basis Vectors for the Fine Structure

we find our matrix $\langle M_L\ M_S \mid \hat{H}_{so} \mid M_L\ M_S\rangle$ to be:

$$\begin{bmatrix} 1/2 & 0 & 0 & 0 & 0 & 0 \\ 0 & 0 & \sqrt{1/2} & 0 & 0 & 0 \\ 0 & \sqrt{1/2} & -1/2 & 0 & 0 & 0 \\ 0 & 0 & 0 & -1/2 & \sqrt{1/2} & 0 \\ 0 & 0 & 0 & \sqrt{1/2} & 0 & 0 \\ 0 & 0 & 0 & 0 & 0 & 1/2 \end{bmatrix} \qquad \textbf{(2.1-9)}$$

The next step is to solve for the eigenvalues of the matrix by diagonalizing it. This would be difficult to do for a 6 × 6 matrix, except that the matrix is already in a block diagonalized for. The largest block matrix that needs to be solved is a 2 × 2. The block diagonalization of this perturbation matrix is a result of the ladder operators defining the allowable states which can be reached as a result of the spin orbit interaction. This is an important result which later makes it easy for us to solve for the allowable states of the hyperfine structure caused by the nuclear interaction. The block diagonalization makes it trivial to solve for the eigenvalues and eigenfunctions of the matrix. Solving for the eigenvalues, we realize the $\hat{L}\cdot\hat{S}$ perturbation does not entirely remove the degeneracy of the original eigenstates. One level is two fold degenerate and the other is four fold degenerate. This is in agreement with the quantum mechanical rule for degeneracy: 2J+1. For the upper $^2P_{1/2}$ level the eigenvalue of $\lambda_1 = -1$ has a degeneracy of 2, and for the lower $^2P_{3/2}$ level the eigenvalue of $\lambda_2 = 1/2$ has a degeneracy of 4. Using these two eigenvalues and the spin-orbit interaction constant ξ_0, we define an energy splitting ΔE between the $^2P_{1/2}$ and $^2P_{3/2}$ levels:

$$\Delta E = | (\lambda_1 - \lambda_2)\xi_0 | \qquad \textbf{(2.1-10)}$$

This leads to:

$$| \xi_0 | = (2/3)\, T_0 \qquad \textbf{(2.1-11)}$$

Where $T_0 = 7602.9768\ cm^{-1}$ is the experimentally determined value of the total energy splitting of the spin-orbit interaction [10].

The nuclear state of the system is examined next. The iodine nucleus has a spin quantum number of I = 5/2. The magnetic quantum number for the nuclear spin can be defined by M_I = I, I-1, ..., -I. The eigenvectors are labeled $| I M_I \rangle$, and the nuclear state of the system is summarized in Table 2-3.

The hyperfine structure is defined by further splitting of the fine structure due to interactions between the nucleus and the total angular momentum of the electrons. The LS-coupling scheme can be extended to perform the vector addition of the spin angular momentum of the nucleus and the total angular momentum of the electrons. A new total

$\| I M_I \rangle$
$\| 5/2 \quad 5/2 \rangle$
$\| 5/2 \quad 3/2 \rangle$
$\| 5/2 \quad 1/2 \rangle$
$\| 5/2 \quad -1/2 \rangle$
$\| 5/2 \quad -3/2 \rangle$
$\| 5/2 \quad -5/2 \rangle$

Table 2-3 Eigenvectors for the Nuclear State of the System

angular momentum quantum number F is defined which takes the values: F = { | J+I | , | J+I-1 | ,..., | I-J | }. The upper state $^2P_{1/2}$ branches into two levels F = 3,2 and the lower state $^2P_{3/2}$ branches into 4 levels F = 4,3,2,1. The total vector space is defined by $| J M_J \rangle | I M_I \rangle$. $| J M_J \rangle | I M_I \rangle$ is rewritten as $| E, F M_F \rangle$, where E indicates the $^2P_{1/2}$ or $^2P_{3/2}$ level. For the upper $^2P_{1/2}$ level, $| E, F M_F \rangle$ is seen in Figure 2-2. For the lower $^2P_{3/2}$ level $| E, F M_F \rangle$ is seen in Figure 2-3.

The Hamiltonian for the hyperfine structure $\hat{H}_{hf}$ can be written as a combination of an electric quadrupole interaction and a magnetic dipole interaction:

$$\hat{H}_{hf} = \hat{H}_{md} + \hat{H}_{eq} \qquad \textbf{(2.1-12)}$$

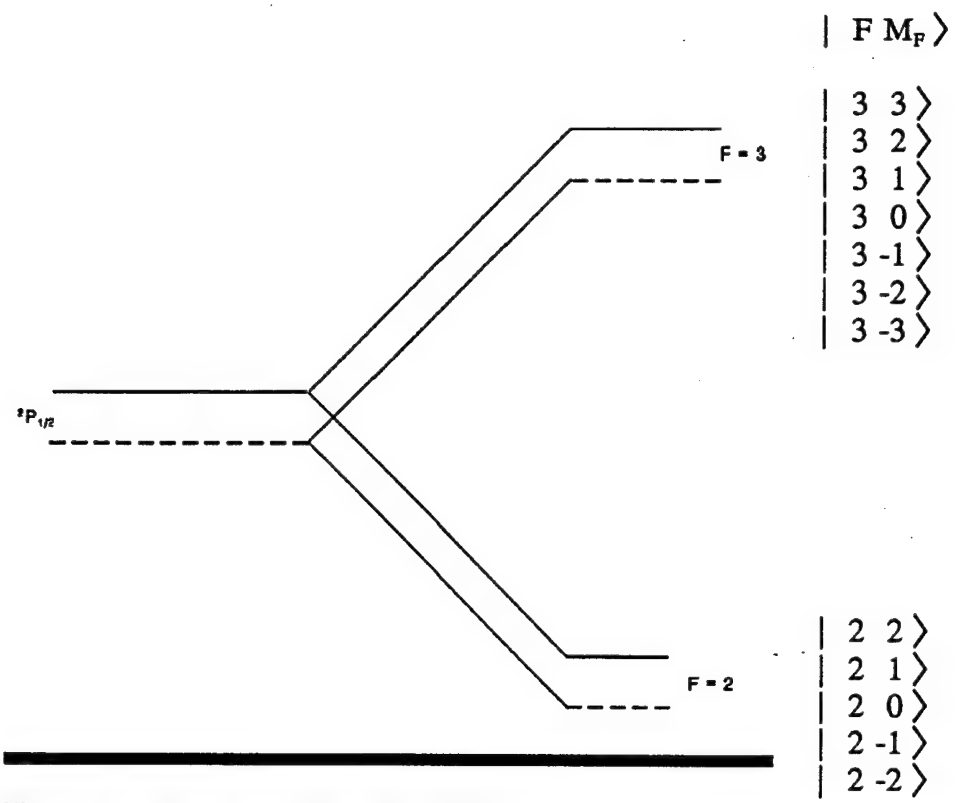

Figure 2-2 Upper Level Hyperfine Splitting

The entire Hamiltonian for the iodine atom may now be written as:

$$\hat{H} = \hat{H}_0 + \hat{H}_{so} + \hat{H}_{hf} \qquad \textbf{(2.1-13)}$$

Because the relative strengths of $\hat{H}_0$, $\hat{H}_{so}$, and $\hat{H}_{hf}$ are fixed: $E_0 \rangle E_{so} \rangle E_{hf}$ it is possible to treat $\hat{H}_{hf}$ as a perturbation relative to $\hat{H}_0$, $\hat{H}_{so}$. From this point on, to distinguish between levels, the hyperfine Hamiltonian operator $\hat{H}_{hf}$ will be written $\hat{H}_{U,L}$. The subscript U denotes the upper $^2P_{1/2}$ level and the subscript L denotes the lower $^2P_{3/2}$ level.

The procedure for determining the energies of the states in the hyperfine structure is similar to the procedure used to determine the fine structure. The first step is to expand the Hamiltonian $\hat{H}_{U,L}$ in the M_J, M_I basis. This creates two matrices with elements $\langle M_J\, M_I \mid \hat{H}_{U,L} \mid M_J\, M_I \rangle$. The matrix for the upper $^2P_{1/2}$ level is a 12 X 12 and the matrix for the lower $^2P_{3/2}$ is a 24 × 24. The Hamiltonian operator has been determined to be [11]:

$$\hat{H} = A_{(U,L)}\left(\hat{J}_Z\hat{I}_Z + \frac{1}{2}\hat{J}_+\hat{I}_- + \tfrac{1}{2}J_-I_+\right)$$

$$+ \frac{B_{(U,L)}}{2I(2I-1)\,J(2J-1)}\left[\frac{1}{2}\left(3\hat{J}_Z^2 - J(J+1)\right)\right.$$

$$\cdot\left[3\hat{I}_Z^2 - I(I+1)\right] + \frac{3}{4}\left(\left[\hat{J}_Z\hat{J}_+ + \hat{J}_+\hat{J}_Z\right]\left[\hat{I}_Z\hat{I}_- + \hat{I}_-\hat{I}_Z\right]\right. \qquad \textbf{(2.1-14)}$$

$$+ \left[\hat{J}_Z\hat{J}_- + \hat{J}_-\hat{J}_Z\right]\left[\hat{I}_Z\hat{I}_+ + \hat{I}_+\hat{I}_Z\right]$$

$$\left.\left. + \left[\hat{I}_+^2\hat{J}_-^2 + \hat{I}_-^2\hat{J}_+^2\right]\right)\right]$$

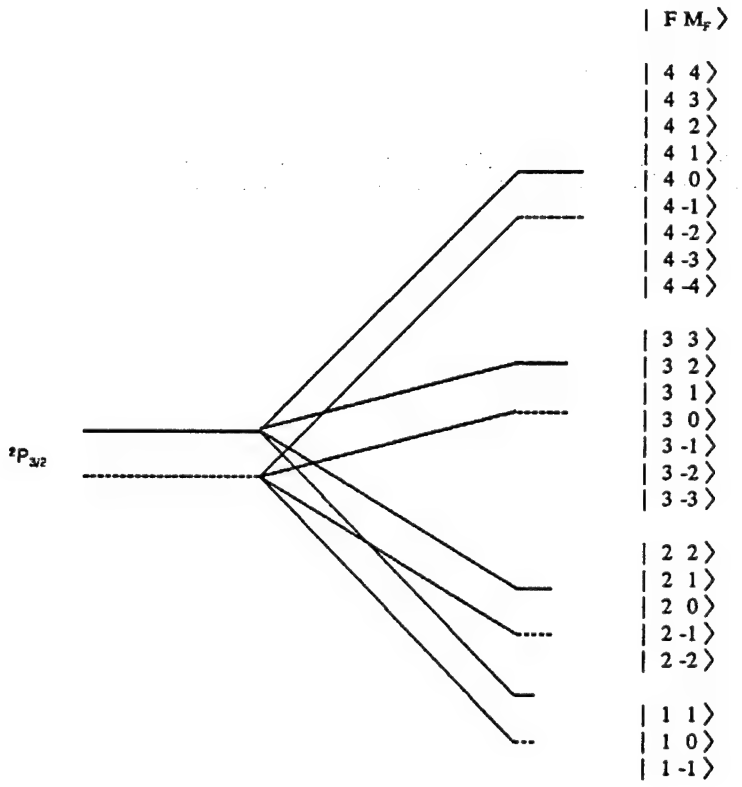

Figure 2-3 Lower Level Hyperfine Splitting

The strength of the magnetic dipole portion $\hat{H}_{md}$ is governed by the empirical constants $A_{U,L}$. The accepted experimental values are [12]:

$$A_U = 0.21973\ cm^{-1} \qquad A_L = 0.02759\ cm^{-1}$$

The strength of the electric quadrupole portion $\hat{H}_{eq}$ is governed by the empirical constants $B_{U,L}$.

$$B_U = 0\ cm^{-1} \qquad B_L = 0.03812\ cm^{-1}$$

As seen before, I = 5/2 is the magnetic quantum number for the nuclear spin and J = 1/2, 3/2 is the total electronic angular momentum quantum number. $\hat{I}_z$, $\hat{J}_z$, $\hat{I}_+$, $\hat{J}_+$, $\hat{I}_-$, and $\hat{J}_-$ are all operators which follow the general rules for quantum mechanical angular momentum as outlined previously in the discussion of the fine structure.

Generating the matrices for the upper and lower levels is simply a matter of book keeping similar to that of the spin-orbit case, and can easily be performed on a computer. The next step, finding the energy eigenvalues, is accomplished by diagonalizing the matrices. This is no trivial task for a 12 × 12 matrix, not to mention a 24 × 24 matrix. The problem is simplified; however, due to the nature of the ladder operators involved. As seen previously in the fine structure case, the vector space is set up such that it is

	$\lvert M_J\ M_I \rangle$	$M_F = M_J + M_I$		$\lvert M_J\ M_I \rangle$	$M_F = M_J + M_I$
1.	$\lvert 1/2\ \ 5/2 \rangle$	3	7.	$\lvert 1/2\ -1/2 \rangle$	0
2.	$\lvert -1/2\ \ 5/2 \rangle$	2	8.	$\lvert -1/2\ -1/2 \rangle$	-1
3.	$\lvert 1/2\ \ 3/2 \rangle$	2	9.	$\lvert 1/2\ -3/2 \rangle$	-1
4.	$\lvert -1/2\ \ 3/2 \rangle$	1	10.	$\lvert -1/2\ -3/2 \rangle$	-2
5.	$\lvert 1/2\ \ 1/2 \rangle$	1	11.	$\lvert 1/2\ -5/2 \rangle$	-2
6.	$\lvert -1/2\ \ 1/2 \rangle$	0	12.	$\lvert -1/2\ -5/2 \rangle$	-3

Table 2-4 Basis Vectors for the Upper $^2P_{1/2}$ Level

1.	$\|$	3/2	5/2 $\rangle$	4	13. $\|$	1/2	-1/2 $\rangle$	0
2.	$\|$	1/2	5/2 $\rangle$	3	14. $\|$	3/2	-3/2 $\rangle$	0
3.	$\|$	3/2	3/2 $\rangle$	3	15. $\|$	-3/2	1/2 $\rangle$	-1
4.	$\|$	-1/2	5/2 $\rangle$	2	16. $\|$	-1/2	-1/2 $\rangle$	-1
5.	$\|$	1/2	5/2 $\rangle$	2	17. $\|$	1/2	-3/2 $\rangle$	-1
6.	$\|$	3/2	1/2 $\rangle$	2	18. $\|$	3/2	-5/2 $\rangle$	-1
7.	$\|$	-3/2	5/2 $\rangle$	1	19. $\|$	-3/2	-1/2 $\rangle$	-2
8.	$\|$	-1/2	3/2 $\rangle$	1	20. $\|$	-1/2	-3/2 $\rangle$	-2
9.	$\|$	1/2	1/2 $\rangle$	1	21. $\|$	1/2	-5/2 $\rangle$	-2
10.	$\|$	3/2	-1/2 $\rangle$	1	22. $\|$	-3/2	-3/2 $\rangle$	-3
11.	$\|$	-3/2	3/2 $\rangle$	0	23. $\|$	-1/2	-5/2 $\rangle$	-3
12.	$\|$	-1/2	1/2 $\rangle$	0	24. $\|$	-3/2	-5/2 $\rangle$	-4

Table 2-5 Basis Vectors for the Lower $^2P_{3/2}$ Level

For the upper level:

F	Degeneracy	Energy Eigenvalue
3	7	$5/4\ A_U = .2746\ cm^{-1}$
2	5	$-7/4\ A_U = -.3845\ cm^{-1}$

For the lower level:

F	Degeneracy	Energy Eigenvalue
4	9	$15/4\ A_L + 1/4\ B_L = .1130\ cm^{-1}$
3	7	$-1/4\ A_L - 11/20\ B_L = -.02786\ cm^{-1}$
2	5	$-13/4\ A_L - 1/10\ B_L = -.09348\ cm^{-1}$
1	3	$-21/4\ A_L + 7/10\ B_L = -.1182\ cm^{-1}$

Table 2-6 Eigenvalues of the Perturbation Matrix

already block diagonalized. The ladder operators determine which states within the basis can be reached. For the upper $^2P_{1/2}$ level, the largest block matrix is a 2×2 and for the lower $^2P_{3/2}$ the largest block matrix is a 4×4. Thus the problem can be solved numerically quite easily. A computer program is used to perform the numerics involved in building the block diagonalized perturbation matrix and solving for the energy eigenstates. The basis states for the upper $^2P_{1/2}$ level are set up in the computer as shown in Table 2-4. For the lower $^2P_{3/2}$ level the basis states are set up in the computer as shown in Table 2-5. The matrices, given by $\langle M_J M_I \mid \hat{H}_{U,L} \mid M_J M_I \rangle$, are too unwieldy to print, but it can be seen that the eigenvalues follow the quantum mechanical rule for degeneracy: 2F+1. This resulting eigenvalue calculation is seen in Table 2-6. This set of calculations leads to the energy level diagram for atomic iodine seen in Figure 2-4.

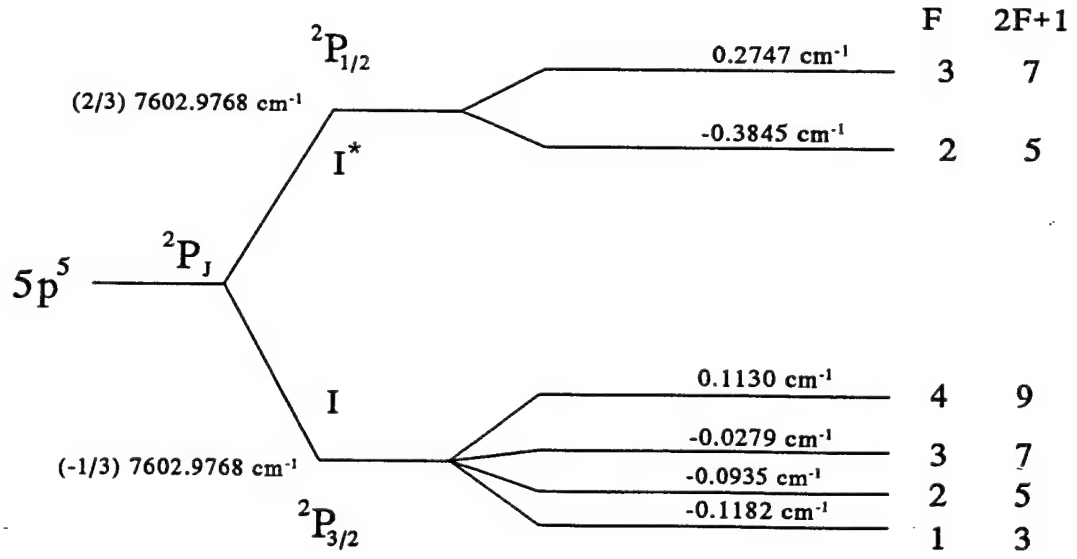

Figure 2-4 Energy Level Diagram for Atomic Iodine

2.2 Processes in the Atomic Iodine Photodissociation Laser

Once the energy eigenstates of the hyperfine Hamiltonian are determined, processes which distribute population between the states can be discussed. Figure 2-5 summarizes the most significant of the processes which might occur in the gain medium of an iodine photodissociation laser. The processes can be divided into two categories: radiative processes and non-radiative processes. The radiative processes are those which cause light to be emitted or absorbed. In atomic iodine, the only processes which are strong enough for this to occur are the magnetic dipole transitions. These processes include stimulated emission, stimulated absorption, and spontaneous emission. The remaining processes are non-radiative and are primarily associated with collisions between the atoms present in the gas mixture. The non-radiative processes include hyperfine relaxation and quenching. Other processes critical to this sort of laser are photodissociation, recombination, and dimerization. Hyperfine relaxation and quenching work through collisions to distribute population in a statistical manner in the gas mixture. Photodissociation, recombination, and dimerization contribute to the total population of atomic iodine in the mixture. The radiative processes will be discussed first, since they follow directly from the vector model and are the most significant in characterizing laser action in an atomic iodine laser. Following the discussion of the radiative processes, non-radiative processes important in characterizing lasing will be considered. Both hyperfine relaxation and quenching will be analyzed, and finally photodissociation, recombination, and dimerization will be discussed.

The radiative processes in atomic iodine arise from magnetic dipole transitions between energy states in the hyperfine structure. From an analysis of the parity conditions for multipole fields [13], the selection rule for which magnetic dipole transitions may occur is $\Delta F=0, \pm 1$. This gives six transitions: 3-4, 3-3, 3-2, 2-3, 2-2, and 2-1. These transitions are seen in Figure 2-6 with an experimentally measured gain spectrum for atomic iodine [14]. The relative absorptions or linear small signal gains of each of these six transitions and the frequency at which they occur are the two basic features which make up the emission/absorption spectrum in Figure 2-6. The position of any given transition is determined directly from the energy eigenvalues of the

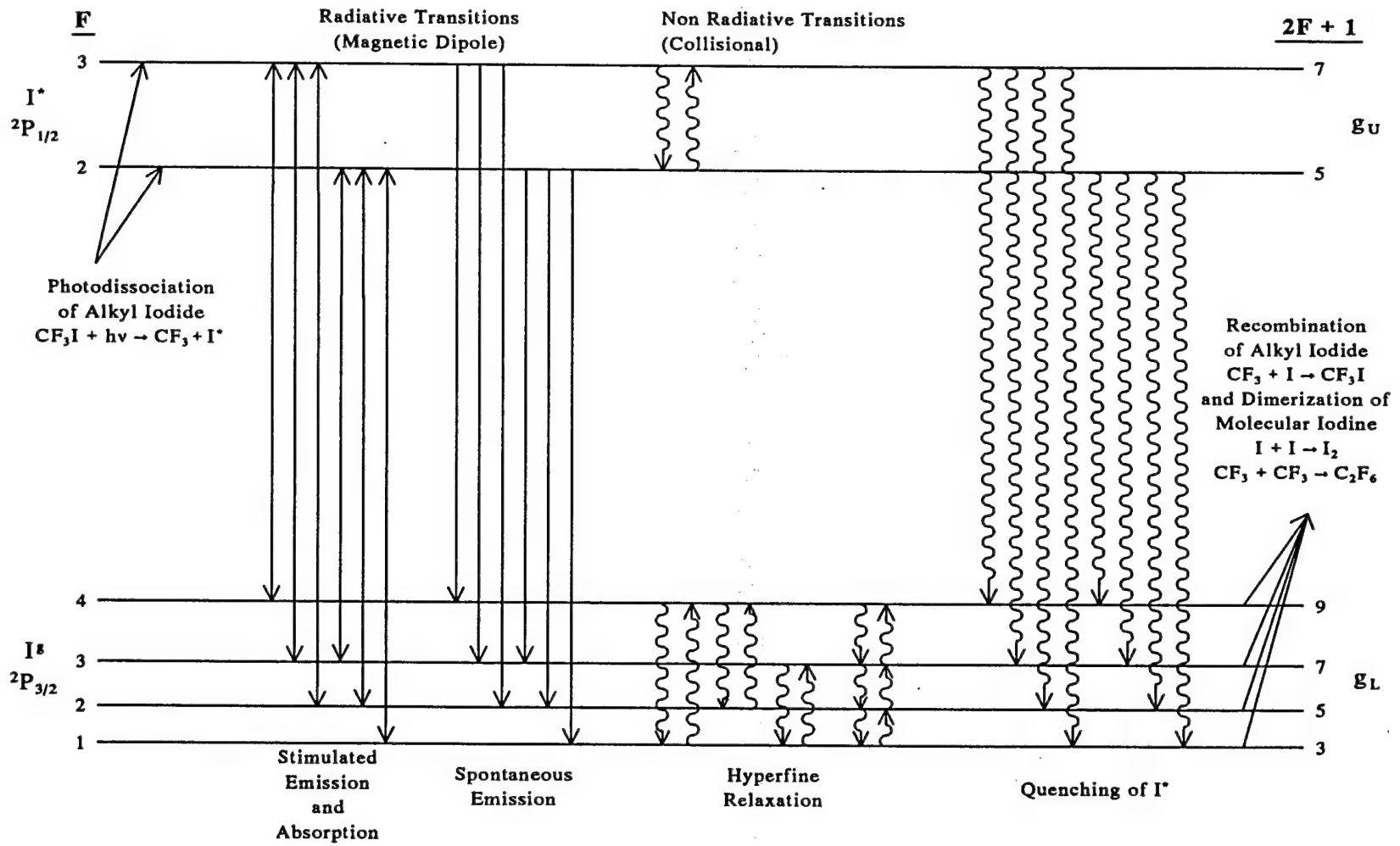

Figure 2-5 Kinetic Processes Associated with an Iodine Photodissociation Laser

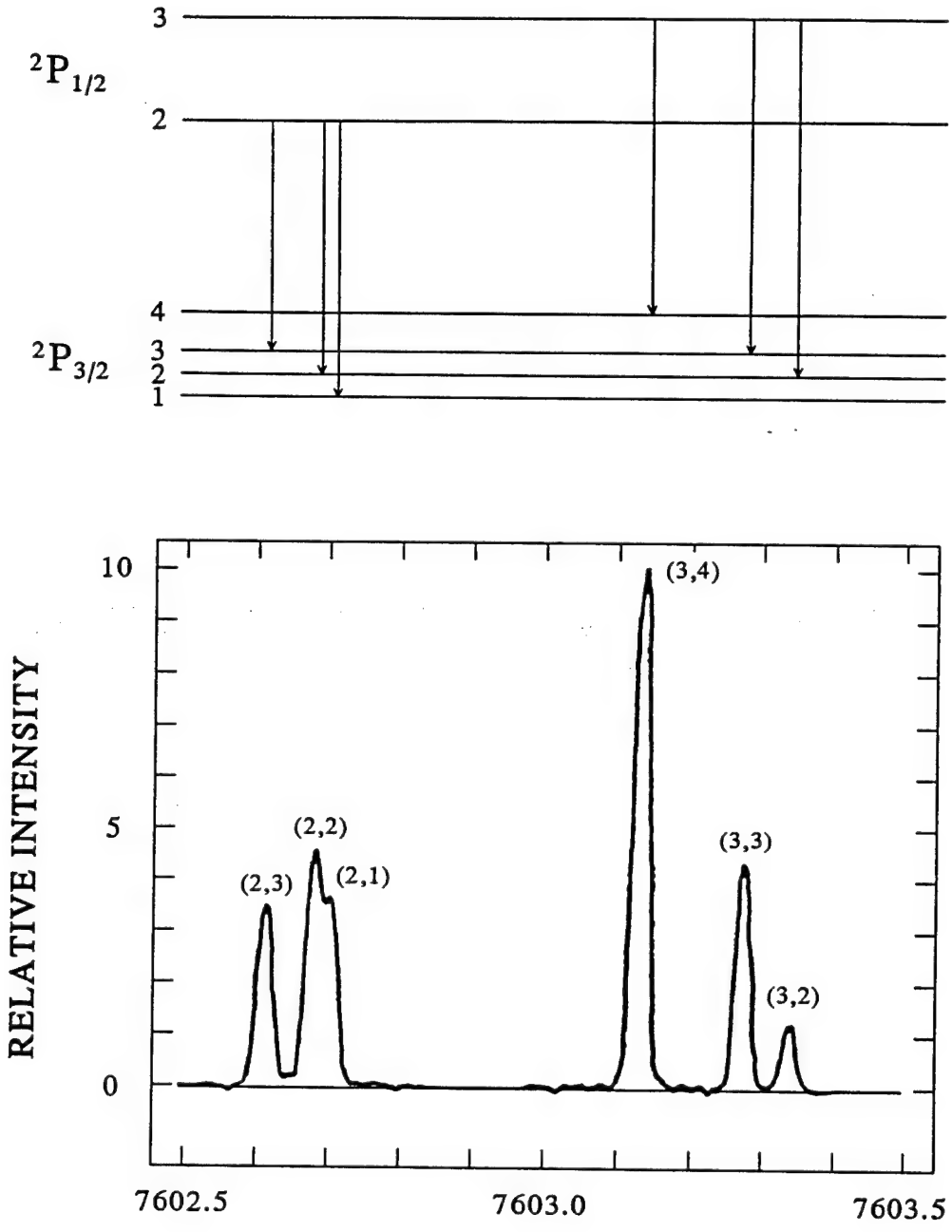

Figure 2-6 Gain Spectrum of Atomic Iodine

Hamiltonian. The linear gain is determined by the original states, the energy eigenvalues of the Hamiltonian, and the gas temperature and pressure. First we will discuss the transition positions or frequencies and then we will discuss their linear gains.

The line positions, or frequencies, are basically the energies of the allowed transitions, which can be determined directly from the eigenvalues of the hyperfine perturbation. The frequencies, expressed in wave numbers, are determined by [15]:

$$E(F_U, F_L) = T_0 + E(F_U) - E(F_L) \qquad (2.2\text{-}1)$$

where U and L signify the upper and lower levels. This gives us:

Transition	Energy (cm^{-1})
3-4	7603.1385
3-3	7603.2794
3-2	7603.3450
2-3	7602.6202
2-2	7602.6858
2-1	7602.7105

Table 2-7 Energies of the Allowed Radiative Transitions

The linear gain coefficients, or absorption coefficients, of each of the individual transitions require a little more computation. The general expression for the linear gain coefficient for a given transition is [16]:

$$\alpha_{U\text{-}L}(\nu) = \frac{\lambda^2_{U\text{-}L}\, A_{U\text{-}L}}{8\pi} \left[[N_U] - \frac{g_U}{g_L}[N_L] \right] f_v(\nu) \qquad (2.2\text{-}2)$$

The small signal gain can also be expressed in terms of a gain cross section $\sigma_{U\text{-}L}(\upsilon)$ [17]:

$$\alpha_{U\text{-}L}(\nu) = \sigma_{U\text{-}L}(\nu) \left[[N_U] - \frac{g_U}{g_L} [N_L] \right] \qquad \textbf{(2.2-3)}$$

where

$$\sigma_{U\text{-}L}(\nu) = \frac{\lambda_{U\text{-}L}^2 A_{U\text{-}L}}{8\pi} f_V(\nu) \qquad \textbf{(2.2-4)}$$

$\lambda_{U\text{-}L}$ is the wavelength of the transition between the upper state U and the lower state L, $A_{U\text{-}L}$ is the Einstein A-coefficient of the transition, $[N_{U,L}]$ are the population densities of each state, and $f_v(\upsilon)$ is the Voigt lineshape function. g_U and g_L are the degeneracies of the upper and lower levels. The A-coefficient is given by [18]:

$$A_{U\text{-}L} = \frac{64\pi^4 \mu_B^2}{3h\lambda_{U\text{-}L}^3} | \langle \psi_L | \hat{L} + 2\hat{S} | \psi_U \rangle |^2 \qquad \textbf{(2.2-5)}$$

Determining the A-coefficient requires another calculation involving the basis vectors and the quantum mechanical angular momentum operators. We know the Bohr magneton is $\mu_B = 0.92741 \times 10^{-20}$ erg/gauss and Planck's constant is $h = 6.62625 \times 10^{-27}$ erg s [19]. Following the standard procedure outlined earlier, the operator $\hat{L} + 2\hat{S}$ operates on the wavefunctions $| \Psi_L \rangle$ and then the integration is performed to find the matrix elements. This is outlined in some detail in Kelly's dissertation. The A-coefficients for the allowed transitions are shown in Table 2-8. Relative small signal gains, normalized to the 3-4 transition can be determined from just the A-coefficients and the degeneracies of the levels. Normalizing the expression for the linear gain for a given transition to that of the 3-4 transition leads to:

$$\frac{\alpha_{U\text{-}L}}{\alpha_{3\text{-}4}} = \frac{A_{U\text{-}L}}{A_{3\text{-}4}} \frac{g_U}{g_L} \qquad \textbf{(2.2-6)}$$

Transition	A-coefficient
3-4	5.08 s^{-1}
3-3	2.20 s^{-1}
3-2	0.63 s^{-1}
2-3	2.46 s^{-1}
2-2	3.07 s^{-1}
2-1	2.37 s^{-1}

Table 2-8 A-coefficients of the Allowed Radiative Transitions

This gives the following values for linear gain normalized to the 3-4 transition. These values are also proportional to the strengths of the transitions.

Transition	Gain
3-4	1.000
3-3	0.433
3-2	0.124
2-3	0.346
2-2	0.432
2-1	0.333

Table 2-9 Values for Linear Gain Normalized to the 3-4 Transition

The final thing which is needed in order to construct the gain spectrum of the iodine atom is the lineshape function $f(\nu)$. There are two basic types of line broadening: homogeneous and inhomogeneous line broadening. Inhomogeneous broadening, usually referred to as collisional or pressure broadening consists of multiple contributions from the various gas phase species present in the laser gain medium and is modeled with a Lorentzian lineshape function. Homogeneous broadening or Doppler broadening is caused by the thermal motion of the gas and is described by a Gaussian lineshape

function. The total line broadening of a gas laser can be modeled using a combination of these two lineshape functions called a Voigt lineshape function. Collisional broadening will be discussed first, then Doppler broadening, and finally the two will be convolved to describe a Voigt lineshape function.

The general expression for the normalized Lorentzian lineshape function is [20]:

$$f_L(\nu) = \frac{\frac{\Delta\nu_L}{2\pi}}{(\nu - \nu_0)^2 + \left(\frac{\Delta\nu_L}{2}\right)^2} \qquad \textbf{(2.2-7)}$$

The full width at half maximum (FWHM) of the lineshape is described by $\Delta\nu_L$. This lineshape function describes both natural broadening and collisional broadening. For natural (or lifetime) broadened transitions the Lorentzian lineshape has a linewidth described by [21]:

$$\Delta\nu_N = \frac{1}{\pi}\left(\frac{1}{\tau_R} + \frac{1}{\tau_{NR}}\right) \qquad \textbf{(2.2-8)}$$

τ_R is the radiative lifetime and τ_{NR} is the contribution due to inelastic collisions with other atomic systems. At room temperature the natural broadening is typically two orders of magnitude less than the collisional broadening [22], thus we will neglect the contribution of the natural lifetime and rely on the linewidth $\Delta\nu_L = \Delta\nu_C$ for collision broadened transitions. The expression for $\Delta\nu_C$ is:

$$\Delta\nu_C = \sum_i \alpha_i P_i \qquad \textbf{(2.2-9)}$$

Where P_i is the partial pressure of a given species in the gas mixture and α_i is the respective pressure broadening coefficient of that species. Evaluating the collision broadened Lorentzian function (Equation 2.2-7) at line center yields:

$$f_L(\nu_0) = \frac{2}{\pi}\frac{1}{\Delta\nu_L} \qquad (2.2\text{-}10)$$

The general expression for the normalized Gaussian lineshape function is [23]:

$$f_G(\nu) = \frac{2\sqrt{\ln 2}}{\sqrt{\pi}\,\Delta\nu_D}\exp\left(\frac{-4\ln 2(\nu-\nu_0)^2}{(\Delta\nu_D)^2}\right) \qquad (2.2\text{-}11)$$

Where the FWHM of the Doppler broadened lineshape function is expressed by [24]:

$$\Delta\nu_D = 2\nu_0\sqrt{\frac{2kT\ln 2}{Mc^2}} \qquad (2.2\text{-}12)$$

The Doppler broadened Gaussian lineshape function (Equation 2.2-11) evaluated at line center yields:

$$f_G(\nu_0) = \frac{2}{\Delta\nu_D}\sqrt{\frac{\ln 2}{\pi}} \qquad (2.2\text{-}13)$$

At low pressures, the Doppler line broadening effects dominate and it is suitable to model the linewidth with a Gaussian lineshape function. At high pressures, collisional effects take over and a Lorentzian lineshape function is more appropriate. For intermediate pressures, however, both effects play a significant role and their lineshape functions must be convolved to form a Voigt lineshape function.

The Voigt lineshape function is the convolution of the collisional broadening with the Doppler broadening. This can be expressed by the convolution integral [25]:

$$f_V(\nu) = f_L \circledast f_G = \int_{+\infty}^{-\infty} f_L(\nu)\, f_G(\nu_0 - \nu)\, d\nu \qquad (2.2\text{-}14)$$

Taking the normalized Gaussian and Lorentzian functions in Equations 2.2-11 and 2.2-7, and applying the convolution integral, we get:

$$f_V(\nu) = \frac{\Delta\nu_L}{\Delta\nu_D}\frac{\sqrt{\ln 2}}{\pi\sqrt{\pi}} \int_{-\infty}^{+\infty} \frac{\exp\left(-\frac{(\nu' - \nu)^2}{\left(\frac{\Delta\nu_D}{2\sqrt{\ln 2}}\right)^2}\right)}{(\nu_0 - \nu')^2 + \left(\frac{\Delta\nu_L}{2}\right)^2}\, d\nu' \qquad (2.2\text{-}15)$$

To solve the integral, the reader is referred to Abramowitz and Stegun Handbook of Mathematical Functions [26]. The integral is basically:

$$\int_{+\infty}^{-\infty} \frac{\exp\left(-\frac{(x' - x)^2}{a^2}\right)}{(x_0 - x')^2 + b^2}\, dx' = \frac{\pi}{b}\,\mathrm{Re}\, w\left[\frac{x_0 - x + ib}{a}\right] \qquad (2.2\text{-}16)$$

Where the complex error function w(z) can be written as a series expansion in terms of the complex variable z and the gamma function Γ:

$$w(z) = \sum_{n=0}^{\infty} \frac{(iz)^n}{\Gamma\left(\frac{n}{2} + 1\right)} \qquad (2.2\text{-}17)$$

If we let:

$$a = \frac{\Delta\nu_D}{2\sqrt{\ln 2}} \qquad b = \frac{\Delta\nu_L}{2} \qquad (2.2\text{-}18)$$

Then the normalized Voigt lineshape function is:

$$f_V(\nu) = \frac{2\sqrt{\ln 2}}{\Delta\nu_D\sqrt{\pi}} \text{ Re } w\left[\frac{\nu_0 - \nu + \frac{i\Delta\nu_L}{2}}{\frac{\Delta\nu_D}{2\sqrt{\ln 2}}}\right] \qquad \textbf{(2.2-19)}$$

Which can also be expressed as:

$$f_V(\nu) = f_0(0) \text{ Re } w(z) \qquad \textbf{(2.2-20)}$$

Where:

$$z = x + iy = \frac{(\nu_0 - \nu)\,2\sqrt{\ln 2}}{\Delta\nu_D} + i\frac{\Delta\nu_L}{\Delta\nu_D}\sqrt{\ln 2} \qquad \textbf{(2.2-21)}$$

The expression for the Voigt lineshape function at line center is then found from 2.2-19:

$$f_V(\nu_0) = f_G(\nu_0) \text{ Re } w\left[\frac{\Delta\nu_L}{\Delta\nu_D}\sqrt{\ln 2}\right] \qquad \textbf{(2.2-22)}$$

The complex error function w(z) is solved using computer algorithm number 363 from the ACM library which uses the approximation:

$$w(z) = \exp(-z^2)\,\text{erfc}(-iz) \qquad \textbf{(2.2-23)}$$

where the complimentary error function erfc(x) is solved using an algorithm based on solving the Fresnel integrals. This approximation is good up to at least 10 significant digits [27].

The theoretical gain spectrum for a CF_3I photodissociation laser, broadened by a Voigt lineshape function is seen in Figure 2-7. The pressure broadening effects are due to the 50 Torr of CF_3I present in the gas mixture. The radiative processes that make up this spectrum are stimulated emission, stimulated absorption, and spontaneous emission. In a laser of this sort, population is introduced into the upper $^2P_{1/2}$ levels of the hyperfine

structure. Spontaneous emission is the process where an atom in one of the upper energy levels transitions to a lower energy (due to the natural lifetime of the excited state

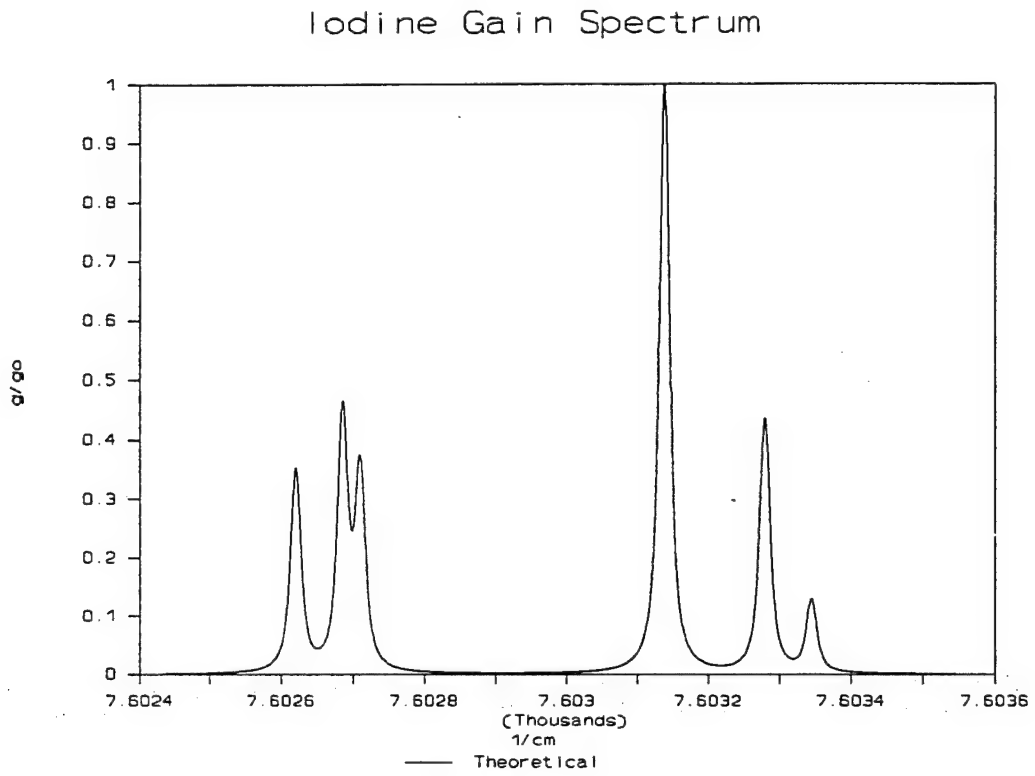

Figure 2-7 Theoretical Gain Spectrum

expiring) and emits a photon of light. This is written:

$$I^* \rightarrow I + h\nu_{1.315} \qquad \textbf{(2.2-24)}$$

Stimulated emission occurs when an existing photon of the proper state interacts with an excited state iodine atom causing the atom to transition to the ground state and emit a photon in the process:

$$h\nu_{1.315} + I^* \rightarrow I + 2h\nu_{1.315} \qquad \textbf{(2.2-25)}$$

Stimulated absorption occurs when a photon interacts with a ground state iodine atom

forcing it to transition to the excited state. The entire energy of the photon is expended in this process:

$$h\nu_{1.315} + I \rightarrow I^* \qquad (2.2\text{-}26)$$

Laser action is achieved through these processes. Spontaneous emission provides a small amount of light which is directed back through the gain medium with resonator mirrors. This stimulates the emission of more photons, and a laser pulse grows out of the noise. Lasing occurs as long as a population inversion exists; that is as long as the population in the upper level is greater than the degeneracy ratio times the population in the lower level of a transition [28].

$$[N_U] = \frac{g_U}{g_L}[N_L] \qquad (2.2\text{-}27)$$

Differential equations can be written to describe how the radiative processes affect population in the different energy levels, and how light flux interacts with the gain medium. The two sets of rate equations, number density and intensity, are coupled and must be solved simultaneously in order to model laser action, but for now we will concentrate on the contribution by the radiative processes to the number density in the hyperfine energy levels. The general equation describing the time rate of change in population for an upper hyperfine energy level due to magnetic dipole processes is [29]:

$$\left.\frac{d[N_U]}{dt}\right|_{md} = -\sum_L \left(\sigma_{U-L} \frac{\bar{I}_{U-L}}{h\nu_{U-L}} \right) - \sum_L \left(A_{U-L}[N_U] \right) \qquad (2.2\text{-}28a)$$

For a lower level the general form is:

$$\left.\frac{d[N_L]}{dt}\right|_{md} = \sum_U \left(\sigma_{U-L} \frac{\bar{I}_{U-L}}{h\nu_{U-L}} \right) + \sum_U \left(A_{U-L}[N_U] \right) \qquad (2.2\text{-}28b)$$

$[N_U]$ and $[N_L]$ are populations of individual upper and lower levels. A_{U-L} is the A-

coefficient for the transition U-L (2.2-5), and $\sigma_{U\text{-}L}$, is the gain cross section (2.2-4). h is Planck's constant and $\nu_{U\text{-}L}$ is the frequency of the transition. The product $h\nu_{U\text{-}L}$ is the energy of the transition. $\bar{I}_{U\text{-}L}$ is the two way circulating intensity in the laser cavity which can be described generally by a set of flux equations [30]. These intensity equations will be discussed in much greater detail in Section 2.3. For now it is important only to realize that they couple to the number density rate equations.

Looking again at the radiative contribution to the number density equations, it can be seen that the spontaneous emission plays a very small part after lasing starts. It acts initially as a noise term to begin the lasing process, spontaneously producing photons at a rate described by the A-coefficients which are on the order of several transitions per second. Thus after laser action starts, the stimulated emission and absorption terms dominate and the noise term can be eliminated from the equations:

$$\left.\frac{d[N_U]}{dt}\right|_{stim} = -\sum_{L}\left(\sigma_{U\text{-}L}\,\frac{\bar{I}_{U\text{-}L}}{h\nu_{U\text{-}L}}\right) \qquad \textbf{(2.2-29a)}$$

$$\left.\frac{d[N_L]}{dt}\right|_{stim} = \sum_{U}\left(\sigma_{U\text{-}L}\,\frac{\bar{I}_{U\text{-}L}}{h\nu_{U\text{-}L}}\right) \qquad \textbf{(2.2-29b)}$$

The radiative contributions to the number density can be written out to describe the time rate of change in population for each level. For the upper $^2P_{1/2}$ levels:

$$\begin{aligned}\left.\frac{d[I_3^*]}{dt}\right|_{md} = &-\sigma_{34}\left([I_3^*] - \frac{7}{9}[I_4^g]\right)\frac{\bar{I}_{34}(t)}{h\nu_{34}} - \sigma_{33}\left([I_3^*] - [I_3^g]\right)\frac{\bar{I}_{33}(t)}{h\nu_{33}} \\ &-\sigma_{32}\left([I_3^*] - \frac{7}{5}[I_2^g]\right)\frac{\bar{I}_{32}(t)}{h\nu_{32}} + (A_{34} + A_{33} + A_{32})[I_3^*]\end{aligned} \qquad \textbf{(2.2-30a)}$$

$$\left.\frac{d[I_2^*]}{dt}\right|_{md} = -\sigma_{23}\left([I_2^*] - \frac{5}{7}[I_3^g]\right)\frac{\bar{I}_{23}(t)}{h\nu_{23}} - \sigma_{22}\left([I_2^*] - [I_2^g]\right)\frac{\bar{I}_{22}(t)}{h\nu_{22}}$$
$$- \sigma_{21}\left([I_2^*] - \frac{5}{3}[I_1^g]\right)\frac{\bar{I}_{21}(t)}{h\nu_{21}} + (A_{23} + A_{22} + A_{21})[I_2^*] \qquad \text{(2.2-30b)}$$

For the lower $^2P_{3/2}$ levels:

$$\left.\frac{d[I_4^g]}{dt}\right|_{md} = \sigma_{34}\left([I_3^*] - \frac{7}{9}[I_4^g]\right)\frac{\bar{I}_{34}(t)}{h\nu_{34}} + A_{34}[I_3^*] \qquad \text{(2.2-30c)}$$

$$\left.\frac{d[I_3^g]}{dt}\right|_{md} = \sigma_{33}\left([I_3^*] - [I_3^g]\right)\frac{\bar{I}_{33}(t)}{h\nu_{33}} + \sigma_{23}\left([I_2^*] - \frac{5}{7}[I_3^g]\right)\frac{\bar{I}_{23}(t)}{h\nu_{23}}$$
$$+ A_{33}[I_3^*] + A_{23}[I_2^*] \qquad \text{(2.2-30d)}$$

$$\left.\frac{d[I_2^g]}{dt}\right|_{md} = \sigma_{32}\left([I_3^*] - \frac{7}{5}[I_2^g]\right)\frac{\bar{I}_{32}(t)}{h\nu_{32}} + \sigma_{22}\left([I_2^*] - [I_2^g]\right)\frac{\bar{I}_{22}(t)}{h\nu_{22}}$$
$$+ A_{33}[I_3^*] + A_{22}[I_2^*] \qquad \text{(2.2-30e)}$$

$$\left.\frac{d[I_1^g]}{dt}\right|_{md} = \sigma_{21}\left([I_2^*] - \frac{5}{3}[I_1^g]\right)\frac{\bar{I}_{21}(t)}{h\nu_{21}} + A_{21}[I_2^*] \qquad \text{(2.2-30f)}$$

Now that the radiative contribution to the number density equations has been discussed, other non-radiative processes which adjust the population in each of the hyperfine levels through collisional relaxation can be addressed.

The primary non-radiative processes which occur during lasing are hyperfine relaxation and quenching. Both of these processes are collisional, but quenching occurs on a much slower time scale than the hyperfine relaxation, and generally has little effect on lasing in the short pulsed laser system being studied. Hyperfine relaxation will be dealt with first.

Hyperfine relaxation occurs between the upper two energy states in the hyperfine structure and between the lower four energy states as shown in Figure 2-5. The mechanisms which relax the upper $^2P_{1/2}$ levels must be dealt with separately from those which relax the lower $^2P_{3/2}$ levels. Since hyperfine relaxation is a collisional process, the first step in determining the relevant relaxation mechanism is to find the collision partner for the interaction. In the type of photodissociation laser being studied, the particle species present can be limited to CF_3I, CF_3, I^*, I, I_2 and possibly some buffer gas.

A theoretical analysis by Yukov [31] predicts that the relaxation between the excited state hyperfine levels is due primarily to resonant energy transfer with ground state iodine. Measurements by Thieme and Fill [32] also show that the main contribution to hyperfine relaxation within the upper laser level comes from collisions with iodine atoms in the ground state. This resonant energy transfer, or exchange interaction, occurs when an excited atom transfers its excitation energy to an atom in the ground state. The overall effect of the electronic resonance interaction is the mixing of the two upper hyperfine levels shown in Figure 2-8. The relaxation rate constants for the mixing are

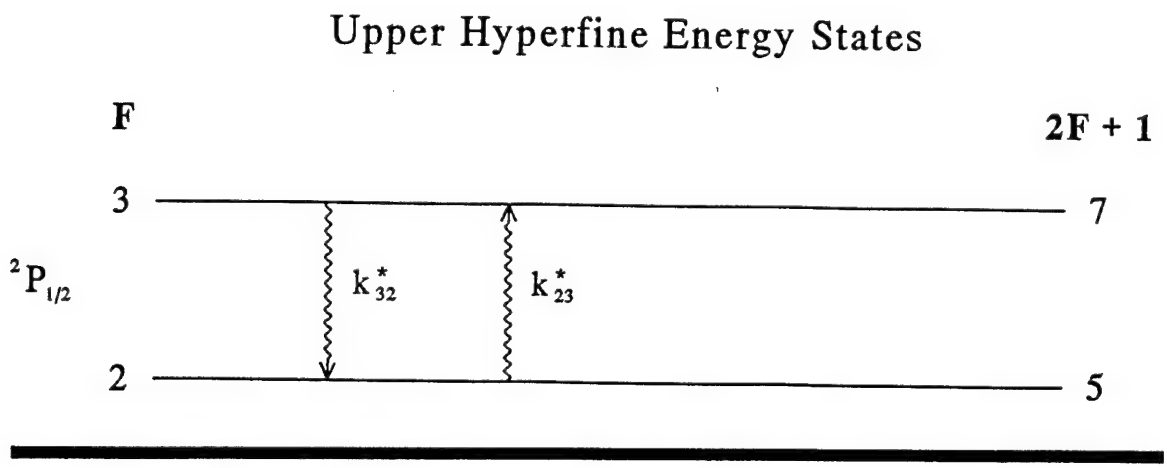

Figure 2-8 Mixing of Population Between Levels in the Excited State

k_{32}^* and k_{23}^* . The contribution to the time rate of change in population of the upper F=3 excited hyperfine state is described by the differential equation:

$$\left.\frac{d[I_3^*]}{dt}\right|_{hf} = -k_{32}^*[I_3^*][M_U] + k_{23}^*[I_2^*][M_U] \qquad \textbf{(2.2-31a)}$$

where $[I_3^*]$ is the population of the upper F=3 level, and $[I_2^*]$ is the population of the upper F=2 level. M_U is the concentration of the collision partner for the upper levels, which has been determined to be primarily ground state iodine.

A similar equation can be written for the upper F=2 excited hyperfine state:

$$\left.\frac{d[I_2^*]}{dt}\right|_{hf} = -k_{23}^*[I_2^*][M_U] + k_{32}^*[I_3^*][M_U] \qquad \textbf{(2.2-31b)}$$

In steady state the populations reach an equilibrium defined by:

$$\left.\frac{d[I_3^*]}{dt}\right|_{hf} = 0 \Rightarrow k_{32}^*[I_3^*]_{eq} = k_{23}^*[I_2^*]_{eq} \qquad \textbf{(2.2-33)}$$

$$\textbf{(2.2-32)}$$

which leads to:

$$\frac{k_{32}^*}{k_{23}^*} = \frac{[I_2^*]_{eq}}{[I_3^*]_{eq}} = \frac{g_2^* e^{\frac{-E_2}{kT}}}{g_3^* e^{\frac{-E_3}{kT}}} \cong \frac{g_2^*}{g_3^*} = \frac{5}{7}$$

where g_2^* is the degeneracy of the upper F=2 level, g_3^* is the degeneracy of the upper F=3 level, and $(E_3 - E_2)$ is the energy separation between the two levels and is much less than kT. The general result of this analysis is:

$$\frac{k_{i-j}}{k_{j-i}} = \frac{g_j}{g_i} \qquad \textbf{(2.2-34)}$$

If we let the downward rate $k_{32}^* = k_U$, then the upward rate can be found to be:

$$k_{23}^{*} = \frac{7}{5}k_U \qquad (2.2\text{-}36)$$

rewriting our rate equations (2.2-31) we get:

$$\left.\frac{d[I_3^*]}{dt}\right|_{hf} = -k_U[M_U]\left([I_3^*] - \frac{7}{5}[I_2^*]\right) \qquad (2.2\text{-}37a)$$

$$\left.\frac{d[I_2^*]}{dt}\right|_{hf} = -k_U[M_U]\left(\frac{7}{5}[I_2^*] - [I_3^*]\right) \qquad (2.2\text{-}37b)$$

Solving these equations in the steady state limit we also find:

$$\left.\frac{d[I_3^*]}{dt}\right|_{hf} = 0 \Rightarrow \frac{[I_3^*]_{eq}}{[I_2^*]_{eq}} = \frac{7}{5} \qquad (2.2\text{-}38)$$

Thus the population in the upper two hyperfine levels relax toward an equilibrium of 7/12 of the excited state population residing in the upper F=3 level and 5/12 residing in the upper F=2 level. Thieme and Fill report a theoretical relaxation time for the upper level of 30-50 ns and an experimental value of about 100 ns for their flash lamp pumped i-C_3F_7I photodissociation laser [33].

Yukov [34] theoretically predicts that relaxation between hyperfine levels in the ground state is independent of the electronic nature of the collision partner. Looking at our possible relaxation partners (CF_3I, CF_3, I, I^*, I_2, and some buffer gas) we see that any of these could play a role in relaxation. The overall effect of the collisions is seen in Figure 2-9. The most abundant species after photodissociation is either CF_3I or some buffer gas. The pressure of the buffer gas could be varied to change the number of

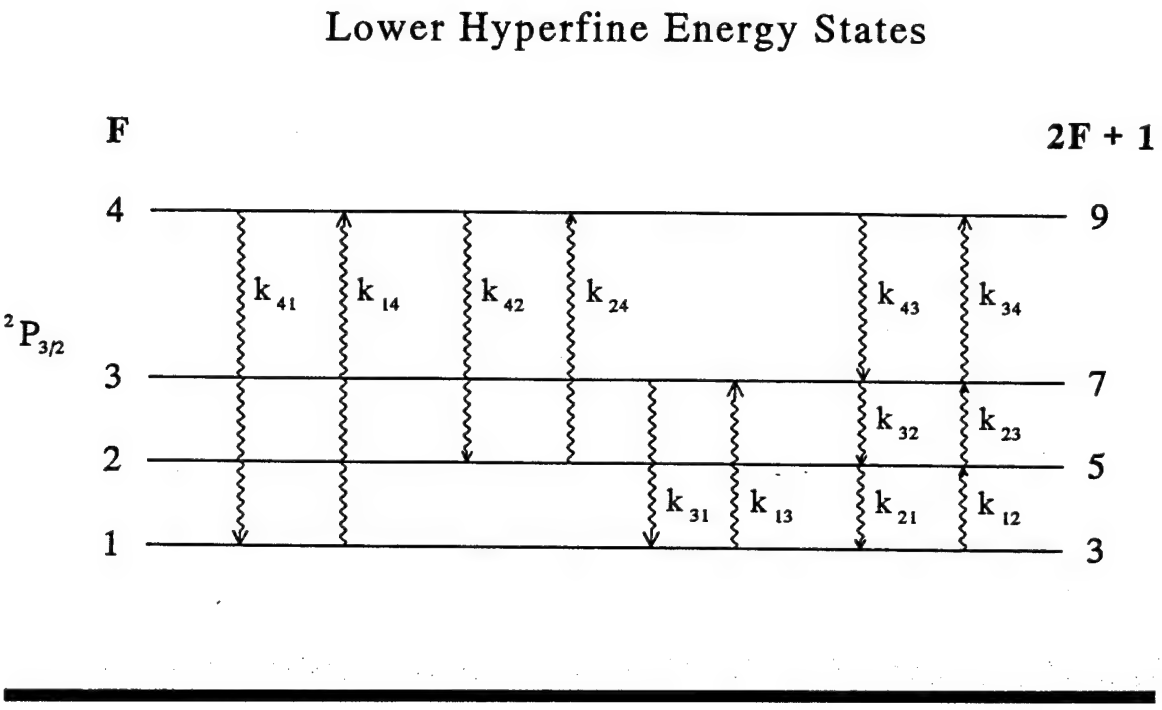

Figure 2-9 Mixing of Population Between Levels in the Ground State

collisions and thus vary the relaxation time in the lower levels. For any given collision partner, the contribution to the population rate equations for the lower F=4 sublevel is written:

$$\left.\frac{d[I_4^g]}{dt}\right|_{hf} = -\left(k_{43} + k_{42} + k_{41}\right)[I_4^g][M_L] + k_{34}[I_3^g][M_L] + k_{24}[I_2^g][M_L] + k_{14}[I_1^g][M_L] \qquad \textbf{(2.2-39a)}$$

where the k's are the general relaxation rate constants, the [I]'s are the population densities of the different levels in the $^2P_{3/2}$ state, and the $[M_L]$ is the density of the collision partner. If it is determined that more than one collision partner play a significant role, then a rate equation for each partner should be written containing the

relevant rate constants and partner densities. The equations for the other sublevels can be written in a similar manner:

$$\left.\frac{d[I_3^g]}{dt}\right|_{hf} = -\left(k_{34} + k_{32} + k_{31}\right)[I_3^g][M_L] + k_{43}[I_4^g][M_L] + k_{23}[I_2^g][M_L] + k_{13}[I_1^g][M_L] \qquad \text{(2.2-39b)}$$

$$\left.\frac{d[I_2^g]}{dt}\right|_{hf} = -\left(k_{24} + k_{23} + k_{21}\right)[I_2^g][M_L] + k_{42}[I_4^g][M_L] + k_{32}[I_3^g][M_L] + k_{12}[I_1^g][M_L] \qquad \text{(2.2-39c)}$$

$$\left.\frac{d[I_1^g]}{dt}\right|_{hf} = -\left(k_{14} + k_{13} + k_{12}\right)[I_1^g][M_L] + k_{41}[I_4^g][M_L] + k_{31}[I_3^g][M_L] + k_{21}[I_2^g][M_L] \qquad \text{(2.2-39d)}$$

If we let all downward rates be equal to a constant k_L,

$$k_{43} = k_{32} = k_{21} = k_{42} = k_{31} = k_{41} = k_L \qquad \text{(2.2-40)}$$

The reverse rates are found to be:

$$\begin{aligned} k_{34} &= (9/7)k_{43} = (9/7)k_L \\ k_{23} &= (7/5)k_{32} = (7/5)k_L \\ k_{12} &= (5/3)k_{21} = (5/3)k_L \\ k_{24} &= (9/5)k_{42} = (9/5)k_L \\ k_{13} &= (7/3)k_{31} = (7/3)k_L \\ k_{14} &= (9/3)k_{41} = (9/3)k_L \end{aligned} \qquad \text{(2.2-41)}$$

The contribution of the hyperfine mixing on the number density equations can be re-written as:

$$\left.\frac{d[I_4^g]}{dt}\right|_{hf} = -3k_L[I_4^g][M_L] + k_L\frac{9}{7}[I_3^g][M_L] + k_L\frac{9}{5}[I_2^g][M_L] + k_L\frac{9}{3}[I_1^g][M_L] \quad \textbf{(2.2-42a)}$$

$$\left.\frac{d[I_3^g]}{dt}\right|_{hf} = -\frac{23}{7}[I_3^g][M_L] + k_L[I_4^g][M_L] + k_L\frac{7}{5}[I_2^g][M_L] + k_L\frac{7}{3}[I_1^g][M_L] \quad \textbf{(2.2-42b)}$$

$$\left.\frac{d[I_2^g]}{dt}\right|_{hf} = -k_L\frac{21}{5}[I_2^g][M_L] + k_L[I_4^g][M_L] + k_L[I_3^g][M_L] + k_L\frac{5}{3}[I_1^g][M_L] \quad \textbf{(2.2-42c)}$$

$$\left.\frac{d[I_1^g]}{dt}\right|_{hf} = -k_L 7[I_1^g][M_L] + k_L[I_4^g][M_L] + k_L[I_3^g][M_L] + k_L[I_2^g][M_L] \quad \textbf{(2.2-42d)}$$

To determine the statistical populations of the levels in the steady state, we let:

$$\left.\frac{d[I_4^g]}{dt}\right|_{hf} = \left.\frac{d[I_3^g]}{dt}\right|_{hf} = \left.\frac{d[I_2^g]}{dt}\right|_{hf} = \left.\frac{d[I_1^g]}{dt}\right|_{hf} = 0 \quad \textbf{(2.2-43)}$$

Imposing these conditions on the Equations 2.2-43 and solving the four resulting equations simultaneously, we find a statistical distribution. In the steady state limit, the lower levels of the hyperfine structure relax toward a statistical equilibrium of 9/24, 7/24, 5/24, and 3/24 for F=4,3,2,1 respectively. Yukov's [35] theoretical analysis

predicts that for the lower levels the relaxation time to reach statistical equilibrium is on the order of subnanoseconds. Thieme and Fill [36] report measuring a relaxation time less than 2 nanoseconds. The fact is, that hyperfine relaxation for the lower hyperfine levels can be expected to be very fast.

From this discussion of hyperfine relaxation, we can see that resonant energy transfer and collisions play a large role in the number density rate equations. This role is to continuously try to pull population into a statistical equilibrium among the levels. If this mixing did not occur, laser action would be significantly different from what it is. If the hyperfine relaxation in an iodine photodissociation laser in both the upper and lower levels were sufficiently slow, population inversion would exist for all six radiative transitions, and lasing would occur on all six lines. Alekseev [37] predicts theoretically that since the lower levels relax on the order of subnanoseconds, and the upper levels mix more slowly, it would be probable to observe laser pulses on both the 3-4 transition and the 2-2 transition. More discussion on multi-line lasing will be made later.

The final nonradiative process to discuss is quenching. This process occurs on a relatively slow time scale compared to hyperfine relaxation, but should still be considered to make the model more complete. Quenching is the process by which excited iodine population is transferred to the ground state through collisions with other species in the mixture (Figure 2-5). Possible quenchers include: CF_3I, CF_3, I_2, and some buffer gas. Quenching rate constants for these are listed below [38]:

Quencher	Rate Constant
CF_3I	3.3×10^{-17} cc/s
CF_3	0.1×10^{-12} cc/s
I_2	3.6×10^{-11} cc/s
Ar	1.3×10^{-19} cc/s

Table 2-10 Quenching Rate Constants

The effect of quenching on the number density equation is simple to describe. Population is lost from the upper two hyperfine levels by:

$$\left.\frac{d[I_3^*]}{dt}\right|_{quench} = -[I_3^*]\sum_q (k_q[M_q]) \qquad \textbf{(2.2-44a)}$$

$$\left.\frac{d[I_2^*]}{dt}\right|_{quench} = -[I_2^*]\sum_q (k_q[M_q]) \qquad \textbf{(2.2-44b)}$$

where k_q is the quenching rate constant for the number density of the relative quencher $[M_q]$. For the lower levels, population lost from the upper levels is assumed to be distributed statistically:

$$\left.\frac{d[I_4^g]}{dt}\right|_{quench} = \frac{9}{24}\left([I_3^*] + [I_2^*]\right) \sum_q (k_q[M_q]) \qquad \textbf{(2.2-44c)}$$

$$\left.\frac{d[I_3^g]}{dt}\right|_{quench} = \frac{7}{24}\left([I_3^*] + [I_2^*]\right) \sum_q (k_q[M_q]) \qquad \textbf{(2.2-44d)}$$

$$\left.\frac{d[I_2^g]}{dt}\right|_{quench} = \frac{5}{24}\left([I_3^*] + [I_2^*]\right) \sum_q (k_q[M_q]) \qquad \textbf{(2.2-44e)}$$

$$\left.\frac{d[I_1^g]}{dt}\right|_{quench} = \frac{3}{24}\left([I_3^*] + [I_2^*]\right) \sum_q (k_q[M_q]) \qquad \textbf{(2.2-44f)}$$

To see what sort of a role quenching can play on number density, suppose that the most

important quencher is I_2 [39]. Also assume that we have a partial pressure of I_2 that is equal to the room temperature vapor pressure:

$$P_{I_2 300K} = 0.403 \text{ Torr}$$

We know that the population of I^* is defined by:

$$\left.\frac{d[I^*]}{dt}\right|_{quench} = -k_{q(I_2)}[I^*][I_2] \qquad (2.2\text{-}45)$$

The solution to equation (2.2-45), assuming $[I_2]$ is constant, is

$$\frac{[I^*]}{[I^*]_0} = e^{-k_{q(I_2)}[I_2]t} = e^{-(3.6\times10^{-11})(1.3\times10^{-16})t} \qquad (2.2\text{-}46)$$

at

$$\frac{[I^*]}{[I^*]_0} = \frac{1}{2} \Rightarrow t = 1.48\,\mu\text{sec}$$

Thus quenching occurs on the order of microseconds.

The final group of processes to discuss are those which add to and subtract from the population of atomic iodine. These processes include photodissociation, recombination, and dimerization. Photodissociation is the process by which excited atomic iodine is introduced into the laser gain medium. The process is described by:

$$CF_3I + h\nu \rightarrow CF_3 + I^* \qquad (2.2\text{-}47)$$

Recombination is where atomic iodine is removed from the medium by reforming an

alkyl iodide:

$$CF_3 + I \rightarrow CF_3I \qquad (2.2\text{-}48)$$

Dimerization is where atomic iodine is removed from the medium by the formation of molecular iodine:

$$I + I \rightarrow I_2 \qquad (2.2\text{-}49)$$

or where two radicals pair up:

$$CF_3 + CF_3 \rightarrow C_2F_6 \qquad (2.2\text{-}50)$$

We will look at photodissociation first.

The photodissociation of alkyl iodide (2.2-47) can be written more generally as:

$$RI + h\nu \rightarrow R + I^* \qquad (2.2\text{-}51)$$

where R is the free radical of the dissociation: CF_3, C_3F_7, C_4F_8, CH_3, etc. $h\nu$ is the photodissociation energy, which is generally in the ultraviolet for this sort of laser. A graph of photodissociation cross sections is seen in Figure 2-10 [40].

At 248 nm, the photodissociation cross section for CF_3I is:

$$\sigma = 3 \times 10^{-18}\ cm^2$$

The quantum yield of this reaction has been measured to be close to 100%. Measured quantum yields of CF_3I are listed in Table 2-11 [41]. The quantum yield is defined to be:

$$f(I^*) = \frac{[I^*]}{[I^*] + [I]} \qquad (2.2\text{-}52)$$

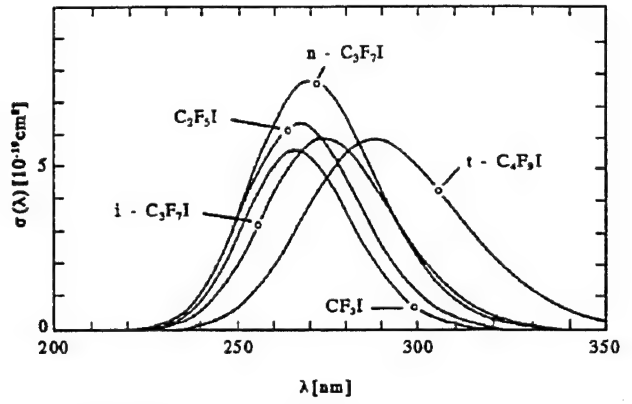

Figure 2-10 Photodissociation Cross Sections

QUANTUM YIELD	REFERENCE
0.91 ± 0.003	Donahue
0.91 ± 0.005	Ershov
0.98 ± 0.02	Ivanov
0.83 ± 0.05	Gerek
0.75 ± 0.05	Gerek

Table 2-11 Quantum Yields following uv-photolysis of CF_3I

Thus by assuming the quantum yield is high, we can assume that 100% of the atomic iodine produced in the photolysis is introduced into the excited $^2P_{1/2}$ state. We will also assume for now that as photodissociation occurs, the F=3 and F=2 levels of the excited state are filled statistically [42]. This will be seen experimentally later.

To see how photodissociation affects the number density equations, we will develop a pumping term. The first step is to describe the source of the photodissociation. We will assume our source is a gaussian pulse from a KrF excimer laser at 248 nm, and is pumping transverse to the gain medium (Figure 2-11a).

The absorption cross section of CF_3I at 248 nm is $\sigma = 3 \times 10^{-19}$ cm^2 [43]. The number density of CF_3I can be found using the ideal gas law [44]:

$$\frac{n}{V} = \frac{P}{RT} \rightarrow \frac{[CF_3I]}{V} = \frac{P}{(82.1)(300)(760)} N_{av} \qquad (2.2\text{-}53)$$

At 60 Torr this works out to be 1.93×10^{18} atoms/cc. Using Beers law and transversely pumping 2 cm of CF_3I we find:

$$\frac{\bar{I}_0}{\bar{I}_I} = e^{-\sigma[CF_3I]\ell} \sim \frac{E_0}{E_I} = e^{-1.158} = 0.314 \qquad (2.2\text{-}54)$$

The energy absorbed into the CF_3I is the difference between the energy incident on the cell, and the energy measured after the cell. If the excimer pump energy is 175 mJ the energy deposited in the 60 Torr of gas can be found by:

$$E_{ABSORBED} = E_{IN} - E_{OUT} = 175(1 - 0.314) = 120.05 \text{ mJ} \qquad (2.2\text{-}55)$$

To define useful gain, the energy absorbed within the extraction volume must be considered. Figure 2-11a defines the extraction volume. The extraction volume is a cylinder since the aperture within the I^* laser cavity is a circle. The energy within this cylinder can be approximated by taking the ratio of the volume of the cylinder to the volume of the box enclosing the cylinder multiplied by the energy within the box. The energy within the box is found by integration:

$$\begin{aligned} E_2 - E_1 &= \int_0^t \bar{I}_0(t) - \bar{I}_0(t)\, e^{-\sigma[CF_3I]z_2} dt \; - \; \int_0^t \bar{I}_0(t) - \bar{I}_0(t)\, e^{-\sigma[CF_3I]z_1} dt \\ &= E_{IN}\left((1 - e^{-\sigma[CF_3I]z_2}) - (1 - e^{-\sigma[CF_3I]z_1})\right) \end{aligned} \qquad (2.2\text{-}56)$$

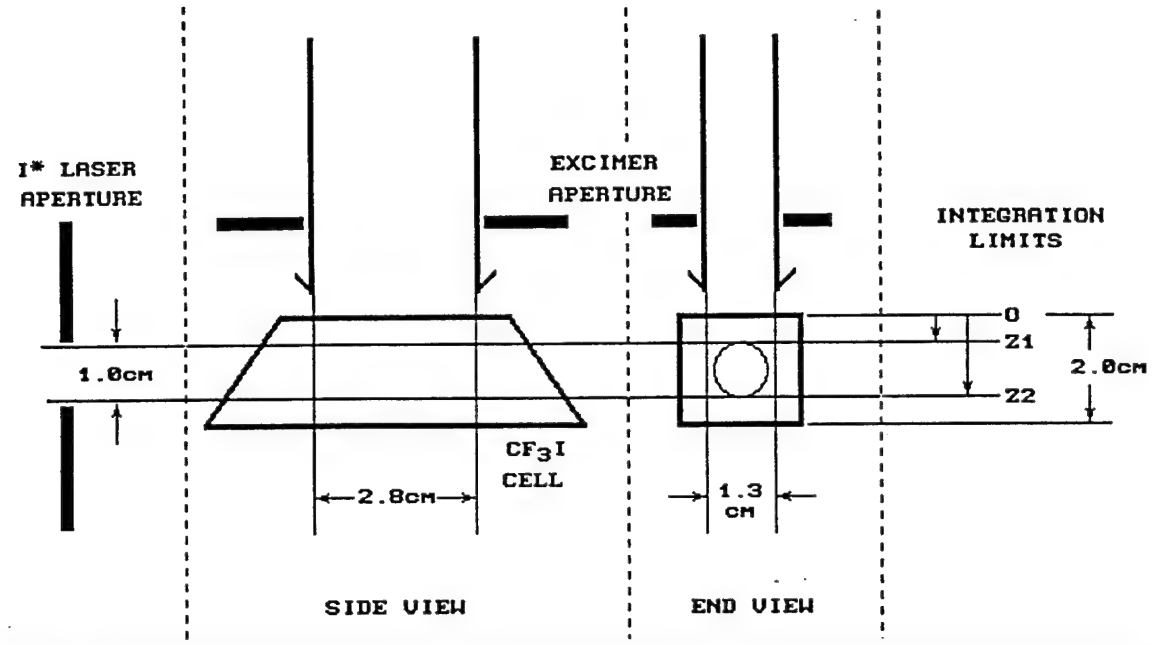

Figure 2-11a Orthographic View of Cell Geometry

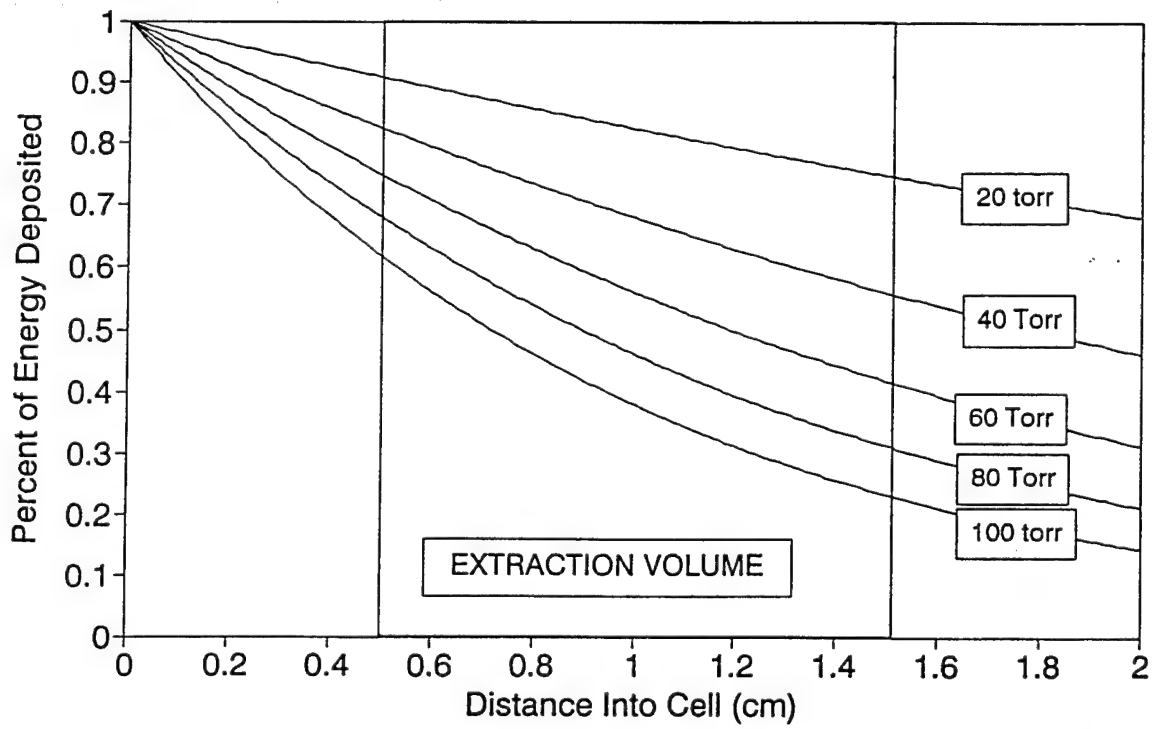

Figure 2-11b Linearity of CF_3I Photodissociation

For 60 Torr and an aperture with a diameter of 1 cm centered in the gain region, the energy absorbed within the extraction volume works out to be

$$\frac{V_{CYLINDER}}{V_{BOX}}(E_2 - E_1) = 34.79 \text{ mJ} \qquad (2.2\text{-}57)$$

where

$$E_2 - E_1 = 175\left(e^{-0.579(0.5)} - e^{-0.579(1.5)}\right) = 57.585 \text{ mJ} \qquad (2.2\text{-}58)$$

The approximation of the volume ratios at 60 Torr is valid since absorption within the cylinder is close to linear (Figure 2-11b). Integrating over the cylindrical volume yields 34.64 mJ. The error of the approximation increases as the pressure increases, and goes to zero as the pressure decreases.

The density of excited iodine atoms within the extraction volume is [45]:

$$\frac{[I^*]}{V} = \frac{34.79}{h\nu_{248}} \frac{1}{V_{CYLINDER}} = 1.97 \times 10^{16} \ \ I^* \text{ atoms/cc} \qquad (2.2\text{-}59)$$

Since we know the number density of excited iodine atoms produced, we can distribute this over time with our gaussian. If we center our gaussian around some time t_0, our pumping term becomes:

$$W_{I^*}(t) = [I^*] \frac{2\sqrt{\ln(2)}}{\sqrt{\pi}\,\Delta t} \exp\left(\frac{-4\ln(2)\,(t - t_0)^2}{\Delta t^2}\right) \qquad (2.2\text{-}60)$$

Δt is the width of our excimer pulse. Population is introduced statistically into our number density equations through this pumping term.

$$\left.\frac{d[I_3^*]}{dt}\right|_{pump} = \frac{7}{12} f(I^*) W_I \cdot(t) \qquad \textbf{(2.2-61a)}$$

$$\left.\frac{d[I_2^*]}{dt}\right|_{pump} = \frac{5}{12} f(I^*) W_I \cdot(t) \qquad \textbf{(2.2-61b)}$$

$$\left.\frac{d[I_4^g]}{dt}\right|_{pump} = \frac{9}{24} (1 - f(I^*)) W_I \cdot(t) \qquad \textbf{(2.2-61c)}$$

$$\left.\frac{d[I_3^g]}{dt}\right|_{pump} = \frac{7}{24} (1 - f(I^*)) W_I \cdot(t) \qquad \textbf{(2.2-61d)}$$

$$\left.\frac{d[I_2^g]}{dt}\right|_{pump} = \frac{5}{24} (1 - f(I^*)) W_I \cdot(t) \qquad \textbf{(2.2-61e)}$$

$$\left.\frac{d[I_1^g]}{dt}\right|_{pump} = \frac{3}{24} (1 - f(I^*)) W_I \cdot(t) \qquad \textbf{(2.2-61f)}$$

After photolysis of the CF_3I recombination and dimerization come into play. Recombination is written in general terms as:

$$\mathbf{R + I \rightarrow RI} \qquad \textbf{(2.2-62)}$$

Dimerization is written in general terms as:

$$I + I \rightarrow I_2 \qquad (2.2\text{-}63)$$

$$R + R \rightarrow 2R \qquad (2.2\text{-}64)$$

The effect of these processes can be easily taken into consideration by writing several rate equations to couple to the number density equations. For recombination:

$$\frac{d[CF_3I]}{dt} = k_R[CF_3][I] - W_I\cdot(t) \qquad (2.2\text{-}65)$$

$$\frac{d[CF_3]}{dt} = W_I\cdot(t) - k_R[CF_3][I] \qquad (2.2\text{-}66)$$

where $k_R = (1.6 \pm 0.3) \times 10^{-11}$ (cm^3/molecule · s) is the recombination rate constant [33]. For dimerization of I_2:

$$\frac{d[I_2]}{dt} = \sum_i k_i [M_i][I^g]^2 \qquad (2.2\text{-}67)$$

where k_i is the rate constant for the relevant species $[M_i]$. These are given in Table 2-12 [34].

MOLECULE M_i	k_i (cm^6/molecule^2·s)
CF_3I	1.3×10^{-31}
Ar	$(6.6 \pm 0.3) \times 10^{-33}$
I_2	$(3.9 \pm 0.6) \times 10^{-30}$

Table 2-12 Rate constants for dimerization process

For dimerization of C_2F_6:

$$\frac{d[C_2F_6]}{dt} = k_D[CF_3]^2 \qquad \textbf{(2.2-68)}$$

where $k_D = (5.5 \pm 1.2) \times 10^{-12}$ (cm^3/molecule · s) is the dimerization rate constant for the free radicals. Recombination and dimerization affect the population in the lower levels as follows:

$$\left.\frac{d[I_4^g]}{dt}\right|_{RD} = -k_R[I_4^g][CF_3] - [I_4^g]^2 \sum_i (k_i[M_i]) \qquad \textbf{(2.2-69a)}$$

$$\left.\frac{d[I_3^g]}{dt}\right|_{RD} = -k_R[I_3^g][CF_3] - [I_3^g]^2 \sum_i (k_i[M_i]) \qquad \textbf{(2.2-69b)}$$

$$\left.\frac{d[I_2^g]}{dt}\right|_{RD} = -k_R[I_2^g][CF_3] - [I_2^g]^2 \sum_i (k_i[M_i]) \qquad \textbf{(2.2-69c)}$$

$$\left.\frac{d[I_1^g]}{dt}\right|_{RD} = -k_R[I_1^g][CF_3] - [I_1^g]^2 \sum_i (k_i[M_i]) \qquad \textbf{(2.2-69d)}$$

Taking into account all of the processes discussed in this section we can write a complete set of rate equations to describe the change in population in the different hyperfine levels.

$$\frac{d[I_3^*]}{dt} = \frac{7}{12} f(I^*) W_{I^*}(t) + k_{23}^*[I_2^*][M_U] - k_{32}^*[I_3^*][M_U] - (A_{34} + A_{33} + A_{32})[I_3^*]$$

[pump term] [relaxation terms] [spontaneous transition terms]

$$- \sigma_{34}\left([I_3^*] - \frac{7}{9}[I_4^g]\right)\frac{\bar{I}_{34}(t)}{h\nu_{34}} - \sigma_{33}\left([I_3^*] - [I_3^g]\right)\frac{\bar{I}_{33}(t)}{h\nu_{33}} - \sigma_{32}\left([I_3^*] - \frac{7}{5}[I_2^g]\right)\frac{\bar{I}_{32}(t)}{h\nu_{32}} - [I_3^*]\sum_q (k_q[M_q])$$

[stimulated transition terms] [quenching term]

(2.2-70a)

$$\frac{d[I_2^*]}{dt} = \frac{5}{12} f(I^*) W_{I^*}(t) + k_{32}^*[I_3^*][M_U] - k_{23}^*[I_2^*][M_U] - (A_{23} + A_{22} + A_{21})[I_2^*]$$

[pump term] [relaxation terms] [spontaneous transition terms]

$$- \sigma_{23}\left([I_2^*] - \frac{5}{7}[I_3^g]\right)\frac{\bar{I}_{23}(t)}{h\nu_{23}} - \sigma_{22}\left([I_2^*] - [I_2^g]\right)\frac{\bar{I}_{22}(t)}{h\nu_{22}} - \sigma_{21}\left([I_2^*] - \frac{5}{3}[I_1^g]\right)\frac{\bar{I}_{21}(t)}{h\nu_{21}} - [I_2^*]\sum_q (k_q[M_q])$$

[stimulated transition terms] [quenching term]

(2.2-70b)

$$\frac{d[I_4^g]}{dt} = \frac{9}{24}(1 - f(I^*))W_{I^*}(t) + k_{34}[I_3^g][M_L] + k_{24}[I_2^g][M_L] + k_{14}[I_1^g][M_L] - (k_{43} + k_{42} + k_{41})[I_4^g][M_L]$$

[pump term] [relaxation terms]

$$+ \sigma_{34}\left([I_3^*] - \frac{7}{9}[I_4^g]\right)\frac{\bar{I}_{34}(t)}{h\nu_{34}} + A_{34}[I_3^*] + \frac{9}{24}\left([I_3^*] + [I_2^*]\right)\sum_q (k_q[M_q])$$

[stimulated transition terms] [spontaneous transition terms] [quenching term]

$$- k_R[I_4^g][CF_3] - [I_4^g]^2 \sum_i (k_i[M_i])$$

[recombination and dimerization]

(2.2-70c)

$$\frac{d[I_3^g]}{dt} = \frac{7}{24}(1 - f(I^*))W_{I^*}(t) + k_{43}[I_4^g][M] + k_{23}[I_2^g][M] + k_{13}[I_1^g][M] - (k_{34} + k_{32} + k_{31})[I_3^g][M]$$

pump term | relaxation terms

$$+ \sigma_{33}\left([I_3^*] - [I_3^g]\right)\frac{\bar{I}_{33}(t)}{h\nu_{33}} + \sigma_{23}\left([I_2^*] - \frac{5}{7}[I_3^g]\right)\frac{\bar{I}_{23}(t)}{h\nu_{23}} + A_{33}[I_3^*] + A_{23}[I_2^*]$$

stimulated transition terms | spontaneous transition terms

$$+ \frac{7}{24}\left([I_3^*] + [I_2^*]\right)\sum_q\left(k_q[M_q]\right) - k_R[I_3^g][CF_3] - [I_3^g]^2\sum_i\left(k_i[M_i]\right)$$

quenching term | recombination and dimerization

(2.2-70d)

$$\frac{d[I_2^g]}{dt} = \frac{5}{24}(1 - f(I^*))W_{I^*}(t) + k_{42}[I_4^g][M] + k_{32}[I_3^g][M] + k_{12}[I_1^g][M] - (k_{24} + k_{23} + k_{21})[I_2^g][M]$$

pump term | relaxation terms

$$+ \sigma_{32}\left([I_3^*] - \frac{7}{5}[I_3^g]\right)\frac{\bar{I}_{32}(t)}{h\nu_{32}} + \sigma_{22}\left([I_2^*] - [I_2^g]\right)\frac{\bar{I}_{22}(t)}{h\nu_{22}} + A_{32}[I_3^*] + A_{22}[I_2^*]$$

stimulated transition terms | spontaneous transition terms

$$+ \frac{5}{24}[I^*]\sum_q\left(k_q[M_q]\right) - k_R[I_2^g][CF_3] - [I_2^g]^2\sum_i\left(k_i[M_i]\right)$$

quenching term | recombination and dimerization

(2.2-70e)

$$\frac{d[I_1^g]}{dt} = \frac{3}{24}(1 - f(I^*))W_{I^*}(t) + k_{41}[I_4^g][M] + k_{31}[I_3^g][M] + k_{21}[I_2^g][M] - (k_{14} + k_{13} + k_{12})[I_1^g][M]$$

pump term; relaxation terms

$$+ \sigma_{21}\left([I_2^*] - \frac{5}{3}[I_1^g]\right)\frac{\bar{I}_{21}(t)}{h\nu_{21}} + A_{21}[I_2^*] + \frac{3}{24}[I^*]\sum_q (k_q[M_q])$$

stimulated transition term; spontaneous transition term; quenching term

$$- k_R[I_1^g][CF_3] - [I_1^g]^2 \sum_i (k_i[M_i])$$

recombination and dimerization

(2.2-70f)

2.3 Laser Intensity Equations

Now that we are finished covering the number density equations, we can discuss the intensity rate equations in greater detail, and apply these flux equations to the particular laser system under consideration. Recall that the number density equations are coupled to the intensity equations through the stimulated emission term. The intensity equations can be written in the general form which is valid for non-diffracting plane waves [48]

$$\frac{\partial I^+}{\partial t} + c\frac{\partial I^+}{\partial z} = c(\alpha - \mathcal{L})I^+ + Q \qquad \textbf{(2.3-1a)}$$

$$\frac{\partial I^-}{\partial t} - c\frac{\partial I^-}{\partial z} = c(\alpha - \mathcal{L})I^- + Q \qquad \textbf{(2.3-1b)}$$

α is the linear small signal gain (2.2-3), $\mathcal{L}$ is a distributed loss, Q is a noise term, and c is the speed of light. I^+ is the flux traveling to the right through the cavity and I^- is

the flux traveling left. Both I^+ and I^- are functions of position z and time t (Figure 2-12).

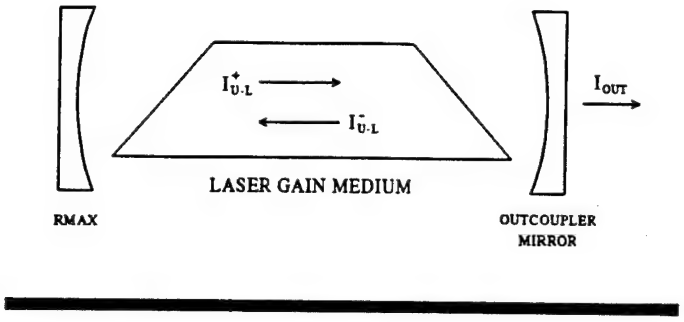

Figure 2-12 Intensity in a Laser

If we use the uniform field approximation, which ignores the spatial dependence of the intracavity field [49], we get:

$$\frac{\partial I^+}{\partial z} = -\frac{\partial I^-}{\partial z} \qquad \textbf{(2.3-2)}$$

Thus the general form for the intensity equations using the uniform field approximation is given by:

$$\frac{d\bar{I}(t)}{dt} = c(\alpha - \mathcal{L})\bar{I}(t) + Q \qquad \textbf{(2.3-3)}$$

To write the intensity equations more specifically for the laser system under consideration, we must define the cavity more exactly than Figure 2-12. The model for the laser cavity is shown in Figure 2-13. We can assume in this model that outside the gain region $\alpha=0$, $\mathcal{L}=0$, and $Q=0$. Inside the gain region $\alpha=\alpha(t)$, $Q=Q(t)$, and $\mathcal{L}$ is constant. If we integrate Equation 2.3-1 over the gain region in Figure 2-13, we get [50]:

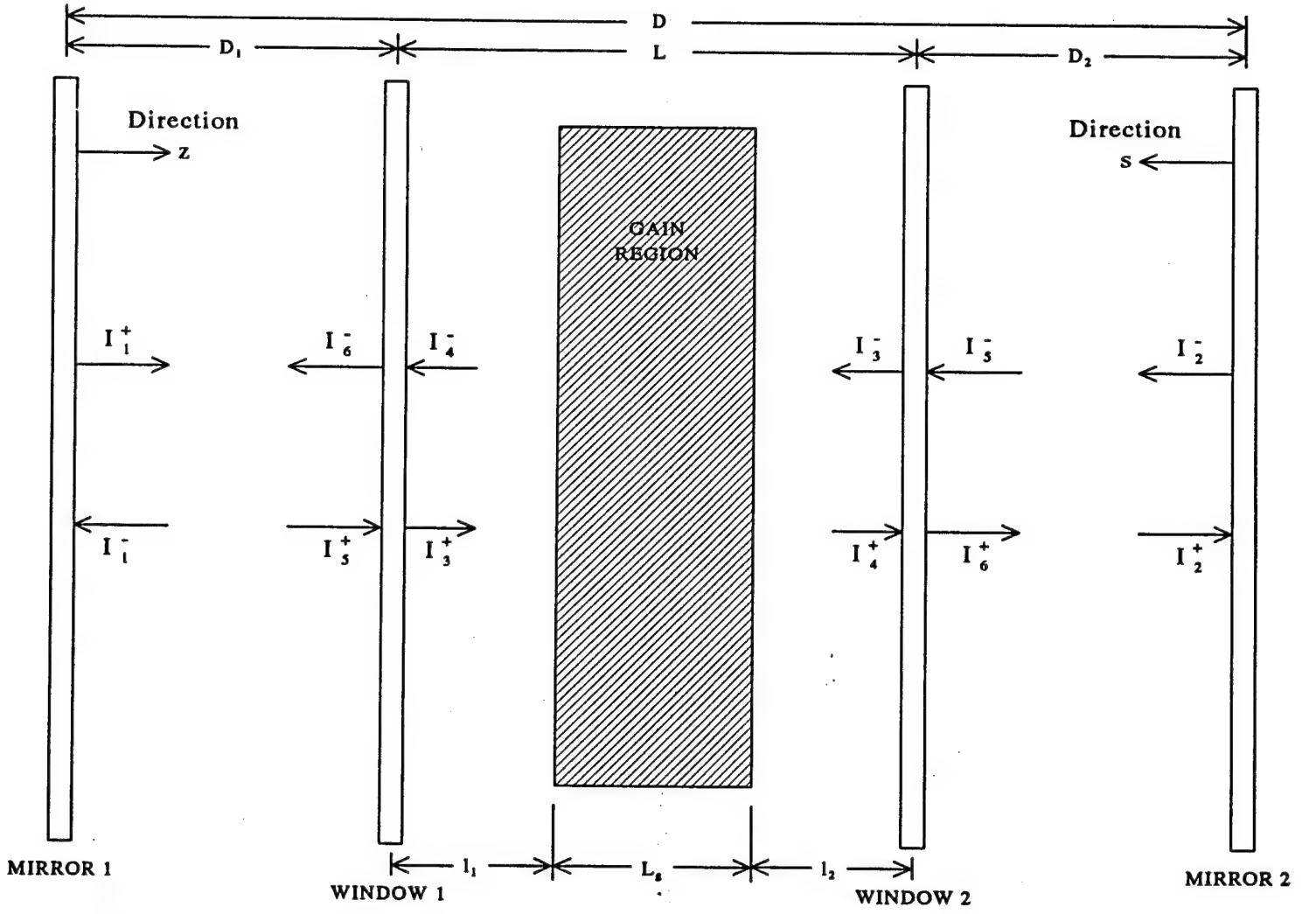

Figure 2-13 Intensity in Laser Cavity

$$\int_{D_1}^{D_1+L} \frac{\partial I^+}{\partial t}\,dz + c\left[I_4^+ - I_3^+\right] = c(\alpha - \mathfrak{L}) \int_{D_1+\ell_1}^{D_1+L-\ell_2} I^+ dz + QL_g \qquad (2.3\text{-}4)$$

$$\int_{D_2}^{D_2+L} \frac{\partial I^-}{\partial t}\,ds + c\left[I_4^- - I_3^-\right] = c(\alpha - \mathfrak{L}) \int_{D_2+\ell_2}^{D_2+L-\ell_1} I^- ds + QL_g \qquad (2.3\text{-}5)$$

Next we define an average two way circulating intensity within the region between window 1 and window 2 [51]:

$$\bar{I} \equiv \frac{1}{L} \int_{D_1}^{D_1+L} I^+ dz + \frac{1}{L} \int_{D_2}^{D_2+L} I^- ds \qquad (2.3\text{-}6)$$

Adding Equations 2.3-4 and 2.3-5 together and using the above equation (2.3-6) we find an equation for the two way circulating intensity between the two windows:

$$\frac{\partial \bar{I}}{\partial t} + \frac{c}{L}\left[I_4^+ - I_3^+ + I_4^- - I_3^-\right] = \frac{cL_g}{L}(\alpha - \mathfrak{L})\bar{I} + 2Q\frac{L_g}{L} \qquad (2.3\text{-}7)$$

where

$$\bar{I}L_g = \int_{D_1+\ell_1}^{D_1+\ell_1-\ell_2} I^+ dz + \int_{D_2+\ell_2}^{D_2+\ell_2-\ell_1} I^- ds \qquad (2.3\text{-}8)$$

Next we perform a similar integration over Equations 2.3-1 for the region between mirror 1 and window 1, and define an average two way circulating intensity for this region:

$$\bar{I}_1 \equiv \frac{1}{D_1}\int_0^{D_1} I^+ dz + \frac{1}{D_1}\int_{D_2+L}^{D} I^- ds \qquad (2.3\text{-}9)$$

Similarly, we find the equation for the two way circulating intensity in the region between mirror 1 and window 1 to be:

$$\frac{\partial \bar{I}_1}{\partial t} + \frac{c}{D_1}\left[I_5^+ - I_1^+ + I_1^- - I_6^-\right] = 0 \qquad \textbf{(2.3-10)}$$

This same procedure is followed for the region between window 2 and mirror 2. The average two way circulating flux is defined as:

$$\bar{I}_2 \equiv \frac{1}{D_2}\int_0^{D_2} I^- ds + \frac{1}{D_2}\int_{D_1+L}^{D} I^+ dz \qquad \textbf{(2.3-11)}$$

The two way circulating intensity between window 2 and mirror 2 is:

$$\frac{\partial \bar{I}_2}{\partial t} + \frac{c}{D_2}\left[I_2^+ - I_6^+ + I_5^- - I_2^-\right] = 0 \qquad \textbf{(2.3-12)}$$

The next logical step is to link the two way circulating flux equations for each of the regions by applying boundary conditions at the interfaces of each region. The boundary conditions for the windows are defined by the transmission losses across the windows:

$$\begin{aligned} I_6^+ &= t_2 I_4^+ \qquad & I_3^+ &= t_1 I_5^+ \\ I_3^- &= t_2 I_5^- \qquad & I_6^- &= t_1 I_4^- \end{aligned} \qquad \textbf{(2.3-13)}$$

where t_1 is the transmission of window 1 and t_2 is the transmission of window 2.

The boundary conditions of the mirrors are defined by the reflectance of the

mirrors:

$$I_1^+ = R_1 I_1^- \qquad I_2^- = R_2 I_2^+ \tag{2.3-14}$$

where R_1 is the reflectivity of mirror 1 and R_2 is the reflectivity of mirror 2.

At this point it is convenient to bring in the uniform field approximation again and apply it to each of the regions. For the region between window 1 and window 2 we assume $I^+ + I^-$ is constant to get:

$$I_3^+ + I_4^- = I_3^- + I_4^+ = \bar{I} \tag{2.3-15}$$

For the region between mirror 1 and window 1 we assume $I^+ + I^-$ is constant to get:

$$I_5^+ + I_6^- = I_1^- + I_1^- = \bar{I}_1 \tag{2.3-16}$$

For the region between mirror 2 and window 2 we assume $I^+ + I^-$ is constant to get:

$$I_2^+ + I_2^- = I_5^- + I_6^+ = \bar{I}_2 \tag{2.3-17}$$

Equations 2.3-15, 2.3-16, and 2.3-17 can be re-arranged to form the following relationships between flux within the three regions:

$$I_1^+ = \frac{R_1 \bar{I}_1}{1 + R_1} \qquad I_1^- = \frac{\bar{I}_1}{1 + R_1} \tag{100}$$

$$I_2^+ = \frac{\bar{I}_2}{1 + R_2} \qquad I_2^- = \frac{R_2 \bar{I}_2}{1 + R_2}$$

$$I_5^+ = \frac{\bar{I}_1 - t_1 \bar{I}}{1 - t_1^2} \qquad I_5^- = \frac{\bar{I}_2 - t_2 \bar{I}}{1 - t_2^2} \tag{2.3-18}$$

$$I_6^+ = I_2 - \frac{\bar{I}_2 - t_2\bar{I}}{1 - t_2^2} = t_2\frac{(\bar{I} - t_2\bar{I}_2)}{1 - t_2^2}$$

$$I_6^- = I_1 - \frac{\bar{I}_1 - t_1\bar{I}}{1 - t_1^2} = t_1\frac{(\bar{I} - t_1\bar{I}_1)}{1 - t_1^2}$$

Substituting the flux relationships (2.3-18) into the equations for two way circulating intensity in each of the regions (Equations 2.3-7 through 2.3-12) we arrive at a set of three coupled differential equations which describe the two way circulating intensity in each of the three regions [52]:

$$\frac{d\bar{I}_1}{dt} + \frac{c}{D_1}\left[\frac{2(\bar{I}_1 - t_1\bar{I})}{1 - t_1^2} - \frac{2R_1}{1 + R_1}\bar{I}_1\right] = 0 \qquad \textbf{(2.3-19a)}$$

$$\frac{d\bar{I}_2}{dt} + \frac{c}{D_2}\left[\frac{2(\bar{I}_2 - t_2\bar{I})}{1 - t_2^2} - \frac{2R_2}{1 + R_2}\bar{I}_2\right] = 0 \qquad \textbf{(2.3-19b)}$$

$$\frac{d\bar{I}}{dt} + \frac{c}{L}\left\{\frac{1}{t_1}\bar{I}_1 + \frac{1}{t_2}\bar{I}_2 - \left(\frac{1 + t_1^2}{t_1}\right)\left(\frac{\bar{I}_1 - t_1\bar{I}}{1 - t_1^2}\right)\right.$$

$$\left. - \left(\frac{1 + t_2^2}{t_2}\right)\left(\frac{\bar{I}_2 - t_2\bar{I}}{1 - t_2^2}\right)\right\} = \frac{cL_g}{L}(\alpha - \mathcal{L})\bar{I} + 2Q\frac{L_g}{L} \qquad \textbf{(2.3-19c)}$$

Further simplification can be made by assuming the transit time of the photons between the windows and mirrors is negligible. To do this we assume:

$$I_5^+ \equiv I_1^+ \qquad I_2^+ \equiv I_6^+$$
$$I_1^- \equiv I_6^- \qquad I_5^- \equiv I_2^- \tag{2.3-20}$$

Thus ignoring the photon transit time from window to mirror, we get the relationships:

$$I_3^+ = t_1 I_1^+ \qquad I_4^+ = \frac{I_2^+}{t_2}$$

$$I_3^- = t_2 I_2^- \qquad I_4^- = \frac{I_1^-}{t_1} \tag{2.3-21}$$

Using the relationships found in Equation 14 we get a new set of flux relationships

$$I_1 = \frac{t_1(1+R_1)\bar{I}}{1+R_1 t_1^2} \qquad I_2 = \frac{t_2(1+R_2)\bar{I}}{1+R_2 t_2^2} \tag{2.3-22}$$

Substituting these equations into 2.3-19 and replacing L with D to conserve the overall transit time we find the overall general form for the two way circulating equations to be:

$$\frac{d\bar{I}}{dt} = \frac{cL_g}{D}(\alpha - \mathcal{L})\bar{I} + 2Q\left(\frac{L_g}{D}\right) - \frac{c}{D}\bar{I}\left[\frac{1-R_2 t_2^2}{1+R_2 t_2^2} + \frac{1-R_1 t_1^2}{1+R_1 t_1^2}\right]$$

(2.3-25)

The form of this equation is very similar to Equation 2.3-3, but losses in windows and mirrors are taken into account separately, rather than being lumped into a distributed loss $\mathcal{L}$.

Equation 2.3-23 can be written in a more comprehensible form by defining a cavity loss rate [53]:

$$\gamma_{cav} \equiv \frac{c}{D}\left[\mathcal{L}L_g + \frac{1-R_1t_1^2}{1+R_1t_1^2} + \frac{1-R_2t_2^2}{1+R_2t_2^2}\right] \qquad \textbf{(2.3-24)}$$

This allows Equation 2.3-23 to be written as:

$$\frac{d\bar{I}(t)}{dt} = \underbrace{\frac{cL_g}{D}\alpha_{U\text{-}L}\bar{I}(t)}_{\text{gain term}} - \underbrace{\gamma_{cav}\bar{I}(t)}_{\text{loss term}} + \underbrace{2Q\frac{L_g}{D}}_{\text{noise term}} \qquad \textbf{(2.3-25)}$$

The cavity loss rate can be simplified further by the approximation:

$$\frac{2(1-R_1t_1^2R_2t_2^2)}{(1+R_1t_1^2)(1+R_2t_2^2)} \approx +\frac{1}{2}\ln\left(\frac{1}{R_1R_2t_1^2t_2^2}\right) \qquad \textbf{(2.3-26)}$$

By letting $t_1=t_2=1$ we arrive at a definition for threshold gain similar to that given by Verdeyen [54]:

$$\alpha_{th} \equiv \frac{1}{2D}\ln\frac{1}{R_1R_2} \qquad \textbf{(2.3-27)}$$

Our cavity loss rate term works out to be:

$$\gamma_{cav} = c(\mathcal{L}' + \alpha_{th}) \qquad \textbf{2.3-28}$$

where α_{th} is the loss due to outcoupling energy from the cavity, and $\mathcal{L}'=\mathcal{L}L_g/D$ is the remaining loss, both of which are distributed over the length of the cavity.

The remaining portion of the intensity rate equations which must be addressed is the noise term Q. A small amount of intensity is introduced into the system of rate equations through the spontaneous emission process (Figure 2-5). Verdeyen writes the noise term [55] as the rate of increase of photons in the $TEM_{0,0,1}$ cavity mode due to spontaneous emission:

$$\left.\frac{d\phi_p}{dt}\right|_{spont} = \left(A_{U-L}[N_U]V_M\right)\left[f_v(\nu)\frac{c}{2D}\right]\frac{1}{\left(\frac{8\pi\nu^2}{c^3}\right)\left(\frac{c}{2D}\right)V_m} \qquad (2.3\text{-}29)$$

where A_{U-L} is the A-coefficient, $[N_U]$ is the population density of the state from which the transition is originating, V_m is the mode volume, $f_v(\nu)$ is the Voigt lineshape function, and c/2D is the longitudinal mode spacing within the cavity. By canceling terms and recalling our definition for gain cross section σ_{U-L}, this equation can be reduced to a more compact form:

$$\left.\frac{d\phi_p}{dt}\right|_{spont} = [N_U]\,c\left[A_{U-L}\frac{\lambda^2}{8\pi}f_v(\nu)\right] = [N_U]\,c\,\sigma_{U-L} \qquad (2.3\text{-}30)$$

To convert total flux to photon density [56]:

$$\bar{I} = \frac{c\,\phi\,h\nu}{AD} \quad \Rightarrow \quad \frac{d\bar{I}}{dt} = \frac{c\,h\nu}{AD}\frac{d\phi}{dt} \qquad (2.3\text{-}31)$$

where $h\nu$ is the energy of the photon and AD is the mode volume. Thus for the spontaneous emission noise term we get:

$$\left.\frac{d\bar{I}}{dt}\right|_{spont} = \frac{c^2\,h\nu\,\sigma_{U-L}}{AD}[N_U] \qquad (2.3\text{-}32)$$

factoring in the ratio of gain length to cavity length squared we find:

$$\left.\frac{d\bar{I}}{dt}\right|_{spont} = 2Q\frac{L_g}{D} = \left(\frac{L_g}{D}\right)^2\left(\frac{c^2 h\nu\,\sigma_{U\text{-}L}}{AD}\right)[N_U] \qquad \textbf{(2.3-33)}$$

To complete the discussion of the intensity equations, we must realize that the general expression in Equation 2.3-25 must be applied to each of the radiative transitions. The following list summarizes the intensity equations for all six of the possible radiative transitions in the atomic iodine laser under consideration:

$$\frac{d\bar{I}_{34}(t)}{dt} = \sigma_{34}\left([I_3^*] - \frac{7}{9}[I_4^g]\right)\frac{L_g c}{d}\bar{I}_{34}(t) - \gamma_{cav}\bar{I}_{34}(t) + 2Q\frac{L_g}{d}$$

(2.3-34a)

$$\frac{d\bar{I}_{33}(t)}{dt} = \sigma_{33}\left([I_3^*] - [I_3^g]\right)\frac{L_g c}{d}\bar{I}_{33}(t) - \gamma_{cav}\bar{I}_{33}(t) + 2Q\frac{L_g}{d}$$

(2.3-34b)

$$\frac{d\bar{I}_{32}(t)}{dt} = \sigma_{32}\left([I_3^*] - \frac{7}{5}[I_2^g]\right)\frac{L_g c}{d}\bar{I}_{32}(t) - \gamma_{cav}\bar{I}_{32}(t) + 2Q\frac{L_g}{d}$$

(2.3-34c)

$$\frac{d\bar{I}_{23}(t)}{dt} = \sigma_{23}\left([I_3^*] - \frac{5}{7}[I_3^g]\right)\frac{L_g c}{d}\bar{I}_{23}(t) - \gamma_{cav}\bar{I}_{23}(t) + 2Q\frac{L_g}{d}$$

(2.3-34d)

$$\frac{d\bar{I}_{22}(t)}{dt} = \sigma_{22}\left([I_2^*] - [I_2^g]\right)\frac{L_g c}{d}\bar{I}_{22}(t) - \gamma_{cav}\bar{I}_{22}(t) + 2Q\frac{L_g}{d}$$

(2.3-34e)

$$\frac{d\bar{I}_{21}(t)}{dt} = \sigma_{21}\left([I_3^*] - \frac{5}{3}[I_3^g]\right)\frac{L_g c}{d}\bar{I}_{21}(t) - \gamma_{cav}\bar{I}_{21}(t) + 2Q\frac{L_g}{d}$$

(2.3-34f)

2.4 Numerical Results

The theory required to model a short pulsed excimer pumped atomic Iodine laser was outlined in the previous sections in fairly rigorous detail. Several approximations were made which simplified the modeling. The purpose of this section is to determine which approximations can be made and then demonstrate the workings of the model using a computer to solve the system of equations.

The most rigorous approach is the paraxial wave equation approach (Equations 2.3-1) which involves solving the intensity equations with respect to both time and space within the cavity. There are several situations in which it may be necessary to include the spatial dependence as well as the time dependence of the intensity within the cavity. One such system is the modeling of extremely short pulsed systems which involve pulse propagation within the laser cavity. Another situation is systems which have both a spatially dependent gain and a fairly short pulse length relative to cavity length. An example of a system with a spatially dependent gain is one with a longitudinal pumping configuration and a long gain length. A third system which may require modification of the paraxial wave equation approach is a very low pressure amplifier system in which it takes the velocities of the excited species a significant amount of time to reach a Boltzmann distribution [57].

The system which I am studying involves a transverse pumping configuration, which removes the z-dependence of the gain. Previous studies by E.E. Fill show pulse durations between 2-12 ns FWHM [58]. My own experimental measurements show pulse durations between 20-100 ns FWHM for a 16 cm cavity. It is seen that the uniform field approximation is definitely valid for a 20 ns pulse in a 16 cm cavity since the speed of light is 30 cm/ns and a 20 ns pulse would be easily distributed evenly over a 16 cm cavity at any given point in time. Concern about velocity distribution is not necessary around 50 Torr of CF_3I. The mixture reaches a Boltzmann distribution almost immediately upon photodissociation due to the high pressure of CF_3I [59]. The uniform field approximation leads to the equations 2.3-34. The intensity equations with the

number density equations yield a full set of sixteen coupled differential equations (2.2-65 to 2.2-68, 2.2-70, and 2.3-34).

Various other approximations can be made to the sixteen equation model with little or no effect. One such approximation is to assume that quenching plays little or no role in laser action, thus eliminating the quenching terms from Equations 2.2-70 and eliminating altogether 2.2-65 through 2.2-68. This reduces the total number of equations to 12: six number density and six intensity. The validity of this approximation is seen in Equation 2.2-46 where quenching of I^* by I_2 is seen to occur on a microseconds time scale. The spontaneous emission terms in the number density equations can also be neglected since the contribution to the overall population in each level is small. This is due to the A-coefficients being on the order of a few transitions per second. The noise term in the intensity equation is sufficient to create the impetus to drive the set of equations. Both quenching and spontaneous emission terms are retained, however; to maintain completeness and a detailed balance.

Another set of approximations deals with hyperfine relaxation. Previous work has

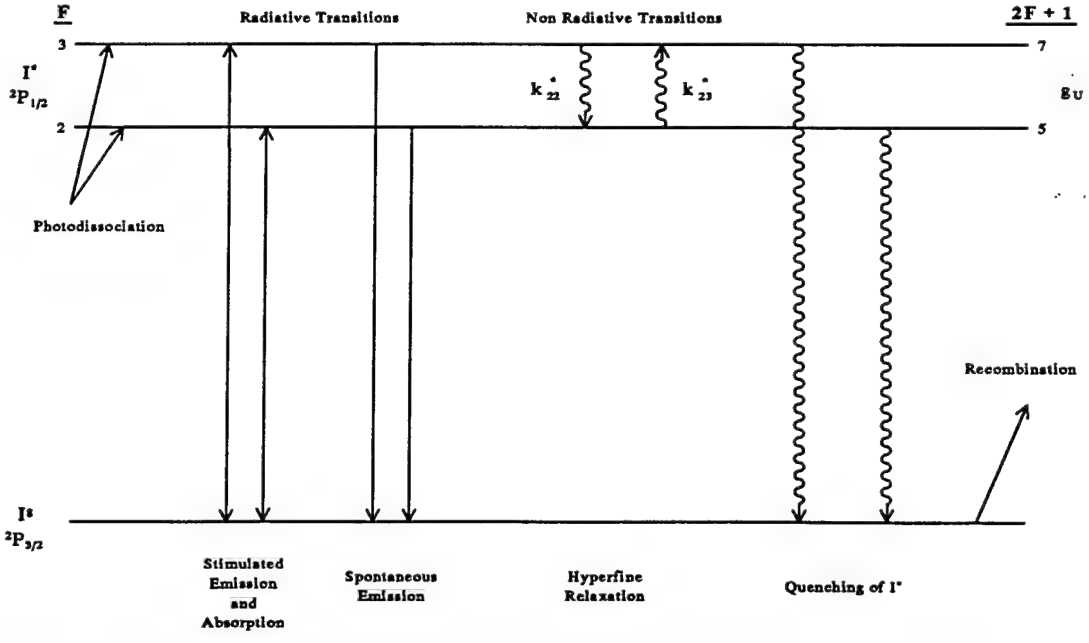

Figure 2-14 Processes Assuming Lower Level Relaxation Fast

shown that relaxation between the lower hyperfine levels occurs on a sub-nanosecondtime scale while relaxation between the upper levels occurs on a much slower time scale (tens of nanoseconds) [60]. An approximation which Alekseev makes [61] is that the population distribution in the lower levels during lasing is statistical, while the upper two levels mix at the same finite rate. This approximation leads to three number density equations and two intensity equations describing population in the upper two hyperfine levels, the lower ground level, and the two-way circulating intensity from the upper F=3 sublevel to ground, and the upper F=2 sublevel to ground. The statistical distribution in the ground state fixes the population and allows only two possible radiative transitions instead of six. The processes for this nine equation model are seen graphically in Figure 2-14. The number density equations for this approximation can be written:

$$\frac{d[I_3^*]}{dt} = \frac{7}{12} f(I^*) W_{I^*}(t) + k_{23}^*[I_2^*][M_U] - k_{32}^*[I_3^*][M_U] - (A_{34} + A_{33} + A_{32})[I_3^*]$$

$$- \sigma_{34}\left([I_3^*] - \frac{7}{24}[I^g]\right)\frac{\bar{I}_{34}(t)}{h\nu_{34}} - [I_3^*]\sum_q (k_q[M_q]) \qquad \textbf{(2.4-1a)}$$

$$\frac{d[I_2^*]}{dt} = \frac{5}{12} f(I^*) W_{I^*}(t) + k_{32}^*[I_3^*][M_U] - k_{23}^*[I_2^*][M_U] - (A_{23} + A_{22} + A_{21})[I_2^*]$$

$$- \sigma_{22}\left([I_2^*] - \frac{5}{24}[I^g]\right)\frac{\bar{I}_{22}(t)}{h\nu_{22}} - [I_2^*]\sum_q (k_q[M_q]) \qquad \textbf{(2.4-1b)}$$

$$\frac{d[I^g]}{dt} = (1 - f(I^*)) W_{I^*}(t) + \sigma_{34}\left([I_3^*] - \frac{7}{24}[I^g]\right)\frac{\bar{I}_{34}(t)}{h\nu_{34}} + \sigma_{22}\left([I_2^*] - \frac{5}{24}[I^g]\right)\frac{\bar{I}_{22}(t)}{h\nu_{22}}$$

$$+ (A_{34} + A_{33} + A_{32})[I_3^*] + (A_{23} + A_{22} + A_{21})[I_2^*] + \left([I_3^*] + [I_2^*]\right)\sum_q (k_q[M_q])$$

$$- k_R[I^g][CF_3] - [I^g]^2 \sum_i (k_i[M_i]) \qquad \textbf{(2.4-1c)}$$

Intensity equations only need to be written for two transitions due to the nature of the approximation:

$$\frac{d\bar{I}_{34}(t)}{dt} = \sigma_{34}\left([I_3^*] - \frac{7}{24}[I^g]\right)\frac{L_g c}{d}\bar{I}_{34}(t) - \gamma_{cav}\bar{I}_{34}(t) + 2Q\frac{L_g}{d}$$

(2.4-1d)

$$\frac{d\bar{I}_{22}(t)}{dt} = \sigma_{22}\left([I_2^*] - \frac{5}{24}[I^g]\right)\frac{L_g c}{d}\bar{I}_{22}(t) - \gamma_{cav}\bar{I}_{22}(t) + 2Q\frac{L_g}{d}$$

(2.4-1e)

Equations 2.2-65 through 2.2-68 are coupled in for recombination. This approximation can be taken a step further by assuming the hyperfine relaxation between the upper two levels is fast enough to keep the populations statistical. In this case the 3-4 transition will be the only transition to lase. The seven equation model can be described graphically:

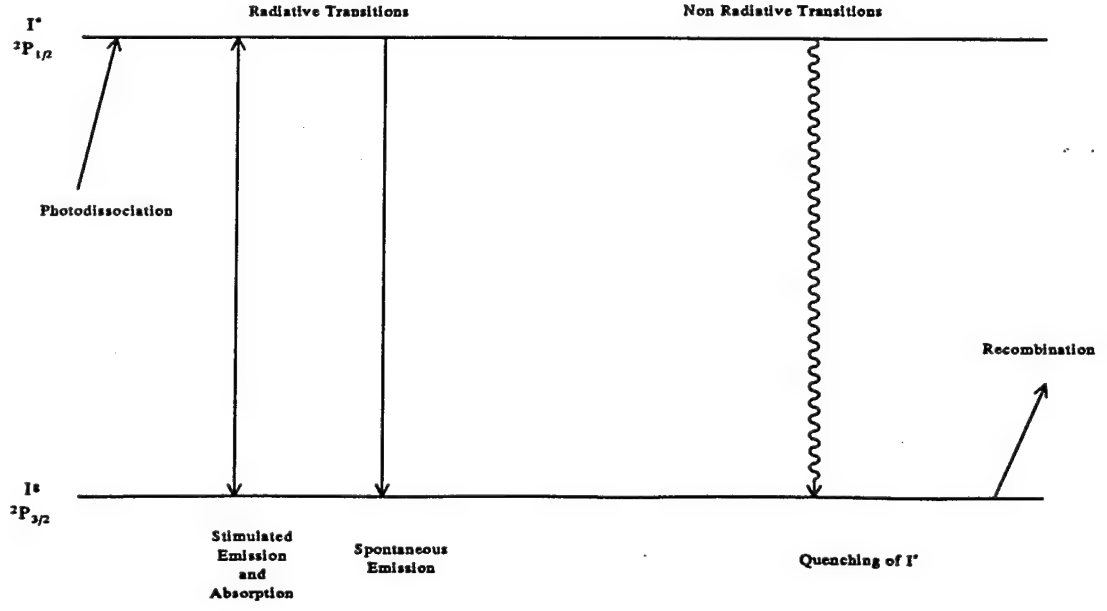

Figure 2-15 Processes Assuming Relaxation Fast in Both Levels

The rate equations for these simplified processes work out to be:

$$\frac{d[I^*]}{dt} = f(I^*)W_{I^*}(t) - (A_{34} + A_{33} + A_{32} + A_{23} + A_{22} + A_{21})[I^*]$$

$$- \sigma_{34}\left([I^*] - \frac{1}{2}[I^g]\right)\frac{7}{12}\frac{\bar{I}_{34}(t)}{h\nu_{34}} - [I^*]\sum_q (k_q[M_q]) \qquad \textbf{(2.4-2a)}$$

$$\frac{d[I^g]}{dt} = (1 - f(I^*))W_{I^*}(t) + \sigma_{34}\left([I^*] - \frac{1}{2}[I^g]\right)\frac{7}{12}\frac{\bar{I}_{34}(t)}{h\nu_{34}}$$

$$+ (A_{34} + A_{33} + A_{32} + A_{23} + A_{22} + A_{21})[I^*] + [I^*]\sum_q (k_q[M_q])$$

$$- k_R[I^g][CF_3] - [I^g]^2\sum_i (k_i[M_i]) \qquad \textbf{(2.4-2b)}$$

$$\frac{d\bar{I}_{34}(t)}{dt} = \sigma_{34}\left([I^*] - \frac{1}{2}[I^g]\right)\frac{7}{12}\frac{L_g c}{d}\bar{I}_{34}(t) - \gamma_{cav}\bar{I}_{34}(t) + 2Q\frac{L_g}{d}$$

(2.4-2c)

In addition, equations 2.2-65 through 2.2-68 are coupled in for recombination. The combinations of approximations are limitless, but several different combinations of the approximations above were tried and compared. I chose to use the sixteen equation model for completeness of the population equations. The seven equation model lacked the effect of hyperfine relaxation on the pulse shape. This effect is an exponential tail on the trailing side of the I^* laser pulse caused by a finite relaxation time. The nine equation model did a better job showing this tail, but the sixteen equation model was chosen to include the effects of mixing in the lower levels.

The set of sixteen coupled differential equations (2.2-65 — 2.2-68, 2.2-70, and 2.3-34) are solved over time using the double precision FORTRAN version of the Livermore Solver for Ordinary Differential Equations (DLSODE). This solver uses an Adams-Bashford technique for solving differential equations which allows for the stiffness of the problem [62]. A listing of the FORTRAN program which drives the equation solver is in Appendix B.

Outputs from the code include a graph of laser pulse intensities, number densities within each of the hyperfine levels, small signal gains for each of the radiative transitions, and a listing of input parameters, output parameters, and solver statistics. Examples of these outputs are shown in Figures 2-16 through 2-18 and Table 2-13. Time is incremented from 0 to 1500 ns. At about 100 ns an excimer laser pulse modeled

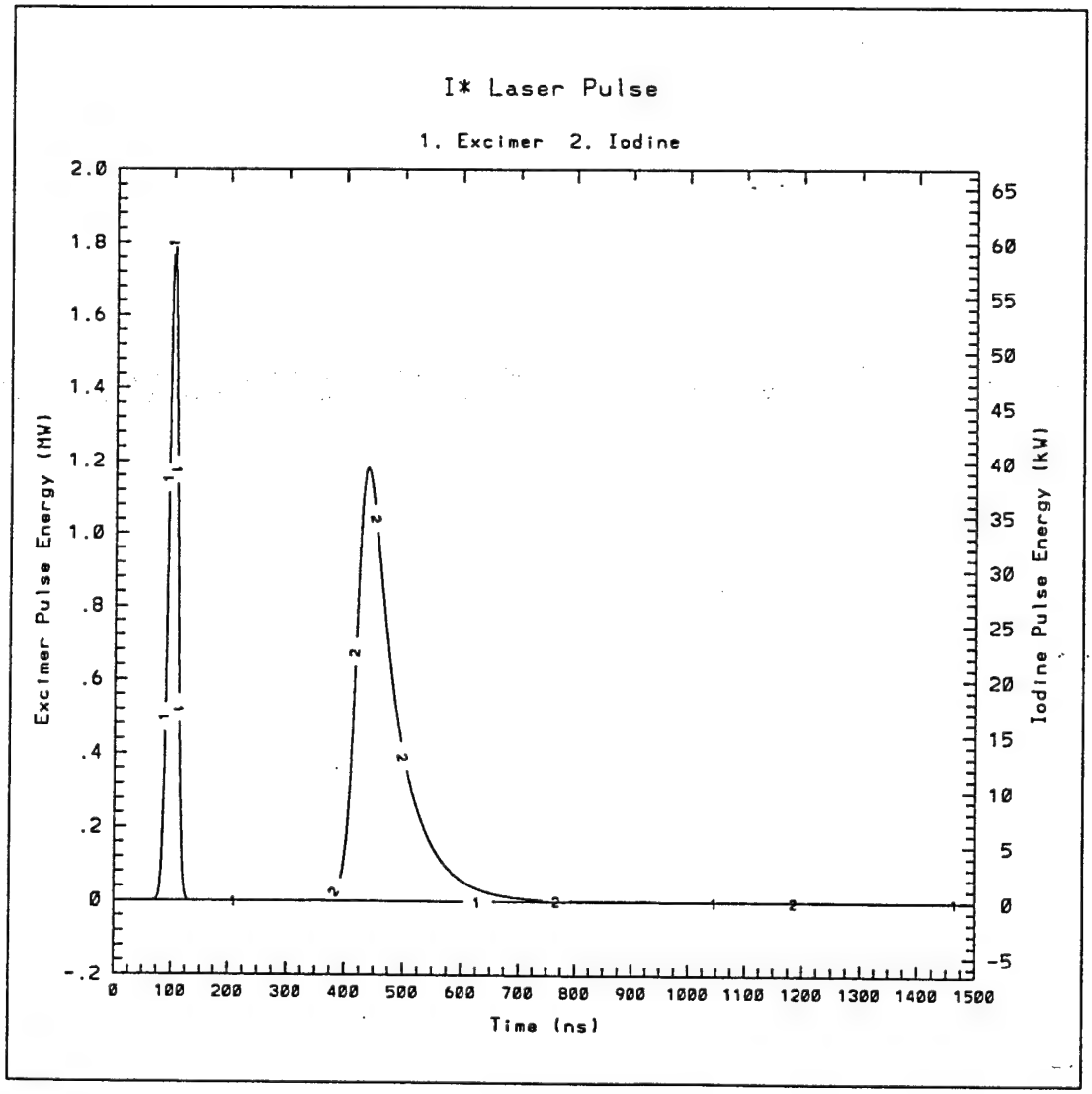

Figure 2-16 I* Laser Intensities

with a gaussian pulse peaks out (Figure 2-16). At the peak of the excimer pulse, half of the energy within the pulse has been dumped into the CF_3I gain medium, and in Figure 2-17 it is seen that the population has increased half way to its maximum. After the excimer pulse has fully passed, population in the upper two levels is at a maximum (Figure 2-17). The population is distributed statistically between these two levels: 7/12 in the upper

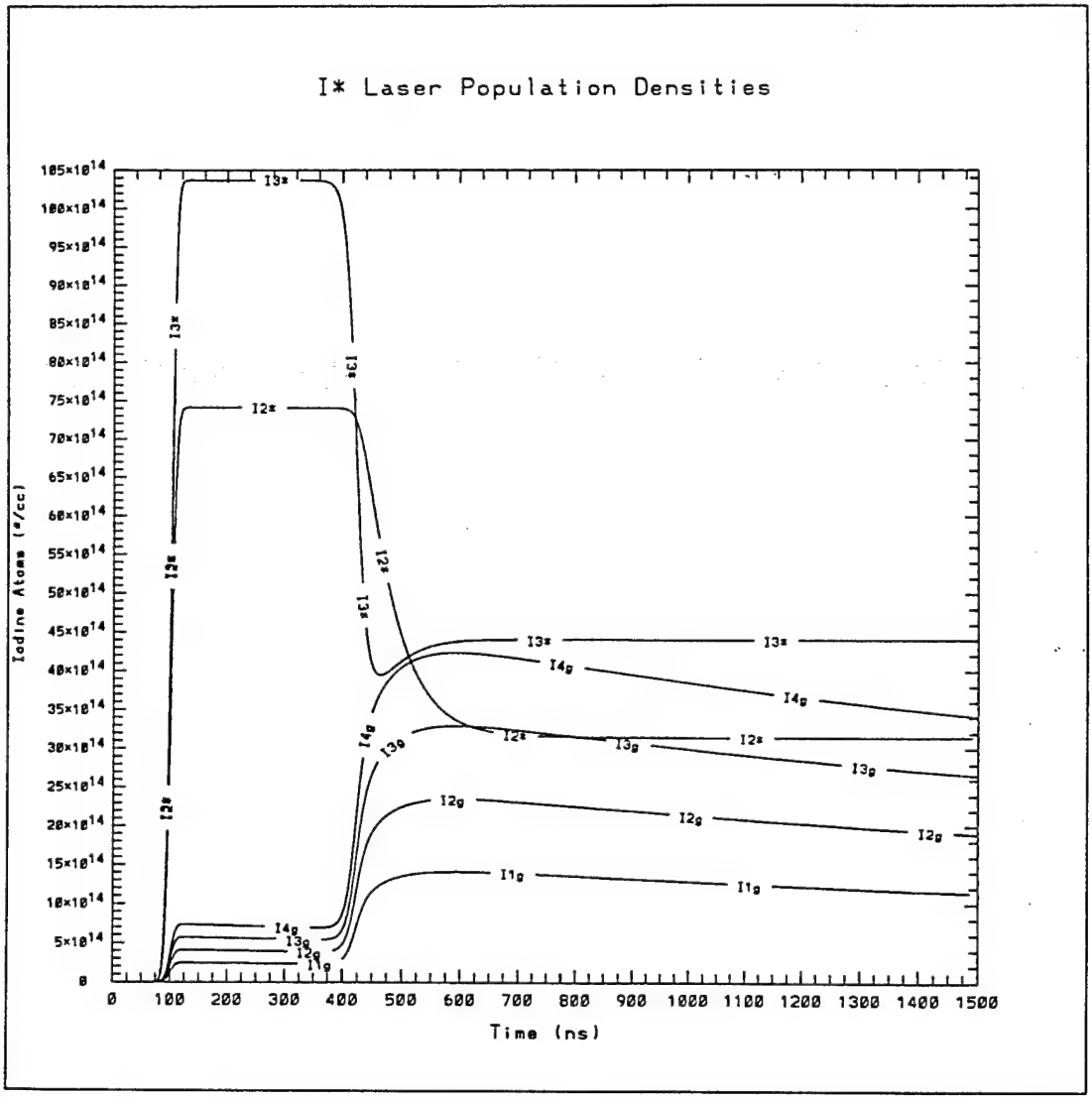

Figure 2-17 I* Laser Population Densities

F=3 level, and 5/12 in the upper F=2 level. After a period of time commonly referred to as the cavity build-up time, or mode build-up time, the stimulated emission terms in the differential equations take over and a laser pulse emerges from the spontaneous emission noise on the 3-4 transition (Figure 2-16). This action dumps population from

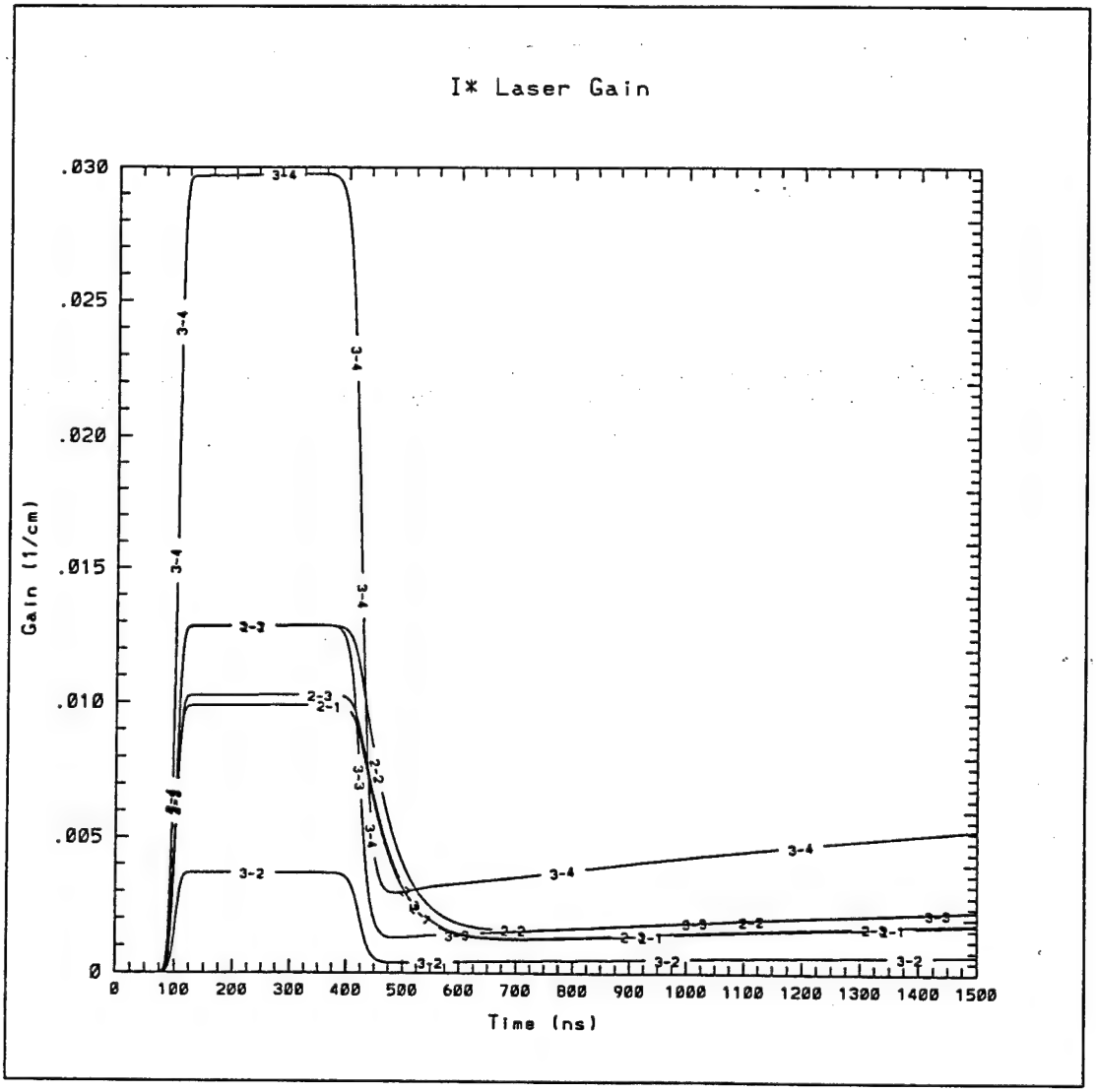

Figure 2-18 I* Laser Gain

Pulsed I^* 16 Equation Model I/O Parameters

gain length =	2.800 cm.
cavity length =	16.000 cm.
uv pump energy =	0.175 Joules
i* yield =	90.000 %
pump pulse width =	0.180E-07 secs fwhm
output mirror reflectivity =	0.964 %
internal loss =	0.000 %
iodide pressure =	60.000 torr
argon pressure =	0.000 torr
upper level relaxation rate constant =	1.50E-09 cc/s
lower level relaxation rate constant =	0.40E-09 cc/s
window transmission =	1.000
scattering losses =	0.000
excimer energy deposited in gain region =	3.48E-02 Joules
extracted energy =	3.21E-03 Joules
cavity build-up time =	3.38E+02 nsec
maximum small signal gain =	2.94E-03 /cm

no. steps = 10094 no. f-s = 12873 no. j-s = 1860

Table 2-13 Input and Output Parameters of Computer Model

the upper F=3 level to the lower F=4 level (Figure 2-17). Following this laser action hyperfine relaxation terms came into play to pull population back into statistical equilibrium. Relaxation time constants used are those calculated by Alekseev [63] Once again $[I_3^*]$ and $[I_2^*]$ are at 7/12 and 5/12 respectively. $[I_4^g]$, $[I_3^g]$, $[I_2^g]$ and $[I_1^g]$ are at 9/24, 7/24, 5/24, and 3/24. Recombination and dimerzation remove population from the lower levels. Figure 2-18 shows how the small signal gain evolves with time. Table 2-13 lists

input parameters, output parameters, and solver statistics.

Input parameters seen in Table 2-13 which are of particular interest include output coupler reflectivity, CF_3I pressure, and cavity length. Figures 2-19 through 2-20 show the output from the code as each of the parameters is varied. All cases assume no losses.

Figure 2-19 is a comparison between output laser pulses as the outcoupling mirror changes. Pressure is kept constant at 60 Torr and cavity length is 16 cm. Figure 2-19a shows the theoretically predicted laser pulses for values of outcoupling mirrors between 86% and 98% as listed. Since we have assumed no cavity losses aside from outcoupling, the mirror with the least amount of outcoupling loss should have the highest energy. The energy for each pulse is plotted in Figure 2-19b. As predicted, the 98% outcoupler is seen to have the highest energy. This is not necessarily true in a system with losses. It is important to understand, however; that before we start introducing losses into the system the energy will approach a theoretical maximum as the outcoupling losses go to zero. This theoretical maximum is found by taking the amount of UV energy deposited in the CF_3I, converting it into equivalent energy in terms of 1.315 μm photons, and multiply by the quantum efficiency (2/3 from Figure 2-4 or 2.1-11). This works out to be:

$$(34.8\ \text{mJ})\left(\frac{248\ \text{nm}}{1315\ \text{nm}}\right)\left(\frac{2}{3}\right) \Rightarrow 4.375\ \text{mJ}$$

Figure 2-19b demonstrates that this is predicted by the rate equation model.

Figure 2-20 demonstrates varying CF_3I pressure keeping the cavity length at 16 cm and the outcoupler reflectivity at 96.4%. Pressures range between 10 and 100 Torr as listed. At low pressures, the energy is low due to the lack of CF_3I to produce I^*. At high pressures, a good percentage of UV light is absorbed before it reaches the extraction volume, thus the energy should fall off after some optimal pressure. Figure 2-20b shows this effect.

Figure 2-21 demonstrates how laser pulse characteristics change with increasing cavity length. The pressure is 60 Torr and the outcoupler is 96.4%. Varying the cavity length in steps of 16 cm from 16 cm out to 112 cm has the simple result of increasing

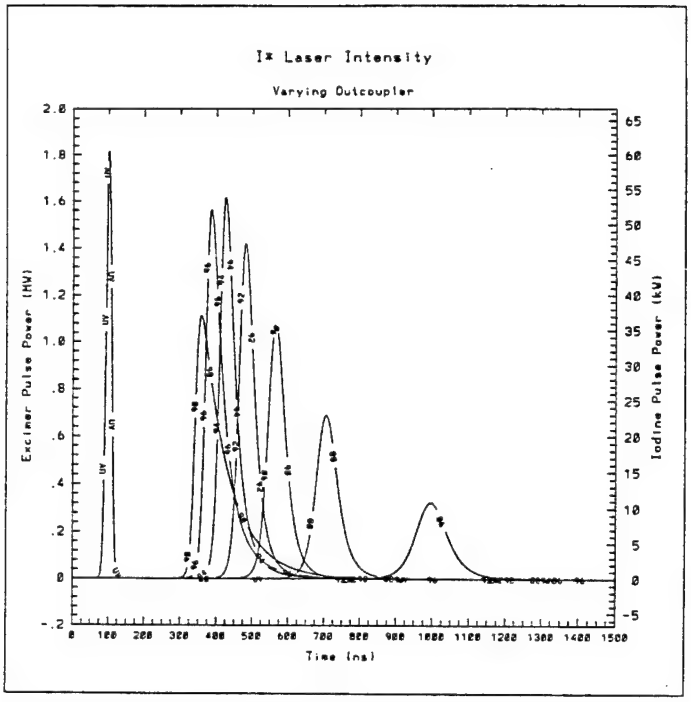

Figure 2-19a I* Laser Intensities for Various Outcoupling Mirrors

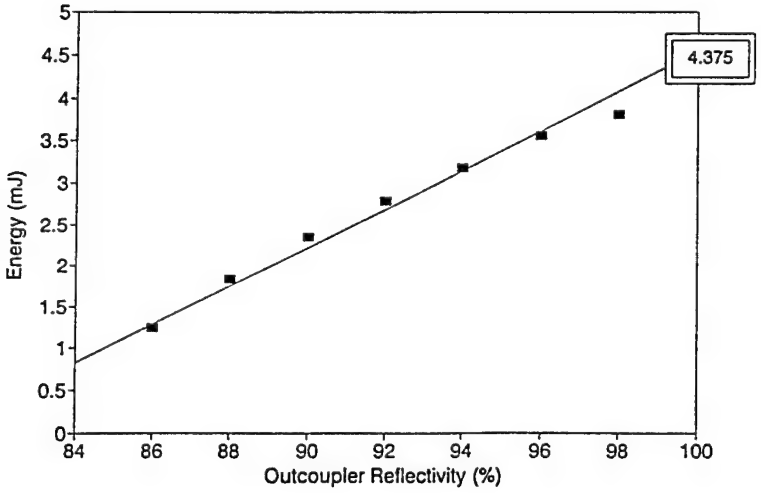

Figure 2-19b I* Laser Energy versus Outcoupler Reflectivity

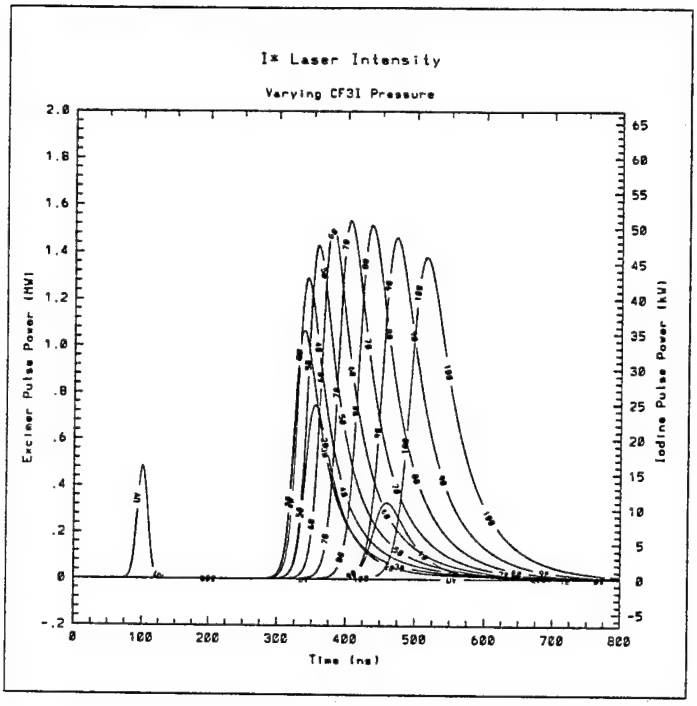

Figure 2-20a I^* Laser Intensities for Various CF_3I Pressures

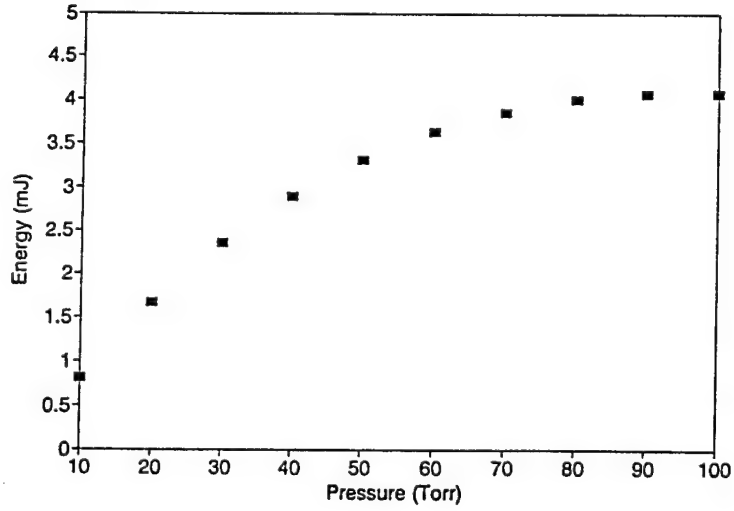

Figure 2-20b I^* Laser Energy versus CF_3I Pressure

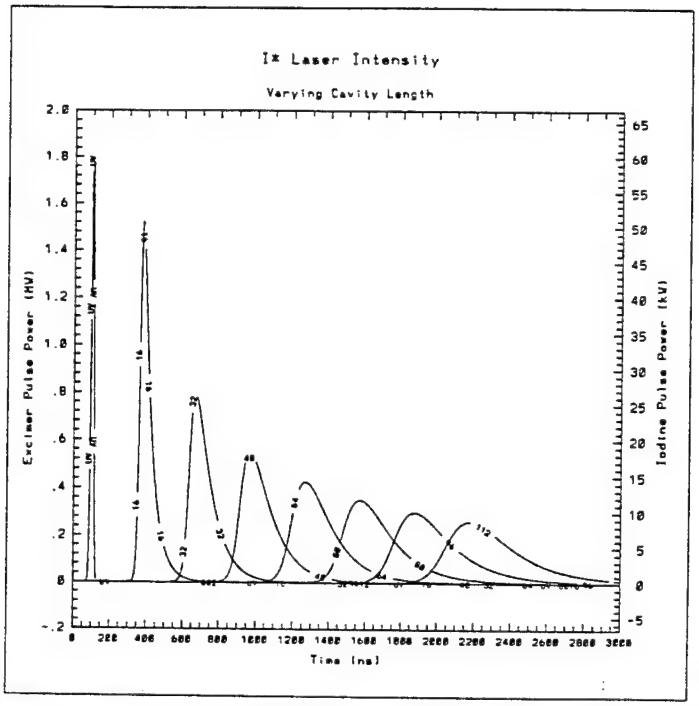

Figure 2-21a I* Laser Intensities for Various Cavity Lengths

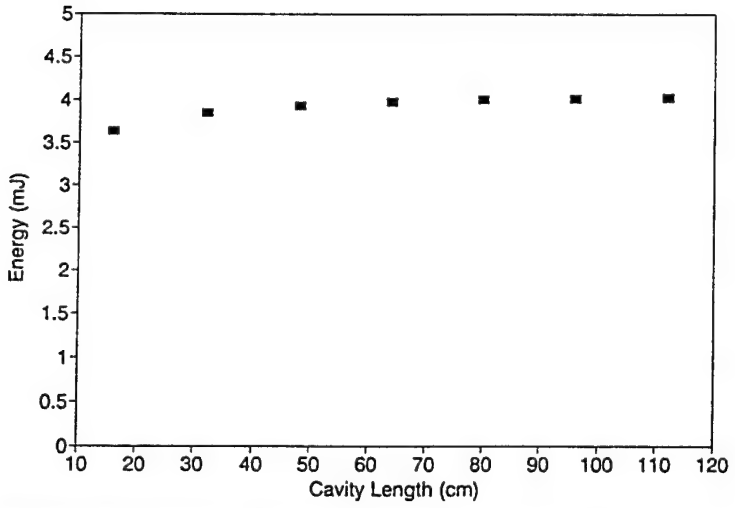

Figure 2-21b I* Laser Energy versus Cavity Length

the round trip time of the photons in the cavity. This has the expected effect of a linear increase in both cavity buildup time and pulse width. Since the photon time in the cavity is the only variable, the energy of each pulse should be constant. This is seen in Figure 2-21b.

There are several interesting effects which the model can be used to demonstrate. One such effect mentioned earlier in Section 2.2 in the discussion of hyperfine relaxation is the possibility of multiple line lasing. If hyperfine relaxation between the upper two energy states was sufficiently slow, two line lasing could occur. If lower level hyperfine mixing were also slow, more lines could lase. With the code, conditions might be simulated such that all six transitions could develop laser pulses. One way to test this case is to adjust the relaxation rate for the system used in the above examples. The pressure is fixed at 60 Torr, the cavity length at 16 cm, and the outcoupling mirror at 96.4%. Excimer energy is increased to ensure gain on the radiative transitions is above threshold. The hyperfine relaxation rate constant for the upper levels is set to zero. Figure 2-22 shows plots of the number density and the intensity for the lasing conditions. As was expected, two lines were forced to lase. By setting the lower level relaxation rate constant to zero also, we stop the mixing in the lower sublevels to try and force more lines to lase. Figure 2-23 demonstrates the result. A more realistic way to demonstrate the multiple line lasing effect, as mentioned earlier, is to lower the CF_3I pressure and longitudinally pump the laser. With some modification to the pump term in Section 2.2 this longitudinal pumping scheme can simulated. Figure 2-24 shows the two line lasing using the longitudinal pumping scheme, a CF_3I pressure of 0.100 Torr, cavity length of 600 cm, gain length of 500 cm, a pump energy of 500 mJ, and an outcoupling mirror of 80%.

Another interesting effect dealing with hyperfine relaxation which has not been mentioned yet is relaxation oscillation [64]. This occurs when a gain medium is pumped with a large amount of energy over a long pump pulse duration. In this phenomena, lasing occurs on the 3-4 transition, dumping population out of the upper F=3 level, and decreasing laser intensity as the level is depopulated. Relaxation occurs to repopulate the F=3 level, and at the same time more CF_3I is being photodissociated due to the long pump pulse, and thus the F=3 level is populated rapidly. This gives rise to an increase

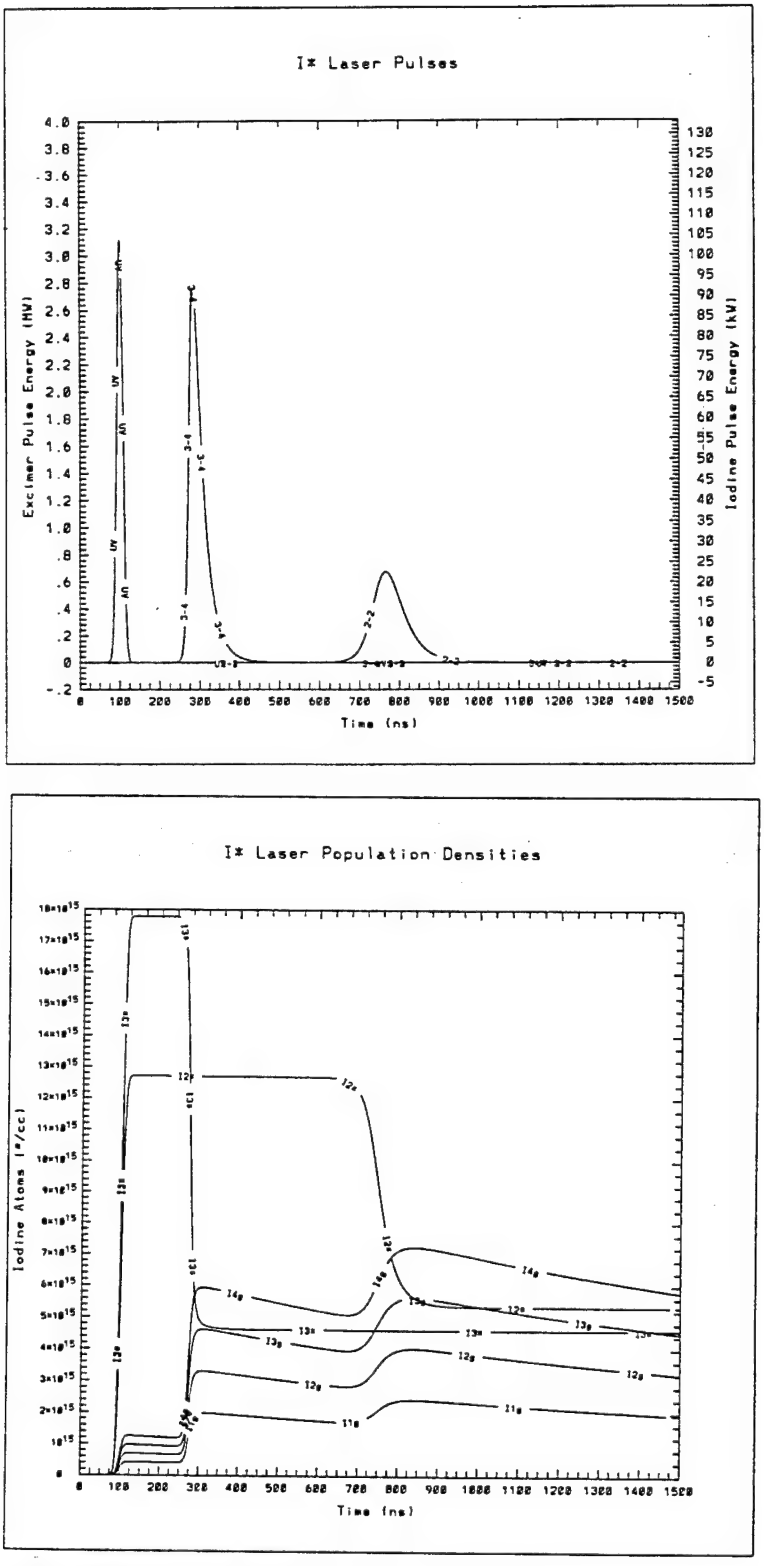

Figure 2-22 Two Line Lasing

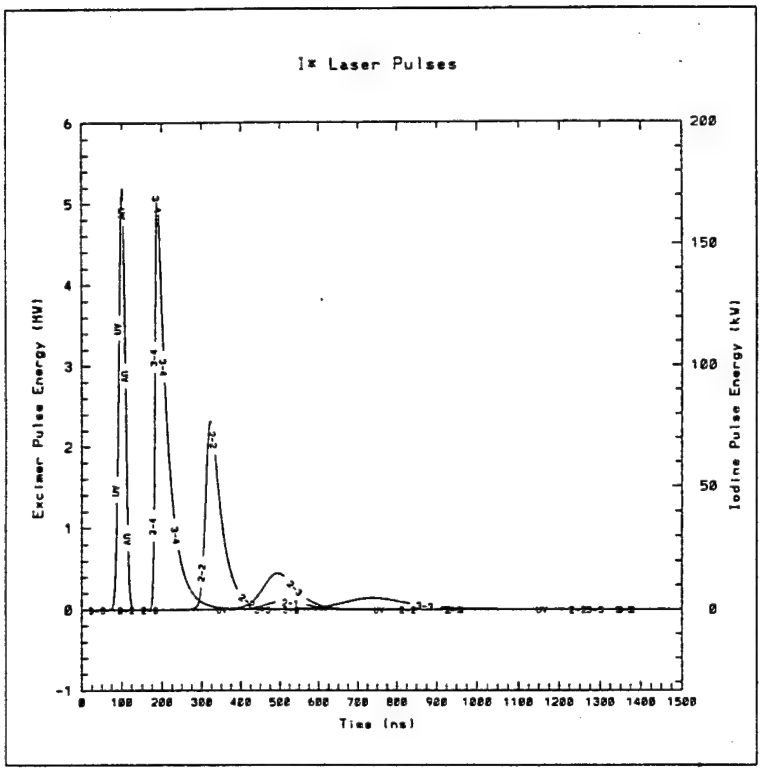

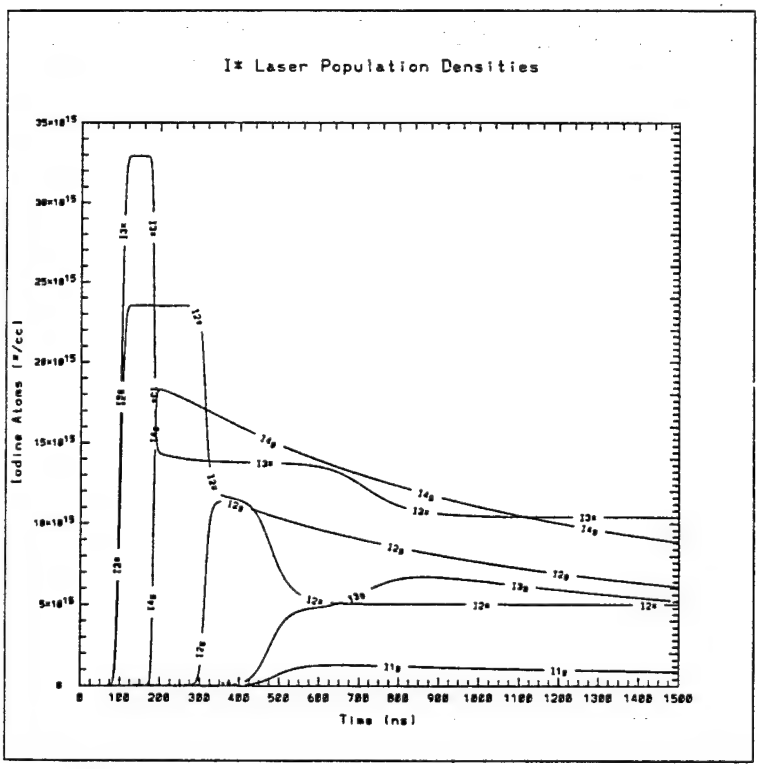

Figure 2-23 Multi-Line Lasing

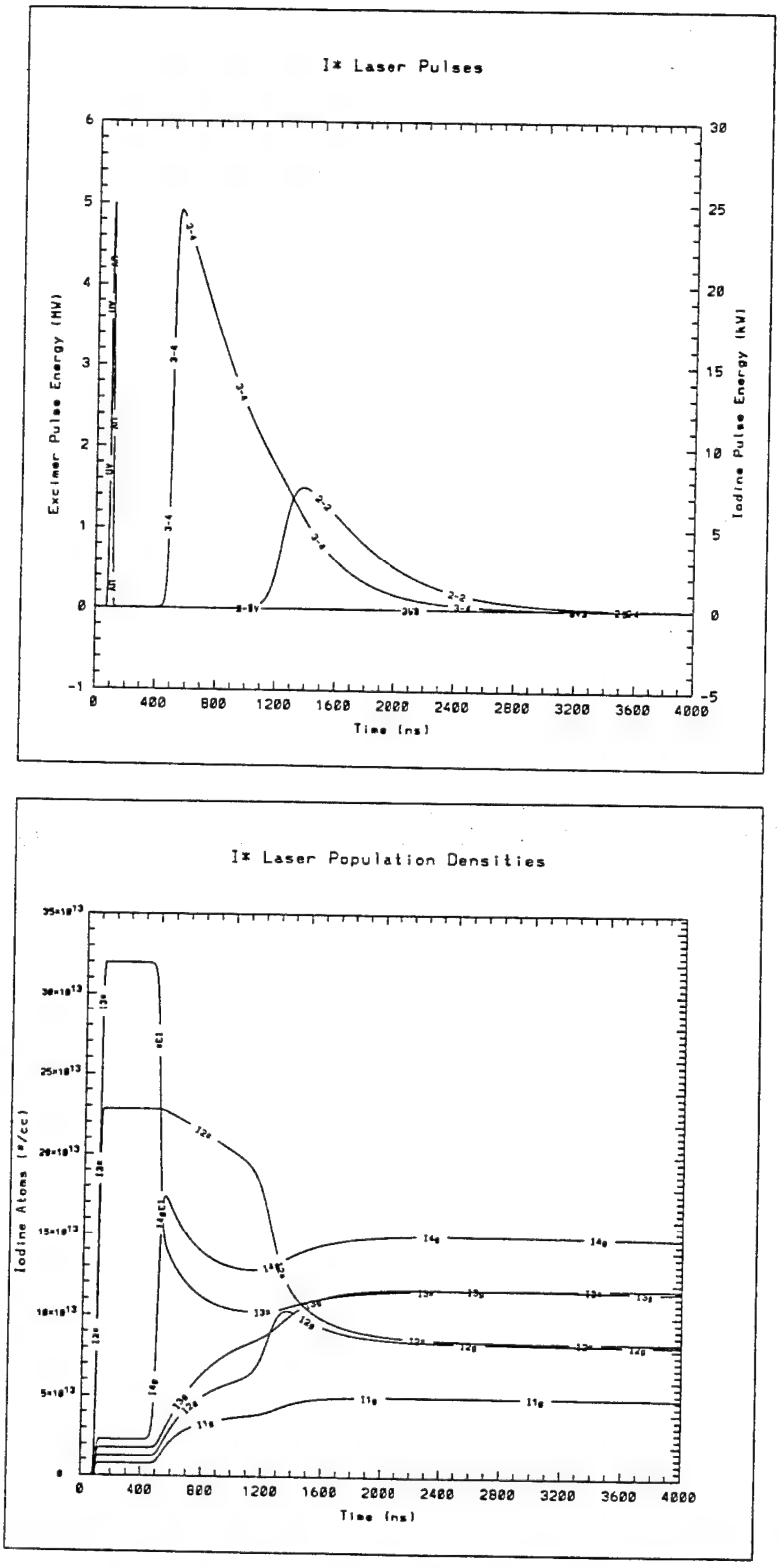

Figure 2-24 Two Line Lasing Induced by Laser Design

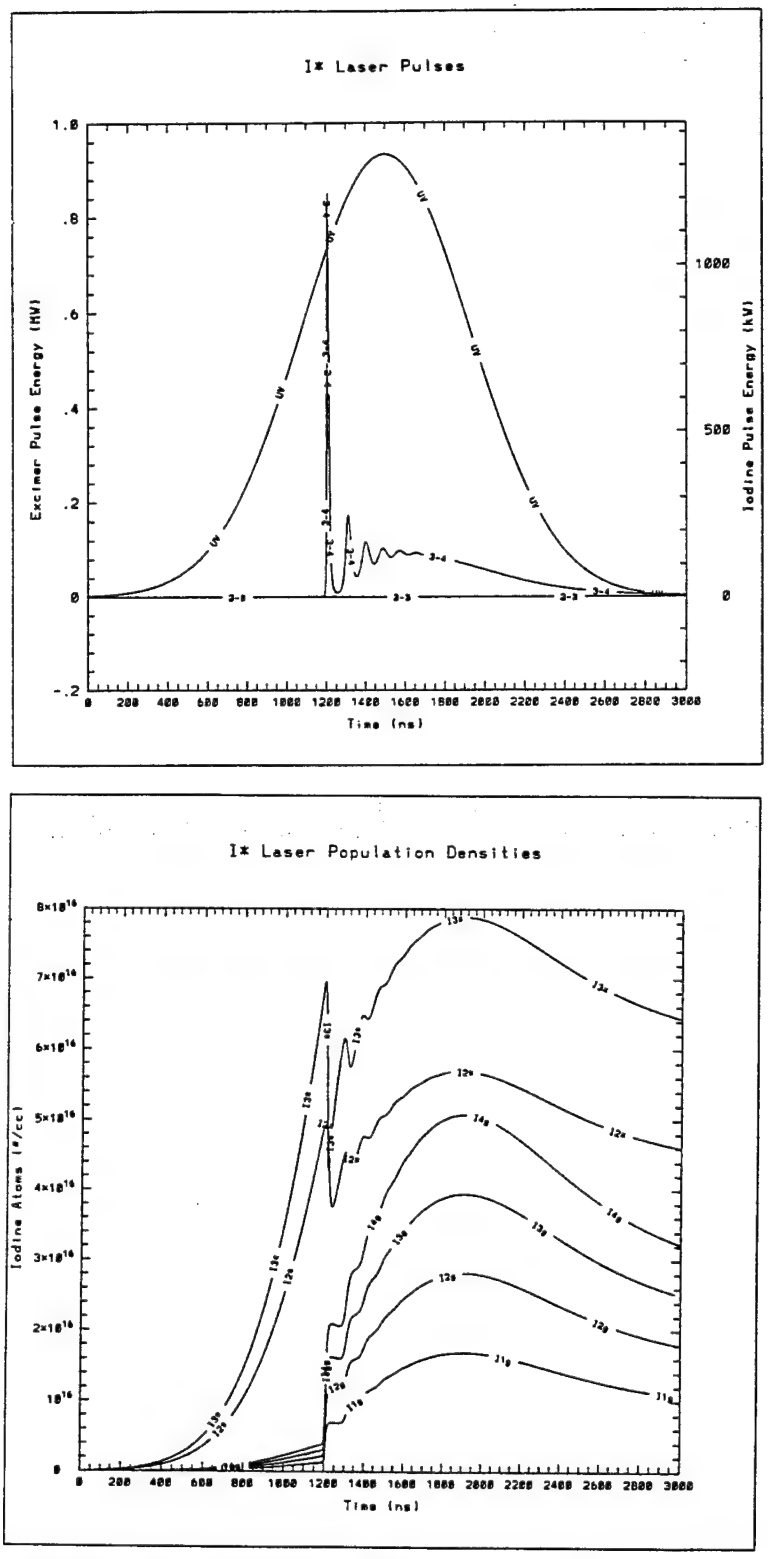

Figure 2-25 Relaxation Oscillation

in intensity on the 3-4 transition. Thus this oscillation in intensity continues until the pump pulse is expended. This action is seen in Figure 2-25.

Until now we have assumed no losses in the system. The model was tested assuming no losses to ensure it was performing in a reasonable manner and to predict several phenomena which may occur in such a system of rate equations. To truly quantitatively model such a laser system, inter-cavity losses must be incorporated in the model. A standard approach to incorporating losses into a laser system is to distribute the loss over the entire cavity. Another approach is to lump the losses in particular spots within the cavity such as in the mirrors or windows. As seen earlier, the model which we are looking at uses both approaches by including a distributed loss and window transmission losses. Mirror absorption losses and scattering losses are included in the final integration of the energy. Figure 2-26 shows the effect on outcoupled energy and cavity buildup time as a result of changing the distributed loss in the system. Figure 2-27 shows the effect on outcoupled energy and cavity buildup time as a result of changing the window transmission loss. The intensity predictions are presented in terms of energy versus outcoupler transmission plots, which is analogous to the standard Rigrod approach used to model gain, loss, and saturation intensity in CW lasers. The approach is useful in this instance as a comparison to lossless situation seen in Figure 2-19b. Both types of losses appear to have a similar effect on the energy plots and the cavity buildup time plots.

Now that we have seen that the computer code behaves in a reasonable manner, we can predict the behavior of the experimental measurements in the following sections.

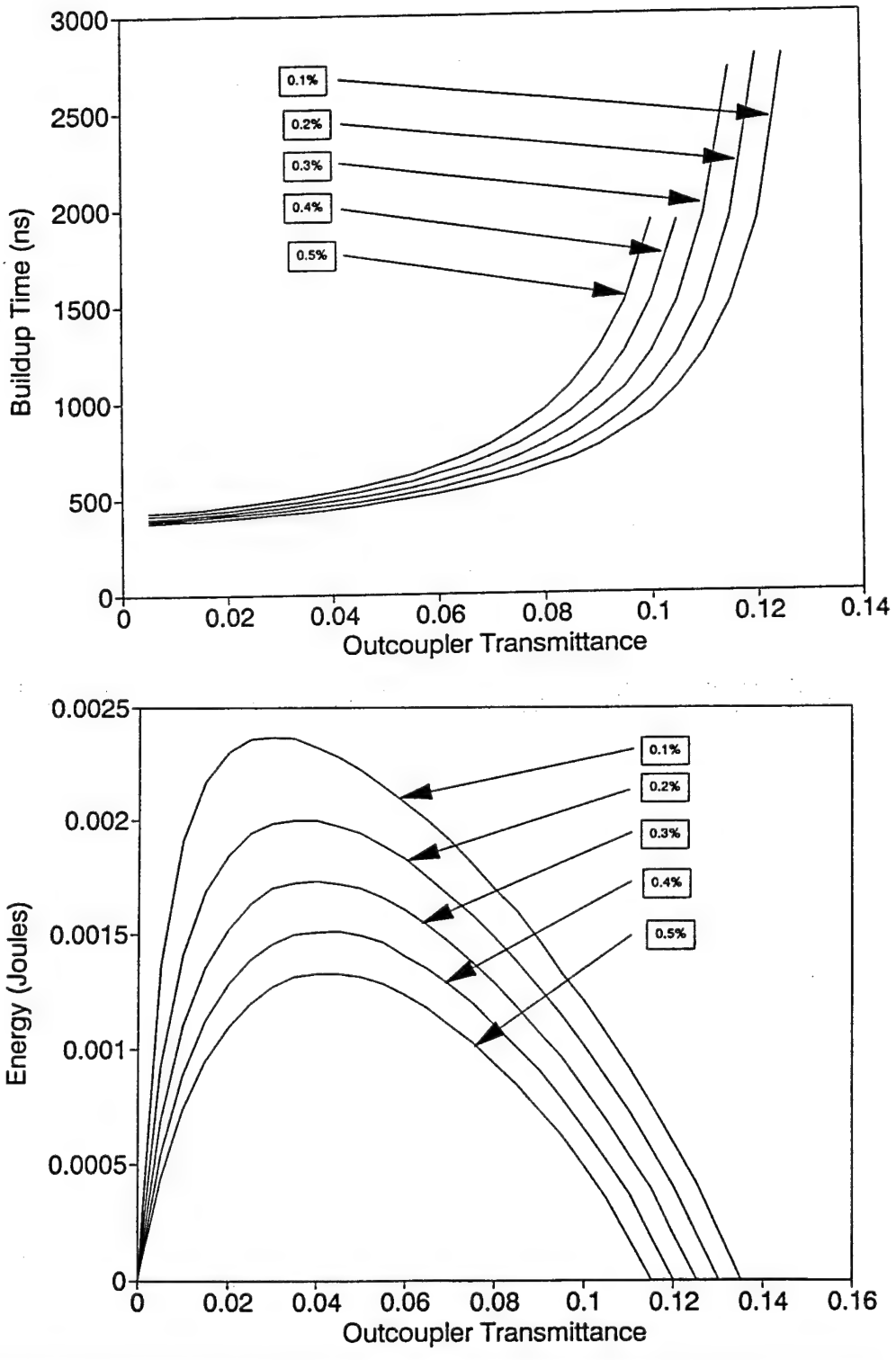

Figure 2-26 Result of Adding Distributed Loss

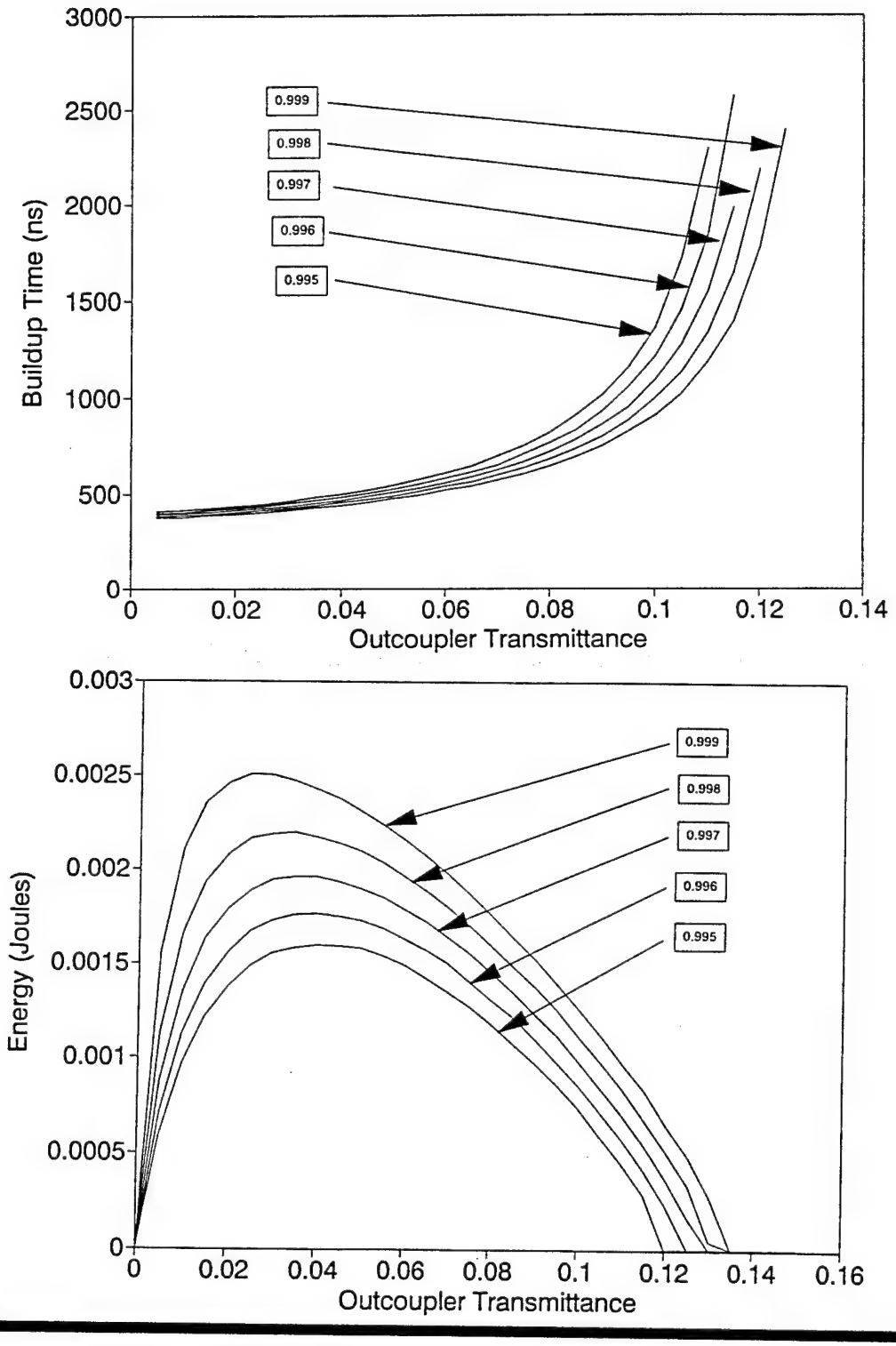

Figure 2-27 Result of Adding Window Transmission Loss

3. EXPERIMENT

3.1 Apparati

There are two experimental apparati which are used to make several measurements. The first is a laser set up which is used to make parametric measurements on the CF_3I photodissociation laser. The second is a "pump and probe" apparatus which uses a tunable diode laser to measure unloaded gain of the cell used in the laser setup. The following is a detailed description of each apparatus including both equipment and measurement technique.

The laser apparatus is seen in Figure 3-1. The pump source is a Queztec excimer laser with a KrF fill. This gives a pump source of around 200 mJ of unpolarized 248 nm light. The beam is apertured to a 1.3 cm by 2.8 cm rectangle to transversely couple into a cell of CF_3I through UV grade water-free quartz windows. A schematic drawing of the stainless steel cell is seen in Figure 3-2. The nature of CF_3I is such that when it is photolyzed, I_2 forms in the cell. Thus the system either has to be flowed or evacuated between photolysis events. The cell is designed for either; however, I decided to use a static fill for each measurement. Between each photolysis event, an Alcatel pump and cold trap are used to evacuate the cell below 0.030 Torr. This pressure is sufficiently low since the CF_3I fills range between 10 - 100 Torr.

The amount of 248 nm light which makes it through the aperture and through the cell is measured with an ED-500 Gentec joulemeter on the opposite side of the cell. This arrangement allows us to measure the amount of UV energy deposited into the CF_3I. With no CF_3I in the cell, about 175 mJ of 248 nm light make it through the aperture and the quartz windows. Any difference between energy measured without CF_3I in the cell and energy measured with CF_3I present can be attributed to photodissociation. The temporal dependence of the excimer pulse is measured using an FND-100Q fast detector.

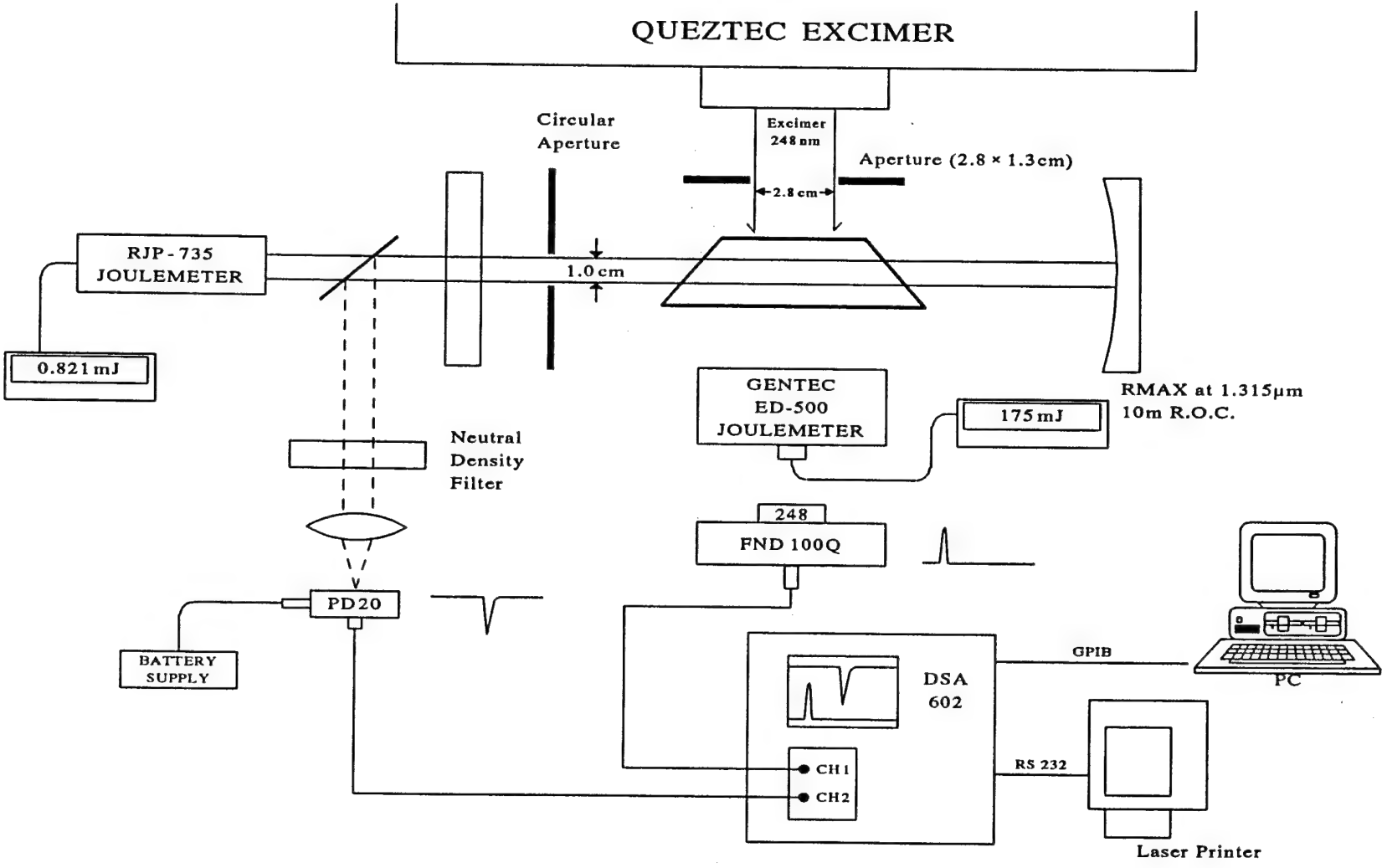

Figure 3-1 I^* Laser Apparatus

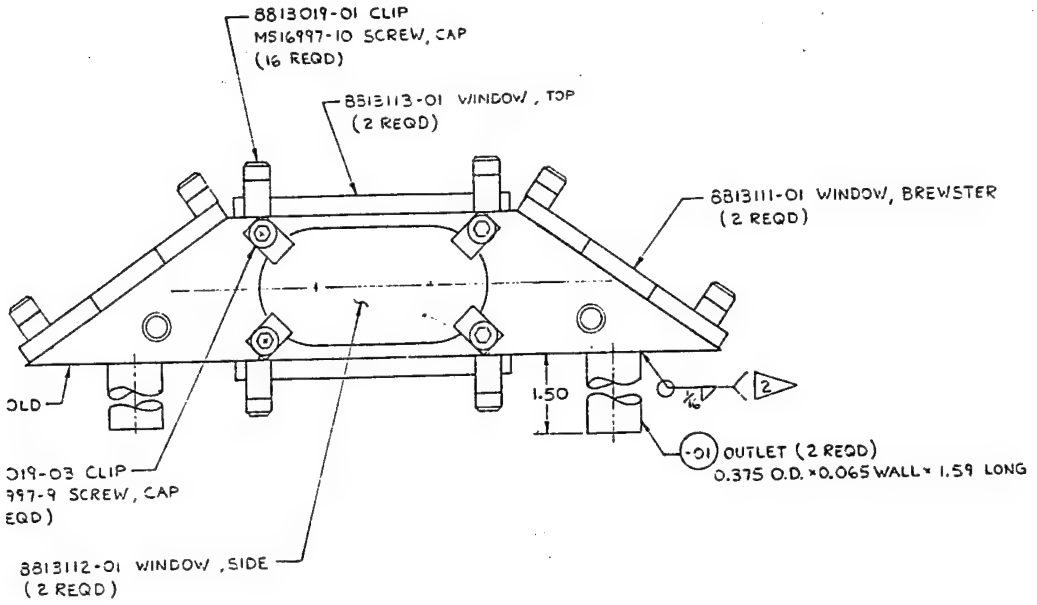

Figure 3-2 CF_3I Cell Schematic

This detector is sufficiently fast enough to measure the 18 ns FWHM excimer pump pulse. The detector is also equipped with a quartz window to allow transmission of 248 nm light. The detector is placed at an angle such that it picks up the excimer laser pulse without saturating.

Energy from the gain medium is extracted orthogonal to the pump laser through a 1 cm circular aperture. The aperture defines a specific extraction volume. The cell windows in the lasing direction are made of water-free quartz and are oriented at Brewsters angle for maximum transmission of 1.315 μm light [65]:

$$\tan\theta_B = \frac{n'}{n} \rightarrow \theta_B = \tan^{-1}\left(\frac{1.44702}{1}\right) = 55.3526^\circ \qquad (3.1\text{-}1)$$

The resonator mirrors are placed in a stable hemispherical configuration. The high reflector is designed to maximize reflectivity at 1.315 μm and has a radius of curvature of 10 meters. The outcoupler is a flat (∞ radius of curvature) with a specified

reflectivity at 1.315 μm. The spacing between the mirrors never exceeds 10 meters; thus the resonator is stable. For most measurements the mirror spacing is on the order of 16 cm.

Infrared energy extracted from the laser is measured on a sensitive Laser Precision joulemeter (Model RJP-735) capable of measuring microjoules. The temporal dependence of the laser pulse is monitored by taking 8% of the 1.315 μm light off with a microscope slide, passing it through a neutral density filter, and focussing the reduced signal onto a small area fast detector. The fast detector for the 1.315 μm light is an Electro-Optics PD20 ultra-fast detector capable of measuring a 4 GHz bandwidth. Both the FND-100Q and the PD20 detectors are fed into a Tektronics DSA 602 Digital Oscilloscope with an analog bandwidth of 500 MHz. The scope is set to trigger off the excimer pulse. Noise generated by the excimer's thyratrons firing was a significant problem. Coaxial cables leading from the fast detectors to the scope were double shielded and aluminum foil was used to cover areas such as switches and connectors where excimer noise may couple into the lines. The detectors were both run off batteries inside shielded boxes, and a ground loop isolation transformer was used to isolate the oscilloscope.

A special procedure for alignment of the resonator mirrors and the fast detector was developed using a 1.315 μm diode laser Figure 3-3. The laser precision joulemeter is removed and a collimated diode laser beam at 1.315 μm is sent back through the microscope slide beam splitter into the resonator. The front mirror is removed and the back mirror is aligned by using an IR sensitive card to direct the beam back into itself. Precise alignment is achieved by watching the diode laser's spectrum change as feedback from the mirror alters its lasing characteristics. The front mirror is aligned in a similar manner. A 30dB faraday isolator is used in the diode laser path to keep the feedback from damaging the diode. Once the resonator is aligned, the PD20 fast detector must be aligned.

The small area of the PD20 detector makes it quite difficult to align. The alignment is accomplished by placing a chopper in the diode laser path, removing the neutral density filter from between the beamsplitter and the focussing lens, and adding a $\times$20 amplifier between the PD20 and the scope. The system is aligned when the small

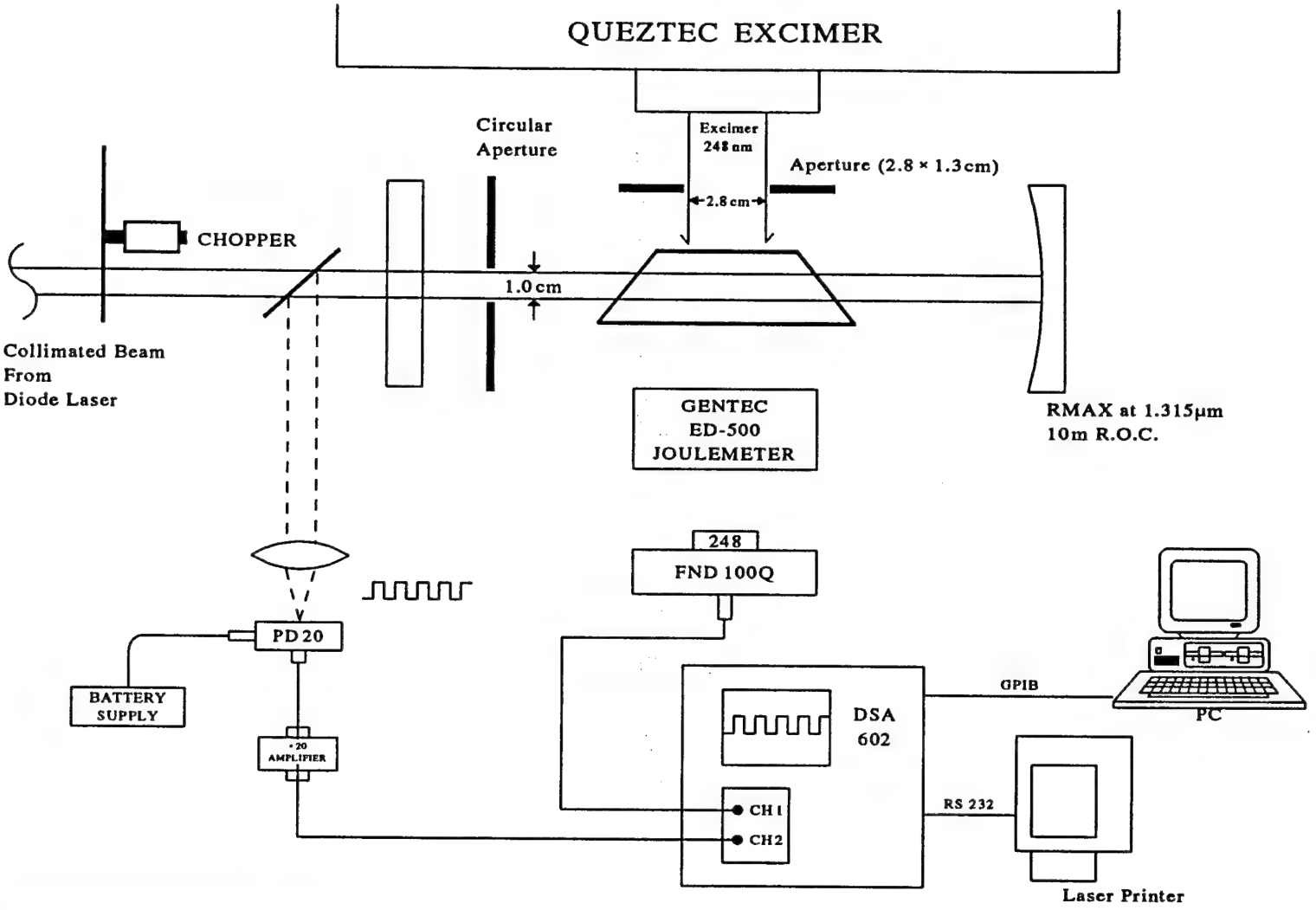

Figure 3-3 Alignment Setup for I* Laser

chopped signal from the diode laser is optimized on the oscilloscope. To make the measurement, the diode laser is turned off, the laser precision joulemeter and the neutral density filter are returned to their proper places, the ×20 amplifier is removed, and the scope is set to trigger off the excimer pulse. The resulting acquisition is seen in Figure 3-4.

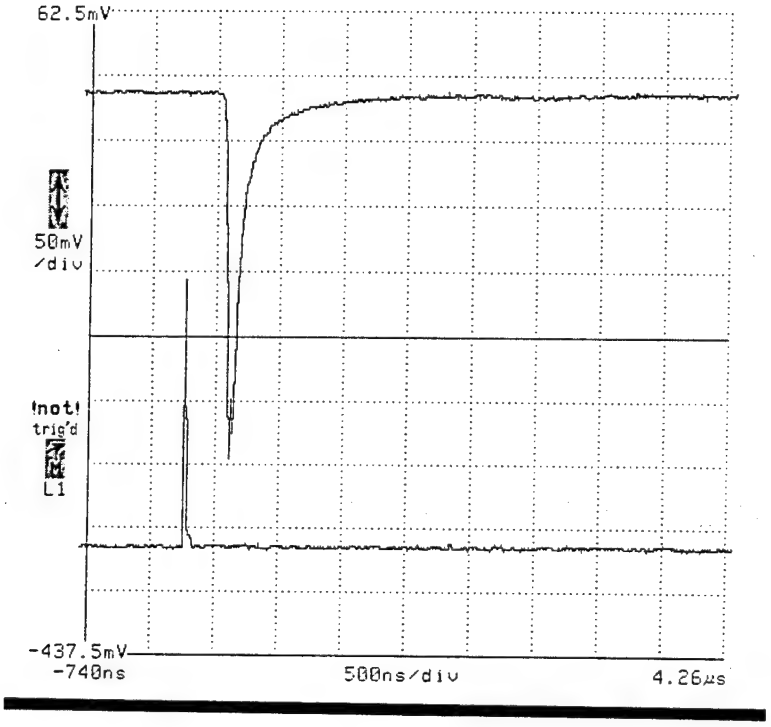

Figure 3-4 Measured I^* Laser Intensity

The first pulse is the excimer pump pulse measured with the FND-100Q detector. The second pulse is the Iodine lase pulse measured with the PD20 detector. This pulse is inverted since the PD20 is a negative going detector.

The experimental apparatus which involves using a tunable diode laser to measure small signal gain is seen in Figure 3-5. The same pumping configuration and cell as in the laser setup is used. The resonator mirrors are removed and an InGaAsP diode laser at 1.315 μm in a frequency narrowed single mode operation is locked on one of the six radiative transitions of atomic iodine. The diode laser is chopped for alignment purposes and to provide a baseline for the gain measurement. The chopper is removed while the

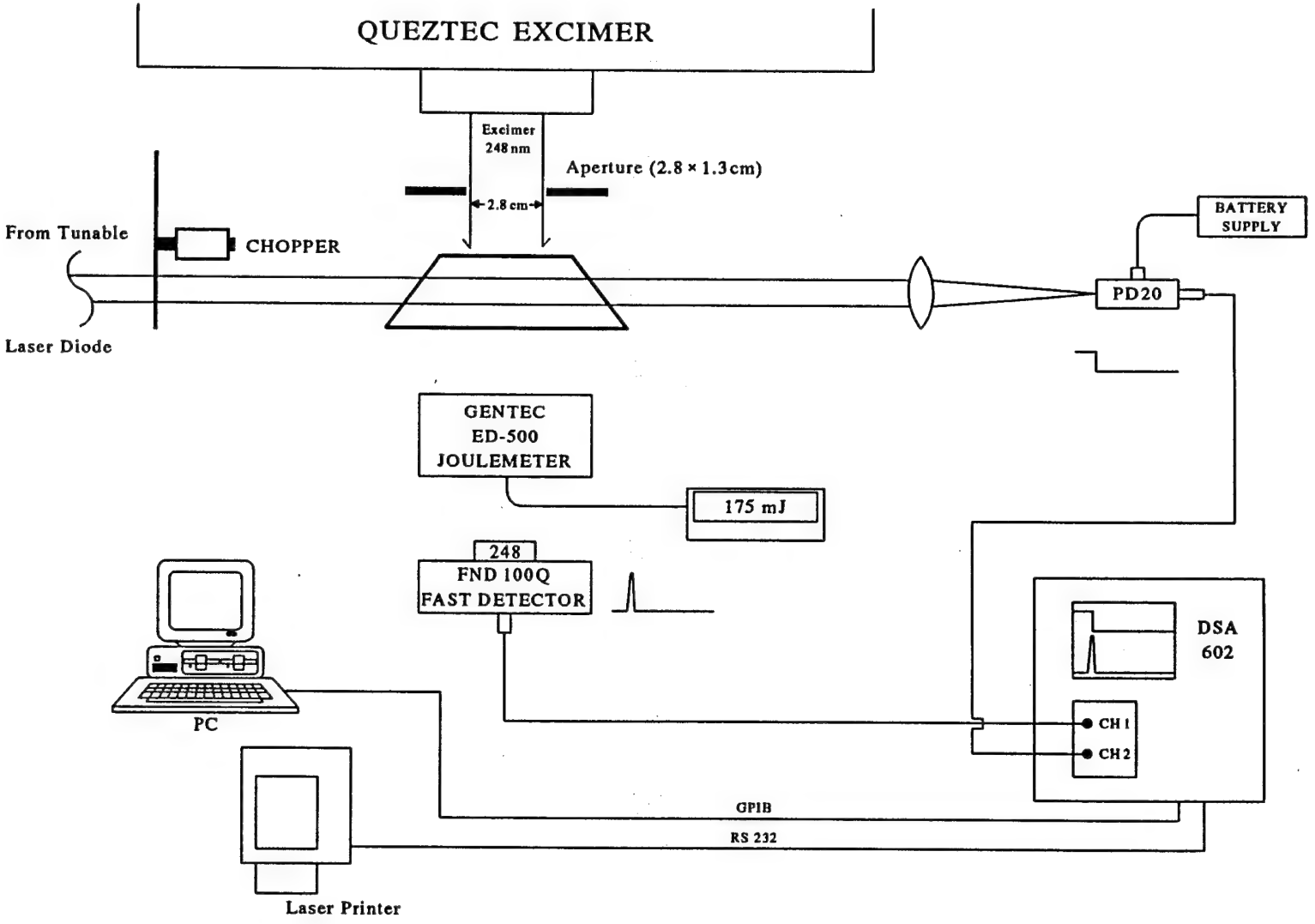

Figure 3-5 Gain Measurement Setup

gain measurement is being made. Amplification within the cell, which basically amounts to gain plus loss, is measured by comparing the change in the diode laser signal to the baseline established by the chopper. If the baseline established by the chopper is ΔV_B and the amplification by the gain medium within the cell is ΔV_g then the small signal gain plus loss follows Beer's law:

$$\frac{\Delta V_B + \Delta V_g}{\Delta V_B} = e^{\alpha_o L_g} \quad \Rightarrow \quad \alpha_o = \frac{1}{L_g} \ln\left(\frac{\Delta V_B + \Delta V_g}{\Delta V_B}\right) \qquad (3.1\text{-}1)$$

where α_o is gain plus loss and L_g is the 2.8 cm gain length.

The most critical part of this apparatus is the tunable diode laser illustrated in Figure 3-6. The diode laser used is a 3-6 mWatt InGaAsP multimode diode made by Hitachi. The model number is the HLP 5400, wavelength selected at the factory to lase at 1.318 μm at 25°C. The diode was selected at this wavelength and temperature for a

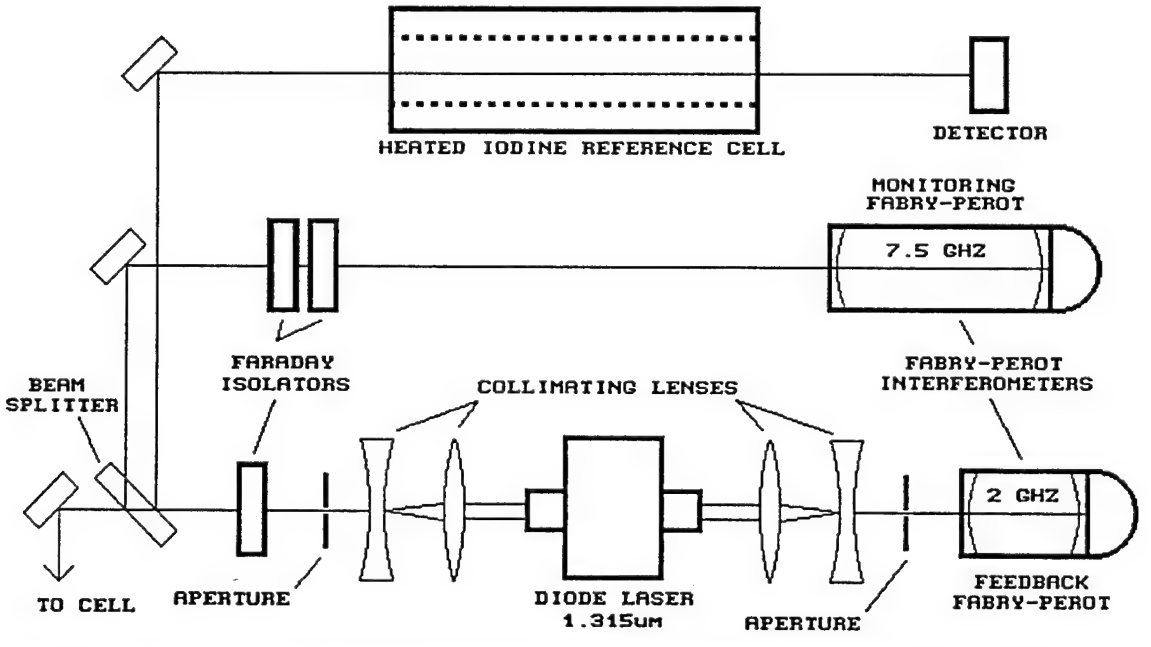

Figure 3-6 Tunable Diode Laser Setup

specific reason. By lowering the temperature and adjusting the current of the diode selected, it can be operated close to the threshold right around 1.315 μm. The temperature controller, current source, and laser diode mount used to impose these conditions on the diode were made by ILX Lightwave specifically for laser diode control. At about 18 °C and 25 mA the wavelength selected diode laser spectrum overlaps the 3-4 transition in atomic iodine. This is seen by an absorption, as part of the diode laser is directed up through a heated iodine reference cell.

The heated iodine reference cell is a glass cell with molecular iodine crystals heated to about 600°C. At this temperature the iodine no longer exists as a dimer, but rather as atomic iodine. A detector placed at the opposite end of the cell is used to sense absorption of the diode laser as it turns through the atomic iodine spectrum.

Once the transition of interest is found, feedback from a tech optics fabry-perot interferometer is used to force the diode to narrow and suppress the side modes to where the diode is functioning in virtually a single mode operation. The spectrum of the diode laser is observed on another tech-optics fabry-perot interferometer. A 30dB Faraday isolator is placed between the diode laser and the experiment to insure that feedback from the experiment does not affect diode laser operation. A 60dB Faraday isolator is placed between the diode laser and the monitoring fabry-perot for the same purpose. The feedback fabry-perot can thus be solely adjusted to optimize the laser diode.

Noise from the excimer laser is a major problem in this apparatus. The diode laser electronics are highly susceptible to electromagnetic noise. In the end, the brute force method was used to reduce the noise: the entire laser diode setup was encased in a make-shift Faraday cage of copper and aluminum along with a Topaz ground loop isolation transformer as a power source. The result was that the noise was reduced sufficiently.

Figure 3-7 shows an example of typical gain measurements made using this apparatus. The top signal is the change in flux seen by the detector due to amplification by the cell. This change is ΔV_g. The bottom signal is the baseline signal generated by the chopper measured prior to ΔV_g. This change is ΔV_B. Applying these measurements to Equation 3.1-1 we get the small signal gain plus loss on the transition selected by the diode laser.

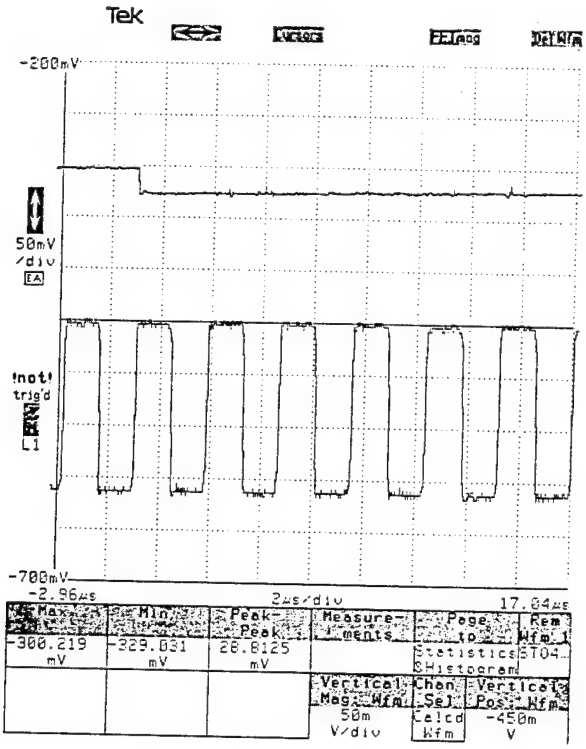

Figure 3-7 Typical Gain Measurement

3.2 I^* Laser Data

A large amount of data was taken using the laser apparatus of Figure 3-1. Several different parameters in the laser device can be varied to alter lasing characteristics. These parameters include mirror reflectivity, CF_3I pressure, cavity length, and gain length. Measurements were performed several times on different days to insure reproducibility. The following set of measurements was taken 4 November 1992.

The first group involves using a CF_3I pressure of 60 Torr, a cavity length of 16 cm, while varying the outcoupler reflectivity. A set of outcouplers were measured by the metrology center at the Phillips Laboratory. The set includes reflectivities of 98.8%, 96.415%, 89.5%, 85.8%, and 80.1%. Lasing did not occur at 80.1%. Plots of pulses

which did occur can be seen in Figure 3-8. Laser pulse energies and cavity build-up times are given below each plot.

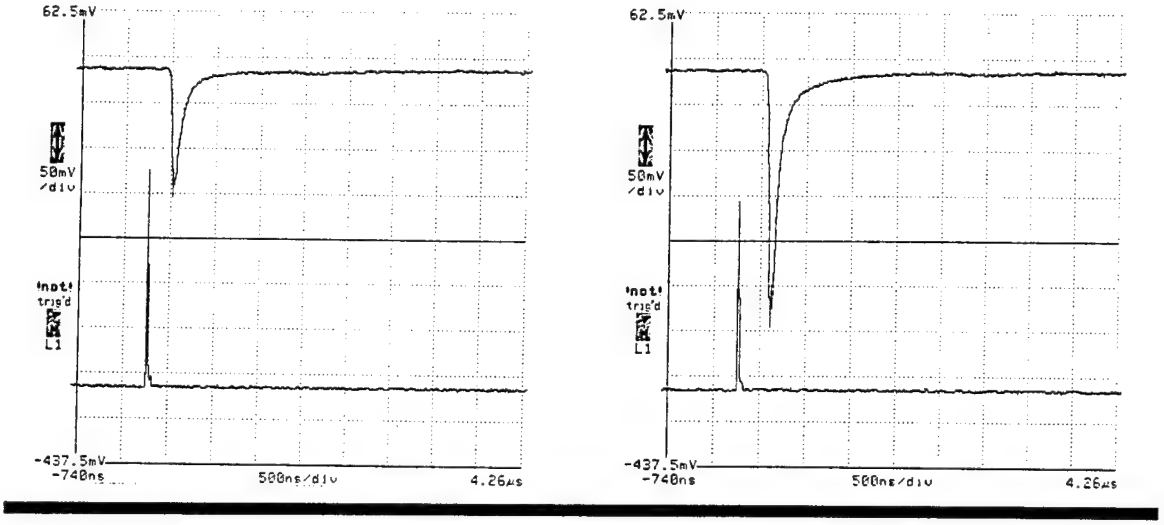

R = 98.8% E = 0.235mJ τ = 210ns

R = 96.4% E = 0.430mJ τ = 300ns

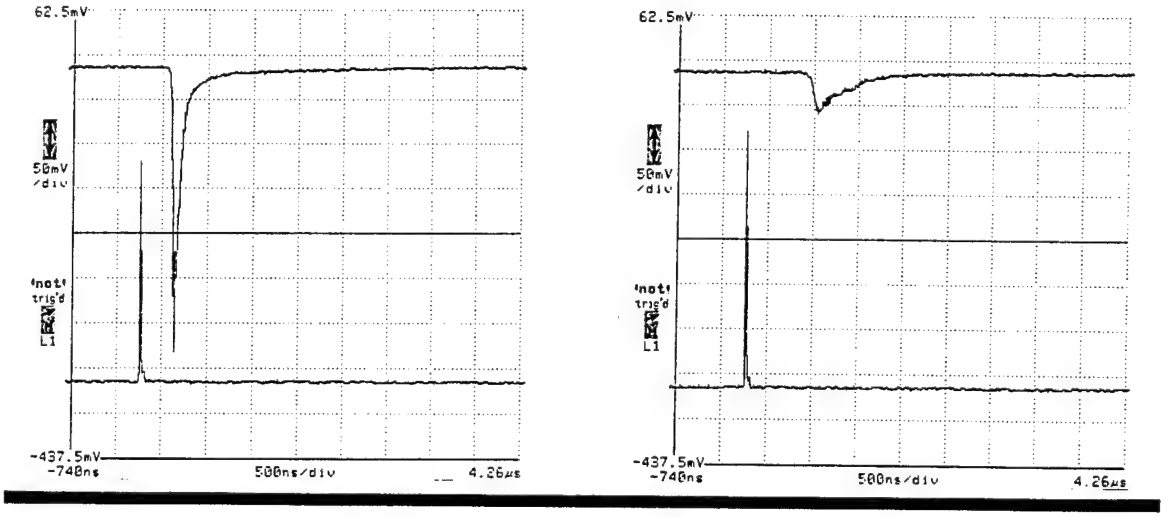

R = 89.5% E = 0.269mJ τ = 320ns

R = 85.8% E = 0.150mJ τ = 690ns

Figure 3-8 Varying Outcoupler Reflectivity

The next group involves varying the pressure of CF_3I in the cell and measuring lasing characteristics. As the pressure is changed, the amount of UV energy deposited

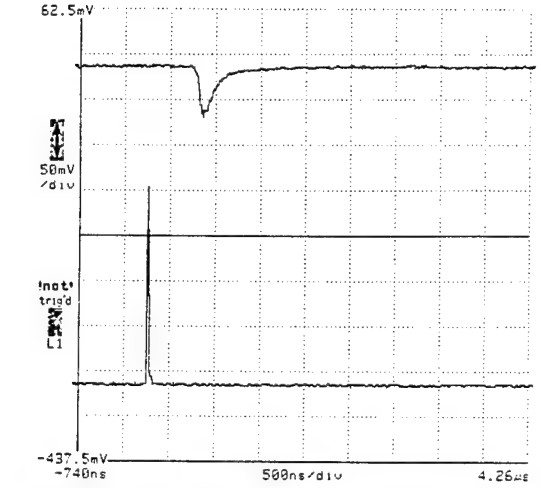

P = 10 Torr E_D = 29mJ
E = 0.124mJ τ = 500ns

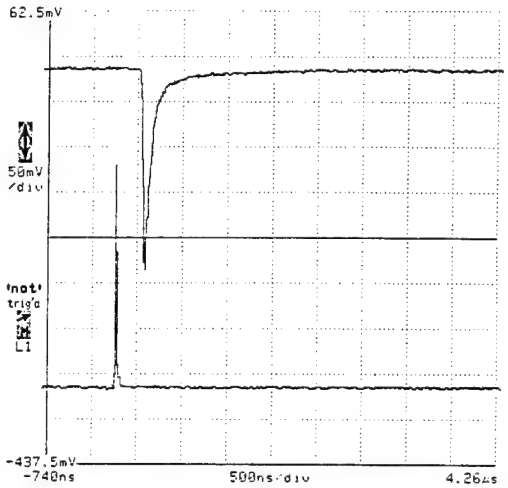

P = 20 Torr E_D = 52mJ
E = 0.311mJ τ = 270ns

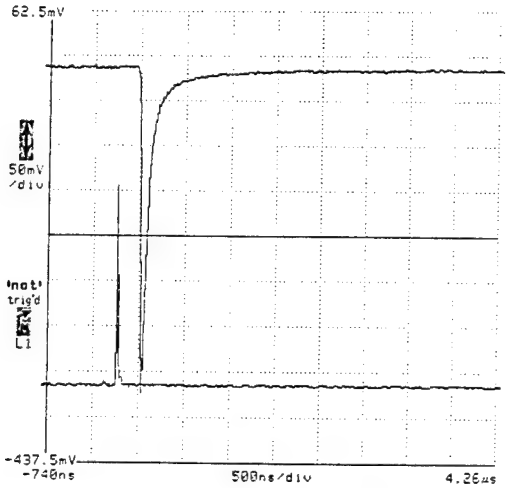

P = 30 Torr E_D = 72mJ
E = 0.419mJ τ = 220ns

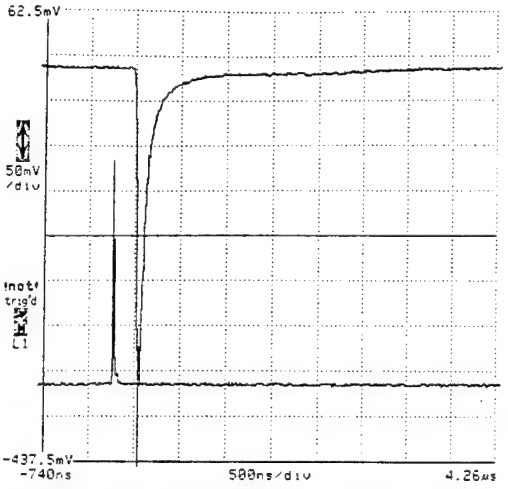

P = 40 Torr E_D = 90mJ
E = 0.520mJ τ = 230ns

Figure 3-9 Varying CF_3I Pressure

in the CF_3I also changes. Pressures are varied between 10 Torr and 100 Torr in steps of 10 Torr. Figure 3-9 shows the resulting laser intensities along with cavity buildup, laser

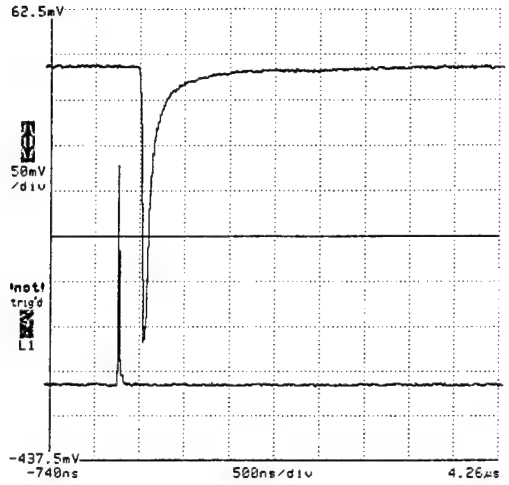

P = 50 Torr E_D = 104mJ
E = 0.510mJ τ = 240ns

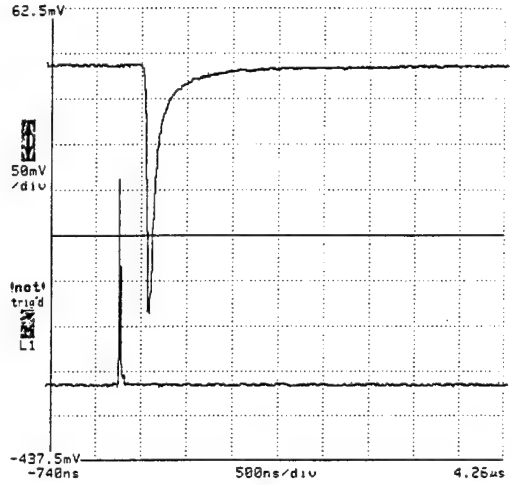

P = 60 Torr E_D = 115mJ
E = 0.446mJ τ = 260ns

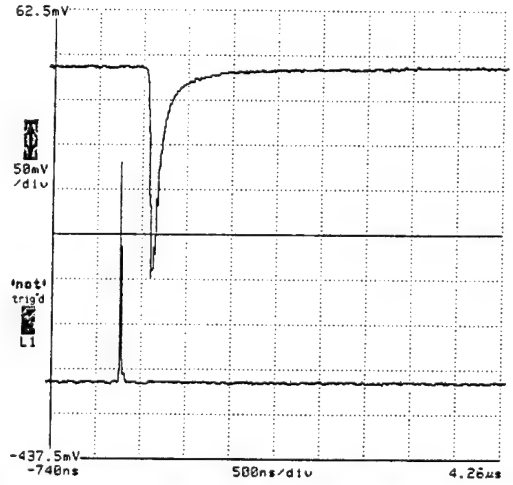

P = 70 Torr E_D = 126mJ
E = 0.405mJ τ = 290ns

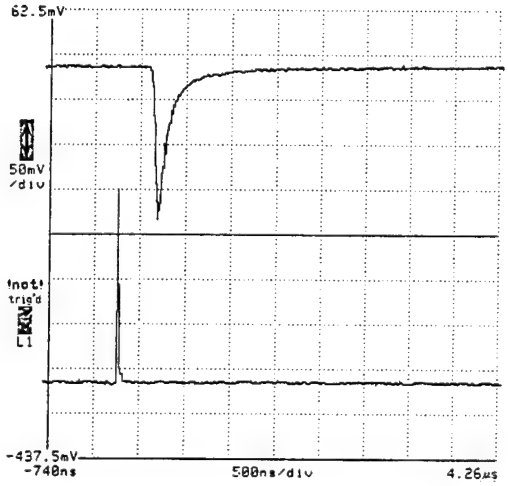

P = 80 Torr E_D = 135mJ
E = 0.360mJ τ = 350ns

Figure 3-9 Varying CF_3I Pressure (continued)

energy, and deposited energy listed below.

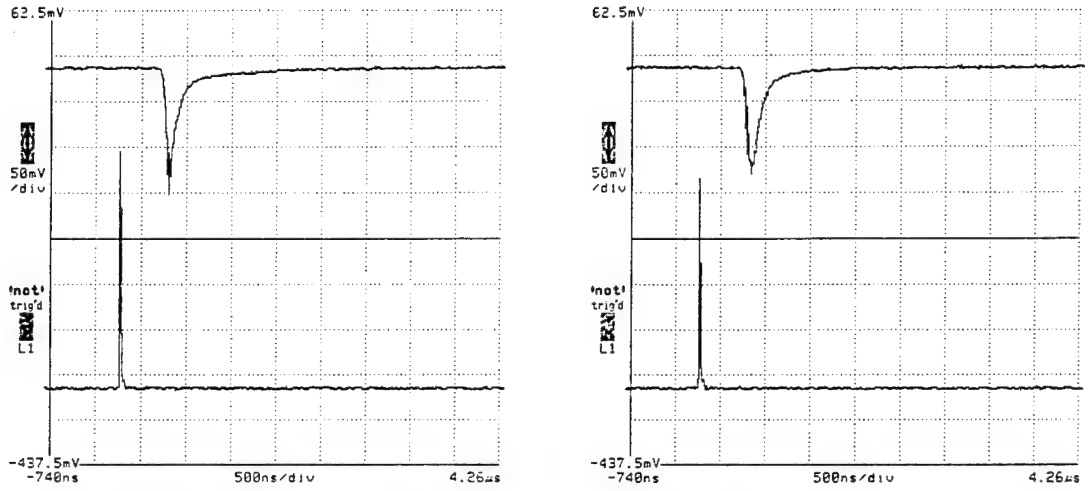

P = 90 Torr E_D = 142mJ
E = 0.258mJ τ = 440ns

P = 100 Torr E_D = 146mJ
E = 0.215mJ τ = 490ns

Figure 3-9 Varying CF_3I Pressure (continued)

The third group of laser measurements involves varying the cavity length. The pressure is kept constant at 60 Torr and the outcoupler is 96.415%. The cavity length is increased from 16 cm to 112 cm in steps of 16 cm. Figure 3-10 shows these plots with cavity buildup time and pulse energy listed below each.

The final set of laser measurements performed on 4 November 1992 involved decreasing the gain length of the laser from 2.8 cm to where it ceased to lase (Figure 3-11). The outcoupler is fixed at 96.415% and the gas pressure is kept at 60 Torr. Pulse energy, cavity build-up time, and energy deposited in the CF_3I are listed below each plot. Data was taken every 0.2 cm; however, for practical reasons only selected plots are shown.

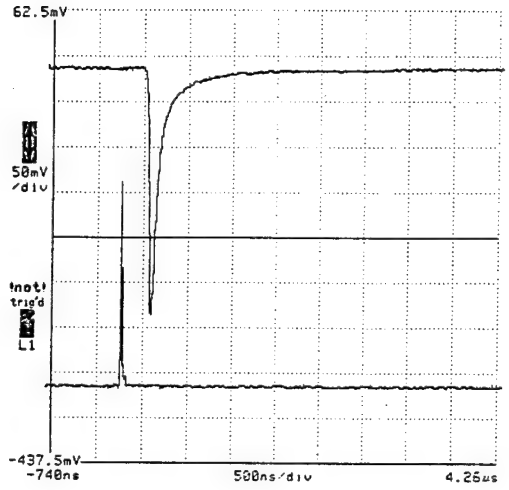

D = 16 E = 0.446mJ τ = 260ns

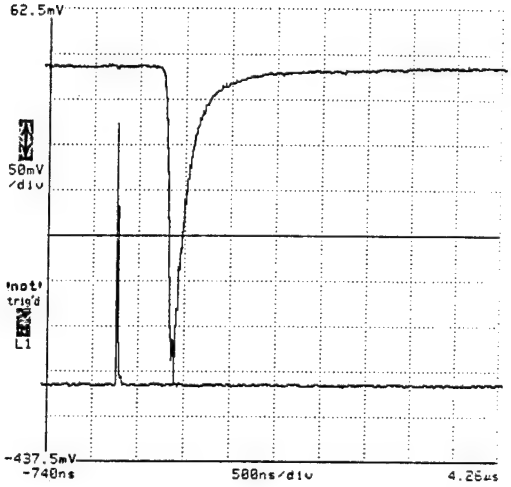

D = 32cm E = 0.591mJ τ = 510ns

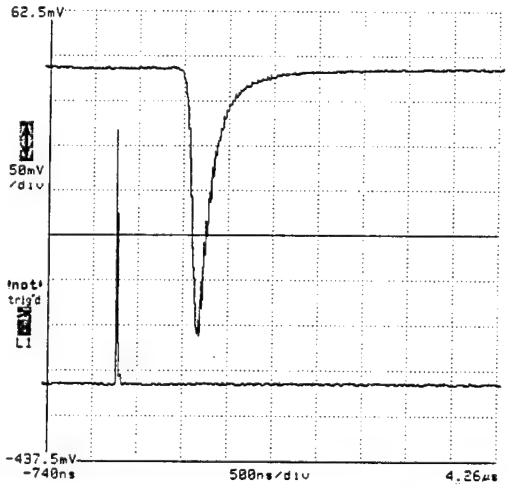

D = 48cm E = 0.463mJ τ = 750ns

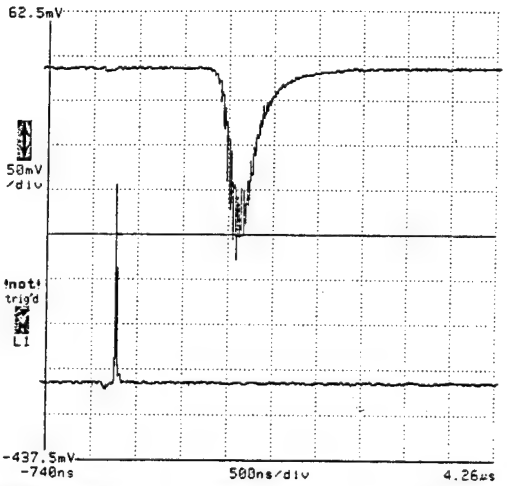

D = 64cm E = 0.332mJ τ = 1.1μs

Figure 3-10 Varying Cavity Length

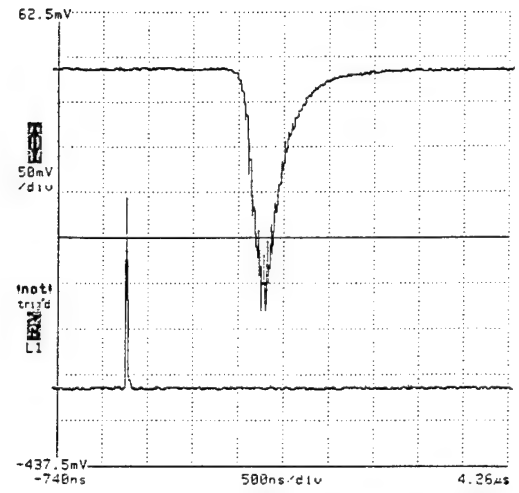

D = 80 E = 0.474mJ τ = 1.25μs

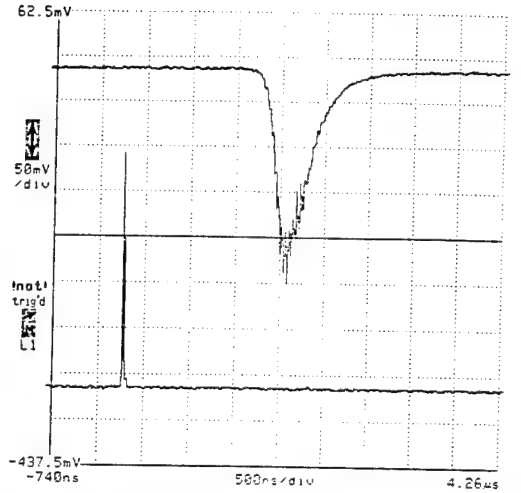

D = 96cm E = 0.432mJ τ = 1.53μs

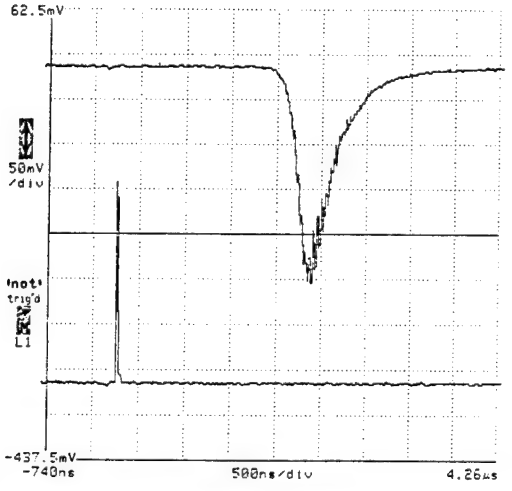

D = 112cm E = 0.508mJ τ = 1.81μs

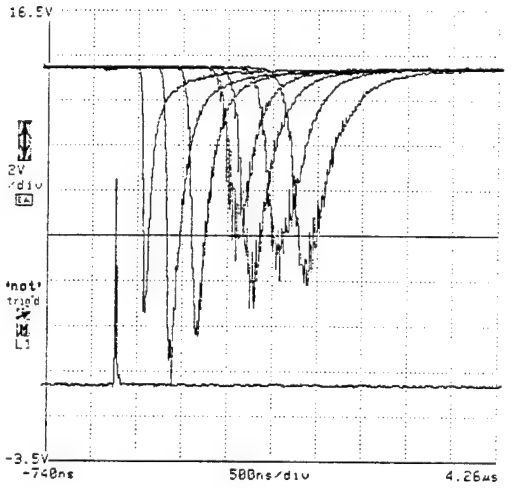

Summary of Measurements

Figure 3-10 Varying Cavity Length (continued)

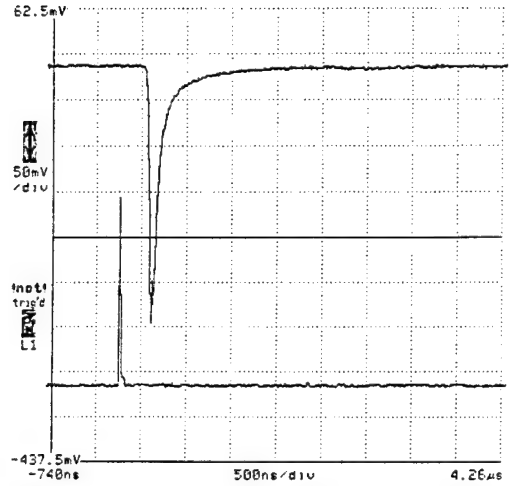

L_g = 2.8cm E_D = 111mJ
E = 0.473mJ τ = 260ns

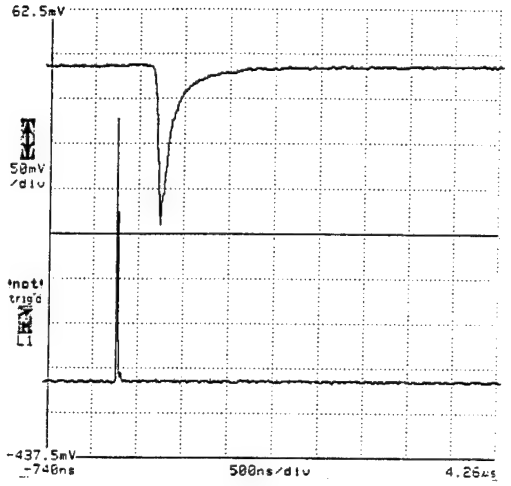

L_g = 2.2cm E_D = 93.4mJ
E = 0.353mJ τ = 400ns

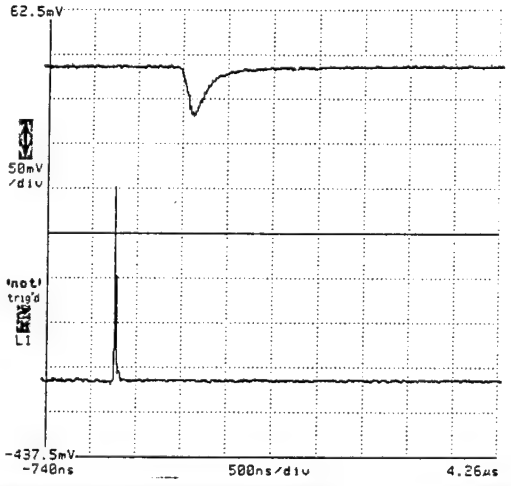

L_g = 1.8cm E_D = 76.6mJ
E = 0.153mJ τ = 940ns

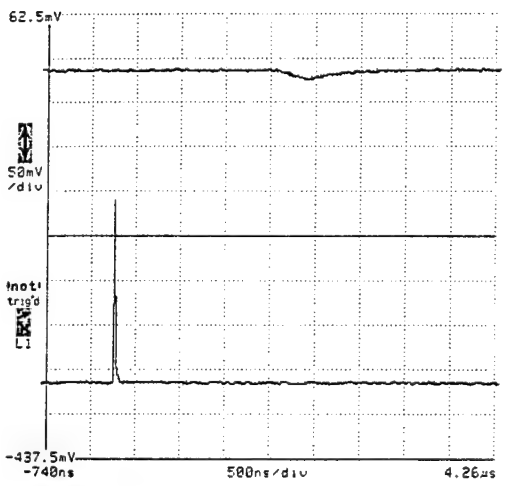

L_g = 1.4cm E_D = 56.2mJ
E = 0.055mJ τ = 1.87μs

Figure 3-11 Varying Gain Length

3.3 I* Gain Data

Gain measurements made with apparatus in Figure 3-5 were limited to a single pressure of 60 Torr. Gain was measured; however, on all six radiative transitions in the atomic Iodine spectrum. These measurements were repeated to insure reproducibility. The main problem encountered was that the diode laser could not be forced into true single mode. Feedback narrowed the diode laser lines and partially suppressed the side modes, but several side modes still existed. The effect of the side modes on the intensity measurement can be taken into account by factoring the intensity in the side modes into the final gain measurement. Since the intensity of each mode is proportional to the area under the mode, a correction factor can be determined by measuring the area under the side modes. This is quickly accomplished in Figure 3-12 by the digital oscilloscope. Figure 3-12 shows four sets of two plots to compare area under each of the diode laser modes. Each set shows a plot of the mode structure of the diode laser within the free spectral range of the interferometer above a plot of one of the individual modes.

An equation can be derived to determine how to factor in the effect of the side modes. The assumption is that the area under each mode is proportional to the intensity of the mode. Figure 3-13 shows the intensities before and after the cell assuming the strongest mode of the diode laser is on the radiative transition being measured. The ratio of the intensity after the cell over the intensity before the cell becomes:

$$\frac{\bar{I}_o}{\bar{I}_i} = \frac{\bar{I}_1 e^{\alpha_o L_g} + \bar{I}_2 + \bar{I}_3 + \bar{I}_4}{\bar{I}_1 + \bar{I}_2 + \bar{I}_3 + \bar{I}_4}$$

Solving this for gain plus loss α_o:

$$\alpha_o = \frac{1}{L_g} \ln \left[\frac{\bar{I}_i}{\bar{I}_1} \left[\frac{\bar{I}_o}{\bar{I}_i} - 1 \right] + 1 \right]$$

Thus with this equation, gain measurements can be corrected to account for the fact that the diode laser was not operating in a true single mode.

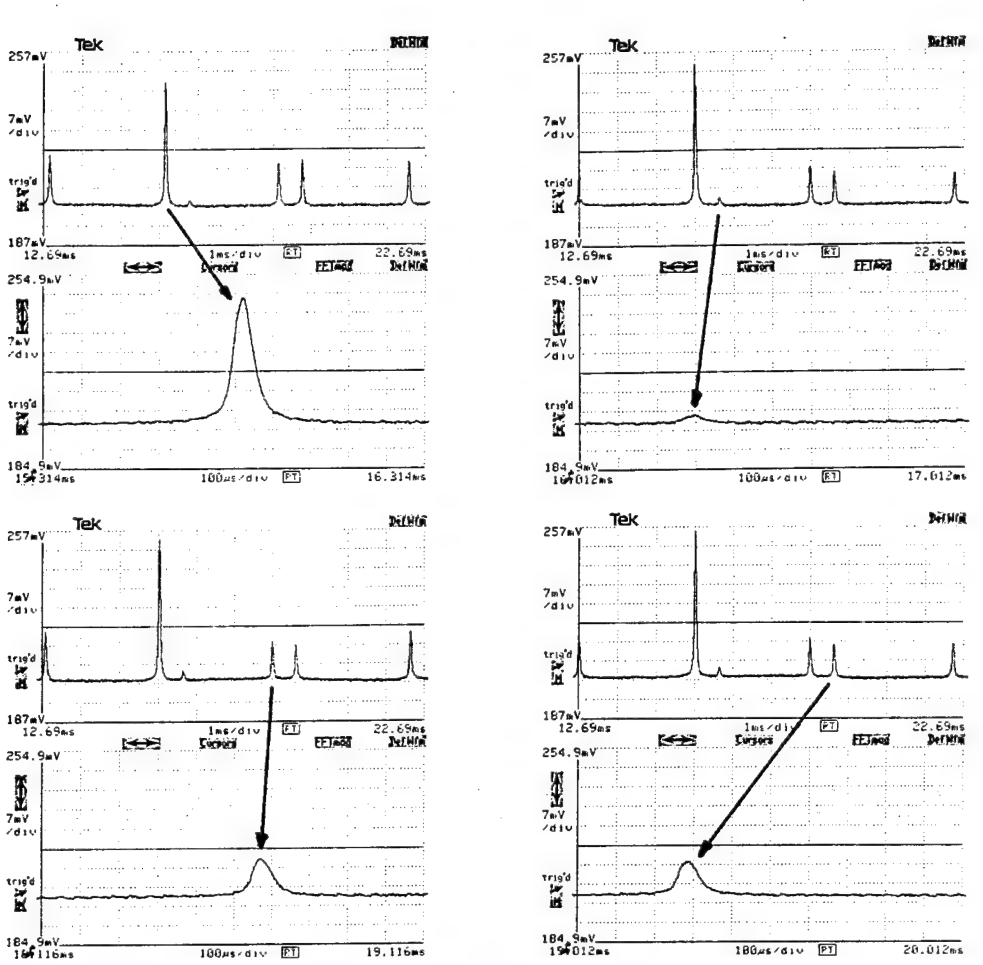

Figure 3-12 Diode Laser Mode Structure

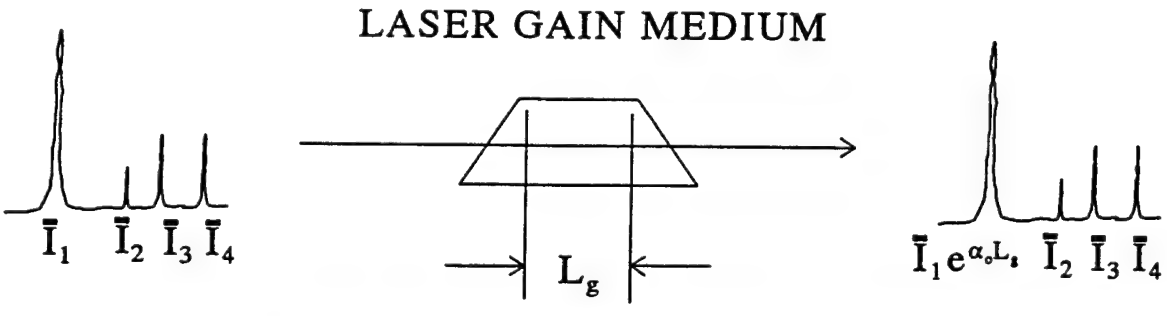

Figure 3-13 Intensity Amplified by Cell

Figure 3-14 shows gain measurements made for all six radiative transitions on 8 October 1992 for a CF_3I pressure of 60 Torr. Amplitude scales and time scales vary

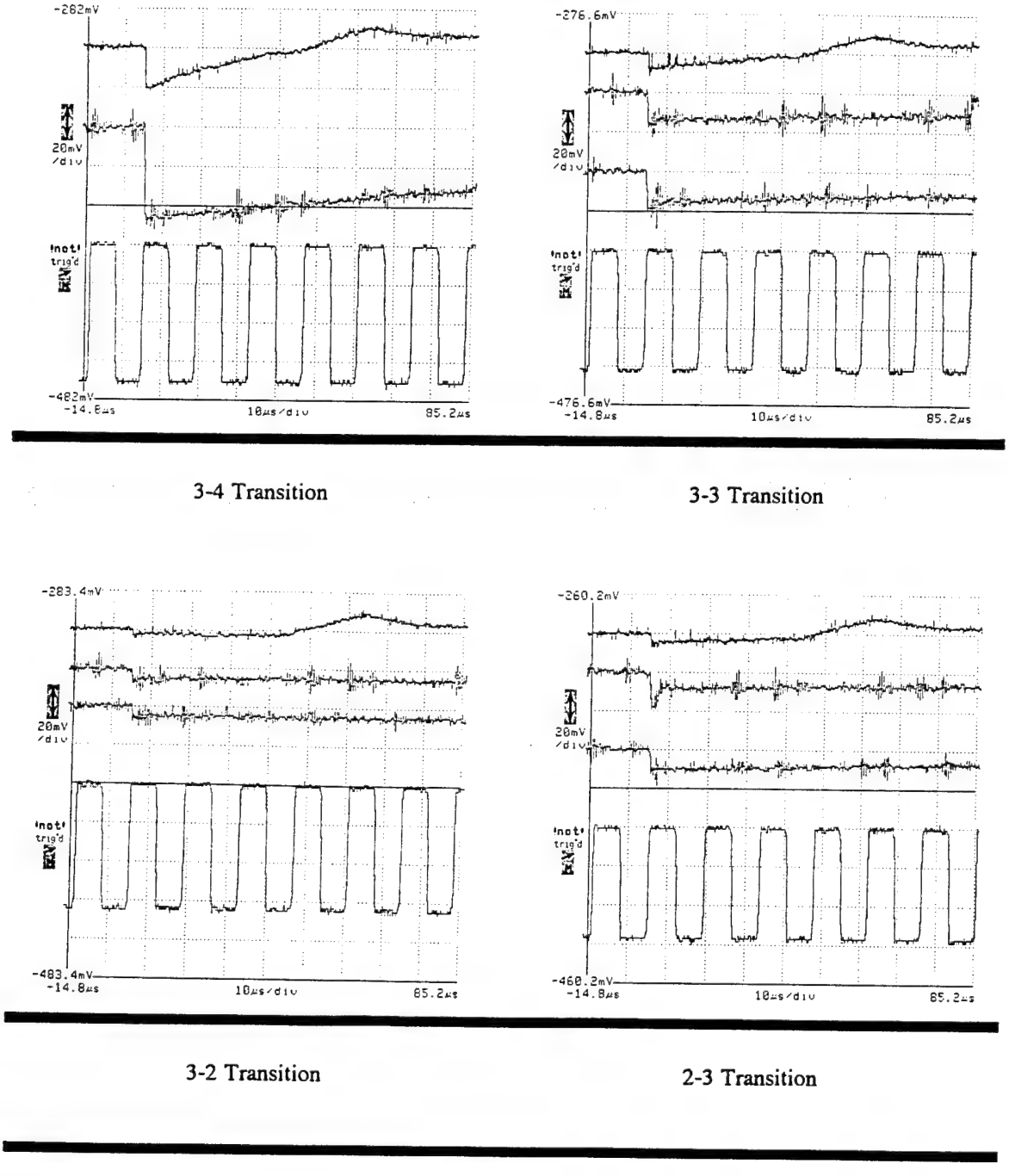

3-4 Transition

3-3 Transition

3-2 Transition

2-3 Transition

Figure 3-14 Gain Measurements (8 OCT 92)

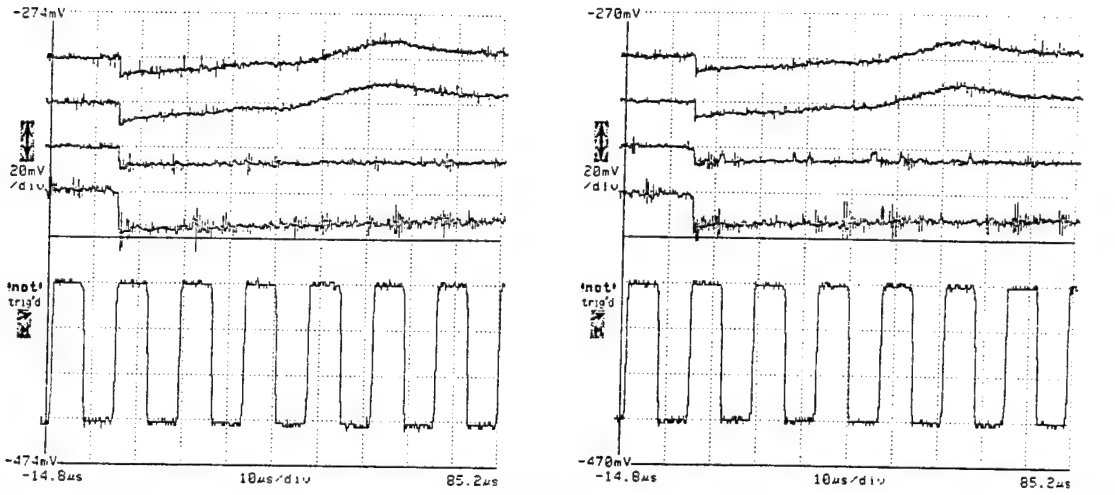

2-2 Transition

2-1 Transition

Figure 3-14 Gain Measurements (8 OCT 92) (continued)

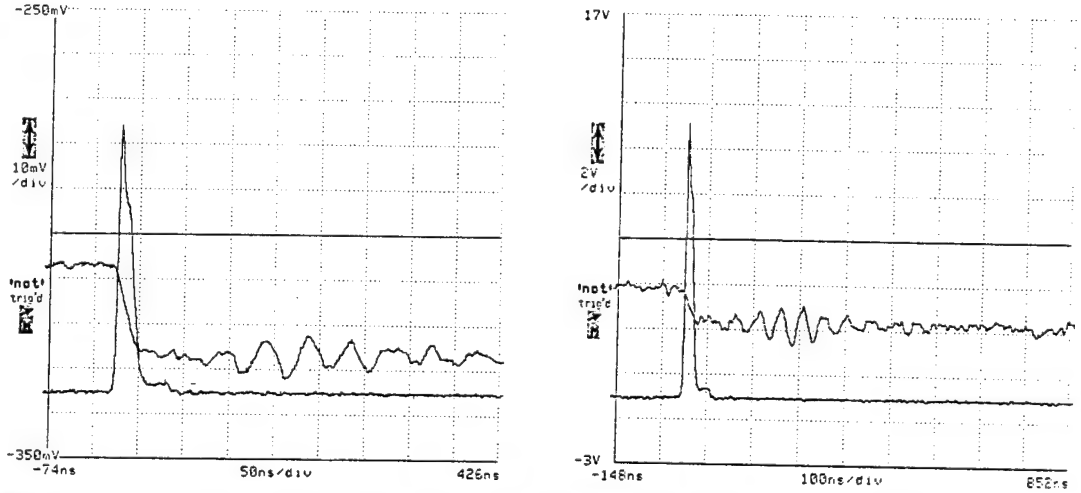

3-4 Transition

3-3 Transition

Figure 3-15 Transient Gain Measurements (9 OCT 92)

between traces. Actual gain will be extracted from these plots in a later section. Figure 3-15 shows gain measurements made for all six radiative transitions on 9 October 1992

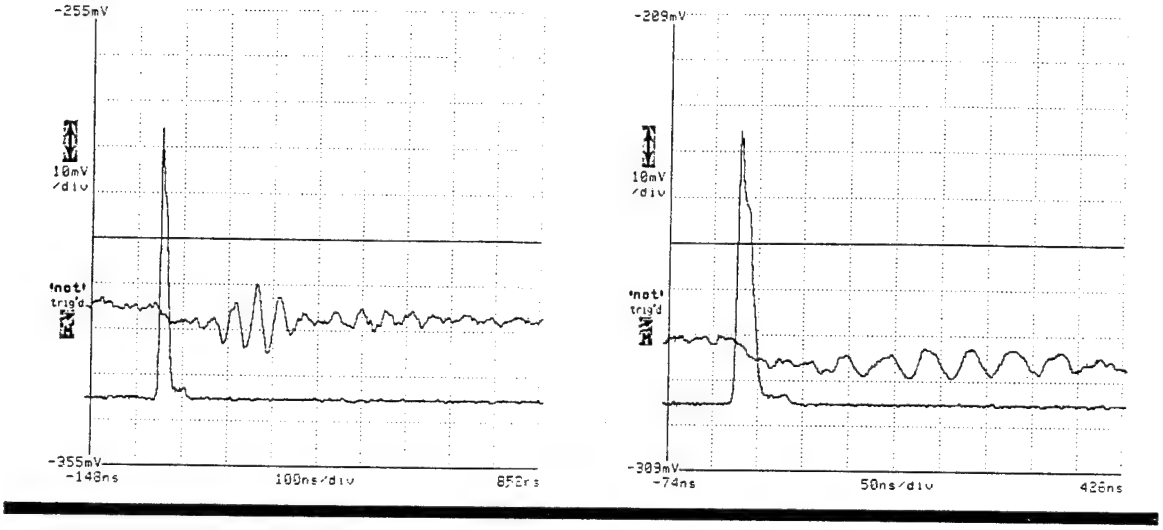

3-2 Transition

2-3 Transition

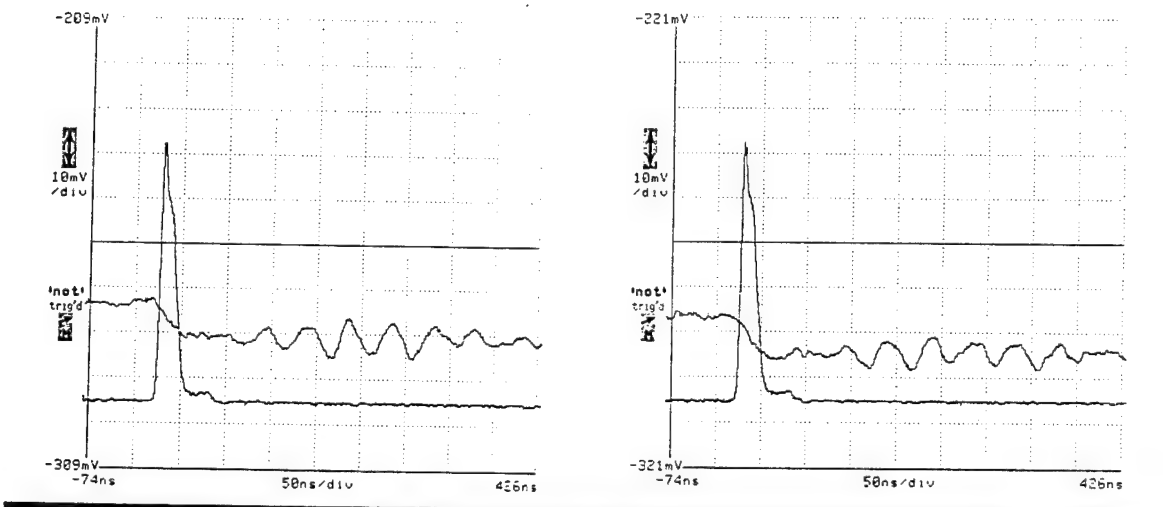

2-2 Transition

2-1 Transition

Figure 3-15 Transient Gain Measurements (9 OCT 92) (continued)

for a pressure of 60 Torr. The time scale is displayed with the excimer photodissociation pulse to show how gain occurs on the time scale of the photolysis.

4. Results And Discussion

4.1 Comparison of Gain Measurements

A theoretical value for the small signal gain can be determined from a measurement of the amount of UV energy deposited in the CF_3I. Knowing the amount of the energy deposited in the CF_3I and that the photon yield is 100%, the number of I^* produced can be determined, and from this a maximum small signal gain can be calculated. The expression for the small signal gain on line center of the 3-4 transition is:

$$\alpha_{34} = \frac{A_{34}\lambda^2}{8\pi}\left(N_3^U - \frac{7}{9}N_4^L\right) f(\nu_0) \qquad \textbf{(2.2-2)}$$

The Einstein A coefficient for the 3-4 transition in atomic Iodine is 5.0 /s and the wavelength $\lambda = 1.315\ \mu m$. The absorption cross section of CF_3I at 248 nm is $\sigma = 3 \times 10^{-19}\ cm^2$. At 60 Torr the number density of CF_3I is 1.93×10^{18} atoms/cc. Using Beers law and transversely pumping 2 cm of CF_3I we find:

$$\frac{\bar{I}_0}{\bar{I}_I} = e^{-\sigma[CF_3I]\ell} \sim \frac{E_0}{E_I} = e^{-1.158} = 0.314 \qquad \textbf{(2.2-69)}$$

The energy absorbed by the CF_3I is the difference between the energy incident on the cell, and the energy measured after the cell. If the excimer pump energy is 175 mJ the energy deposited in the 60 Torr of gas is 120 mJ. Figure 4-1 shows the measured UV energy deposited in the gas plotted on top of the theoretically predicted Beer's Law curve for a pump energy of 175 mJ.

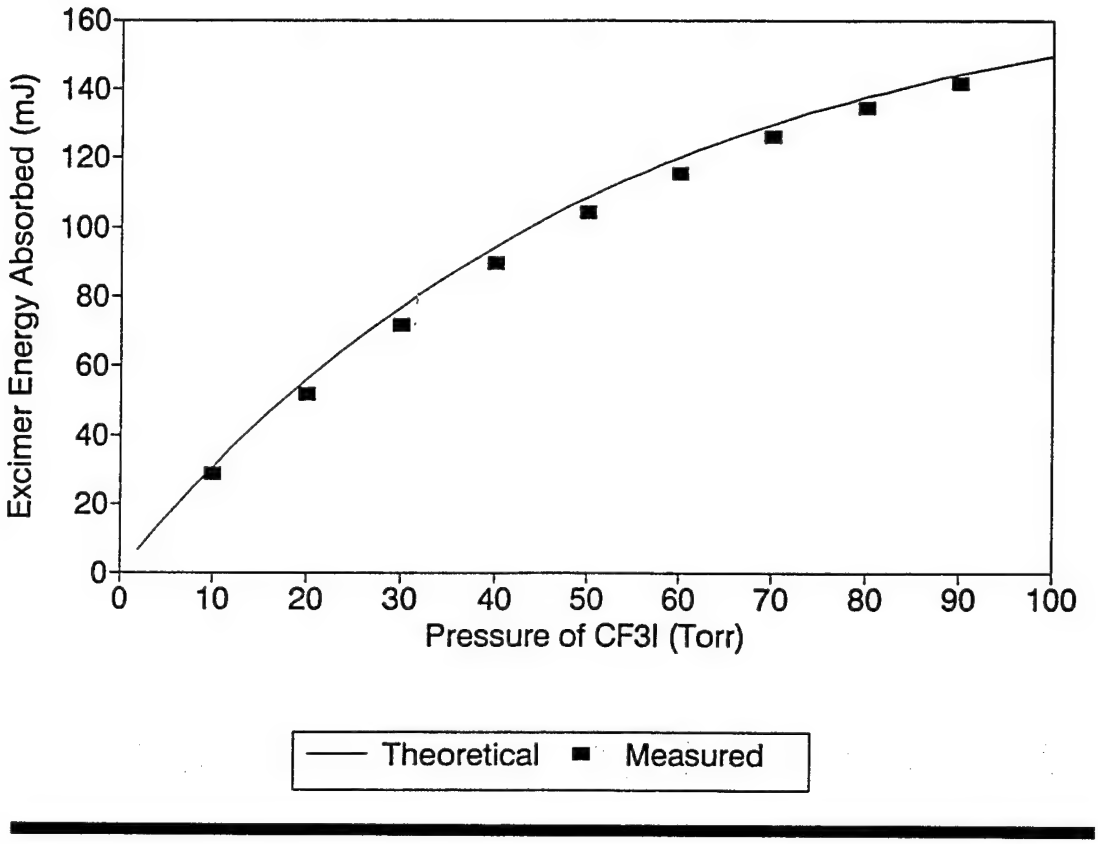

Figure 4-1. UV Energy Deposited in the CF_3I.

To define useful gain, the energy absorbed within the extraction volume was considered. For 60 Torr and an extraction aperture with a diameter of 1 cm centered in the gain region, the energy absorbed within the extraction volume is 34.79 mJ. The density of excited Iodine atoms within the extraction volume is calculated to be 1.99×10^{16} atoms/cc. The line shape function $f(\nu)$ can be approximated by a Lorentzian. At line center:

$$f_L(\nu_0) = \frac{2}{\pi}\frac{1}{\Delta\nu} \qquad \textbf{(2.2-10)}$$

Where $\Delta\nu$ is the sum of the products of the partial pressure of each species and their

broadening coefficients. Since the contribution from I and I* is small, $\Delta\nu$ can be approximated by just using the contribution from CF_3I. For a CF_3I pressure of 60 Torr and pressure broadening coefficient of 11.3 MHz/Torr we get $\Delta\nu$ = 678 MHz. The small signal gain for the 3-4 transition is then calculated to be 3.72%/cm. Since no losses are taken into account, this number can be considered a theoretical maximum value for the small signal gain within the extraction volume for the given pumping conditions.

Gain measurements using the tunable diode laser are shown in Figure 3-14. Comparing the change in intensity to the reference signal the gain plus loss for the 3-4 transition in the cell was found to be between 2.4%/cm to 3.1%/cm. This was done for each of the six possible laser transitions (Table 4-1). Figure 4-2 shows the resulting gain

Transition	Theory	Measured	Normalized
2-3	0.353	1.265	0.340
2-2	0.466	1.819	0.489
2-1	0.375	1.600	0.440
3-4	1.000	3.720	1.000
3-3	0.436	1.525	0.410
3-2	0.130	0.472	0.127

Table 4-1. Iodine Gain Measurements

measurements normalized to the 3-4 transition and plotted on top of a theoretical spectrum broadened with a Voigt lineshape function. An interesting phenomena that was observed is seen in Figure 3-15. Comparing transitions from the upper F=3 level to the lower F=2 level it is seen that gain appears on all transitions as the excimer photodissociates the CF_3I. This demonstrates that, on the time scale of the experiment, population must be born statistically in the upper two levels of the hyperfine structure.

The second set of gain measurements involved measuring the energy extracted from the I* laser while varying the reflectivity of the outcoupling mirror. This data is presented in Figure 4-3 in terms of I* laser energy and outcoupling mirror transmittance.

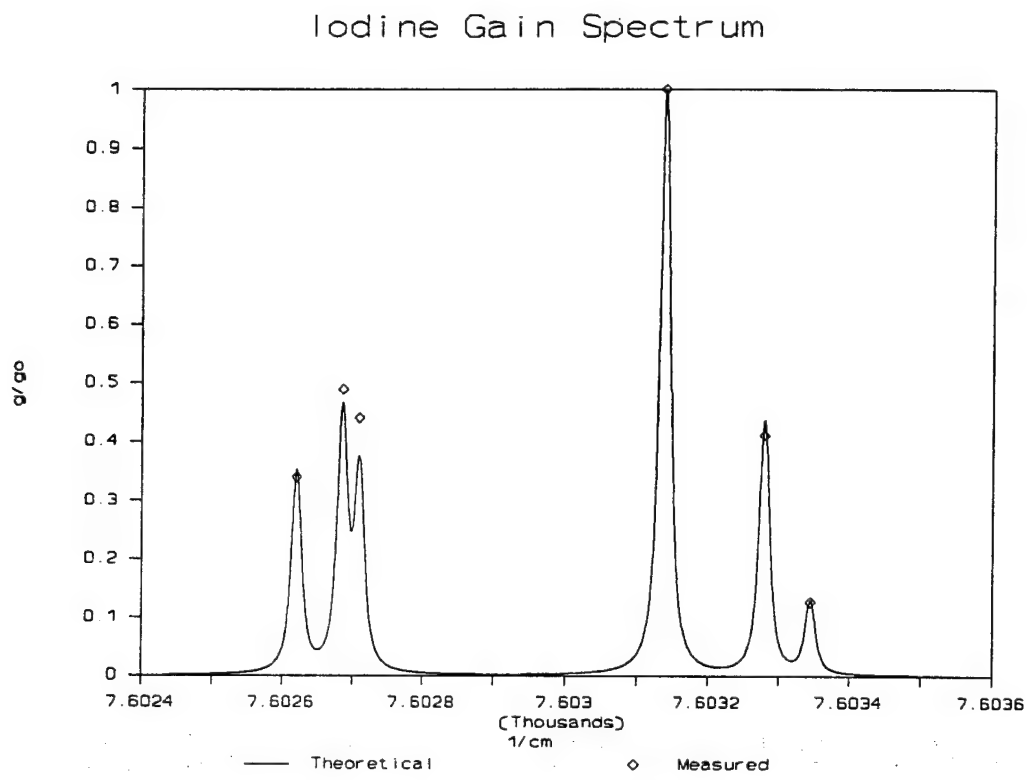

Figure 4-2 Normalized Gain Plotted on Theoretical Spectrum

At the peak of this curve, laser losses are matched optimally to the geometric parameters of the laser to give a maximum output energy. As the transmission of the outcoupler is decreased laser losses play a greater role and force the energy to drop. As the outcoupler transmission is increased, the threshold for lasing increases, and the extracted energy drops. In the limit as the energy goes to zero, the small signal gain equals the threshold gain, which can be expressed in terms of the geometric parameters of the laser:

$$\alpha_0 = \alpha_{th} = \frac{1}{2L_g} \ln \frac{1}{R_1 R_2} - \mathcal{L} \qquad (4.1\text{-}1)$$

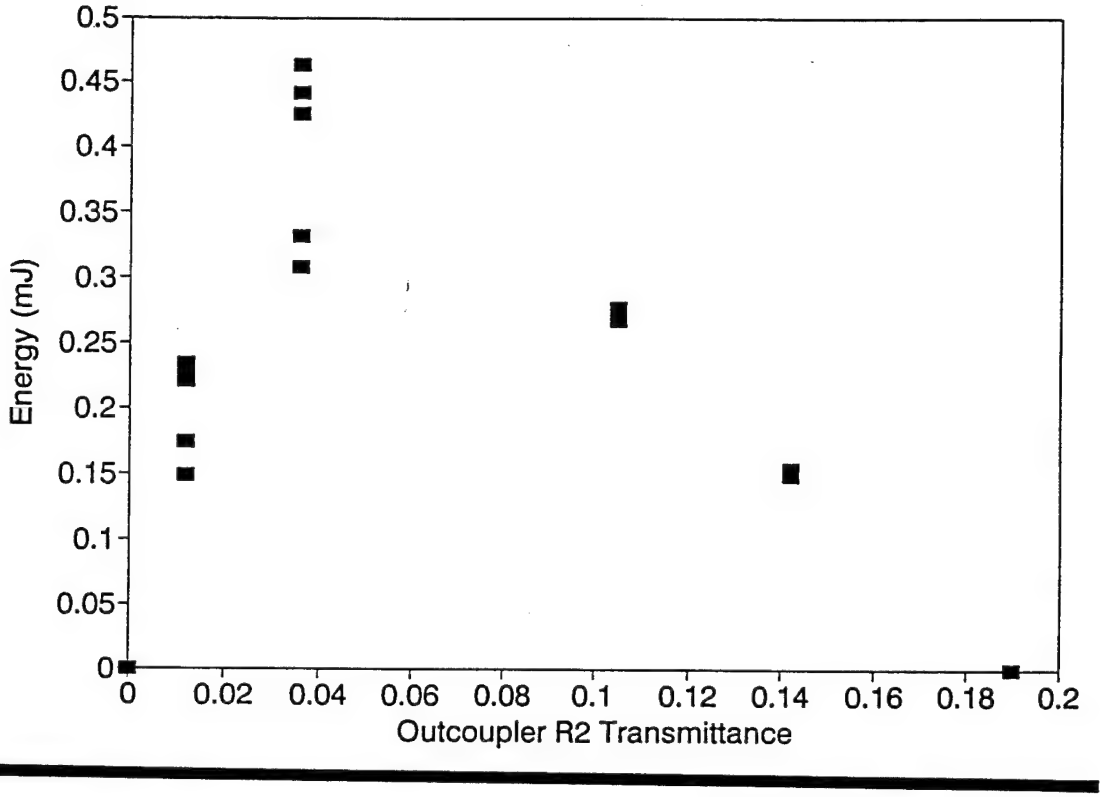

Figure 4-3 I^* Laser Energy versus Outcoupler Transmittance

If we assume our losses $\mathcal{L}$ are small, we can calculate our gain to be bounded between 2.7%/cm and 3.8%/cm By extrapolating we can get a nominal value of 81.5% for the outcoupler reflectivity which gives us a gain plus loss of 3.65%/cm. It is important to note here that even if there is some ambiguity in the exact values of energy measured, the fact that the laser lased at R2 = 85.8% and did not lase at R2 = 81% is enough to bound the gain plus loss.

4.2 Qualitative Comparison of Data to Rate Equation Model

In the last section we saw a quantitative comparison between small signal gain; theoretically calculated, and measured using several techniques. It is important to pin down a specific parameter of the laser system and understand it in a quantitative sense, but a deeper understanding of the system can be achieved by a comparison of the

measured laser pulse characteristics to the full rate equation model.

The following comparisons are introduced in a qualitative sense. A quantitative analysis will follow shortly after, using a select few of the data, bounded by theoretical error bars. The qualitative analysis will contain a study of outcoupling mirror reflectivities, various pressures, and finally varying cavity lengths. In the following plots, traces marked with numbers 1 or 2 are measured while traces marked with 3 or 4 are theoretical. Traces marked 1 or 3 are the excimer pump pulses and traces marked 2 or 4 are the I^* laser pulses. They are more easily distinguished by the theoretical pulses being smooth and the measured pulses being rough due to noise.

Figure 4-4 compares theoretical pulses to measured. Pressure is held constant at 60 Torr and cavity length is 16 cm. The Model assumes losses are negligible for this set of calculations. By adding in losses, the comparison between pulse energy is more favorable, but calculated pulse shape and cavity buildup time do not match the measured data. The experimental pulse shape for the 85.8% outcoupler is distorted most likely due to the fact that it is lasing close to threshold. Near threshold laser action is far from

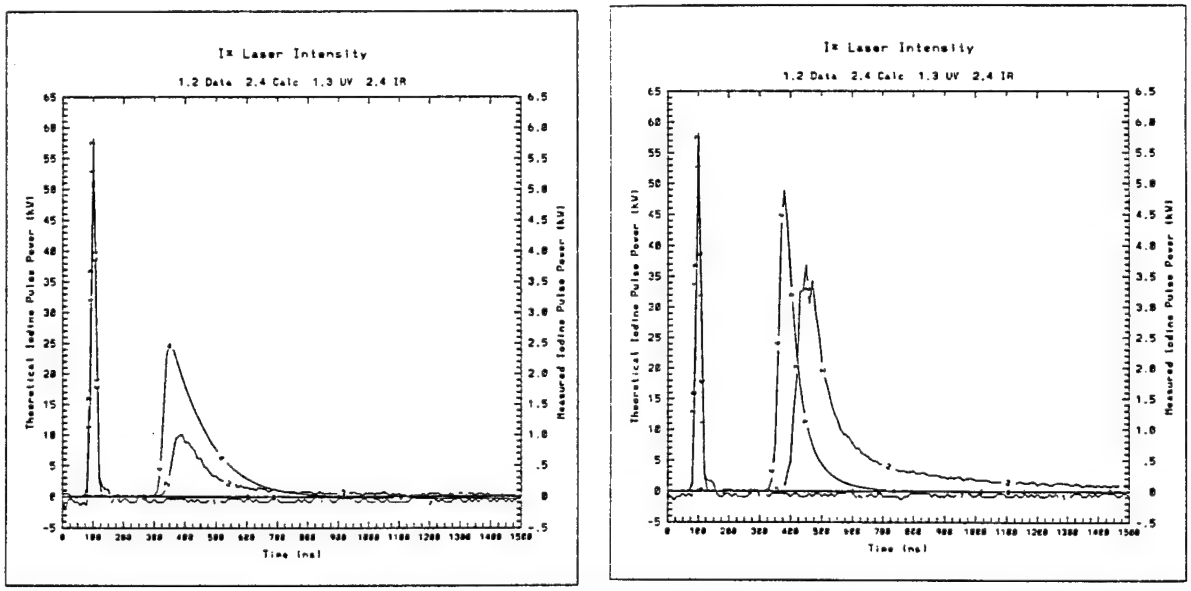

R = 98.8% R = 96.4%

Figure 4-4 Qualitative Comparison of Laser Pulses for Various Outcoupling Mirrors

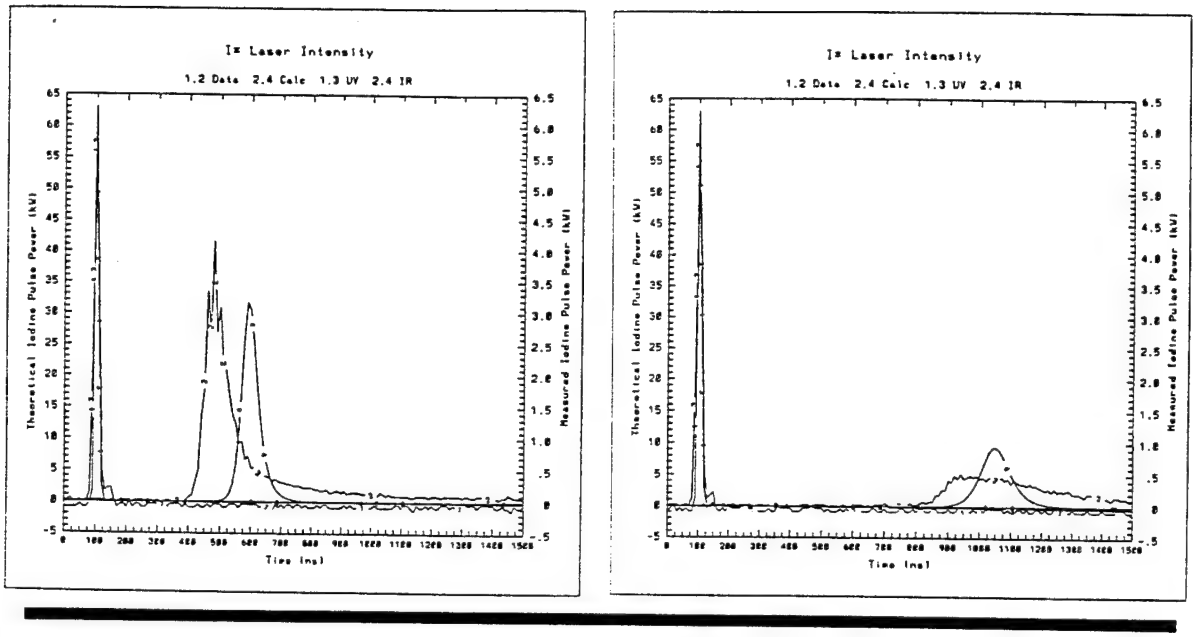

R = 89.5%

R = 85.8%

Figure 4-4 Qualitative Comparison of Laser Pulses for Various Outcoupling Mirrors (continued)

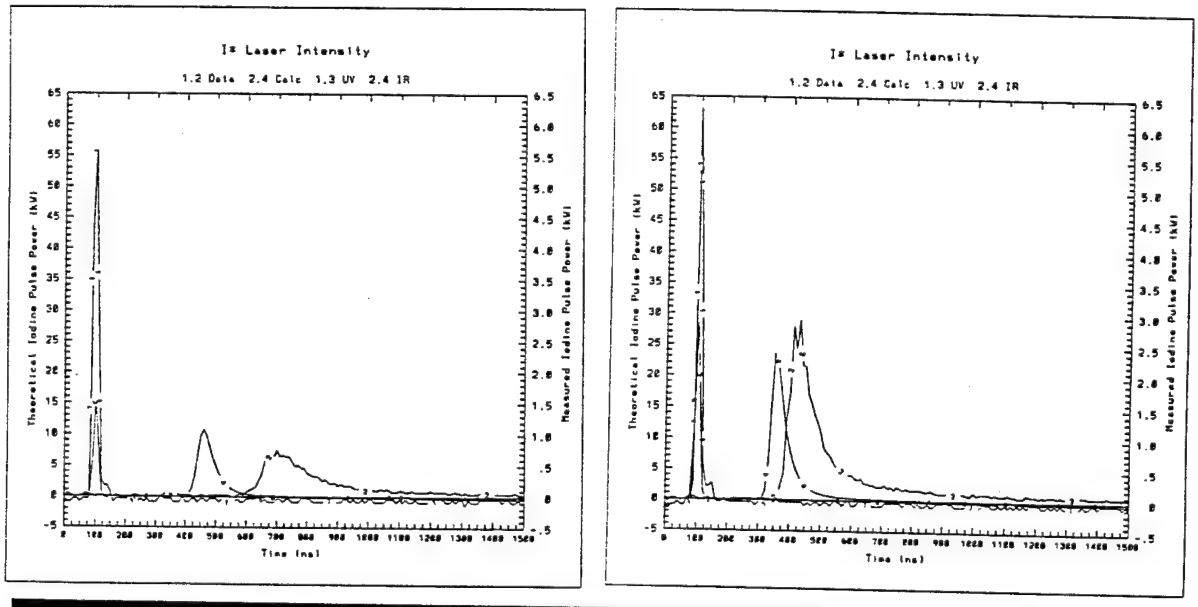

P = 10 Torr

P = 20 Torr

Figure 4-5 Qualitative Comparison of Laser Pulses for Varying Pressures

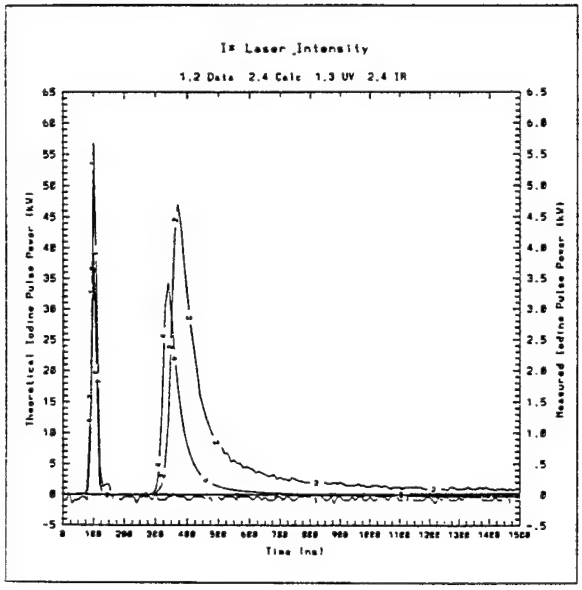

P = 30 Torr

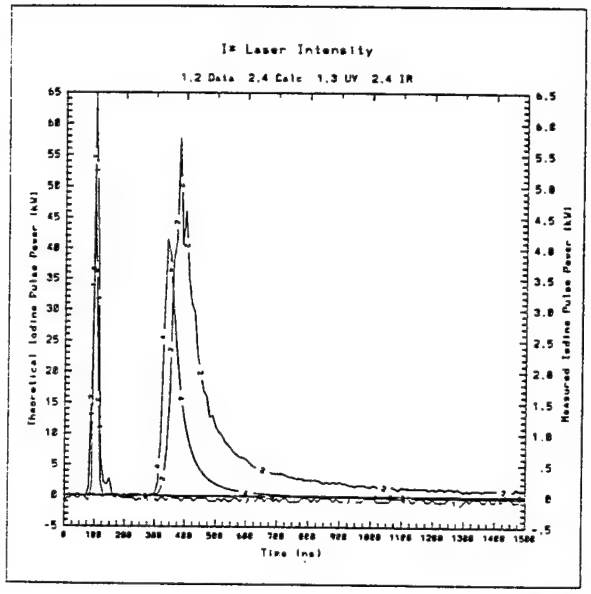

P = 40 Torr

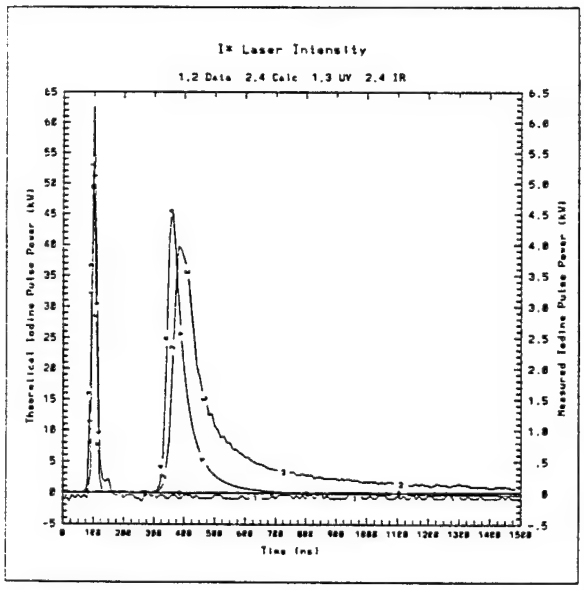

P = 50 Torr

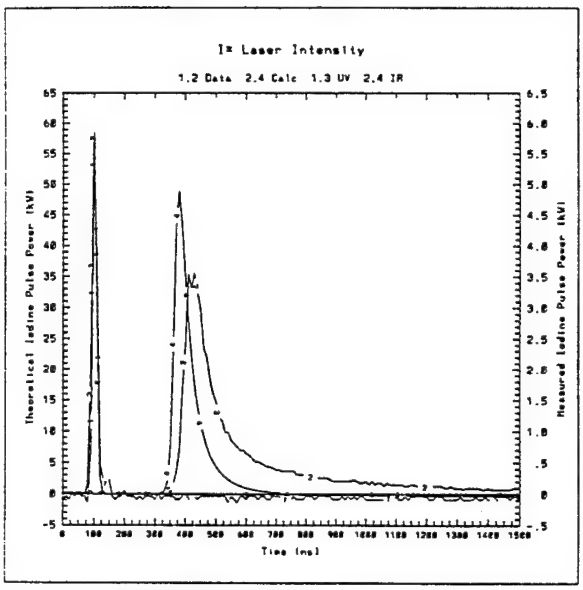

P = 60 Torr

Figure 4-5 Qualitative Comparison of Laser Pulses for Varying Pressures (continued)

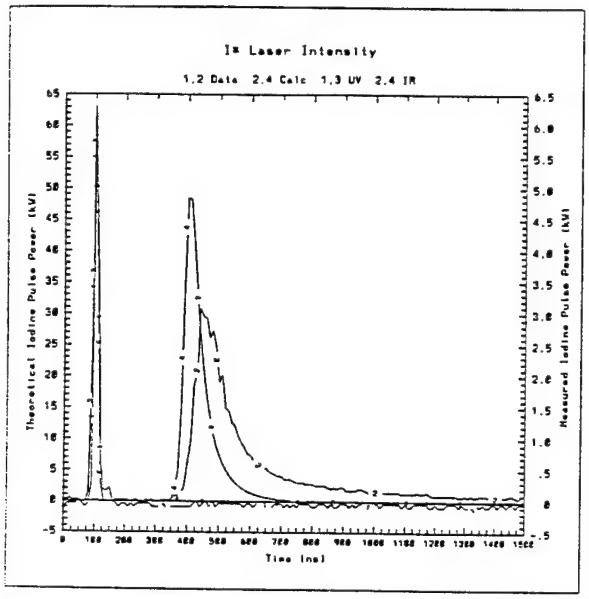

P = 70 Torr

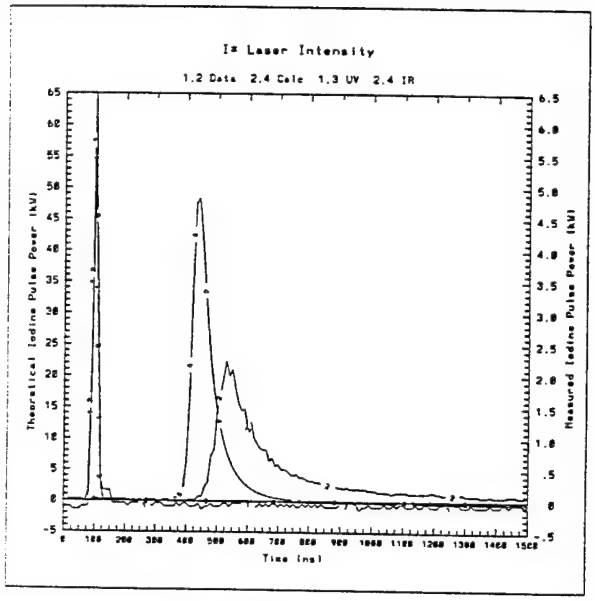

P = 80 Torr

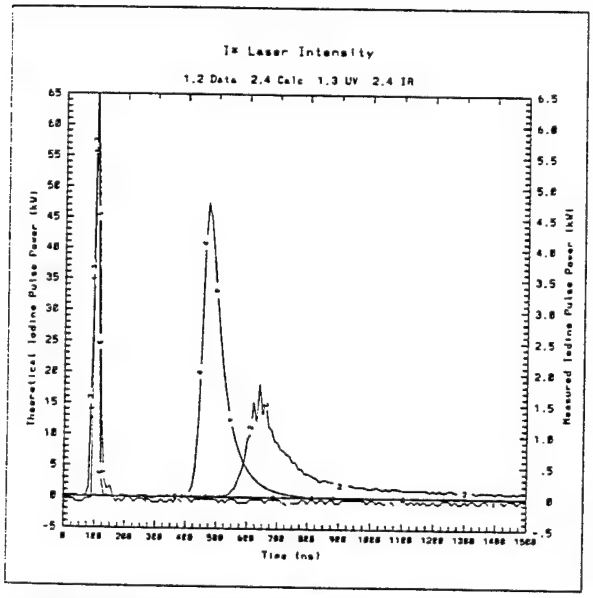

P = 90 Torr

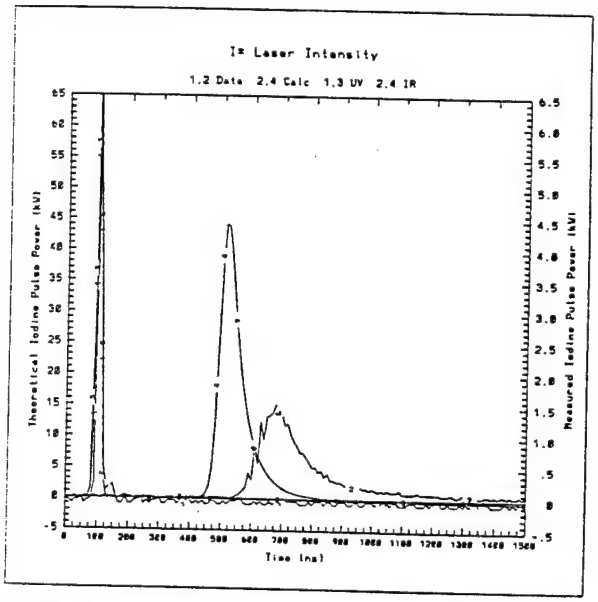

P = 100 Torr

Figure 4-5 Qualitative Comparison of Laser Pulses for Varying Pressures (continued)

ideal.

Figure 4-5 compares theory to experiment as pressure ranges from 10 Torr out to 100 Torr. Cavity length is 16 cm and outcoupler reflectivity is 96.4%. Modeling again assumes no losses. It is important to see that for low pressures the pulse is wide and the buildup time is large. As the pressure increases, the pulse width decreases, and the buildup time shortens. After 30 or 40 Torr the buildup time increases again and so does the pulse width.

Figure 4-6 shows how the lasing characteristics change with cavity length. Pressure is fixed at 60 Torr and outcoupler reflectivity is 96.4%. The model assumes no losses. As it was discussed in Section 2.4, cavity length variations affect buildup time and pulse width. Figure 4-6 show that theoretical and measured buildup times and pulse widths compare favorably as well as the actual shape of the pulse. The last two plots in Figure 4-6 summarize the effect nicely. From this set of comparisons it is seen that both theory and experiment compare favorably in a qualitative sense. The rate equation model, assuming no losses, produces theoretical laser pulses which act similar to the

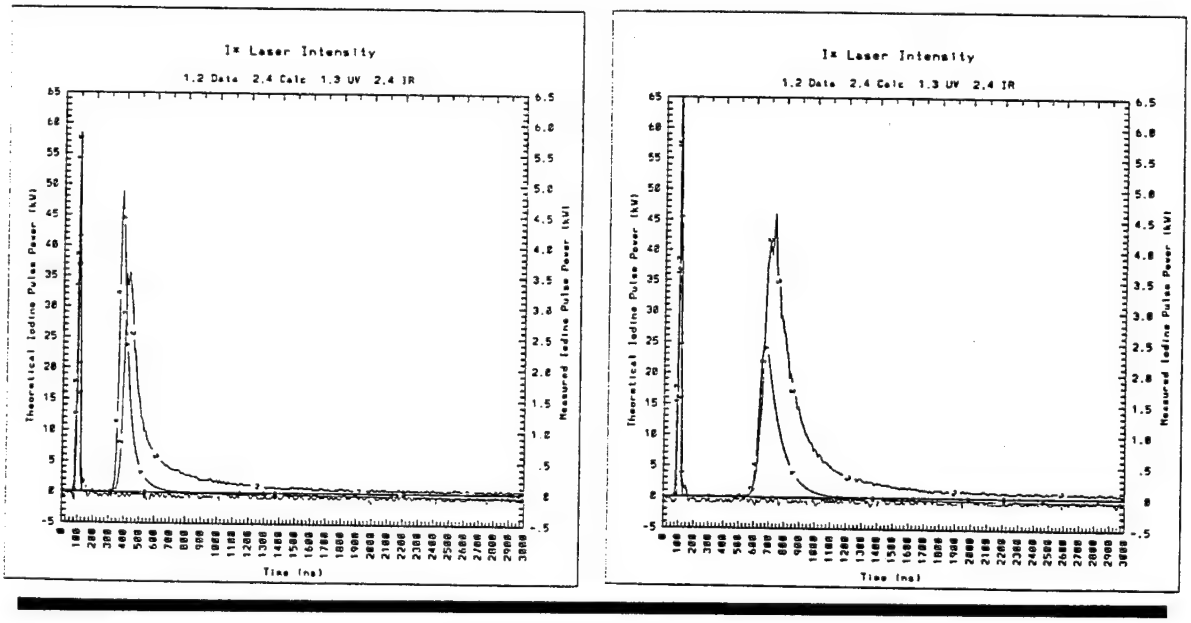

D = 16 cm D = 32 cm

Figure 4-6 Qualitative Comparison of Laser Pulses for Varying Cavity Lengths

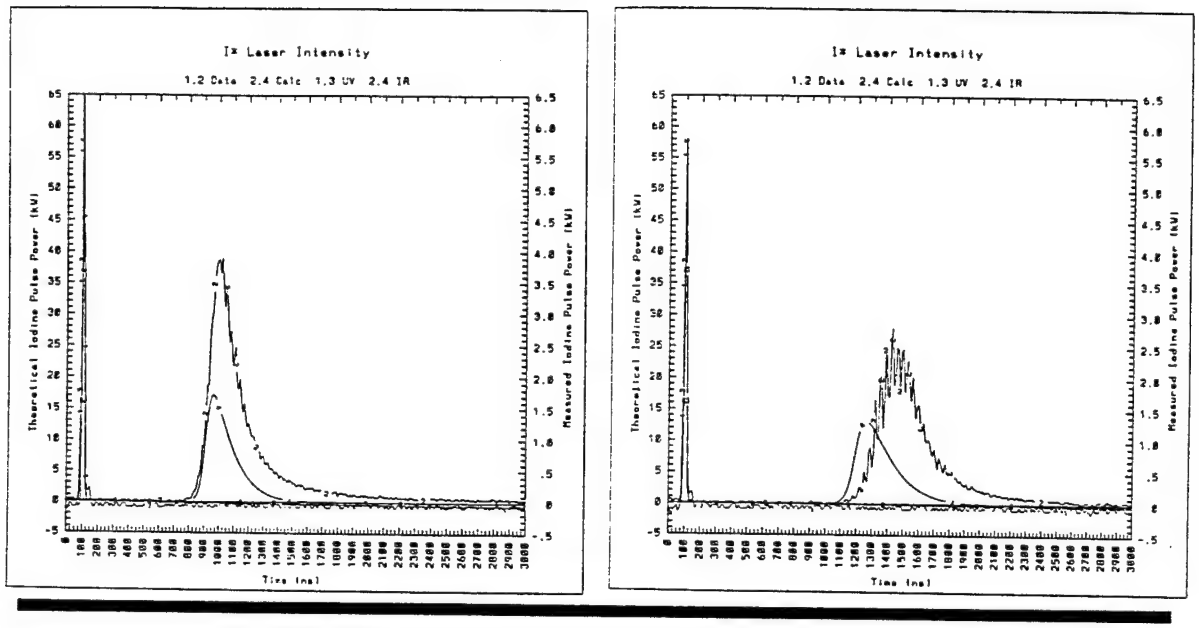

D = 48 cm

D = 64 cm

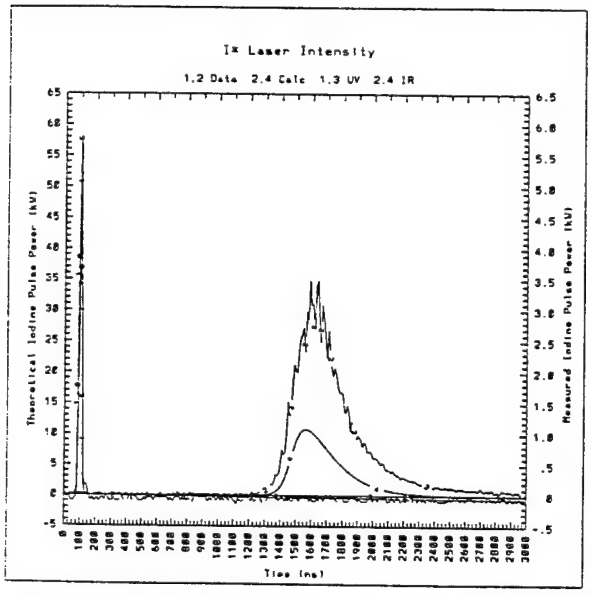

D = 80 cm

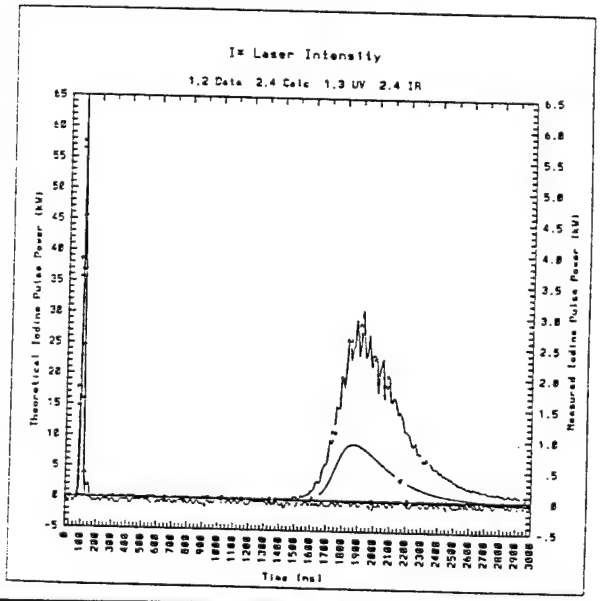

D = 96 cm

Figure 4-6 Qualitative Comparison of Laser Pulses for Varying Cavity Lengths (continued)

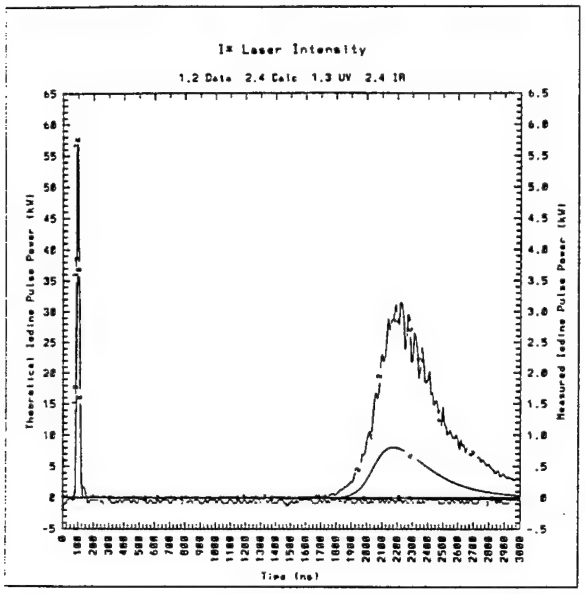

D = 112 cm

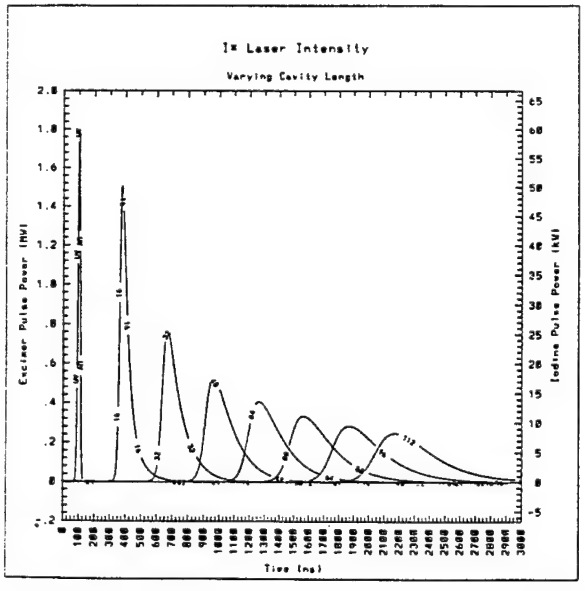

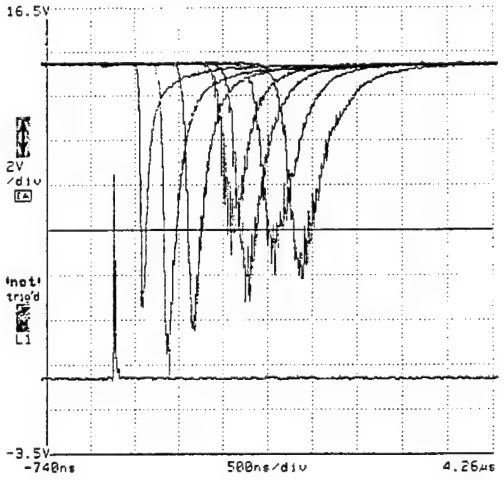

Summary of Theoretical

Summary of Measured

Figure 4-6 Qualitative Comparison of Laser Pulses for Varying Cavity Lengths (continued)

measured intensities as parameters are varied. The next section will deal with a qualitative comparison, introducing error bars on theory and experiment, and explaining any discrepancies between the two.

4.3 Error Analysis and Quantitative Discussion of I^* Laser Data and Rate Equation Model

Looking back and comparing Figure 2-26 to Figure 4-3 we see that there is a fairly large disagreement between theoretical and measured intensity despite the reasonable qualitative comparison of the last section. The purpose of this section is to analyze possible causes of this discrepancy and suggest reasonable modifications to the rate equation model to bring theory into line with experiment. This quantitative discussion will include an error analysis which will show how possible sources of uncertainty influence the final solution of the rate equation model.

The first step in any quantitative analysis is to determine all possible sources of error. Both the experiment and the rate equation model have many variables which must be considered. The code has been developed and tested over a period of several years and the approximations and assumptions which have made it numerically tractable have been discussed and justified in Chapter 2. Despite this thoroughness there is still the possibility that something may have been overlooked. Numerical accuracy of the equation solver must be considered, as well as uncertainty in the input parameters to the code. One thing that was not discussed in Chapter 2 but which may have bearing on the theoretical analysis is the mode structure of the laser and the simplistic resonator model assumed by the code. Experimental technique has also been perfected over a period of several years and reproducibility has been achieved through the method of exhaustion. Error which must be considered for the experiment may include measurement device precision and accuracy and the idealness of experimental conditions such as gas purity, beam quality, and mirror reflectivity.

The first source of error that I wish to discuss is the numerics involved in solving sixteen stiff coupled differential equations. Stiffness is a term used to describe the behavior of a system of differential equations. Fundamentally this can be described by

how quickly the solution changes with respect to the ordinary time increment of the integrator or solver. A more in-depth discussion about stiffness can be found in [66]. The system of equations used in the model is definitely stiff. The I^* laser pulse builds rapidly out of the noise and this must be taken into account by the time step of the integration. The DLSODE solver, mentioned in Section 2.4, uses the Adams-Bashford technique to compensate for stiffness. This technique basically uses the jacobian of the system of equations to adjust the time step used during stiff portions of the integration. There are two limits in which the numerics of the problem make it difficult for the solver to integrate. One limit is when outcoupling losses are close to the threshold gain, and the other is when outcoupling losses and other internal losses are close to zero. The first case is seen in Figure 2-27. The second case is seen in the variation from linearity of the plot in Figure 2-19b as plot approaches the discontinuity at zero outcoupled loss. Except at these limits, the solver appears to behave well.

There are many parameters which serve as inputs to the model. These are seen in Table 2-13. Gain length and cavity length are precise. An aperture is used to define gain length and the mirror spacing of the stable resonator is closely measured. Small variations (1-2%) in either parameter do not have a significant effect on the output of the code. Spatial linearity of the pump beam incident on the gain region is questionable. Care was taken to use the aperture to select what appeared to be a fairly linear region of the pump beam. A burn mark from the pump laser is seen in Figure 4-7. The pump

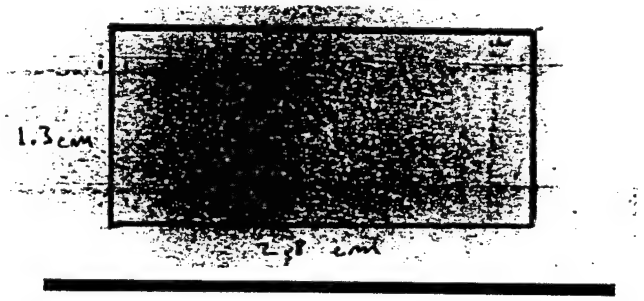

Figure 4-7 Spatial Characteristics of Pump Pulse

energy measurement is fairly reliable. Pump pulse energy measurements by three

different joulemeters compared favorably. The meters, however, are still only accurate to within 10%. The temporal characteristics of the photodissociation pulse are not quite the Gaussian assumed by the code, but differences should have insignificant effect on the final comparison since photodissociation occurs some time prior to lasing. Out of all the pump pulse errors mentioned thus far, the 10% uncertainty of the total photodissociation energy seems like it would have the largest influence on the final solution. Figure 4-8 shows that as excimer energy is varied, the extracted energy changes as well as the cavity buildup time. A distributed loss of 0.1%/cm is assumed as well as 100% quantum yield. Data is plotted as solid black triangles. Quantitatively the extracted energy is brought into better agreement while cavity buildup time agreement is made worse. Most likely, this error alone cannot account for the difference between data and theory.

Iodide pressure is another input parameter which is known with a large degree of certainty. A frequently calibrated set of 100 Torr baratron heads are used to determine the pressure to within 1%. There is a definite change in pressure (and temperature) immediately upon photodissociation which is hardly noticeable since it returns to normal upon recombination. This could introduce an acoustic noise within the cell, but the size of the cell dictates that the acoustic wave be on the order of 6 kHz. This is much slower than the time scale of the experiment. Thermal velocities, as mentioned earlier in the beginning of Section 2.4, reach a Boltzmann distribution on a much shorter time scale than the experiment due to the pressure range under consideration. At lower pressures thermalization of velocities could become a significant problem. At 17 Pa of n-C_3F_7I it takes about 5 μs to reach a Boltzmann velocity distribution [67].

The I^* quantum yield is another input parameter in question. Measured values of this are seen in Table 2-11 to vary between 75% to 98%. I would guess that this difference in measured quantum yields is due to differences in the purity of the gasses used. In the early stages of my experiment I found a difference in I^* laser energy between two bottles of CF_3I purchased from the same company. After this observation, all measurements were made from the same bottle of CF_3I. A filter using copper wool was also added before the bottle to remove possible iodide impurities. Attempts to use a freeze thaw method of purification were considered but never made. This would be

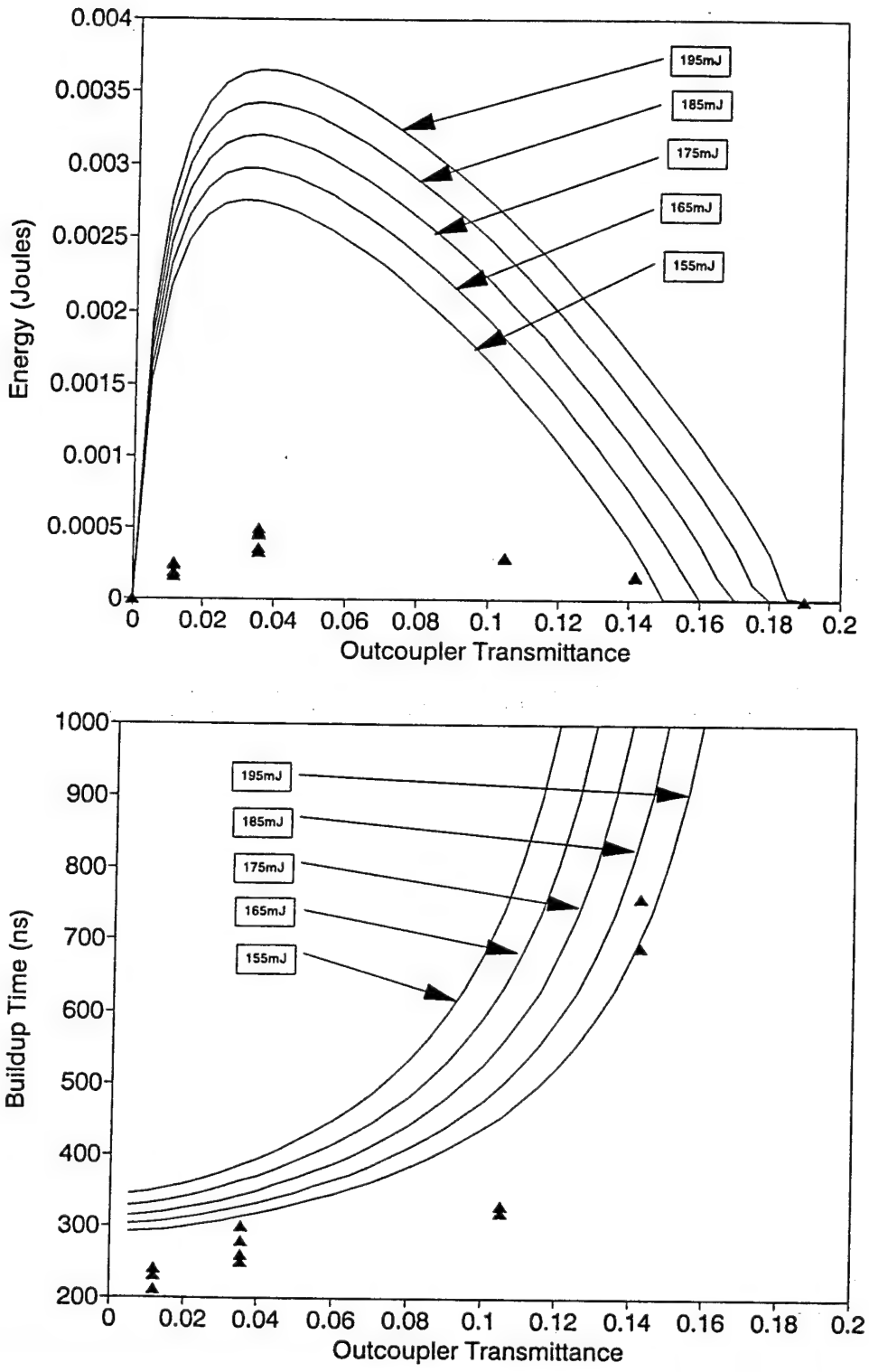

Figure 4-8 Error Bounds Due to Pump Pulse Energy Uncertainty

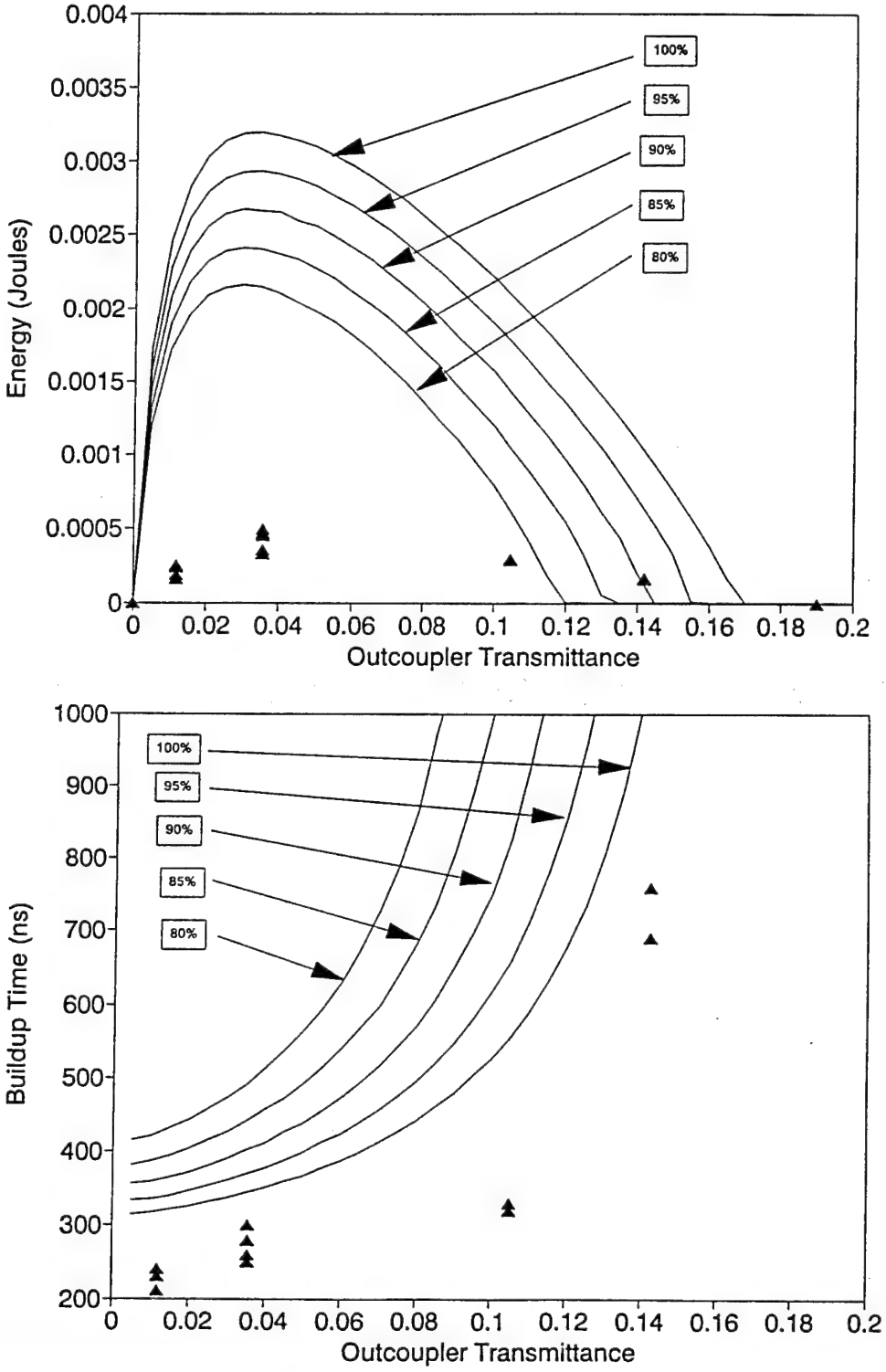

Figure 4-9 Error Bounds Due to Uncertainty of Quantum Yield

highly recommended for future work if precise quantitative measurements are desired and the time and facilities are available. Figure 4-9 Shows that the influence of varying the quantum yield is similar to that of varying the pump energy. This is intuitive since both contribute to the total I^* population. The two errors might have a compensating effect on one another. Most likely, error here can also be dismissed since there is a tradeoff in agreement between energy an cavity buildup time.

The hyperfine relaxation rate constants are input parameters which are not very well known. The influence of these rate constants is seen mainly in the I^* laser pulse shape. Figure 4-10 shows the effect of varying the upper level relaxation rate constant. The lower level relaxation rate constant is assumed to be fast. The discrepancy seen in the energy plot when the rate constant is 1.0×10^{-10} cc/s due to the two line lasing effects observed in Figure 2-22. At an outcoupler transmittance less than about 5% two line lasing does not occur, but greater than 5% two line lasing becomes apparent. Little more than an estimate is known of the hyperfine relaxation rates. Observation of where the two line lasing occurs may be suggested as a method for determining the upper level rate constant. For now we must assume a calculated value of 1.5×10^{-9} cc/s.

Significant parameters within the laser cell which introduce error include distributed loss and window transmission loss. Upon photodissociation, I_2 forms in the cell. This is seen after several shots as crystalline deposits on the cell walls. Quenching by I_2 is slow (2.2-46) and is accounted for in the model, but absorption of UV or IR light by the dimer must be factored into the code as a loss if deposits occur on windows or if residue I_2 remains in the cell from previous shots. The cell is evacuated to less than 0.050 Torr between shots to remove residual I_2. It was noticed, however, after about three test days there would be a significant drop in I^* laser energy. It was found that this could be attributed to I_2 deposits on the windows which could not be removed by vacuum. These deposits can be modeled with a window transmission loss or by distributing it over the cavity, but the best way to take care of the problem to ensure the least amount of error in modeling is to clean the windows before every test day. Since cleaning the windows opens the cell up to atmosphere and introduces water vapor (another possible distributed loss and quencher!), the precautions taken were to clean the windows the night before testing and let the system pump out any water vapor overnight.

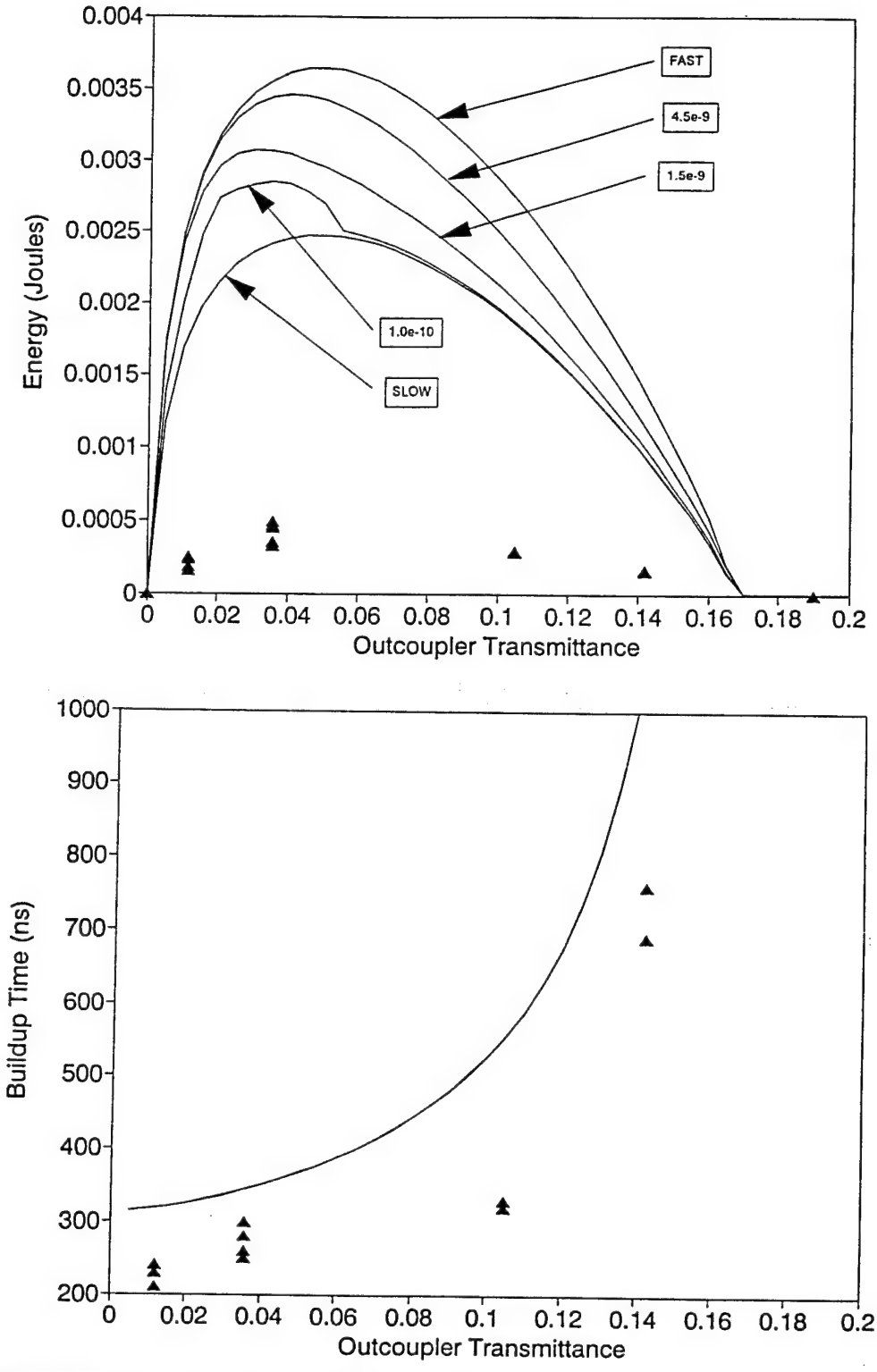

Figure 4-10 Influence of Uncertainty in Hyperfine Relaxation Rate Constant

A heating coil was used to "bake" any water out of the system. As it was seen in Figures 2-26 and 2-27, window transmission loss and distributed loss affect laser performance in a similar manner, thus it is possible to lump the window losses into the distributed loss. The gain of Section 4.1 bounds this loss to be less than 1 %/cm. A nominal value is 0.07 %/cm. The theoretical calculations of Figure 2-26 suggest that it is less than 0.1 %/cm. All this speculation is based on equation 4.1-1. Figure 4-11 shows the influence of adding a distributed loss. Similar to the energy and yield uncertainty, there is a tradeoff in comparison between energy and buildup time. In addition to this, baseline calculations give a very reasonable estimate of distributed loss. Most likely, good comparison cannot be achieved through adjusting our distributed loss.

Error introduced outside the cell but still within the resonator can be described by mirror scattering and absorption losses and accuracy of outcoupling mirror reflectivities. The set of outcoupling mirrors was measured several times at the Phillips Laboratory Metrology lab. A list of transmissions and reflectivities measured for some of the mirrors at 1.315 μm is seen in Table 4-2. From these values a scattering plus absorption loss might be estimated, except for the fact that a few of the measurements hint that several of the mirrors have a small amount of gain associated with them. The precision of the measurements may be questionable, but the accuracy should be close enough to provide a good input parameter for the code. Scattering and absorption losses appear to be negligible: 0.001 is a reasonable value for most clean mirrors. Uniformity of the mirror coating was checked and found to be satisfactory.

Alignment of the laser is another factor. The alignment procedure developed using the diode laser was discussed in Section 3.1. A suggestion for improving alignment technique is to flow the CF_3I and adjust the energy to a maximum through alignment. Another option is to use t-C_4F_9I. t-C_4F_9I has been found to have much better recombination characteristics than CF_3I which allows for multiple shots off a single fill [68]. I satisfied myself with the diode laser alignment technique by reproducibility of the measurements.

Error outside the cavity can be limited to the beamsplitter, the joulemeter, and the fast detector. The fast detector is the least likely source of any error. The 4 GHz bandwidth is sufficient to measure a 50 ps pulse, as long as the detector was not

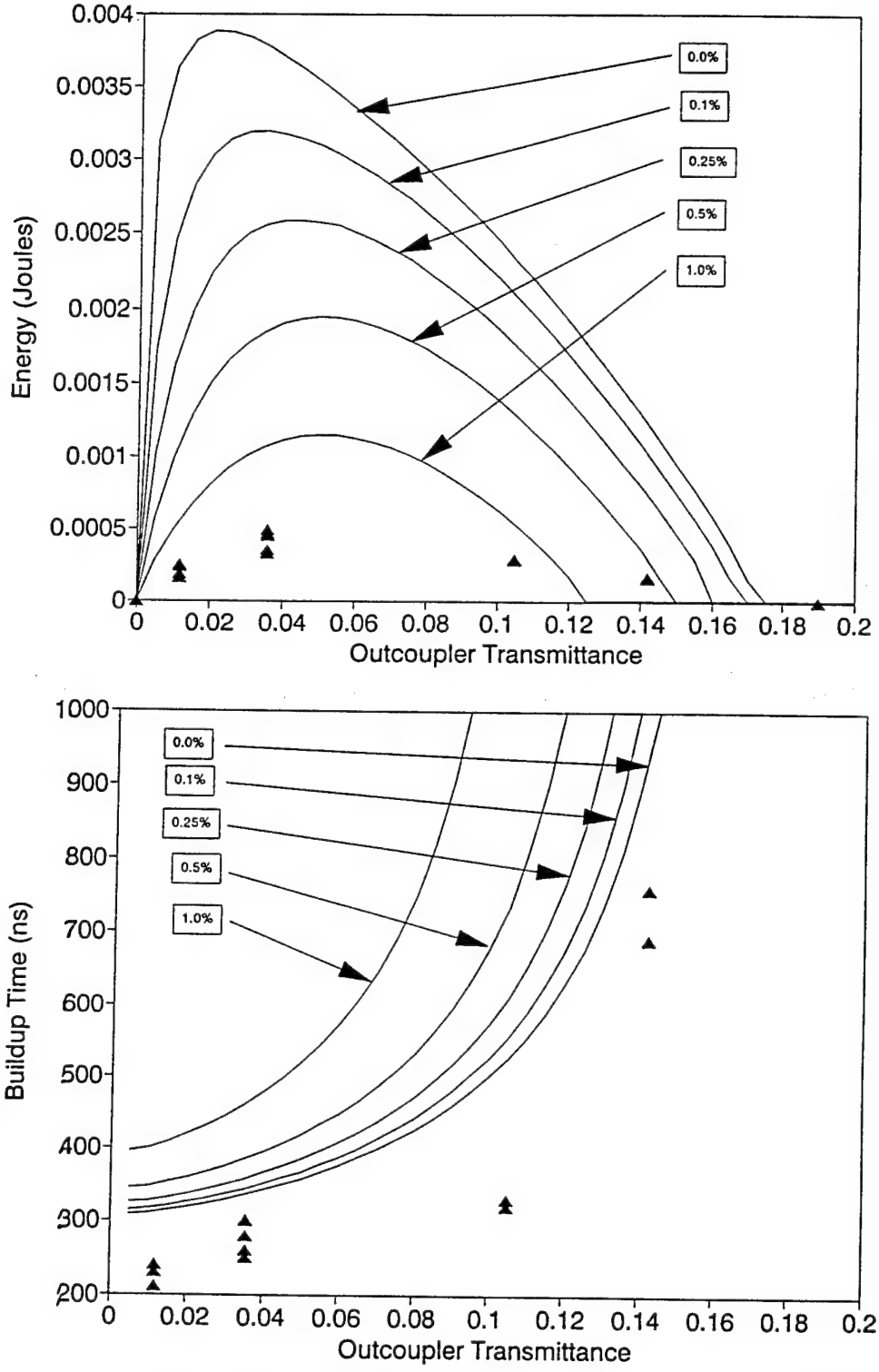

Figure 4-11 Influence of Distributed Loss

saturated! The beamsplitter at 7% per surface and a stack of neutral density filters were used to ensure that no saturation occurred. The detector was not used to measure absolute energy, but only cavity buildup time and pulse shape. The transmittance of the beamsplitter was measured with the diode laser at the proper orientation to the

Serial Number	Reflectance	Transmittance
92629-01	0.97958	0.00970
92629-02	0.81869	0.18480
92629-03	0.90694	0.08748
92629-04	0.96415	0.04153
92629-05	0.69951	0.30370
91509-01	0.987	
91509-02	0.988	
91509-03	0.941	
91509-04	0.934	
91509-05	0.814	
91509-06	0.793	
91509-07	0.858	
91509-08	0.851	
91509-09	0.893	
91509-10	0.895	

Table 4-2 Measured Outcoupler Transmission and Reflectivity

polarization of the light and found to have an 86% transmission (7% loss per surface is assumed), and this was factored into the energy measurement. Energy was measured with three joulemeters with slightly different results. The best, most expensive, and most suitable joulemeter for low energy short pulsed measurements was chosen to be believed. The outcoupled energy reading can be believed to be accurate to within a factor of two.

Obviously the largest source of error outside the cavity is the energy reading. However, we may safely assume that it is within a factor of two. One other important fact to note is that I never got a reading on the joulemeter without seeing a pulse on the fast detector, and seldom was a pulse seen on the fast detector that couldn't be measured

with the joulemeter. Care must be taken with some joulemeters which measure low energy since they are often susceptible to electrical as well as acoustic noise.

The final source of error which must be mentioned to conclude the quantitative analysis is the mode structure of the laser. The resonator model used in the code is a simple plane parallel resonator. The configuration used in the experiment is a hemispherical resonator. The code also assumes the laser is operating in a single transverse mode; the TEM_{00} mode. More than likely, the actual device is operating in many transverse modes. It is likely that these modes introduce losses which cannot be modeled as a distributed loss, but significantly affect the outcoupled power of the laser. To solve the problem, it might be suggested to aperture the cavity down to the TEM_{00} mode. The size of aperture required to do this can be found by calculating the spot size of the TEM_{00} mode at the location of the aperture within the cavity. Placing the aperture close to the flat outcoupling mirror R_2 we calculate the resonator parameters to be $g_1 = 0.984$ and $g_2 = 1.0$ from [69]:

$$g_1 = 1 - \frac{D}{R_1} \qquad g_2 = 1 - \frac{D}{R_2} \qquad \textbf{(4.3-1)}$$

The spot size is found to be [70]:

$$w_2 = \left(\frac{D\lambda}{\pi}\right)^{\frac{1}{2}} \left(\frac{g_2}{g_1(1 - g_1 g_2)}\right)^{\frac{1}{4}} = 0.73\,\text{mm} \qquad \textbf{(3.1-1)}$$

From this calculation we see that most likely the laser which used a 1.0 cm aperture was running in a multi-transverse mode. The problem with aperturing the system to a single mode introduces difficulties with alignment. There is also some uncertainty that the aperture will not select the TEM_{00} mode but will select one of the transverse modes to lase on instead.

The extraction volume is well defined by a 1.0 cm diameter aperture, but if the transverse mode structure is not known, there may be some uncertainty associated with this parameter in the model. Figure 4-12 shows the effect of varying the size of the aperture. The calculations use a distributed loss of 0.1%, a pump energy of 175 mJ, and a yield of 100%. If the experiment were favoring single mode operation, or at least the intensity across the laser beam were concentrated in the single transverse mode, I could decrease the aperture in the experiment down close to single mode with little or no effect on intensity, and thus achieve the effect in Figure 4-12. Experience in the lab, however, tells me that if I were to close the aperture down to the single mode, the energy would also drop nearly proportional to the square of the radius of the aperture. This was seen when the energy dropped from a few mJ's down to half a mJ when the 1 cm aperture was added to the system. Current work also shows that the energy falls off nearly proportional to the square of the radius of the aperture. If this is truly the case, most likely the resonator model in the code is valid; however, the modeling of losses due to the higher order transverse modes may not be appropriate.

Looking at all of the error studies performed thus far, the only two parameters which can be adjusted to bring the modeling into full quantitative agreement with the experimental measurements include changing the aperture size of the extraction area or multiplying the measured energy by a factor due to a possible factor of two error in the joulemeter used to measure I^* laser energy. Even the error in the energy measurement cannot alone account for the discrepancy observed. To bring the model in line with experiment it would seem justifiable to adjust the aperture accordingly. Figure 4-13 illustrates an optimal aperture size of 3.8 mm diameter to fit the data.

The only other possibility of adjusting the model to match the data lies in the noise term in the intensity equations. A factor multiplying the noise term in the intensity equations was varied and the resulting effect plotted in Figure 4-14. Changing this noise term factor in combination with the distributed loss was attempted with unsatisfactory results. The noise term discussed in Section 2.3 is fairly accurate to within a factor of two or three theoretically. A factor of 10,000 cannot be physically justified without some sort of injection seeding of photons occurring in the cavity. The noise term can be adjusted slightly, however, to bring the theoretical cavity buildup time closer to

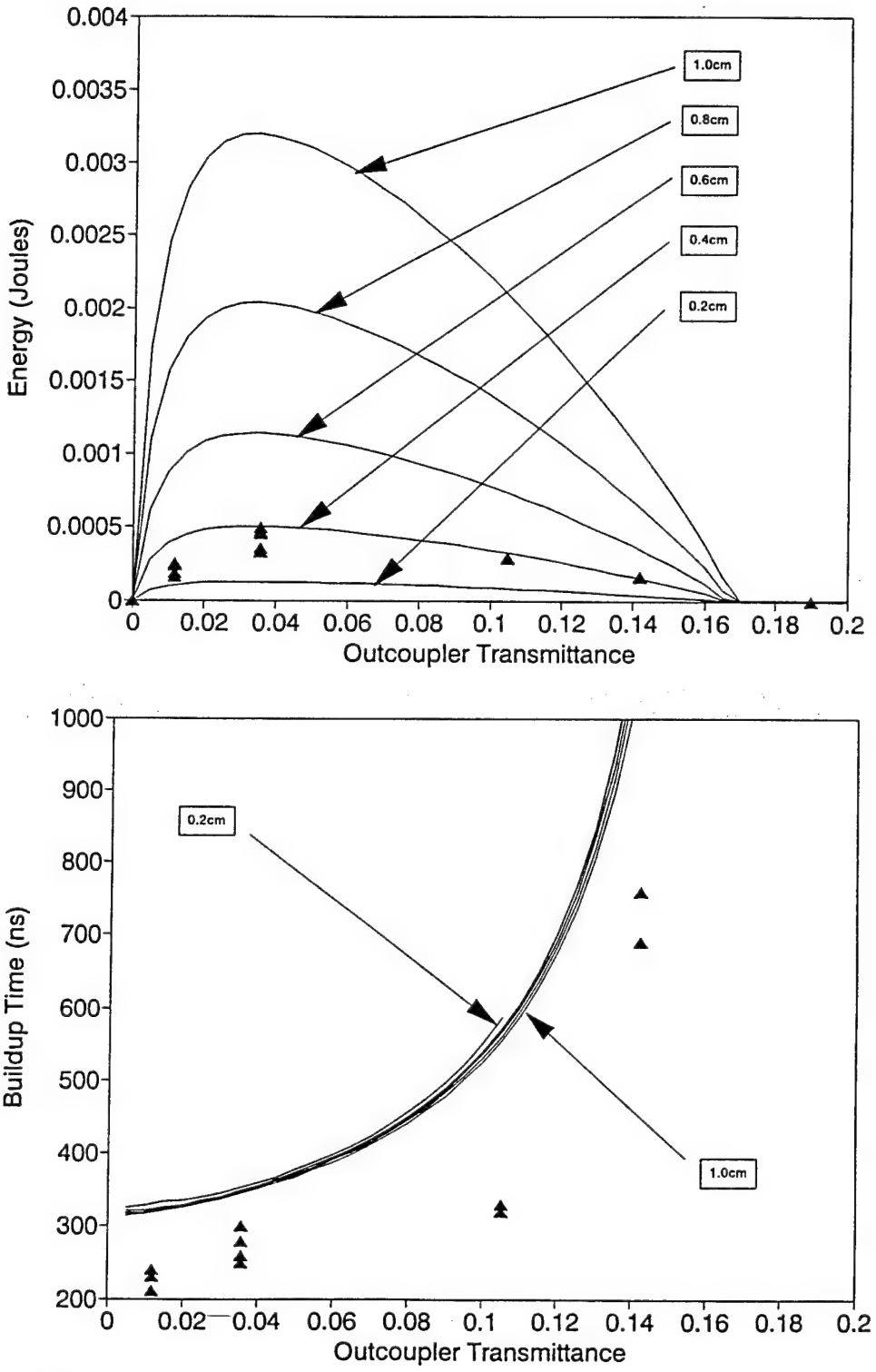

Figure 4-12 Influence of Aperture Size

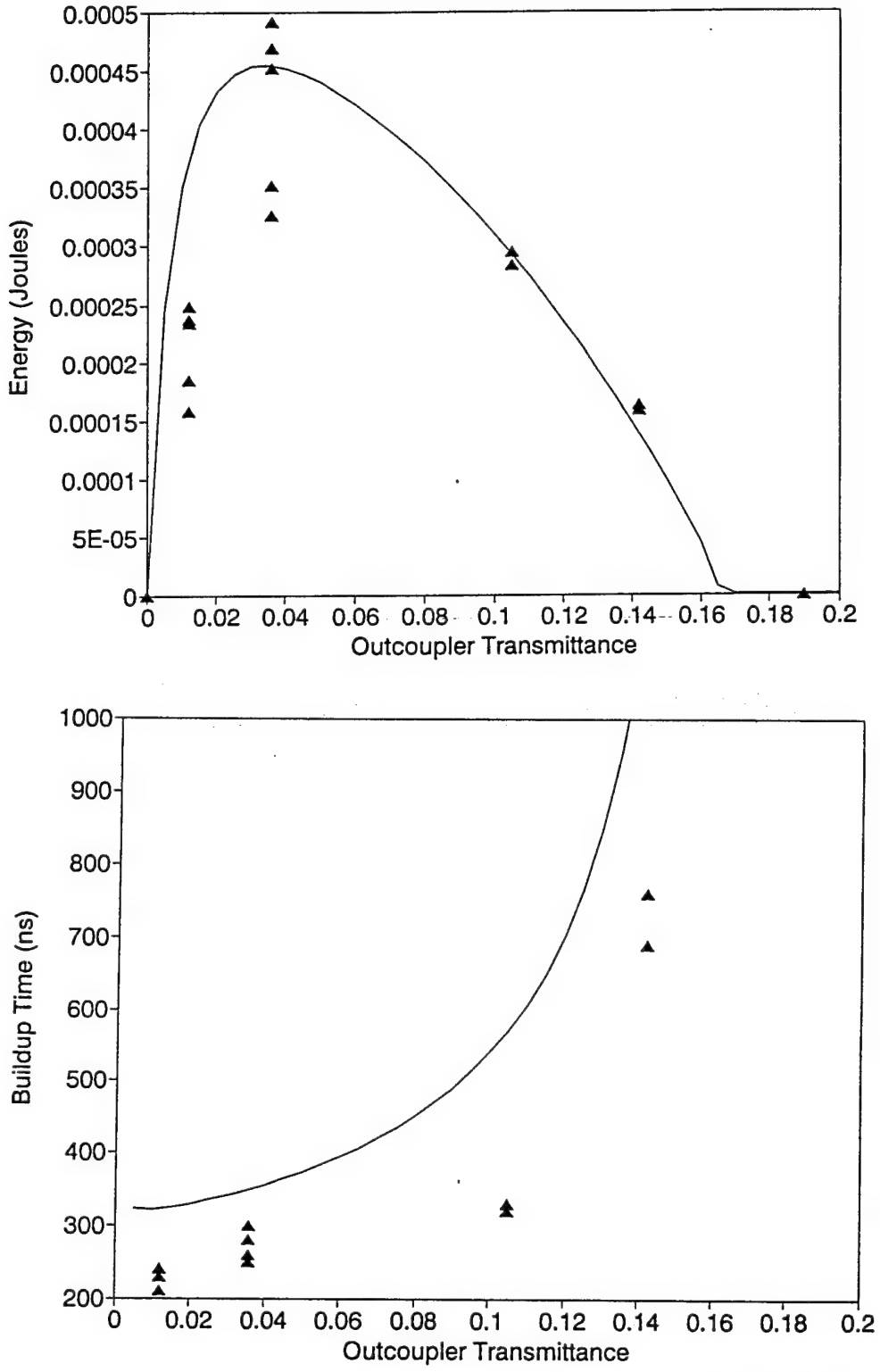

Figure 4-13 Aperture Adjusted to Fit Data

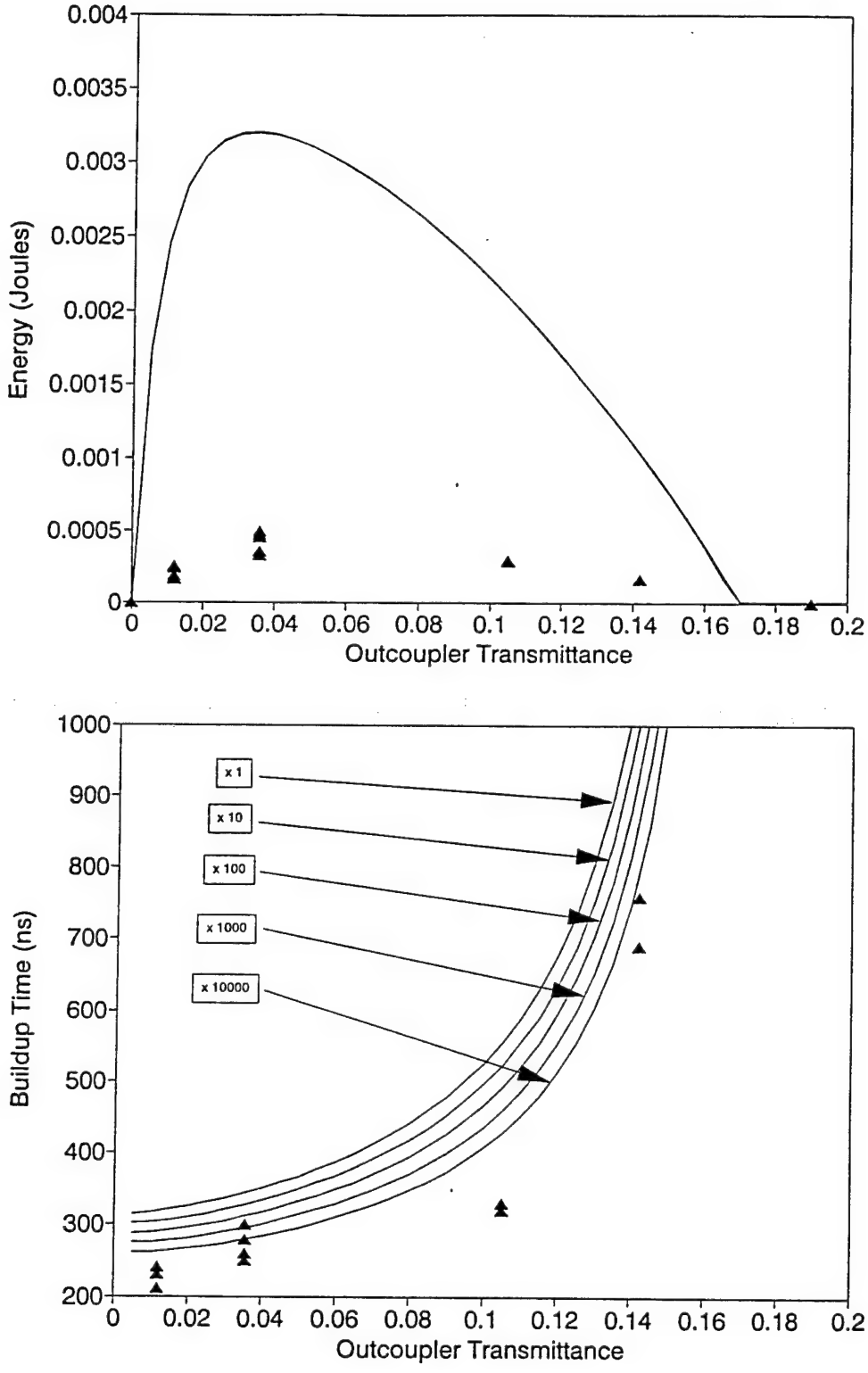

Figure 4-14 Influence of Noise Term Factor

measured data without an effect on the intensity values.

A final test of this method of adjusting aperture size to bring the theory into line with the experiment is to compare the newly adjusted theory to the pressure measurements and cavity length measurements illustrated in the last section. These comparisons are made in Figure 2-15 and Figure 2-16. A fairly good quantitative agreement between theoretical calculations and experimental measurements has been achieved. Difference in the energy plot of 4-15 is due most likely to the nonuniformity of the gain region as seen in Figure 2-11b.

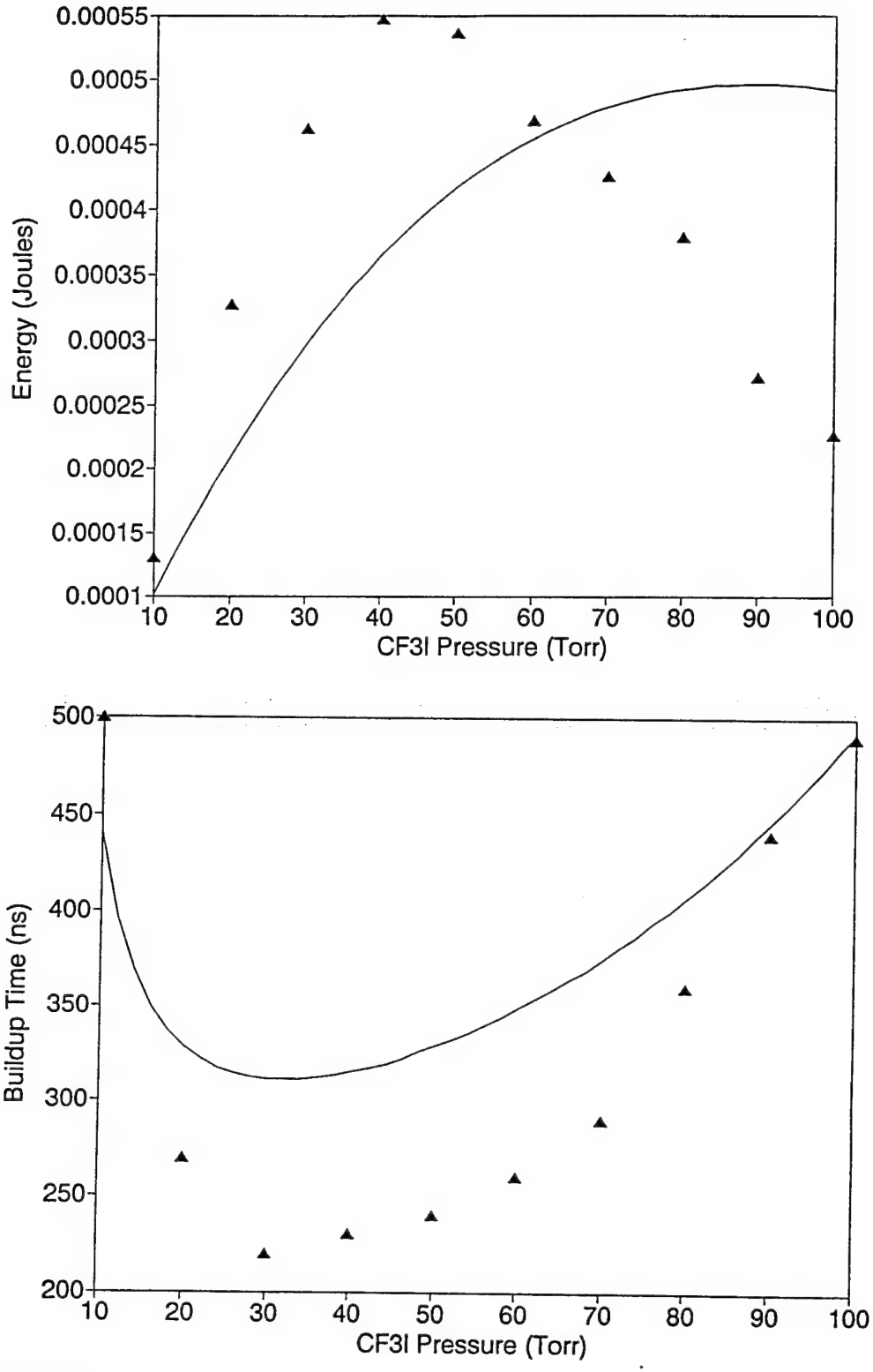

Figure 4-15 Comparison Between Theoretical and Measured Pressure Variations

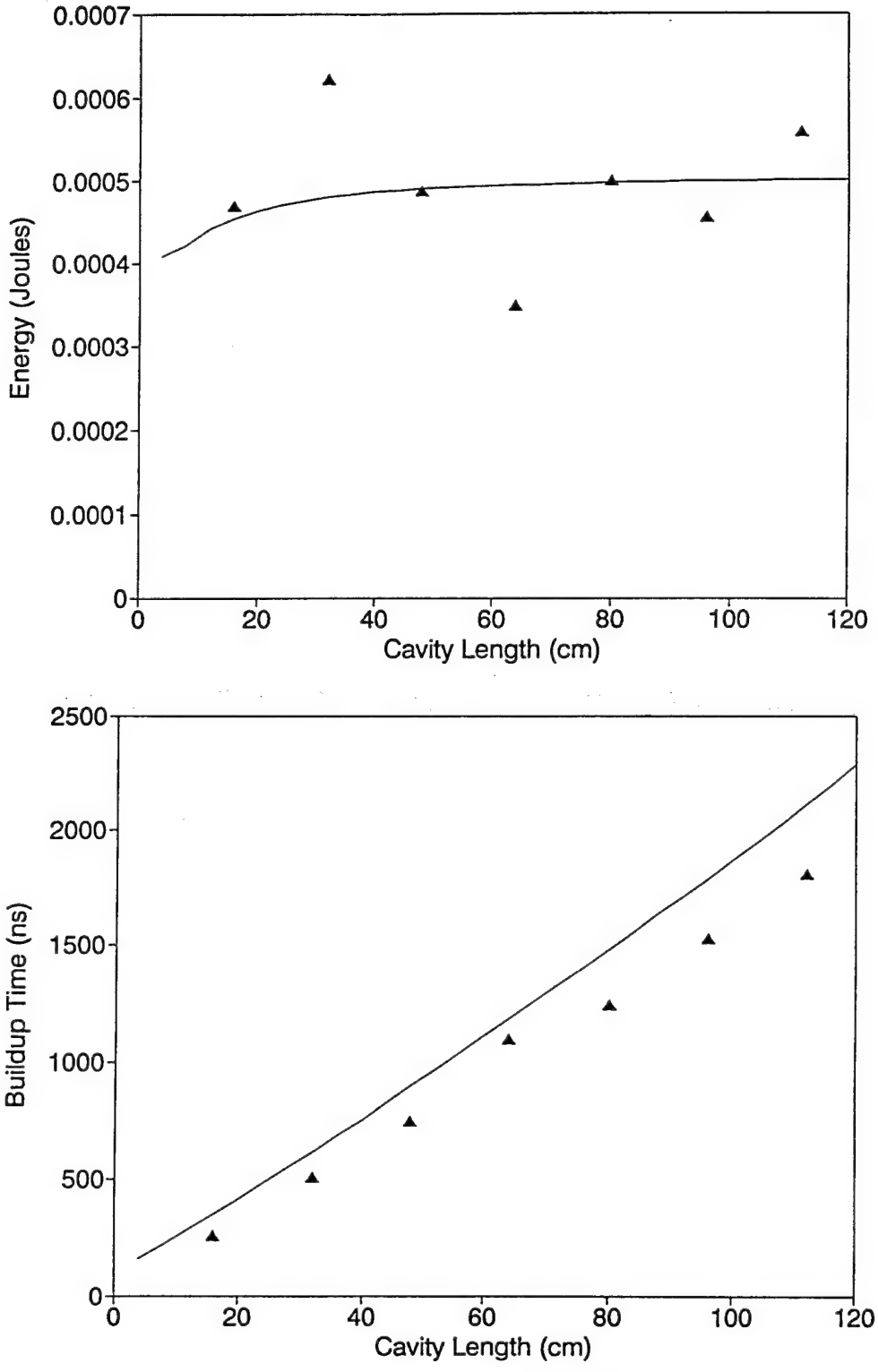

Figure 4-16 Comparison Between Theoretical and Measured Cavity Length Variations

5. CONCLUSIONS

A theoretical rate equation model for a short pulse atomic iodine photodissociation laser was developed and tested. Approximations made to make the model numerically tractable were justified through physical arguments. Calculations were performed to predict I^* laser action as parameters of the experimental laser setup were varied. Other phenomena such as two line lasing and relaxation oscillation were predicted using the model. The rate equation model was evaluated and shown to perform satisfactorily.

Three different approaches were used to determine the gain in the short pulsed KrF excimer pumped atomic Iodine laser. The first technique used a tunable diode laser to directly measure the transient gain of all six hyperfine transitions. The gain on the dominant 3-4 transition was found to be between 2.4 %/cm and 3.1 %/cm. The second method involved measuring the energy extracted from the laser for various outcoupling mirrors and applying the threshold gain condition to determine the small signal gain of the 3-4 laser transition. This yielded a nominal gain of 3.65 %/cm. A maximum theoretical gain of 3.72 %/cm was calculated by measuring the amount of energy deposited in the CF_3I. Both experimental gain measurements compared favorably to the theoretically calculated value.

A qualitative analysis using the rate equation model was performed to demonstrate similarities between the theory and the experiment. Outcoupler reflectivity, pressure, and cavity length were varied in both the model and the experiment. Theoretical and measured cavity buildup time and pulse shape of the I^* laser compared quite favorably in a qualitative sense. There was, however, a consistent discrepancy in the extracted energy: The theoretical energy was consistently higher than the measured energy by a factor of about seven.

A exhaustive error analysis was performed to determine possible causes of discrepancy between theory and experiment. It was found that by adjusting the

extraction aperture in the code, a better agreement between theory and experiment can be achieved. This could possibly be related to the transverse mode structure of the laser and the failure of the code to model losses in higher order transverse modes. A discrepancy in pressure measurements was found that could be due to the non-uniformity of the gain region caused by Beer's law photodissociation. In general, however, the rate equation model and the experiment compared quite favorably once the adjustment to the aperture size was made.

REFERENCES

[1] W. Thieme and E.E. Fill, "Relaxation between the hyperfine levels of iodine atoms in the $^2P_{1/2}$ state," Journal of Applied Physics, Vol. 12, Great Britain (1979), p. 2037.

[2] G. Herzberg, Atomic Spectra & Atomic Structure, Dover Publications, New York (1944), pp. 71-94.

[3] M.A. Kelly, Zeeman Spectroscopy of Photolytically Pumped Atomic Iodine, The University of New Mexico, Albuquerque (1989), pp. 7-21.

[4] E.A. Yukov, "Elementary processes in the active medium of an iodine photodissociation laser," Soviet Journal of Quantum Electronics, Vol. 3, No. 2, Sept. (1973), pp. 117-120.

[5] R. Engleman, Jr., R.A. Keller and B.A. Palmer, "Hyperfine structure and isotope shift of the 1.3 μm transition of ^{129}I," Applied Optics, Vol. 19, (1980), p. 2767.

[6] G. Herzberg, Atomic Spectra & Atomic Structure, Dover Publications, New York (1944), p. 129.

[7] M.A. Kelly, Zeeman Spectroscopy of Photolytically Pumped Atomic Iodine, The University of New Mexico, Albuquerque (1989), p. 13.

[8] G. Herzberg, Atomic Spectra & Atomic Structure, Dover Publications, New York (1944), p. 135.

[9] M.A. Kelly, Zeeman Spectroscopy of Photolytically Pumped Atomic Iodine, The University of New Mexico, Albuquerque (1989), p. 31.

[10] R. Engleman, Jr., R.A. Keller and B.A. Palmer, "Hyperfine structure and isotope shift of the 1.3 μm transition of ^{129}I," Applied Optics, Vol. 19, (1980), p. 2769.

[11] M.A. Kelly, Zeeman Spectroscopy of Photolytically Pumped Atomic Iodine, The University of New Mexico, Albuquerque (1989), p. 94.

[12] R. Engleman, Jr., R.A. Keller and B.A. Palmer, "Hyperfine structure and isotope shift of the 1.3 μm transition of ^{129}I," Applied Optics, Vol. 19, (1980), p. 2769.

[13] M.A. Kelly, Zeeman Spectroscopy of Photolytically Pumped Atomic Iodine, The University of New Mexico, Albuquerque (1989), p. 163.

[14] J.K.G Krug and K.-J. Witte, "Physical and chemical substances related to the atomic iodine laser," Max-Planck-Institut Fur Quantenoptik, M. P. Q. 61, (1982), p. 34.

[15] M.A. Kelly, Zeeman Spectroscopy of Photolytically Pumped Atomic Iodine, The University of New Mexico, Albuquerque (1989), p. 189.

[16] P.W. Milonni and J.H. Eberly, Lasers, John Wiley & Sons, New York (1988), p. 185.

[17] P.W. Milonni and J.H. Eberly, Lasers, John Wiley & Sons, New York (1988), p. 185.

[18] I.N. Levine, Molecular Spectroscopy, John Wiley & Sons, New York (1975),

p. 122.

[19] CRC Handbook of Chemistry and Physiscs, 57th ed., R.C. Weast (ed.), CRC Press, Cleveland (1976), p. F-243.

[20] H. Weichel and L.S. Pedrotti, Electro-Optical Systems Design (EOSD) Handout, Department of Physics, AFIT, Wright-Patterson AFB, Ohio.

[21] H. Weichel and L.S. Pedrotti, Electro-Optical Systems Design (EOSD) Handout, Department of Physics, AFIT, Wright-Patterson AFB, Ohio.

[22] M.A. Kelly, Zeeman Spectroscopy of Photolytically Pumped Atomic Iodine, The University of New Mexico, Albuquerque (1989), pp. 260.

[23] H. Weichel and L.S. Pedrotti, Electro-Optical Systems Design (EOSD) Handout, Department of Physics, AFIT, Wright-Patterson AFB, Ohio.

[24] H. Weichel and L.S. Pedrotti, Electro-Optical Systems Design (EOSD) Handout, Department of Physics, AFIT, Wright-Patterson AFB, Ohio.

[25] M.V. Klein and T.E. Furtak, Optics, 2nd. Ed., John Wiley & Sons, New York (1986), p. 372.

[26] Handbook of Mathematical Functions, M. Abramowitz and I.A. Stegun, (eds.), Dover Publications, Inc., New York (1970), p. 297.

[27] ACM Library, Algorithm 363 Documentation.

[28] J.T. Verdeyen, Laser Electronics, Prentice Hall, Inc., New Jersey (1981), p. 159.

[29] Class Notes, EECE 464, Lesson 18.

[30] Class Notes, EECE 464, Lesson 17.

[31] E.A. Yukov, "Elementary processes in the active medium of an iodine photodissociation laser," Soviet Journal of Quantum Electronics, Vol. 3, No. 2, Sept. (1973), pp. 117-120.

[32] W. Thieme and E.E. Fill, "Hyperfine relaxation in the iodine photodissociation laser," Optics Communications, Vol. 36, No. 5, Mar. (1981), p. 364.

[33] W. Thieme and E.E. Fill, "Hyperfine relaxation in the iodine photodissociation laser," Optics Communications, Vol. 36, No. 5, Mar. (1981), p. 364.

[34] E.A. Yukov, "Elementary processes in the active medium of an iodine photodissociation laser," Soviet Journal of Quantum Electronics, Vol. 3, No. 2, Sept. (1973), pp. 117-120.

[35] E.A. Yukov, "Elementary processes in the active medium of an iodine photodissociation laser," Soviet Journal of Quantum Electronics, Vol. 3, No. 2, Sept. (1973), pp. 117-120.

[36] W. Thieme and E.E. Fill, "Hyperfine relaxation in the iodine photodissociation laser," Optics Communications, Vol. 36, No. 5, Mar. (1981), p. 364.

[37] V.A. Alekseev, T.L. Andreeva, V.N. Volkov and E.A. Yukov, "Kinetics of the generation spectrum of a photodissociation iodine laser," Soviet Physics JETP, Vol. 36, No. 2, Feb. (1973), p. 234.

[38] J.K.G Krug and K.-J. Witte, "Physical and chemical substances related to the atomic iodine laser," Max-Planck-Institut Fur Quantenoptik, M. P. Q. 61,

(1982), p. 41.

[39] N.P. Machara, Air Force Phillips Laboratory, Albuquerque, NM, private communication.

[40] J.K.G Krug and K.-J. Witte, "Physical and chemical substances related to the atomic iodine laser," Max-Planck-Institut Fur Quantenoptik, M. P. Q. 61, (1982), p. 4.

[41] J.K.G Krug and K.-J. Witte, "Physical and chemical substances related to the atomic iodine laser," Max-Planck-Institut Fur Quantenoptik, M. P. Q. 61, (1982), p. 5.

[42] B.S. Hunt, J.K. McIver and G.D. Hager, "Gain measurements on a short pulsed KrF pumped atomic iodine laser, Lasers' 92 Conference, Houston (1992), p. 7.

[43] J.K.G Krug and K.-J. Witte, "Physical and chemical substances related to the atomic iodine laser," Max-Planck-Institut Fur Quantenoptik, M. P. Q. 61, (1982), p. 5.

[44] G.D. Hager, Air Force Phillips Laboratory, Albuquerque, NM, private communication.

[45] G.D. Hager, Air Force Phillips Laboratory, Albuquerque, NM, private communication.

[46] J.K.G Krug and K.-J. Witte, "Physical and chemical substances related to the atomic iodine laser," Max-Planck-Institut Fur Quantenoptik, M. P. Q. 61, (1982), p. 42.

[47] J.K.G Krug and K.-J. Witte, "Physical and chemical substances related to the atomic iodine laser," Max-Planck-Institut Fur Quantenoptik, M. P. Q. 61, (1982), p. 43.

[48] P. Crowell, Air Force Phillips Laboratory, Albuquerque, NM, private communication.

[49] P.W. Milonni and J.H. Eberly, Lasers, John Wiley & Sons, New York (1988), p. 318.

[50] P. Crowell, Air Force Phillips Laboratory, Albuquerque, NM, private communication.

[51] P. Crowell, Air Force Phillips Laboratory, Albuquerque, NM, private communication.

[52] P. Crowell, Air Force Phillips Laboratory, Albuquerque, NM, private communication.

[53] P. Crowell, Air Force Phillips Laboratory, Albuquerque, NM, private communication.

[54] J.T. Verdeyen, Laser Electronics, Prentice Hall, Inc., New Jersey (1981), p. 160.

[55] J.T. Verdeyen, Laser Electronics, Prentice Hall, Inc., New Jersey (1981), p. 184.

[56] G.D. Hager, Air Force Phillips Laboratory, Albuquerque, NM, private communication.

[57] J.I. Cline, C.A. Taatjes, and S.R. Leone, "Diode laser probing of $I^*(^2P_{1/2})$ doppler profiles: time evolution of a fast, anisotropic velocity distribution in a thermal bath," Journal of Chemical Physics, Vol. 93, No. 9, Nov. (1990), p. 6547.

[58] E.E. Fill, W. Skrlac and K.-J Witte, "An excimer laser pumped atomic iodine laser emitting pulses in the range of 2-12 ns," Optics Communications, Vol. 37, No. 2, Apr. (1981), pp. 123-126.

[59] J.I. Cline, C.A. Taatjes, and S.R. Leone, "Diode laser probing of $I^*(^2P_{1/2})$ doppler profiles: time evolution of a fast, anisotropic velocity distribution in a thermal bath," Journal of Chemical Physics, Vol. 93, No. 9, Nov. (1990), p. 6547.

[60] W. Thieme and E.E. Fill, "Hyperfine relaxation in the iodine photodissociation laser," Optics Communications, Vol. 36, No. 5, Mar. (1981), p. 364.

[61] V.A. Alekseev, T.L. Andreeva, V.N. Volkov and E.A. Yukov, "Kinetics of the generation spectrum of a photodissociation iodine laser," Soviet Physics JETP, Vol. 36, No. 2, Feb. (1973), p. 234.

[62] A.C. Hindmarsh, "ODEPACK, a systemized collection of ODE solvers, in scientific computing," R.S. Stepleman et al. (eds.), North-Holland, Amsterdam, (1983), pp. 55-64.

[63] V.A. Alekseev, T.L. Andreeva, V.N. Volkov and E.A. Yukov, "Kinetics of the generation spectrum of a photodissociation iodine laser," Soviet Physics JETP, Vol. 36, No. 2, Feb. (1973), p. 234.

[64] G.D. Hager, Air Force Phillips Laboratory, Albuquerque, NM, private

communication.

[65] M.V. Klein and T.E. Furtak, Optics, 2nd. Ed., John Wiley & Sons, New York (1986), p. 83.

[66] L.F. Shampine and C.W. Gear, "A user's view of solving stiff ordinary differential equations," Society for Industrial and Applied Mathematics (SIAM) Review, Vol. 21, No. 1, January (1979), pp. 1-17.

[67] J.I. Cline, C.A. Taatjes, and S.R. Leone, "Diode laser probing of $I^*(^2P_{1/2})$ doppler profiles: time evolution of a fast, anisotropic velocity distribution in a thermal bath," Journal of Chemical Physics, Vol. 93, No. 9, Nov. (1990), p. 6547.

[70] I.H. Hwang and K.S. Han, "XeCl laser pumped iodine laser using t-C_4F_9I," Optics Communications, Vol. 70, No. 4, Mar. (1989), pp. 341-344.

[69] H. Weichel and L.S. Pedrotti, Electro-Optical Systems Design (EOSD) Handout, Department of Physics, AFIT, Wright-Patterson AFB, Ohio.

[70] H. Weichel and L.S. Pedrotti, Electro-Optical Systems Design (EOSD) Handout, Department of Physics, AFIT, Wright-Patterson AFB, Ohio.

APPENDICES

APPENDIX A. Vector Model of Atomic Iodine

The hyperfine structure of atomic iodine results from the splitting of the fine structure components due to interactions between the nucleus and the angular momentum of the electrons as outlined in Section 2.1. This splitting leads to six hyperfine energy states, two upper ($^2P_{1/2}$) and four lower ($^2P_{3/2}$). Further splitting of the hyperfine structure occurs in the presence of a magnetic field. This effect is known as Zeeman splitting. The following code treats each of the splitting events as a perturbation to the ground state. If the Zeeman perturbation is neglected, the zero field frequency spectrum of atomic iodine seen in Figure 2-7 is generated.

```
c       This program was originally written by Bob Shea on the
c     Cray at the weapons laboratory when it was running under CTSS.
c     I have made various modifications to get it to run on the Iris
c     workstations at the Chemical Laser Facility.  These
c     modifications include writing a program to block diagonalize
c     matrices to solve for the Eigenvalues of the system to gain
c     independence from the Slatec Libraries on the Cray.  I wrote a
c     graphics driver using NCAR to plot the output to a standard
c     CGM ( Computer Graphics Metafile ) file so that the gain
c     spectrum could be compressed and animated and/or converted to
c     a postscript file and plotted out.  I also converted the X axis
c     array frequency to double precision to avoid the stairstep
c     effect.  I've written several other programs to analyze the
c     output of the code to get plots of frequency vs B field and
c     small signal gain vs B field.
c
c                                        - Lt. B. Scott Hunt
c
c
c       This is the main calling program for calculating the effect
c     of a magnetic field on the iodine laser.  A particular set of
c     basis states is chosen to simplify the problem.  These states
c     are discussed in the routines DRIVEU and DRIVEL.
c       DRIVEU calculates the eigenvalues and eigenvectors
```

```
c     resulting from a combination of the zeeman effect and the
c     hyperfine interaction in the upper laser level.
c        DRIVEL performs the same calculation for the lower state.
c        Subroutine ACOEFF calculates  the a coefficients due to
c     magnetic dipole transitions between upper and lower eigenstates.
c     These eigenstates are a linear combination of basis states. the
c     particular combination is a function of magnetic field strength.
c     The A-coefficients are stored in the arrays AR(i,j), AL(i,j) and
c     AZ(i,j).
c        Subroutine ABSORB calculates the absorption coefficients for
c     each transition.
c        Subroutine SYNTH calculates the total absorption cross section
c     across a doppler profile centered on the F=3->F'=4 laser line.
c        Subroutine SYNTH3 scans all transitions to find the maximum and
c     and minimum absorption.
c        Subroutine SETLIN initializes the array broad with normalized
c     line shape information.
c        Subroutine SCAN finds the range of wavenumbers covered by the
c     transitions.
c        Subroutine GAIN calculates the stimulated emission cross section
c     as a function of wavenumber and polarization.
c
c ******************** TO RUN THIS CODE ************************
c
c     You the user have little to do. There is no separate input stream.
c     The only option you have is to change a few data statements. The
c     statements are located in this main program and the variables
c     are discussed below.
c
c        IMAX  - controls the number of non-zero magnetic fields for
c                which calculations are performed. The code always
c                performs a calculation for zero-field in order to
c                determine parameters it needs for later calculations.
c        FIELD - this array contains the various values of magnetic
c                field (in Gauss). Only the first IMAX elements are
c                used.
c        TEMP  - the gas temperature (degrees K) is only used in INIT
c                to calculate the Doppler linewidth.
c        PRESS - the gas pressure (torr) is used in INIT to calculate
c                the Lorenz linewidth. It is assumed that broadening
c                coefficients are 5 MHz/torr and independent of
c                temperature for all gases. This approximation is
c                crude but should be sufficient for most purposes.
c                It can be upgraded by modifying one line of code
c                in INIT.
c
```

```
c ***********************************************************************
c
      double precision xarray(8000)
      common /upper/   nvecu,evalu(12),evectu(12,12),peturb(12,12)
      common /basisu/  nrepu,idimu(7),rmiu(12),rmju(12),ifu(12)
      common /paramu/  au,bu,gu
      common /lower/   nvecl,evall(24),evectl(24,24),plower(24,24)
      common /basisl/  nrepl,idiml(9),rmil(24),rmjl(24),ifl(24)
      common /paraml/  al,bl,gl
      common /line/    wdopp,wlornz,ratio,voigt0,npts,shape(101),
     a                 rl(101),rr(101),rz(101)
      common /band/    width,nband,bandw(8000),rlwide(8000)
      common /const/   planck,c,pi,alpha,ele,rad,bohr,t0
      common /transit/ wlase(6),wave(12,24),aq(12,24),ar(12,24),
     a                 az(12,24)
      common /ginteg/  gnul(8000),gnur(8000),gnuz(8000),nstep,
     a                 delx(10),xtotal,broad(16000),nbig,ncent,
     b                 xarray,ncount,bigger,nlin,nright,nleft
      common /plotv/   rlsave(101,25),rrsave(101,25),rzsave(101,25),
     a                 field(160),nfield
      common /dipole/  tl(12,24),tr(12,24),tz(12,24)
      common /prob/    pl(12,24),pr(12,24),pz(12,24)
      common /gains/   sv1,sv2,sv3
c
c  This sets up the integers involved in the gain calculations:
c
      delx(1)=0.5
      delx(2)=0.5
      delx(3)=0.5
      delx(4)=0.5
      delx(5)=0.5
      delx(6)=0.5
      delx(7)=1.0
      delx(8)=1.0
      delx(9)=0.4
      delx(10)=0.0
      xtotal=5.4
      nstep=8000
      nbig=16000
      ncent=8001
c
c  This sets up the number of fields to calculate, the unit file to
c  store the data, the temperature, the pressure, and the pressure
c  broadening coefficient:
c
      imax=0
```

```
      ifile=10
      temp=300.0
      press=60.0
      pbroad=11.3e6
c
c  This sets up the magnetic field strengths in gauss:
c
c     fldinc=50.0
c     do 10 i=1,20
c        field(i) = i*fldinc
c  10 continue
c
c     fldinc=100.0
c     do 15 i=21,imax
c        field(i) = field(20+(i-20)*fldinc
c  15 continue
c
c     field(1) = 600.0
c
c  This sets up the file to store the dialogue in:
c
      open(unit=7,file='energies.prn',status='new')
c
c ---------------------------------------------------------------

      call opngks
c
c  This is the loop to do the calculations for zero magnetic field:
c
      do 50 ifile=10,10
         write(7,9200) ifile-10
c
         call init(temp,press,pbroad)
c
         ppbroad=pbroad/1.0e6
         h = 0.0
         ifield = 0
         call driveu(h)
         call drivel(h)
c
c  wlase(1) is the wavenumbver of the f=3 to f=4 transition
c  in zero field:
c
         wlase(1) = t0 + evalu(1) - evall(1)
         wlase(2) = t0 + evalu(1) - evall(2)
         wlase(3) = t0 + evalu(1) - evall(4)
```

```
      wlase(4) = t0 + evalu(2) - evall(2)
      wlase(5) = t0 + evalu(2) - evall(4)
      wlase(6) = t0 + evalu(2) - evall(7)
c
      write(7,9000) imax
      write(6,9000) imax
c
      call acoeff
      call absorb
      call synth
      call synth3
      call output(h,absrb)
      call scan(wavmax,wavmin)
      call setlin(wavmax,wavmin)
      call gain(wavmax,wavmin,ifield)
c
c  This calls the filing routine:
c
      call fileit(ifile,h,temp,press,ppbroad)
c
   50 continue
c
c     stop
c
c ---------------------------------------------------------------------
c
c  This is the loop to do the calculations for a non-zero magnetic
c  field:
c
     do 100 i=1,imax
       write(7,9100) i
       write(6,9100) i
       h = field(i)
       call driveu(h)
       call drivel(h)
c
       call acoeff
       call absorb
       call synth
       call synth3
       call output(h,absrb)
       call scan(wavmax,wavmin)
       call setlin(wavmax,wavmin)
       call gain(wavmax,wavmin,i)
c
c  This calls the filing routine:
```

```
c
        call fileit(i+10,h,temp,press,ppbroad)
c
  100 continue

      call clsgks
c
      stop
 9000 format(1x,'Number of fields to calculate = ',i4)
 9100 format(1x,'Field calculation number = ',i4)
 9200 format(1x,'Initial calculation number = ',i4)
      end
c
c ***********************************************************************
c
      subroutine init(temp,press,pbroad)
c
c       This routine initializes the hyperfine interaction constants.
c     The units are in 1/cm. other constants are identified below:
c
c         rad    - The bohr radius in cm.
c         ele    - The electron charge in esu.
c         alpha  - The fine strcture constant.
c         bohr   - The bohr magneton in units of 1/(cm-gauss)
c         t0     - The separation (in 1/cm) of the unpeturbed spin-orbit
c                  terms.
c
c ---------------------------------------------------------------------
c
      common /upper/  nvecu,evalu(12),evectu(12,12),peturb(12,12)
      common /paramu/ au,bu,gu
      common /basisu/ nrepu,idimu(7),rmiu(12),rmju(12),ifu(12)
      common /lower/  nvecl,evall(24),evectl(24,24),plower(24,24)
      common /paraml/ al,bl,gl
      common /basisl/ nrepl,idiml(9),rmil(24),rmjl(24),ifl(24)
      common /line/   wdopp,wlornz,ratio,voigt0,npts,shape(101),
     a                rl(101),rr(101),rz(101)
      common /band/   width,nband,bandw(8000),rlwide(8000)
      common /const/  planck,c,pi,alpha,ele,rad,bohr,t0
c
      au=0.21973
      bu=0.0
      gu=0.673
c
      al=0.02759
      bl=0.03812
```

```
      gl=1.3333
c
      nvecu=12
c
      nrepu=7
      idimu(1)=1
      idimu(2)=2
      idimu(3)=2
      idimu(4)=2
      idimu(5)=2
      idimu(6)=2
      idimu(7)=1
      rmiu(1)=2.5
      rmiu(2)=2.5
      rmiu(3)=1.5
      rmiu(4)=1.5
      rmiu(5)=0.5
      rmiu(6)=0.5
      rmiu(7)=-0.5
      rmiu(8)=-0.5
      rmiu(9)=-1.5
      rmiu(10)=-1.5
      rmiu(11)=-2.5
      rmiu(12)=-2.5
      rmju(1)=0.5
      rmju(2)=-0.5
      rmju(3)=0.5
      rmju(4)=-0.5
      rmju(5)=0.5
      rmju(6)=-0.5
      rmju(7)=0.5
      rmju(8)=-0.5
      rmju(9)=0.5
      rmju(10)=-0.5
      rmju(11)=0.5
      rmju(12)=-0.5
      ifu(1)=3
      ifu(2)=2
      ifu(3)=2
      ifu(4)=1
      ifu(5)=1
      ifu(6)=0
      ifu(7)=0
      ifu(8)=-1
      ifu(9)=-1
      ifu(10)=-2
```

```
      ifu(11)=-2
      ifu(12)=-3
c
      nvecl=24
c
      nrepl=9
      idiml(1)=1
      idiml(2)=2
      idiml(3)=3
      idiml(4)=4
      idiml(5)=4
      idiml(6)=4
      idiml(7)=3
      idiml(8)=2
      idiml(9)=1
      rmil(1)=2.5
      rmil(2)=2.5
      rmil(3)=1.5
      rmil(4)=2.5
      rmil(5)=1.5
      rmil(6)=0.5
      rmil(7)=2.5
      rmil(8)=1.5
      rmil(9)=0.5
      rmil(10)=-0.5
      rmil(11)=1.5
      rmil(12)=0.5
      rmil(13)=-0.5
      rmil(14)=-1.5
      rmil(15)=0.5
      rmil(16)=-0.5
      rmil(17)=-1.5
      rmil(18)=-2.5
      rmil(19)=-0.5
      rmil(20)=-1.5
      rmil(21)=-2.5
      rmil(22)=-1.5
      rmil(23)=-2.5
      rmil(24)=-2.5
      rmjl(1)=1.5
      rmjl(2)=0.5
      rmjl(3)=1.5
      rmjl(4)=-0.5
      rmjl(5)=0.5
      rmjl(6)=1.5
      rmjl(7)=-1.5
```

```
      rmjl(8)=-0.5
      rmjl(9)=0.5
      rmjl(10)=1.5
      rmjl(11)=-1.5
      rmjl(12)=-0.5
      rmjl(13)=0.5
      rmjl(14)=1.5
      rmjl(15)=-1.5
      rmjl(16)=-0.5
      rmjl(17)=0.5
      rmjl(18)=1.5
      rmjl(19)=-1.5
      rmjl(20)=-0.5
      rmjl(21)=0.5
      rmjl(22)=-1.5
      rmjl(23)=-0.5
      rmjl(24)=-1.5
      ifl(1)=4
      ifl(2)=3
      ifl(3)=3
      ifl(4)=2
      ifl(5)=2
      ifl(6)=2
      ifl(7)=1
      ifl(8)=1
      ifl(9)=1
      ifl(10)=1
      ifl(11)=0
      ifl(12)=0
      ifl(13)=0
      ifl(14)=0
      ifl(15)=-1
      ifl(16)=-1
      ifl(17)=-1
      ifl(18)=-1
      ifl(19)=-2
      ifl(20)=-2
      ifl(21)=-2
      ifl(22)=-3
      ifl(23)=-3
      ifl(24)=-4
c
      planck=6.626176e-27
      c=2.997925e10
      pi=3.14159
      alpha=0.007297351
```

```
      ele=4.803242e-10
      rad=5.291771e-9
      bohr=0.46686e-4
      t0=7602.9768
      npts=101
      width=4.5e10
      nband=8000
c
c -----------------------------------------------------------------
c
c  Initialize the magnetic dipole operator between basis states:
c
      call setul
c
c  Set up the line shape parameter:
c
      wdopp =  sqrt(temp/300.0)*250.e6
      treff = 298.0
      wlornz = (treff/temp)*press*pbroad
      ratio = sqrt(alog(2.))*wlornz/wdopp
c
c  Find line shape factor at line center:
c
      call erf(0.,ratio,rim,re)
      voigt0 = re
c
c  Now include the doppler line shape normalization factor:
c
      voigt0 = voigt0*2.*sqrt(alog(2.)/pi)/wdopp
c
c  Set up the linewidth over which we wish to scan:
c
      call find(start,end)
      del = (end - start)/float(npts-1)
      do 100 i=1,npts
        shape(i) = start + del*(i-1)
  100 continue
c
      return
      end
c
c ***************************************************************************
c
      subroutine setul
c
c       This routine sets up matrix elements of the magnetic dipole
```

```
c     operator between the basis states as defined in the routines
c     driveu and drivel. The usual theorems are used to eveluate
c     the matrix elements in terms of reduced matrix elements.
c     The reduced matrix elements are evaluated assuming l-s coupling.
c       The form of the matrix elements is as follows
c           (upper basis state)*( l + 2*s )*(lower basis state)
c     These matrix elements are stored in arrays tl,tr, and tz,
c     which correspond to the various components of the vector
c     operator.
c       The components of the magnetic dipole operator in a spherical
c     basis are denoted by p(1),p(0),and p(-1). The arrays tl,tr, and
c     tz correspond to the following type of matrix elements
c          tz:     (1/2  m  ::  p(0)  ::  3/2  m  )
c          tl:     (1/2  m  ::  p(1)  ::  3/2  m+1)
c          tr:     (1/2  m  ::  p(-1) ::  3/2  m-1)
c
c
c ---------------------------------------------------------------------
c
      common /upper/  nvecu,evalu(12),evectu(12,12),peturb(12,12)
      common /basisu/ nrepu,idimu(7),rmiu(12),rmju(12),ifu(12)
      common /lower/  nvecl,evall(24),evectl(24,24),plower(24,24)
      common /basisl/ nrepl,idiml(9),rmil(24),rmjl(24),ifl(24)
      common /dipole/ tl(12,24),tr(12,24),tz(12,24)
c
      character*8 msg1(7),msg2(7),msg3(7)
c
      msg1(1)='matrix e'
      msg1(2)='lements '
      msg1(3)='of the d'
      msg1(4)='ipole op'
      msg1(5)='erator f'
      msg1(6)='or q = 0'
      msg1(7)='        '
      msg2(1)='matrix e'
      msg2(2)='lements '
      msg2(3)='of the d'
      msg2(4)='ipole op'
      msg2(5)='erator f'
      msg2(6)='or q = +'
      msg2(7)='1       '
      msg3(1)='matrix e'
      msg3(2)='lements '
      msg3(3)='of the d'
      msg3(4)='ipole op'
      msg3(5)='erator f'
```

```
      msg3(6)='or q = -'
      msg3(7)='1       '
c
c -----------------------------------------------------------------
c
      reduce = -2./sqrt(3.)
      fz = 1./sqrt(6.)
      f1 = .5
      f2 = .5/sqrt(3.)
c
      do 200 i=1,nvecu
        rmj1 = rmju(i)
        rmi1 = rmiu(i)
        if(rmj1.gt.0.0) fr = f2
        if(rmj1.lt.0.0) fr = f1
        if(rmj1.gt.0.0) fl = f1
        if(rmj1.lt.0.0) fl = f2
        do 100 j=1,nvecl
          rmj2 = rmjl(j)
          rmi2 = rmil(j)
          del = reduce*delta(rmi1,rmi2)
          tl(i,j) = del*delta(rmj1,rmj2-1.)*fl
          tr(i,j) = del*delta(rmj1,rmj2+1.)*fr
          tz(i,j) = del*delta(rmj1,rmj2)*fz
  100   continue
  200 continue
c
      call matout(tz,nvecu,nvecl,msg1)
      call matout(tl,nvecu,nvecl,msg2)
      call matout(tr,nvecu,nvecl,msg3)
c
      return
      end
c
c ***************************************************************************
c
      subroutine driveu(h)
c
c       This routine calls appropriate routines to do the calculations
c     for the upper state. The particular basis states are given below.
c     the nuclear spin is 5/2 and the total angular momentum for the
c     upper state is 1/2.
c
c       basis(i)  =  j  i   mj   mi
c
c       basis(1)  =        1/2  5/2
```

```
c       basis(2)  =       -1/2  5/2
c       basis(3)  =        1/2  3/2
c       basis(4)  =       -1/2  3/2
c       basis(5)  =        1/2  1/2
c       basis(6)  =       -1/2  1/2
c       basis(7)  =        1/2 -1/2
c       basis(8)  =       -1/2 -1/2
c       basis(9)  =        1/2 -3/2
c       basis(10) =       -1/2 -3/2
c       basis(11) =        1/2 -5/2
c       basis(12) =       -1/2 -5/2
c
c     This particular choice is convenient since the perturbation
c     only couples pairs such as 2 and 3, 4 and 5, etc.
c        The array evalu(i) contains the energies(eigenvalues) of
c     the diagonalized hamiltonian ands evectu(j,i) contains the
c     corresponding eigenvector.
c
c ---------------------------------------------------------------------
c
      common /upper/  nvecu,evalu(12),evectu(12,12),peturb(12,12)
      common /basisu/ nrepu,idimu(7),rmiu(12),rmju(12),ifu(12)
      common /paramu/ au,bu,gu
      common /const/  planck,c,pi,alpha,ele,rad,bohr,t0
c
      character*8 msg1(7),msg2(7),msg3(7)
c
      msg1(1)='perturba'
      msg1(2)='tion mat'
      msg1(3)='rix for '
      msg1(4)='the doub'
      msg1(5)='let p 1/'
      msg1(6)='2 state '
      msg1(7)='        '
      msg2(1)='matrix o'
      msg2(2)='f eigenv'
      msg2(3)='ectors f'
      msg2(4)='or the d'
      msg2(5)='oublet p'
      msg2(6)=' 1/2 sta'
      msg2(7)='te      '
      msg3(1)='eigenval'
      msg3(2)='ues or e'
      msg3(3)='nergies '
      msg3(4)='for the '
      msg3(5)='doublet '
```

```
      msg3(6)='p 1/2 st'
      msg3(7)='ate     '
c
c -----------------------------------------------------------------
c
c  Generate the perturbation matrix
c
      call setu(h)
c
c  Write out the matrix
c
      if(h.eq.0.0) call matout(peturb,nvecu,nvecu,msg1)
c
c  Calculate the eigenvalues and eigenvectors
c
      call eigen(nvecu,evalu,evectu,peturb,nrepu,idimu)
c
c  Normalize the eigenvectors
c
      call normal(nvecu,evectu)
c
c  Write out matrix of eigenvectors
c
      if(h.eq.0.0) call matout(evectu,nvecu,nvecu,msg2)
c
c  Write out the eigenvalues
c
      write(7,9000) h
      call vecout(evalu,nvecu,msg3)
c
      return
 9000 format(1h1,10x,'Magnetic field strength = ',e12.5,' oe')
      end
c
c ***************************************************************************
c
      subroutine drivel(h)
c
c       This routine calls appropriate routines to do the calculations
c     for the lower state.  The particular basis states are given below.
c     The nuclear spin is 5/2 and the total angular momentum for the
c     lower state is 3/2.
c
c       basis(i)  =  j  i   mj   mi
c
c       basis(1)  =        3/2  5/2
```

```
c       basis(2)  =        1/2  5/2
c       basis(3)  =        3/2  3/2
c       basis(4)  =       -1/2  5/2
c       basis(5)  =        1/2  3/2
c       basis(6)  =        3/2  1/2
c       basis(7)  =       -3/2  5/2
c       basis(8)  =       -1/2  3/2
c       basis(9)  =        1/2  1/2
c       basis(10) =        3/2 -1/2
c       basis(11) =       -3/2  3/2
c       basis(12) =       -1/2  1/2
c       basis(13) =        1/2 -1/2
c       basis(14) =        3/2 -3/2
c       basis(15) =       -3/2  1/2
c       basis(16) =       -1/2 -1/2
c       basis(17) =        1/2 -3/2
c       basis(18) =        3/2 -5/2
c       basis(19) =       -3/2 -1/2
c       basis(20) =       -1/2 -3/2
c       basis(21) =        1/2 -5/2
c       basis(22) =       -3/2 -3/2
c       basis(23) =       -1/2 -5/2
c       basis(24) =       -3/2 -5/2
c
c
c
c       The array evall(i) contains the energies(eigenvalues) of
c     the diagonalized hamiltonian ands evectl(j,i) contains the
c     corresponding eigenvector.
c
c ---------------------------------------------------------------------
c
      common /lower/  nvecl,evall(24),evectl(24,24),plower(24,24)
      common /basisl/ nrepl,idiml(9),rmil(24),rmjl(24),ifl(24)
      common /paraml/ al,bl,gl
      common /const/  planck,c,pi,alpha,ele,rad,bohr,t0
      character*8 msg1(7),msg2(7),msg3(7)
c
      msg1(1)='perturba'
      msg1(2)='tion mat'
      msg1(3)='rix for '
      msg1(4)='the doub'
      msg1(5)='let p 3/'
      msg1(6)='2 state '
      msg1(7)='        '
      msg2(1)='matrix o'
```

```
      msg2(2)='f eigenv'
      msg2(3)='ectors f'
      msg2(4)='or the d'
      msg2(5)='oublet p'
      msg2(6)=' 3/2 sta'
      msg2(7)='te      '
      msg3(1)='eigenval'
      msg3(2)='ues or e'
      msg3(3)='nergies '
      msg3(4)='for the '
      msg3(5)='doublet '
      msg3(6)='p 3/2 st'
      msg3(7)='ate     '
c
c -----------------------------------------------------------------
c
c  Generate the perturbation matrix
c
      call setl(h)
c
c  Write out the matrix
c
      if(h.eq.0.0) call matout(plower,nvecl,nvecl,msg1)
c
c  Calculate the eigenvalues and eigenvectors
c
      call eigen(nvecl,evall,evectl,plower,nrepl,idiml)
c
c  Normalize the eigenvectors
c
      call normal(nvecl,evectl)
c
c  Write out matrix of eigenvectors
c
      if(h.eq.0.0) call matout(evectl,nvecl,nvecl,msg2)
c
c  Write out the eigenvalues
c
      write(7,9000) h
      call vecout(evall,nvecl,msg3)
c
      return
 9000 format(1h1,10x,'Magnetic field strength = ',e12.5,' oe')
      end
c
c ***************************************************************************
```

```
c
      subroutine setu(h)
c
c        The array peturb is the matrix of the peturbation betweeen
c     basis vectors i1 and i2. The quantum numbers mi and mj are
c     calculated from the basis vector indicies.
c        The matrix has the form: basis(i1)*h*basis(i2)
c
c ---------------------------------------------------------------------
c
      common /upper/ nvecu,evalu(12),evectu(12,12),peturb(12,12)
      common /basisu/ nrepu,idimu(7),rmiu(12),rmju(12),ifu(12)
      common /paramu/ au,bu,gu
      common /const/ planck,c,pi,alpha,ele,rad,bohr,t0
c
c ---------------------------------------------------------------------
c
      do 200 i1=1,nvecu
        do 100 i2=1,nvecu
          peturb(i1,i2) = 0.0
  100   continue
  200 continue
c
      zeeman = bohr*gu*h
c
      do 400 i1=1,nvecu
        do 300 i2=1,nvecu
          rmj1 = rmju(i1)
          rmj2 = rmju(i2)
          rmi1 = rmiu(i1)
          rmi2 = rmiu(i2)
c
          f1 = sqrt((.5-rmj2)*(1.5+rmj2)*(2.5+rmi2)*(3.5-rmi2))
          f2 = sqrt((.5+rmj2)*(1.5-rmj2)*(2.5-rmi2)*(3.5+rmi2))
          diag = delta(rmj1,rmj2)*delta(rmi1,rmi2)
          off1 = delta(rmj1,rmj2+1.)*delta(rmi1,rmi2-1.)
          off2 = delta(rmj1,rmj2-1.)*delta(rmi1,rmi2+1.)
          peturb(i1,i2) = zeeman*rmj1*diag + au*rmj1*rmi1*diag
     a                  + .5*au*f1*off1 + .5*au*f2*off2
  300   continue
  400 continue
c
      return
      end
c
c ***********************************************************************
```

```
c
      subroutine setl(h)
c
c        The array plower is the matrix of the peturbation betweeen
c     basis vectors i1 and i2. The quantum numbers mi and mj are
c     taken from arrays rmil and rmjl.
c        Since the algebra for the matrix elements of the operator
c     (i dot j)**2 is messy, it is calculated by first working out
c     the matrix elements of (i dot j) and then multiplying matrices.
c
c ---------------------------------------------------------------------
c
      common /lower/  nvecl,evall(24),evectl(24,24),plower(24,24)
      common /basisl/ nrepl,idiml(9),rmil(24),rmjl(24),ifl(24)
      common /paraml/ al,bl,gl
      common /const/  planck,c,pi,alpha,ele,rad,bohr,t0
c
      dimension temp(24,24)
c
c ---------------------------------------------------------------------
c
      do 200 i1=1,nvecl
        do 100 i2=1,nvecl
          plower(i1,i2) = 0.0
          temp(i1,i2) = 0.0
  100   continue
  200 continue
c
      zeeman = bohr*gl*h
c
      do 400 i1=1,nvecl
        do 300 i2=1,nvecl
          rmj1 = rmjl(i1)
          rmj2 = rmjl(i2)
          rmi1 = rmil(i1)
          rmi2 = rmil(i2)
          f1 = sqrt((1.5-rmj2)*(2.5+rmj2)*(2.5+rmi2)*(3.5-rmi2))
          f2 = sqrt((1.5+rmj2)*(2.5-rmj2)*(2.5-rmi2)*(3.5+rmi2))
          diag = delta(rmj1,rmj2)*delta(rmi1,rmi2)
          off1 = delta(rmj1,rmj2+1.)*delta(rmi1,rmi2-1.)
          off2 = delta(rmj1,rmj2-1.)*delta(rmi1,rmi2+1.)
          temp(i1,i2) = rmj1*rmi1*diag + .5*f1*off1 + .5*f2*off2
  300   continue
  400 continue
c
      do 700 i1=1,nvecl
```

```
        do 600 i2=1,nvecl
          do 500 j=1,nvecl
            plower(i1,i2) = plower(i1,i2) + temp(i1,j)*temp(j,i2)
  500       continue
  600     continue
  700 continue
c
      c1 = bl/20.
      c2 = al + bl/40.
      do 900 i1=1,nvecl
        do 800 i2=1,nvecl
          plower(i1,i2) = c1*plower(i1,i2) + c2*temp(i1,i2)
  800     continue
  900 continue
c
      c3 = -35.0*bl/64.0
      do 1000 i1=1,nvecl
        plower(i1,i1) = zeeman*rmjl(i1) + c3 + plower(i1,i1)
 1000 continue
c
      return
      end
c
c ***************************************************************************
c
      subroutine eigen(n,eval,evect,p,nrep,idim)
c
c       This routine diagonalizes the matrix p and returns the
c     eigenvectors in array evect and the eigenvalues in array
c     eval. The array p is assumed to be in block diagonal form with
c     nrep blocks. The dimension of each block is stored in array
c     idim. Each block is broken out and diagonalized separately.
c     This is done in order to avoid diagonalizing large matrices.
c       The dimensions of the arrays set in this routine
c     assume that at most we will be dealing with a 4 x 4 matrix.
c       jacobi returns the eigenvectors stored as columns in the
c     array a.
c
c ---------------------------------------------------------------------
c
      dimension eval(n),evect(n,n),p(n,n),idim(nrep)
      dimension a(16),e(4),b(16)
c
c ---------------------------------------------------------------------
c
      do 200 i=1,n
```

```
        do 100 j=1,n
          evect(i,j) = 0.0
  100   continue
  200 continue
c
      index = 0
      do 1000 i=1,nrep
        m = idim(i)
        do 500 j=1,m
          do 400 k=1,m
            a(j+(k-1)*m) = p(index+j,index+k)
  400     continue
  500   continue
c
        call jacobi(a,m,m,e,b,nrot)
c
        do 700 j=1,m
          eval(index+j) = e(j)
          do 600 k=1,m
            evect(index+j,index+k) = b(j+(k-1)*m)
  600     continue
  700   continue
c
        index = index + m
 1000 continue
c
      return
      end
c
c ***********************************************************************
c
      subroutine jacobi(a,n,np,d,v,nrot)
c
c ---------------------------------------------------------------------
c
      parameter (nmax=100)
      dimension a(np,np),d(np),v(np,np),b(nmax),z(nmax)
c
c ---------------------------------------------------------------------
c
c     This initializes the identity matrix.
c
      do 12 ip=1,n
        do 11 iq=1,n
          v(ip,iq)=0.
   11   continue
```

```
      v(ip,ip)=1.
   12 continue
c
c     This initializes b and d to the diagonal a.
c     z will accumulate terms in the form of taqp.
c
      do 13 ip=1,n
        b(ip)=a(ip,ip)
        d(ip)=b(ip)
        z(ip)=0.
   13 continue
c
c     This sums the off diagonal elements.
c
      nrot=0
      do 24 i=1,50
        sm=0.
        do 15 ip=1,n-1
          do 14 iq=ip+1,n
            sm=sm+abs(a(ip,iq))
   14     continue
   15   continue
c
c     sm converges to zero as the off diagonal elements go to zero.
c
        if(sm.eq.0.)return
        if(i.lt.4)then
          tresh=0.2*sm/n**2
        else
          tresh=0.
        endif
        do 22 ip=1,n-1
          do 21 iq=ip+1,n
            g=100.*abs(a(ip,iq))
            if((i.gt.4).and.(abs(d(ip))+g.eq.abs(d(ip)))
     a          .and.(abs(d(iq))+g.eq.abs(d(iq))))then
              a(ip,iq)=0.
            else if(abs(a(ip,iq)).gt.tresh)then
              h=d(iq)-d(ip)
              if(abs(h)+g.eq.abs(h))then
                t=a(ip,iq)/h
              else
                theta=0.5*h/a(ip,iq)
                t=1./(abs(theta)+sqrt(1.+theta**2))
                if(theta.lt.0.)t=-t
              endif
```

```
            c=1./sqrt(1+t**2)
            s=t*c
            tau=s/(1.+c)
            h=t*a(ip,iq)
            z(ip)=z(ip)-h
            z(iq)=z(iq)+h
            d(ip)=d(ip)-h
            d(iq)=d(iq)+h
            a(ip,iq)=0.
            do 16 j=1,ip-1
              g=a(j,ip)
              h=a(j,iq)
              a(j,ip)=g-s*(h+g*tau)
              a(j,iq)=h+s*(g-h*tau)
16          continue
            do 17 j=ip+1,iq-1
              g=a(ip,j)
              h=a(j,iq)
              a(ip,j)=g-s*(h+g*tau)
              a(j,iq)=h+s*(g-h*tau)
17          continue
            do 18 j=iq+1,n
              g=a(ip,j)
              h=a(iq,j)
              a(ip,j)=g-s*(h+g*tau)
              a(iq,j)=h+s*(g-h*tau)
18          continue
            do 19 j=1,n
              g=v(j,ip)
              h=v(j,iq)
              v(j,ip)=g-s*(h+g*tau)
              v(j,iq)=h+s*(g-h*tau)
19          continue
            nrot=nrot+1
          endif
21      continue
22    continue
      do 23 ip=1,n
        b(ip)=b(ip)+z(ip)
        d(ip)=b(ip)
        z(ip)=0.
23    continue
24  continue
c
      pause '50 iterations should never happen'
      return
```

```
 9000 format(1x,i4)
 9001 format(1x,f8.4)
      end
c
c ***************************************************************************
c
      subroutine acoeff
c
c       this routine calculates the a-coefficient for the various
c     hyperfine transitions when there is magnetic field splitting.
c     of the possible 288 transitions most are forbidden by the
c     selection rules.
c       the arrays al,ar,and az contain the a coefficients for the
c     left handed circularly polarized, the right handed circularly
c     polarized, and the linearly polarized transitions. these
c     arrays contain matrix elements of the magnetic dipole operator
c     between eigenstates formed from a combination of basis states.
c     recall that the matrix elements of the magnetic dipole operator
c     between basis states are already stored in arrays tl,tr, and tz.
c       the wavenumbers for all possible transitions are stored in
c     the array wave.
c       the age of the galaxy is taken as 5.e17 sec. any transition
c     with a longer lifetime is arbitrarily set to zero.
c
c ---------------------------------------------------------------------
c
      common /upper/   nvecu,evalu(12),evectu(12,12),peturb(12,12)
      common /lower/   nvecl,evall(24),evectl(24,24),plower(24,24)
      common /dipole/  tl(12,24),tr(12,24),tz(12,24)
      common /transit/ wlase(6),wave(12,24),aq(12,24),ar(12,24),
     a                 az(12,24)
      common /prob/    pl(12,24),pr(12,24),pz(12,24)
      common /const/   planck,c,pi,alpha,ele,rad,bohr,t0
c
      ifirst=1
      age=5.e17
c
c ---------------------------------------------------------------------
c
      if(ifirst.gt.1) go to 100
c
c     factor was broken down to avoid the use of double precision
c
        factor = 64.*(pi**4)*(ele*rad*alpha/2.)/planck/3.0
        factor = factor*ele*rad*alpha/2.
        ifirst = ifirst + 1
```

```
  100 continue
c
      do 300 i=1,nvecl
        do 200 j=1,nvecu
          wave(j,i) = (evalu(j) - evall(i)) + t0
  200   continue
  300 continue
c
c     transform matrix elements from basis states to eigenstates
c
      do 700 i=1,nvecu
        do 600 j=1,nvecl
          suml = 0.0
          sumr = 0.0
          sumz = 0.0
          do 500 k=1,nvecu
            do 400 l=1,nvecl
              suml = suml + evectu(k,i)*tl(k,l)*evectl(l,j)
              sumr = sumr + evectu(k,i)*tr(k,l)*evectl(l,j)
              sumz = sumz + evectu(k,i)*tz(k,l)*evectl(l,j)
  400       continue
  500     continue
          pl(i,j) = suml**2
          pr(i,j) = sumr**2
          pz(i,j) = sumz**2
  600   continue
  700 continue
c
      sump = 0.0
      do 900 i=1,nvecu
        do 800 j=1,nvecl
          f1 = factor*wave(i,j)**3
          aq(i,j) = f1*pl(i,j)
          ar(i,j) = f1*pr(i,j)
          az(i,j) = f1*pz(i,j)
          sump = sump + pl(i,j) + pr(i,j) + pz(i,j)
  800   continue
  900 continue
c
      rage = 1./age
      suma = 0.0
      do 1100 i=1,nvecu
        do 1000 j=1,nvecl
          if(aq(i,j).lt.rage) aq(i,j) = 0.0
          if(ar(i,j).lt.rage) ar(i,j) = 0.0
          if(az(i,j).lt.rage) az(i,j) = 0.0
```

```
          suma = suma + aq(i,j) + ar(i,j) + az(i,j)
 1000    continue
 1100 continue
c
      suma = suma/12.
      write(7,9000) sump,suma
c
      return
 9000 format(///,10x,'total transition probability ',e12.6,
     a       ///,10x,'total a-coefficient ',e12.6)
 9500 format(i4,5(e12.5))
      end
c
c ***************************************************************************
c
      function delta(ri,rj)
c
c ---------------------------------------------------------------
c
c       This is the kronecker delta.  It is non-zero only when ri
c     equals rj within round off error.
c
      round=1.e-12
c
      delta = 0.0
      if(abs(ri-rj).lt.round) delta = 1.0
c
      return
      end
c
c ***************************************************************************
c
      subroutine absorb
c
c       In this routine the degeneracy is considered removed and a
c     line center absorption is calculated for each transition.
c
c ---------------------------------------------------------------
c
      common/upper/ nvecu,evalu(12),evectu(12,12),peturb(12,12)
      common/lower/ nvecl,evall(24),evectl(24,24),plower(24,24)
      common/transit/ wlase(6),wave(12,24),aq(12,24),ar(12,24),az(12,24)
      common/sigma/ sigmal(12,24),sigmar(12,24),sigmaz(12,24)
      common/line/ wdopp,wlornz,ratio,voigt0,npts,shape(101),
     a             rl(101),rr(101),rz(101)
      common/const/ planck,c,pi,alpha,ele,rad,bohr,t0
```

```
c
      ifirst=1
c
c ---------------------------------------------------------------
c
      if(ifirst.gt.1) go to 100
         store = voigt0/(8.*pi)
         store = store/12.
         ifirst = ifirst + 1
  100 continue
c
      do 300 i=1,nvecu
         do 200 j=1,nvecl
            sigmal(i,j) = store*aq(i,j)/wave(i,j)**2
            sigmar(i,j) = store*ar(i,j)/wave(i,j)**2
            sigmaz(i,j) = store*az(i,j)/wave(i,j)**2
  200    continue
  300 continue
c
      return
      end
c
c ***************************************************************************
c
      subroutine scan(wavmax,wavmin)
c
c        this routine scans the various transitions to find the
c     max and min wavelengths.
c
c ---------------------------------------------------------------
c
      common/upper/ nvecu,evalu(12),evectu(12,12),peturb(12,12)
      common/lower/ nvecl,evall(24),evectl(24,24),plower(24,24)
      common/transit/ wlase(6),wave(12,24),aq(12,24),ar(12,24),az(12,24)
      common/line/ wdopp,wlornz,ratio,voigt0,npts,shape(101),
     a             rl(101),rr(101),rz(101)
c
c ---------------------------------------------------------------
c
      wavmax = wlase(1)
      wavmin = wlase(1)
      testl = wavmin
      testr = wavmin
      testz = wavmin
c
      do 200 i=1,nvecu
```

```
        do 100 j=1,nvecl
          if(aq(i,j).gt.0.0) testl = wave(i,j)
          if(ar(i,j).gt.0.0) testr = wave(i,j)
          if(az(i,j).gt.0.0) testz = wave(i,j)
          wavmax = amax1(wavmax,testl,testr,testz,7603.50)
          wavmin = amin1(wavmin,testl,testr,testz,7602.35)
  100   continue
  200 continue
c
      return
      end
c
c ***********************************************************************
c
      subroutine gain(wavmax,wavmin,ifield)
c
c       this routine scans a particular wavelength range to find the
c     maximum value of the stimulated emission cross section.
c
c ----------------------------------------------------------------
c
      double precision xarray(8000)
      common/upper/ nvecu,evalu(12),evectu(12,12),peturb(12,12)
      common/lower/ nvecl,evall(24),evectl(24,24),plower(24,24)
      common/transit/ wlase(6),wave(12,24),aq(12,24),ar(12,24),az(12,24)
      common/sigma/ sigmal(12,24),sigmar(12,24),sigmaz(12,24)
      common/line/ wdopp,wlornz,ratio,voigt0,npts,shape(101),
     a             rl(101),rr(101),rz(101)
      common/ginteg/ gnul(8000),gnur(8000),gnuz(8000),nstep,
     a               delx(10),xtotal,broad(16000),nbig,ncent,
     b               xarray,ncount,bigger,nlin,nright,nleft
      common/const/ planck,c,pi,alpha,ele,rad,bohr,t0
      common/gains/ sv1,sv2,sv3
c
c ----------------------------------------------------------------
c
c
      rmax = wavmax + 5.*wdopp/c
      rmin = wavmin - 5.*wdopp/c
      step = (rmax - rmin)/float(nstep - 1)
c
      do 600 i=1,nstep
        gnul(i) = 0.0
        gnur(i) = 0.0
        gnuz(i) = 0.0
  600 continue
```

```
c
      do 300 i=1,nvecu
        do 200 j=1,nvecl
          temp1 = sigmal(i,j)
          temp2 = sigmar(i,j)
          temp3 = sigmaz(i,j)
          r0  = (rmin - wave(i,j))/step
          index = ifix(r0 + sign(.5,r0)) + ncent - 1
          if(index.lt.0) index = 0
          nend = nstep
          nn = nbig - index - nstep
          if(nn.lt.0) nend = nend + nn
          do 100 k=1,nend
            gnul(k) = gnul(k) + temp1*broad(index + k)
            gnur(k) = gnur(k) + temp2*broad(index + k)
            gnuz(k) = gnuz(k) + temp3*broad(index + k)
  100       continue
  200     continue
  300 continue
c
      g0max1 = 0.0
      g0max2 = 0.0
      g0max3 = 0.0
      index1 = 0
      index2 = 0
      index3 = 0
c
      do 400 i=1,nstep
        g0max1 = amax1(g0max1,gnul(i))
        g0max2 = amax1(g0max2,gnur(i))
        g0max3 = amax1(g0max3,gnuz(i))
        if(g0max1.eq.gnul(i)) index1 = i
        if(g0max2.eq.gnur(i)) index2 = i
        if(g0max3.eq.gnuz(i)) index3 = i
  400 continue
c
c     save max gains on first pass through this routine
c     (this is the zero-field case)
      if(ifield.eq.0) sv1 = g0max1
      if(ifield.eq.0) sv2 = g0max2
      if(ifield.eq.0) sv3 = g0max3
c
      rg01 = rmin + step*float(index1 - 1)
      rg02 = rmin + step*float(index2 - 1)
      rg03 = rmin + step*float(index3 - 1)
c
```

```
      write(7,9000) rmin,rmax,step,g0max1,rg01
      write(7,9100)
      write(7,9000) rmin,rmax,step,g0max2,rg02
      write(7,9200)
      write(7,9000) rmin,rmax,step,g0max3,rg03
      write(7,9300)
c
  650 continue
c
c     set up array of wavenumbers so that the entire spectrum can
c     be plotted in PLOTIT5
c     also scale gain arrays to zero field value
      do 700 i=1,nstep
         xarray(i) = dble(rmin) + dble(step)*dble(float(i-1))
         gnul(i) = gnul(i)/sv1
         gnur(i) = gnur(i)/sv2
         gnuz(i) = gnuz(i)/sv3
  700 continue
c
      return
 9000 format(//,5x,'in a wavenumber scan from ',f12.6,' 1/cm to ',
     a       f12.6,' 1/cm in steps of ',e12.6,' 1/cm',/,5x,
     b       'a maximum stimulated emission cross section of ',e12.6,
     c       ' sq cm was found.',/,5x,'this maximum value occurs ',
     d       'at a position of ',f12.6,' 1/cm')
 9100 format(5x,'with left handed polarization ')
 9200 format(5x,'with right handed polarization')
 9300 format(5x,'with linear polarization')
c
      end
c
c ***********************************************************************
c
      subroutine setlin(wavmax,wavmin)
c
c        this routine initializes the array broad with line shape
c     information. the location broad(ncent) contains the center
c     of the symmetric line shape profile.
c
c ---------------------------------------------------------------
c
      double precision xarray(8000)
      common/line/ wdopp,wlornz,ratio,voigt0,npts,shape(101),
     a             rl(101),rr(101),rz(101)
      common /ginteg/  gnul(8000),gnur(8000),gnuz(8000),nstep,
     a                 delx(10),xtotal,broad(16000),nbig,ncent,
```

```
     b                xarray,ncount,bigger,nlin,nright,nleft
      common/const/ planck,c,pi,alpha,ele,rad,bohr,t0
c
c ---------------------------------------------------------------
c
c
      rmax = wavmax + 5.*wdopp/c
      rmin = wavmin - 5.*wdopp/c
      step = c*(rmax - rmin)/float(nstep-1)
      x = 0.0
      call erf(x,ratio,rim,re0)
c
      do 100 i=1,nbig
        broad(i) = 0.0
  100 continue
c
      istart = ncent + 1
      broad(ncent) = 1.0
      delnu = 0.0
      do 200 i=istart,nbig
        delnu = delnu + step
        iback = ncent - (i - ncent)
        x = -2.*sqrt(alog(2.))*delnu/wdopp
        call erf(x,ratio,rim,re)
        broad(i) = re/re0
        broad(iback) = broad(i)
        if(broad(i).lt.1.e-6) go to 300
  200 continue
  300 continue
c
      return
      end
c
c ***************************************************************************
c
      subroutine exprt(wavmax,wavmin)
c
c       this routine searches the integrated gain arrays for
c     comparison with experiment.
c
c ---------------------------------------------------------------
c
      double precision xarray(8000)
      common/line/ wdopp,wlornz,ratio,voigt0,npts,shape(101),
     a             rl(101),rr(101),rz(101)
      common /ginteg/  gnul(8000),gnur(8000),gnuz(8000),nstep,
```

```
     a              delx(10),xtotal,broad(16000),nbig,ncent,
     b              xarray,ncount,bigger,nlin,nright,nleft
      common/const/ planck,c,pi,alpha,ele,rad,bohr,t0
c
c ---------------------------------------------------------------------
c
      g0l = 0.0
      g0r = 0.0
      g0z = 0.0
      do 100 i=1,nstep
        g0l = amax1(g0l,gnul(i))
        if(g0l.eq.gnul(i)) il = i
        g0r = amax1(g0r,gnur(i))
        if(g0r.eq.gnur(i)) ir = i
        g0z = amax1(g0z,gnuz(i))
        if(g0z.eq.gnuz(i)) iz = i
  100 continue
c
      rmin = wavmin - 5.*wdopp/c
      rmax = wavmax + 5.*wdopp/c
      step = (rmax - rmin)/float(nstep - 1)
c
      rnul = rmin + float(il - 1)*step
      rnur = rmin + float(ir - 1)*step
      rnuz = rmin + float(iz - 1)*step
c
c  Divide integrared gains by total integration length
c
      g0l = g0l/xtotal
      g0r = g0r/xtotal
      g0z = g0z/xtotal
c
      write(7,9000)
      write(7,9100) g0l,rnul,g0r,rnur,g0z,rnuz
c
      return
 9000 format(///,50x,'maximum gains',/25x,'polarization',9x,'gain',
     a       10x,'wavenumber',/)
 9100 format(25x,'left handed ',5x,e12.6,5x,f12.6,/,
     a       25x,'right handed',5x,e12.6,5x,f12.6,/,
     b       25x,'linear      ',5x,e12.6,5x,f12.6)
      end
c
c ********************************************************************
c
      subroutine synth
```

```
c
c       this routine calculates the absorption at the position of the
c     3-4 transition in zero field.
c
c ---------------------------------------------------------------------
c
      common /upper/    nvecu,evalu(12),evectu(12,12),peturb(12,12)
      common /lower/    nvecl,evall(24),evectl(24,24),plower(24,24)
      common /transit/ wlase(6),wave(12,24),aq(12,24),ar(12,24),
     a                 az(12,24)
      common /sigma/    sigmal(12,24),sigmar(12,24),sigmaz(12,24)
      common /line/     wdopp,wlornz,ratio,voigt0,npts,shape(101),
     a                 rl(101),rr(101),rz(101)
      common /const/    planck,c,pi,alpha,ele,rad,bohr,t0
c
c ---------------------------------------------------------------------
c
      x = 0.0
      call erf(x,ratio,rim,re0)
c
      do 400 i=1,npts
        rnu = shape(i)*1.e6
        suml = 0.0
        sumr = 0.0
        sumz = 0.0
        do 300 j=1,nvecu
          do 200 k=1,nvecl
            delnu = rnu + c*(wlase(1) - wave(j,k))
            x = -2.*sqrt(alog(2.))*delnu/wdopp
            call erf(x,ratio,rim,re)
            suml = suml + re*sigmal(j,k)/re0
            sumr = sumr + re*sigmar(j,k)/re0
            sumz = sumz + re*sigmaz(j,k)/re0
 200      continue
 300    continue
        rl(i) = suml
        rr(i) = sumr
        rz(i) = sumz
 400  continue
c
      return
      end
c
c ********************************************************************
c
      subroutine synth2(absrb)
```

```
c
c       this routine synthesizes the absorption spectrum over
c     a bandwidth which includes all the lines in the spin-orbit
c     spectrum. this bandwidth is broken up into nband points.
c
c ---------------------------------------------------------------------
c
      common/upper/ nvecu,evalu(12),evectu(12,12),peturb(12,12)
      common/lower/ nvecl,evall(24),evectl(24,24),plower(24,24)
      common/transit/ wlase(6),wave(12,24),aq(12,24),ar(12,24),az(12,24)
      common/sigma/ sigmal(12,24),sigmar(12,24),sigmaz(12,24)
      common/band/ width,nband,bandw(8000),rlwide(8000)
      common/line/ wdopp,wlornz,ratio,voigt0,npts,shape(101),
     a             rl(101),rr(101),rz(101)
      common/const/ planck,c,pi,alpha,ele,rad,bohr,t0
c
c ---------------------------------------------------------------------
c
      start = -width/2.
      del = width/float(nband)
      f = start
      do 300 i=1,nband
        sum = 0.0
        do 200 j=1,nvecu
          do 100 k=1,nvecl
            delnu = f + c*(t0 - wave(j,k))
            x = -2.*sqrt(alog(2.))*delnu/wdopp
            call erf(x,ratio,rim,re)
            sum = sum + re*sigmal(j,k)
  100       continue
  200     continue
        bandw(i) = f
        f = f + del
        rlwide(i) = sum/absrb
  300 continue
c
      return
      end
c
c ***********************************************************************
c
      subroutine synth3
c
c       this routine calculates the absorption at the position of the
c     varius transitions in zero field. maximum and values are stored
c     for future reference.
```

```
c
c ---------------------------------------------------------------
c
      common/upper/ nvecu,evalu(12),evectu(12,12),peturb(12,12)
      common/lower/ nvecl,evall(24),evectl(24,24),plower(24,24)
      common/transit/ wlase(6),wave(12,24),aq(12,24),ar(12,24),az(12,24)
      common/sigma/ sigmal(12,24),sigmar(12,24),sigmaz(12,24)
      common/line/ wdopp,wlornz,ratio,voigt0,npts,shape(101),
     a             rl(101),rr(101),rz(101)
      common/hyper/ amaxl(6),aminl(6),amaxr(6),aminr(6),
     c              amaxz(6),aminz(6)
      common/const/ planck,c,pi,alpha,ele,rad,bohr,t0
c
      istart=26
      iend=76
c     ifirst=1
c
c ---------------------------------------------------------------
c
      do 150 i=1,6
        amaxr(i) = 0.0
        aminr(i) = 1.0
        amaxl(i) = 0.0
        aminl(i) = 1.0
        amaxz(i) = 0.0
        aminz(i) = 1.0
  150 continue
c
      do 500 m=1,6
      do 400 i=istart,iend
        rnu = shape(i)*1.e6
        suml = 0.0
        sumr = 0.0
        sumz = 0.0
        do 300 j=1,nvecu
          do 200 k=1,nvecl
            delnu = rnu + c*(wlase(m) - wave(j,k))
            x = -2.*sqrt(alog(2.))*delnu/wdopp
            call erf(x,ratio,rim,re)
            suml = suml + re*sigmal(j,k)
            sumr = sumr + re*sigmar(j,k)
            sumz = sumz + re*sigmaz(j,k)
  200       continue
  300     continue
        amaxl(m) = amax1(suml,amaxl(m))
        aminl(m) = amin1(suml,aminl(m))
```

```
        amaxr(m) = amax1(sumr,amaxr(m))
        aminr(m) = amin1(sumr,aminr(m))
        amaxz(m) = amax1(sumz,amaxz(m))
        aminz(m) = amin1(sumz,aminz(m))
  400 continue
  500 continue
c
      return
      end
c
c ***********************************************************************
c
      subroutine normal(n,array)
c
c        this routine assumes that the eigenvectors are stored as
c     columns in 'array'. this routine normalizes the eigenvectors.
c
c -----------------------------------------------------------------
c
      dimension array(n,n)
c
c -----------------------------------------------------------------
c
      do 300 i=1,n
         sum = 0.0
         do 100 j=1,n
            sum = sum + array(i,j)**2
  100    continue
         if(sum.eq.0.0) go to 400
         do 200 j=1,n
            array(i,j) = array(i,j)/sqrt(sum)
  200    continue
  300 continue
c
  400 continue
      if(sum.eq.0.0) write(7,9000)
      if(sum.eq.0.0) stop
c
      return
c
 9000 format(1h1,//,10x,'program terminated - zero length '
     a       'eigenvector found')
      end
c
c ***********************************************************************
c
```

```
      subroutine matout(array,n,m,msg)
c
c       This routing writes out the n by m array.
c
c -------------------------------------------------------------
c
      dimension array(n,m)
      character*8 msg(7)
c
c -------------------------------------------------------------
c
      write(7,9000) (msg(i),i=1,7)
      do 100 i=1,n
        write(7,9100) (array(i,j),j=1,m)
  100 continue
c
      return
 9000 format(//,5x,10a8,//)
 9100 format(1x,12(e10.4,1x),/)
c
      end
c
c ***************************************************************************
c
      subroutine vecout(vec,n,msg)
c
c       this routine writes out the vector vec.
c
c -------------------------------------------------------------
c
      dimension vec(n)
      character*8 msg(7)
c
c -------------------------------------------------------------
c
      write(7,9000) (msg(i),i=1,7)
      do 100 i=1,n
        write(7,9100) vec(i)
  100 continue
c
      return
 9000 format(//,5x,10a8,/)
 9100 format(50x,e10.4)
      end
c
c ***************************************************************************
```

```
c
      subroutine output(h,absrb)
c
c        this routine outputs all the transitions, their polarizations,
c     a coefficients and wavenumber.
c
c ---------------------------------------------------------------------
c
      common/upper/ nvecu,evalu(12),evectu(12,12),peturb(12,12)
      common/basisu/ nrepu,idimu(7),rmiu(12),rmju(12),ifu(12)
      common/lower/ nvecl,evall(24),evectl(24,24),plower(24,24)
      common/basisl/ nrepl,idiml(9),rmil(24),rmjl(24),ifl(24)
      common/transit/ wlase(6),wave(12,24),aq(12,24),ar(12,24),az(12,24)
      common/prob/ pl(12,24),pr(12,24),pz(12,24)
      common/line/ wdopp,wlornz,ratio,voigt0,npts,shape(101),
     a             rl(101),rr(101),rz(101)
      common /plotv/   rlsave(101,25),rrsave(101,25),rzsave(101,25),
     a                 field(160),nfield
      common/hyper/ amaxl(6),aminl(6),amaxr(6),aminr(6),
     c              amaxz(6),aminz(6)
c
      icount=0
c
c ---------------------------------------------------------------------
c
      icount = icount + 1
      write(7,9000) h
c
      do 200 i=1,nvecu
        do 100 j=1,nvecl
          if(aq(i,j).gt.0.0) write(7,9100) i,j,ifu(i),ifl(j),pl(i,j),
     a                                     aq(i,j),wave(i,j)
          if(ar(i,j).gt.0.0) write(7,9200) i,j,ifu(i),ifl(j),pr(i,j),
     a                                     ar(i,j),wave(i,j)
          if(az(i,j).gt.0.0) write(7,9300) i,j,ifu(i),ifl(j),pz(i,j),
     a                                     az(i,j),wave(i,j)
  100   continue
  200 continue
c
      write(7,9400)
      do 300 i=1,npts
        write(7,9500) shape(i),rl(i),rr(i),rz(i)
  300 continue
c
      if(icount.gt.1) go to 500
        absrb = 0.0
```

```
        do 400 i=1,npts
          absrb = amax1(absrb,rl(i),rr(i),rz(i))
  400   continue
  500 continue
      write(7,9600) absrb
c
      do 600 i=1,npts
        rl(i) = rl(i)/absrb
        rr(i) = rr(i)/absrb
        rz(i) = rz(i)/absrb
  600 continue
c
      do 700 i=1,npts
        rlsave(i,icount) = rl(i)
        rrsave(i,icount) = rr(i)
        rzsave(i,icount) = rz(i)
  700 continue
c
      write(7,9700)
      do 800 i=1,6
        if(i.le.3) ia = 3
        if(i.gt.3) ia = 2
        if(ia.eq.3) ib = 5 - i
        if(ia.eq.2) ib = 7 - i
        write(7,9800) ia,ib,amaxl(i),aminl(i)
        write(7,9800) ia,ib,amaxr(i),aminr(i)
        write(7,9800) ia,ib,amaxz(i),aminz(i)
  800 continue
c
      return
c
 9000 format(1h1,//,40x,'transitions at a field strength of ',
     a       e12.6,' oe',///,2x,'eigenvector',6x,'mi + mj',19x,
     b       'polarization',14x,'probability',5x,'a-coefficient',
     c       5x,'line position',/,
     c       1x,'upper  lower',3x,'upper  lower',5x,
     d       'left handed  right handed  linear',25x,
     e       '1/sec',13x,'1/cm',/)
 9100 format(1x,i3,4x,i3,5x,i3,4x,i3,t39,'x',t73,f10.8,5x,f12.9,7x,
     a       f11.6)
 9200 format(1x,i3,4x,i3,5x,i3,4x,i3,t53,'x',t73,f10.8,5x,f12.9,7x,
     a       f11.6)
 9300 format(1x,i3,4x,i3,5x,i3,4x,i3,t64,'x',t73,f10.8,5x,f12.9,7x,
     a       f11.6)
 9400 format(1h1,//,33x,'absorption cross section for various '
     a       'polarizations (sq cm)',/,30x,'detuning',7x,'left handed',
```

```
     b       5x,'right handed',8x,'linear',/)
 9500 format(30x,f8.2,7x,e10.4,7x,e10.4,7x,e10.4)
 9600 format(45x,'maximum absorption coefficient ',e12.6,/,45x,
     a       'plots scaled by this factor')
 9700 format(///,10x,'abrorption across line profile for various '
     a       'transitions and polarizations',/,8x,'transition',
     b       32x,'absorption',/,6x,'upper',5x,'lower',23x,'max',
     c       15x,'min')
 9800 format(7x,i2,8x,i2,21x,e12.6,5x,e12.6)
      end
c
c ***************************************************************************
c
      subroutine find(start,end)
c
c        This routine locates the point where the line shape factor
c     has decreased by 3 orders of magnitude. this information is
c     used in setting up the plots. values are returned in mhz.
c
c
c ---------------------------------------------------------------------
c
      common/line/ wdopp,wlornz,ratio,voigt0,npts,shape(101),
     a             rl(101),rr(101),rz(101)
c
c ---------------------------------------------------------------------
c
      del = .1*wdopp
      do 100 i=1,50
        delnu = del*float(i-1)
        x = -2.*sqrt(alog(2.))*delnu/wdopp
        call erf(x,ratio,rim,re)
        if(re.le.0.001) go to 200
  100 continue
  200 continue
c
      start = -delnu*1.e-6
      end = delnu*1.e-6
c
      return
      end
c
c ***************************************************************************
c
      subroutine erf(x,y,rim,re)
c
```

```
c     this program computes the error function for complex values of the
c     argument. it computes the function
c                exp(-z**2)*erfc(-i*z)
c     where z = x + i*y
c     if z = i*a - del, where a = sqrt(alog(2))*wlornz/wdopp
c     and del = 2*sqrt(alog2)*(nu - nu0)/wdopp, then re is the line
c     shape function
c
c
c ----------------------------------------------------------------------
c
      integer capn,nu,n,npl
      real x,y,re,rim
      real h,h2,rlmbda,r1,r2,s1,s2,t1,t2,c,s
      logical b,sign
      cst=1.12837916709551
      sign=.false.
c
c ----------------------------------------------------------------------
c
      if(x.lt.0.0) sign=.true.
c     x=abs(x)
      if(x.lt.0.0) x=0.0-x
      if(y.lt.4.29.and.x.lt.5.33) go to 100
      h=0.0
      capn = 0
      nu = 8
      go to 200
 100  s=(1.0-y/4.29)*sqrt(1.0-x*x/28.41)
      h=1.6*s
      h2=2.0*h
      capn=6.5+23*s
      rlmbda=h2**capn
      nu=9.5+21*s
 200  b=.false.
      if(h.eq.0.0.or.rlmbda.eq.0.0) b=.true.
 400  r1 = 0.0
      r2 = 0.0
      s1 = 0.0
      s2 = 0.0
      nup1=nu+1
      do 600 nn=1,nup1
      n=nu+1-nn
      np1=n+1
      t1=y+h+np1*r1
      t2=x-np1*r2
```

```
      c=.5/(t1*t1+t2*t2)
      r1=c*t1
      r2=c*t2
      if(h.gt.0.0.and.n.le.capn) go to 500
      go to 600
  500 t1=rlmbda+s1
      s1=r1*t1-r2*s2
      s2=r2*t1+r1*s2
      rlmbda=rlmbda/h2
  600 continue
      if(b) go to 700
      rim=cst*s2
      re=cst*s1
      go to 800
  700 rim=cst*r2
      re=cst*r1
  800 if(y.eq.0.0) re=exp(-x*x)
      if(sign) rim=-rim
      return
      end
c
c ***************************************************************************
c
      subroutine fileit(ifile,h,temp,press,ppbroad)
c
c ---------------------------------------------------------------------
c
      double precision xarray(8000)
      common /band/     width,nband,bandw(8000),rlwide(8000)
      common /ginteg/  gnul(8000),gnur(8000),gnuz(8000),nstep,
     a                 delx(10),xtotal,broad(16000),nbig,ncent,
     b                 xarray,ncount,bigger,nlin,nright,nleft
c
c ---------------------------------------------------------------------
c
      real gnulr(8000),big
      real xreal(8000)
c
      character*62 Line2
c
      character*7 s1
      character*6 s2
      character*4 s3
      character*4 s4
c
      iplot = iplot + 1
```

```
c
c     write(ifile,9000) h,temp,press,ppbroad
c
      if (h.ne.0) go to 888
      nlin=0
      nright=0
      nleft=0
      biglin=0.0
      bigright=0.0
      bigleft=0.0
      ncount=0
      big=0
c
  888 do 1 i=1,nstep
          gnulr(i)=0.0
          gnulr(i)=gnul(i)+gnur(i)
          if (h.ne.0) go to 1
          if (gnulr(i).le.big) go to 2
          ncount=i
          big=gnulr(i)
    2     if (gnul(i).le.bigleft) go to 3
          nleft=i
          bigleft=gnul(i)
    3     if (gnur(i).le.bigright) go to 4
          nright=i
          bigright=gnur(i)
    4     if (gnuz(i).le.biglin) go to 1
          nlin=i
          biglin=gnuz(i)
    1 continue
      if (h.eq.0) bigger=big
      do 5 i=1,nstep
          gnulr(i)=gnulr(i)/bigger
    5 continue
c
c convert xarray to a real
c
      do 101 i = 1,8000
        xreal(i) = SNGL(xarray(i))
  101 continue
c
      write (s1, '(f7.1)') h
      write (s2, '(f6.1)') temp
      write (s3, '(f4.1)') press
      write (s4, '(f4.1)') ppbroad
```

```
      Line2 = 'B='        // s1 //
     .        ' Gauss T=' // s2 //
     .        ' K P='     // s3 //
     .        ' Torr PB=' // s4 //
     .        ' MHz/Torr'

c
      call agsetf ('GRID/LEFT.',.10)
      call agsetf ('GRID/RIGHT.',.90)
      call agsetf ('GRID/BOTTOM.',.10)
      call agsetf ('GRID/TOP.',.75)
      call agseti ('LINE/MAXIMUM.', 60)
c
c     Set up the top label
c
      call agsetc ('LABEL/NAME.','T')
      call agseti ('LINE/NUMBER.',80)
      call agsetc ('LINE/TEXT.', Line2)

      call agsetf ('X/MINIMUM.', 7602.25)
      call agsetf ('X/MAXIMUM.', 7603.75)

      call agsetf ('Y/MINIMUM.', 0.0)
      call agsetf ('Y/MAXIMUM.', 1.0)

      call agseti ('AXIS/B/TICKS/MAJOR/SPACING/COUNT.', 3)
      call agsetf ('AXIS/B/NUMERIC/WIDTH/MANTISSA.', 0.05)
      call agsetf ('AXIS/B/NUMERIC/WIDTH/EXPONENT.', 0.03)

      call ANOTAT ('1/cm','G/Go',0,0,0,0)
      call EZXY (xreal,gnuz,nstep,'GAIN SPECTRUM: P POLARIZATION')
c
      return
 9000 format(1x,d25.16,4(e13.8,'  '))
 9100 format(1x,d25.16,2(e13.8,'  '))
      end
```

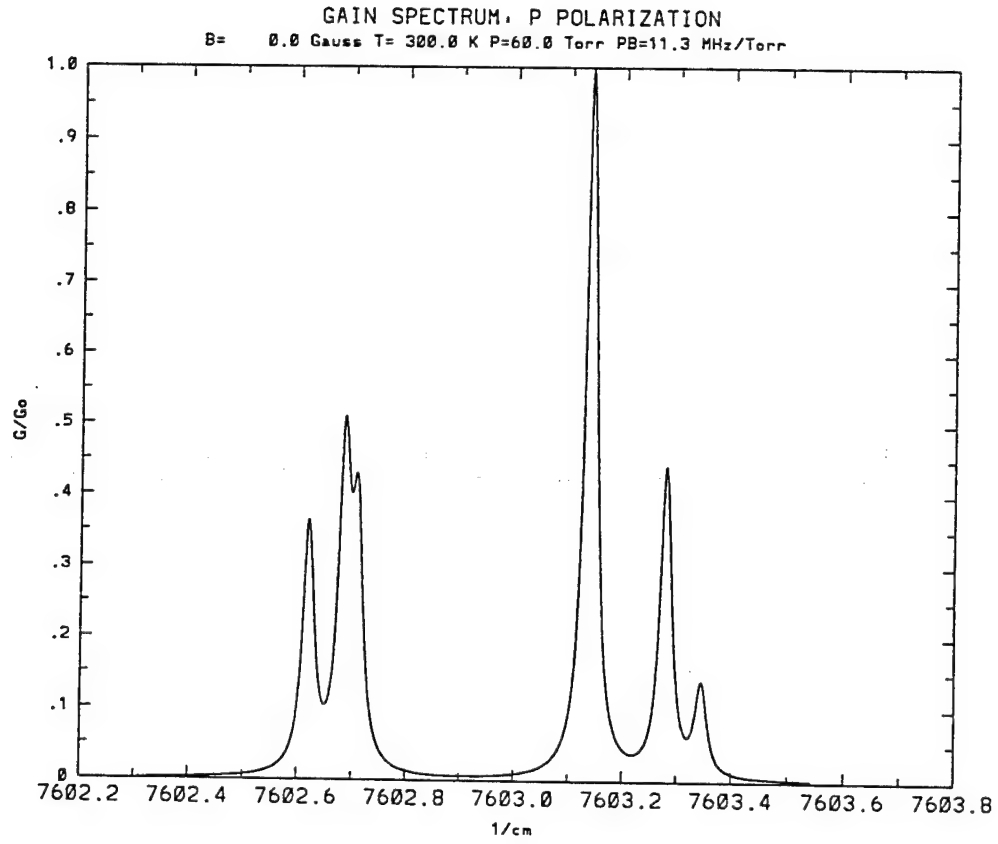

Figure A-1 Output of Vector Model Evaluated for Zero Field

APPENDIX B. Rate Equation Model

The following is a listing of the rate equation model which integrates the kinetic processes of an atomic iodine photodissociation laser over time. The initial effort was started about 1987 by Ralph Tate on a PC/AT computer at the Air Force Weapons Laboratory Chemical Laser Facility. Since 1991, I have changed and added much, using an Iris workstation to perform the calculations. I have produced several different versions of the code, as described in Section 2.4, but only the 15 equation model named I.f and the graphics routines to plot the output are listed below.

Input to I.f is provided by a test file listed below:

```
2.8 16.0 0.175 0.90 0.000000018 0.96415 10.0 0.0 60.0 0.0 0.0000000015 0.0000000004 1.0 0.0
```

The program I.f is compiled with a standard FORTRAN compiler, and the DLSODE library is linked in. A description from the DLSODE library is listed below, including author and version:

```
c
c*** from netlib, Wed Mar 13 16:10:52 EST 1991 ***
c
      subroutine dlsode (f, neq, y, t, tout, itol, rtol, atol, itask,
     1           istate, iopt, rwork, lrw, iwork, liw, jac, mf)
      external f, jac
      integer neq, itol, itask, istate, iopt, lrw, iwork, liw, mf
      double precision y, t, tout, rtol, atol, rwork
      dimension neq(1), y(1), rtol(1), atol(1), rwork(lrw), iwork(liw)
c-----------------------------------------------------------------------
c this is the march 30, 1987 version of
c lsode.. livermore solver for ordinary differential equations.
c this version is in double precision.
c
c lsode solves the initial value problem for stiff or nonstiff
c systems of first order ode-s,
```

```
c     dy/dt = f(t,y) ,  or, in component form,
c     dy(i)/dt = f(i) = f(i,t,y(1),y(2),...,y(neq)) (i = 1,...,neq).
c lsode is a package based on the gear and gearb packages, and on the
c october 23, 1978 version of the tentative odepack user interface
c standard, with minor modifications.
c-----------------------------------------------------------------------
c reference..
c     alan c. hindmarsh,  odepack, a systematized collection of ode
c     solvers, in scientific computing, r. s. stepleman et al. (eds.),
c     north-holland, amsterdam, 1983, pp. 55-64.
c-----------------------------------------------------------------------
c author and contact.. alan c. hindmarsh,
c                      computing and mathematics research div., l-316
c                      lawrence livermore national laboratory
c                      livermore, ca 94550.
c-----------------------------------------------------------------------
```

After the code is compiled, it is executed, producing an output file in a standard binary format. The output file is read by the graphics routines that follow the code listing, and standard Computer Graphics Metafile (CGM) files are produced. The graphics routines were written to be compiled with the NCAR Graphics library. The CGM files produced by the routines in the NCAR Graphics library are translated to postscript and sent to a printer.

```
c **********************************************************************
c
c ATOMIC IODINE PHOTODISSOCIATION LASER RATE EQUATION MODEL
16NIPQRS
c
c **********************************************************************
c
c  B. Scott Hunt
c
c  last modified : 31 JUL 93
c
c **********************************************************************
c
c This code solves the set of 15 first order coupled differential
c equations listed in the subroutine fex.  These equations describe
```

```
c an excimer pumped (248nm) pulsed atomic iodine laser.  The 9 number
c density equations take into account photolysis, stimulated emission,
c spontaneous emission, hyperfine relaxation, quenching, and
c recombination.  The 6 intensity equations describe the intensity
c within the cavity taking into account losses at the cell windows by
c ignoring the transit time of the light between the widows and
c resonator mirrors and lumping them into mirror losses.  A general
c loss is also distributed through the gain region.
c
c ***********************************************************************
c
      implicit real*8 (a-h,o-z)
      parameter(isize = 1500,jsize = 25,nsize = 16,lsize = 6)
      external fex, jex
      dimension y(nsize),rwork(22+9*nsize+nsize*nsize),iwork(20+nsize),
     1          yp(lsize),extrac(lsize),ssg(lsize),ssgold(lsize),
     2          ssgmax(lsize)
      real datar(isize,jsize)
      common /user/ cavlos,sn34,sn33,sn32,sn23,sn22,sn21,fill,hnui,
     1              pump,relax(14),sigma(6),yield,qcf3i,qcf3,qi2,r,
     2              qar,par,temp,a34,a33,a32,a23,a22,a21,ganlen,cavlen,
     3              recf3,dc2f6,di2,dcf3i,dar
c
c This opens the data files:
c
      open(unit=7,file='test',status='old')
      open(unit=8,file='data',form='unformatted',status='new')
      open(unit=9,file='text',status='new')
c
c This reads the input parameter file:
c
      read(7,*) ganlen,cavlen,energy,yield,pdelt,r2,roc,
     1          dloss,pcf3i,par,rrcu,rrcl,t1,s1
    1 format(A)
c
c This writes the parameters out to the screen:
c
      write(9,11)
   11 format(///)
c
      write(9,12)
   12 format(20x,'pulsed I* 16nipqr model '/)
c
      write(9,13) ganlen
   13 format(/5x,'gain length = ',f10.3,' cm.')
c
```

```
      write(9,14) cavlen
   14 format(/5x,'cavity length = ',f10.3,' cm.')
c
      write(9,15) energy
   15 format(/5x,'uv pump energy = ',f10.3,' joules')
c
      write(9,16) yield*100.0
   16 format(/5x,'i* yield = ',f10.3,' %')
c
      write(9,17) pdelt
   17 format(/5x,'pump pulse width = ',e10.3,' secs fwhm')
c
      write(9,18) r2
   18 format(/5x,'output mirror reflectivity = ',f10.3)
c
      write(9,19) dloss*100.0
   19 format(/5x,'internal loss = 'f10.3,' %')
c
      write(9,20) pcf3i
   20 format(/5x,'iodide pressure = ',f10.3,' torr')
c
      write(9,21) par
   21 format(/5x,'argon pressure = ',f10.3,' torr')
c
      write(9,22) rrcu
   22 format(/5x,'upper level relaxation rate constant = ',e10.2)
c
      write(9,23) rrcl
   23 format(/5x,'lower level relaxation rate constant = ',e10.2)
c
      write(9,24) t1
   24 format(/5x,'window transmission = ',f10.3,' cm^3')
c
      write(9,25) s1
   25 format(/5x,'scattering losses = ',f10.3,' cm^3')
c
c ****************************** constants ****************************
c
      hnu248 = 8.015d-19
      hnui = 1.51d-19
      pi = 0.314159d+01
      c = 3.0d10
      temp = 300.0
      r = 9.65d+18
      r1 = 0.998
      t2 = t1
```

```
      s2 = s1
      rad = 0.5
      snfudg = 1.0
c
c cross section of cf3i at 248nm from max-planck
c
      scf3i = 3.d-19
c
c pressure broadening coefficients (hz/torr)
c
      rcf3i = 11.3d6
      rar = 5.1d6
      ri = 16.2d6
c
c  stimulated emission probabilities (1/s)
c
      a34 = 5.08
      a33 = 2.20
      a32 = 0.63
      a23 = 2.46
      a22 = 3.07
      a21 = 2.37
c
c wavelengths of lasing transitions (cm)
c
      wl34 = 1.31521d-4
      wl33 = 1.31519d-4
      wl32 = 1.31518d-4
      wl23 = 1.31530d-4
      wl22 = 1.31529d-4
      wl21 = 1.31529d-4
c
c relaxation rate constants (cc/s)
c
c   relax(1)  ->      u(2-3)         rrcu
c   relax(2)  ->      u(3-2)     (5/7)*u(2-3)
c   relax(3)  ->      l(4-3)         rrcl
c   relax(4)  ->      l(4-2)         rrcl
c   relax(5)  ->      l(4-1)         rrcl
c   relax(6)  ->      l(3-2)         rrcl
c   relax(7)  ->      l(3-1)         rrcl
c   relax(8)  ->      l(2-1)         rrcl
c   relax(9)  ->      l(1-2)     (5/3)*l(2-1)
c   relax(10) ->      l(1-3)     (7/3)*l(3-1)
c   relax(11) ->      l(1-4)     (9/3)*l(4-1)
c   relax(12) ->      l(2-3)     (7/5)*l(3-2)
```

```
c  relax(13) ->      l(2-4)   (9/5)*l(4-2)
c  relax(14) ->      l(3-4)   (9/7)*l(4-3)
c
      relax(1) = rrcu
      relax(2) = (5.0/7.0)*relax(1)
      relax(3) = rrcl
      relax(4) = rrcl
      relax(5) = rrcl
      relax(6) = rrcl
      relax(7) = rrcl
      relax(8) = rrcl
      relax(9) = (5.0/3.0)*relax(8)
      relax(10) = (7.0/3.0)*relax(7)
      relax(11) = (9.0/3.0)*relax(5)
      relax(12) = (7.0/5.0)*relax(6)
      relax(13) = (9.0/5.0)*relax(4)
      relax(14) = (9.0/7.0)*relax(3)
c
c quenching rate constants (cc/molecule s)
c
      qcf3i = 3.3d-17
      qcf3 = 0.1d-12
      qar = 1.3d-19
      qi2 = 3.6d-11
c
c recombination rate constants (cc/molecule s)
c
      recf3 = 1.6d-11
c
c dimerization rate constants of free radicals (cc/molecule s)
c
      dc2f6 = 5.5d-12
c
c dimerization rate constants of iodine (cm^6 molecule^-2 s^-1)
c
      di2   = 3.9d-31
c     dcf3i = 1.3d-31
      dar   = 6.6d-33
      dcf3i = 0.0
c
c Set initial values:
c
      do 51 i=1,isize
        do 52 j=1,jsize
          datar(i,j)=0.0
  52    continue
```

```
   51 continue
      do 53 i=1,nsize
      y(i)=0.0
   53 continue
      do 54 i=1,lsize
      yp(i)=0.0
      extrac(i)=0.0
   54 continue
      y(13) = (r*pcf3i)/temp
      t = 0.0
      tout = 0.0
      deltat = 1.0d-9
      exmr = 0.0
      pump = 0.0
      before = 0.0
      tau = 0.0
c
c calculate losses due to scattering and transmission at r2
c
      omega = t2*(1-r2-s2)/(1+r2*(t2**2))
c
c calculate cavity loss rate from a distributed loss, mirror
c contributions and transmission losses
c
      cavlos = (c/cavlen)*(dloss*ganlen+(1-r1*(t1**2))/(1+r1*(t1**2))
     1          +(1-r2*(t2**2))/(1+r2*(t2**2)))
c
c calculate pump term from cell geometry:
c
      area = pi*(rad*rad)              ! area of aperture
      volabs = ganlen*2.0*rad*1.3
      volext = area*ganlen
      eabs = energy*volext*((1.0-dexp(-(scf3I*y(13)*(1.0+rad))))-
     1              (1.0-dexp(-(scf3I*y(13)*(1.0-rad)))))/volabs
      pwr = eabs/(hnu248*volext)
      pnorm = 2.0*dsqrt(dlog(0.2d+01))/(dsqrt(pi)*pdelt)
      fill = c*ganlen/cavlen
c
c calculate resonator parameters
c
      g1 = 1.0
      g2 = 1.0 - (cavlen/(roc*100.0))
      w1 = dsqrt((cavlen*1.315d-4/pi))*
     1     dsqrt(dsqrt(g2/(1.0-g2)))
      w2 = dsqrt((cavlen*1.315d-4/pi))*
     1     dsqrt(dsqrt(1.0/(g2*(1.0-g2))))
```

```
      spot1 = pi*w1**2
      spot2 = pi*w2**2
c
c  Set up the line shape parameter for a voigt:
c
      wdopp =  dsqrt(temp/300.0)*250.d6
      wlornz = pcf3i*rcf3i+par*rar
      ratio = dsqrt(dlog(.2d+01))*wlornz/wdopp
c
c  Find line shape factor at line center for normalized voigt:
c
      call erf(0.,ratio,rim,re)
c
c  Now include the doppler line shape normalization factor:
c
      press0 = 2.0/(pi*wlornz)
      dopp0  = 2.0*dsqrt(dlog(.2d+01)/pi)/wdopp
      voigt0 = re*dopp0
c
c lower level relaxation collisional partner (ar+cf3i)
c
      cpl = (r*par+r*pcf3i)/temp
c
c initial stimulated emission cross sections (cm**2)
c
      sigma(1) = a34*(wl34**2)*voigt0/(8.0*pi)
      sigma(2) = a33*(wl33**2)*voigt0/(8.0*pi)
      sigma(3) = a32*(wl32**2)*voigt0/(8.0*pi)
      sigma(4) = a23*(wl23**2)*voigt0/(8.0*pi)
      sigma(5) = a22*(wl22**2)*voigt0/(8.0*pi)
      sigma(6) = a21*(wl21**2)*voigt0/(8.0*pi)
c
c calculate noise-term constant Q
c
      sn = snfudg*(c/(2*cavlen))*(c*hnui*ganlen/(area*cavlen))
      sn34 = sn*sigma(1)
      sn33 = sn*sigma(2)
      sn32 = sn*sigma(3)
      sn23 = sn*sigma(4)
      sn22 = sn*sigma(5)
      sn21 = sn*sigma(6)
c
c calculate the initial small signal gain:
c
      ssg(1)=sigma(1)*(y(1)-(7.0/9.0)*y(3))
      ssg(2)=sigma(2)*(y(1)-y(4))
```

```
      ssg(3)=sigma(3)*(y(1)-(7.0/5.0)*y(5))
      ssg(4)=sigma(4)*(y(2)-(5.0/7.0)*y(4))
      ssg(5)=sigma(5)*(y(2)-y(5))
      ssg(6)=sigma(6)*(y(2)-(5.0/3.0)*y(6))
c
c required parameters for integrator
c
      neq = nsize
      lrw = 22+9*nsize+nsize*nsize
      liw = 20+nsize
      mf = 21
      do 101 i=1,lrw
        rwork(i) = 0.0
  101 continue
      do 102 i=1,liw
        iwork(i) = 0
  102 continue
      itol = 1
      rtol = 15.d-15
      atol = 15.d-14
      itask = 1
      istate = 1
      iopt = 1
      iwork(6) = 1000
c
c write initial values out to an array
c
      datar(1,1) = sngl(t)
      datar(1,2) = sngl(yp(1))
      do 151 nout = 1,nsize
        datar(1,nout+2) = sngl(y(nout))
  151 continue
      datar(1,nsize+3) = sngl(pump*hnu248*volext)
      do 152 nout = 1,lsize
        datar(1,nout+nsize+3) = sngl(ssg(nout))
  152 continue
c
c begin do loop
c
      do 1000 iout = 2,isize
c
      call dlsode(fex,neq,y,t,tout,itol,rtol,atol,itask,istate,
     1            iopt,rwork,lrw,iwork,liw,jex,mf)
c
c integrate excimer pump term over time interval
c
```

```
      exmr = exmr + pump*deltat
c
c calculate outcoupled power and
c integrate outcoupled power to get extracted energy
c
      do 201 i=1,lsize
        yp(i) = y(6+i)*area*omega
        extrac(i) = extrac(i) + yp(i)*deltat
        ssgold(i)=ssg(i)
  201 continue
c
c calculate the cavity build-up time
c
      if (yp(1).gt.1000.0) then
        before=10.0
      endif
      if (before.lt.1.0) then
          tau = tau + deltat
      endif
c
c write calculated values out to an array
c
      datar(iout,1) = sngl(t)
      datar(iout,2) = sngl(yp(1))
      do 251 nout = 1,nsize
        datar(iout,nout+2) = sngl(y(nout))
  251 continue
      datar(iout,nsize+3) = sngl(pump*hnu248*volext)
      do 252 nout = 1,lsize
        datar(iout,nout+nsize+3) = sngl(ssg(nout))
  252 continue
c
c  check for error in odepack:
c
      if (istate .lt. 0) go to 1001
c
c calculate pump term
c
      pump = dexp(-(4.0*dlog(0.2d+01)*((t-100.0d-9)**2)/
     1           (pdelt**2)))*pwr*pnorm
      if (pump.lt.1.0) then
          pump = 0.0
      endif
c
c calculate the small signal gain:
c
```

```
      ssg(1)=sigma(1)*(y(1)-(7.0/9.0)*y(3))
      ssg(2)=sigma(2)*(y(1)-y(4))
      ssg(3)=sigma(3)*(y(1)-(7.0/5.0)*y(5))
      ssg(4)=sigma(4)*(y(2)-(5.0/7.0)*y(4))
      ssg(5)=sigma(5)*(y(2)-y(5))
      ssg(6)=sigma(6)*(y(2)-(5.0/3.0)*y(6))
      do 301 i=1,lsize
        if (ssgold(i).gt.ssg(i)) then
          ssgmax(i) = ssgold(i)
        endif
  301 continue
c
c this increments the time by deltat
c
      tout = tout+deltat
c
 1000 continue
c
c end of do loop
c
c ***************************************************************************
c
c This writes the data array out to a binary file:
c
      do 351 iout=1,isize
        do 352 jout=1,jsize
          write(8) datar(iout,jout)
  352   continue
  351 continue
c
c This writes the rest of the parameters to the screen:
c
      write(9,401) exmr*hnu248*volext
  401 format(//5x,'excimer energy =',1pe10.2,' joules')
c
        write(9,402) extrac(1)
  402 format(//5x,'extracted energy =',1pe10.2,' joules')
c
      write(9,403) tau*1e9-50.0
  403 format(//5x,'cavity build-up time =',1pe10.2,' nsec')
c
        write(9,404) ssgmax(1)
  404 format(//5x,'maximum small signal gain =',1pe10.2,' /cm')
c
      write(9,405) iwork(11),iwork(12),iwork(13)
  405 format(//5x,'no. steps =',i6,'   no. f-s =',i6,'   no. j-s =',i6)
```

```
      go to 1002
c
 1001 write(9,451) istate
  451 format(//5x,'fatal error. run aborted with istate =',i3)
 1002 continue
c
c ***********************************************************************
c
      stop
      end
c
c
c ***********************************************************************
c
c     required subroutine fex
      subroutine fex (neq, t, y, ydot)
      implicit real*8 (a-h,o-z)
      parameter(nsize = 16)
      real*8 t, y, ydot
      dimension y(nsize), ydot(nsize)
      common /user/ cavlos,sn34,sn33,sn32,sn23,sn22,sn21,fill,hnui,
     1              pump,relax(14),sigma(6),yield,qcf3i,qcf3,qi2,r,
     2              qar,par,temp,a34,a33,a32,a23,a22,a21,ganlen,cavlen,
     3              recf3,dc2f6,di2,dcf3i,dar
c
c ********** upper level population density rate equations **********
c
c level 3 population density
c
      ydot(1) = (7.0/12.0)*yield*pump
     1 - (sigma(1)*(y(1)-(7.0/9.0)*y(3))*y(7))/hnui
     2 - (sigma(2)*(y(1)-y(4))*y(8))/hnui
     3 - (sigma(3)*(y(1)-(7.0/5.0)*y(5))*y(9))/hnui
     4 - y(1)*(a34+a33+a32)
     5 + (relax(1)*y(2)-relax(2)*y(1))*(y(3)+y(4)+y(5)+y(6))
     6 - (qcf3i*y(13)+qcf3*y(14)+qi2*y(15)+r*qar*par/temp)*y(1)
c
c level 2 population density
c
      ydot(2) = (5.0/12.0)*yield*pump
     1 - (sigma(4)*(y(2)-(5.0/7.0)*y(4))*y(10))/hnui
     2 - (sigma(5)*(y(2)-y(5))*y(11))/hnui
     3 - (sigma(6)*(y(2)-(5.0/3.0)*y(6))*y(12))/hnui
     4 - y(2)*(a23+a22+a21)
     5 + (relax(2)*y(1)-relax(1)*y(2))*(y(3)+y(4)+y(5)+y(6))
     6 - (qcf3i*y(13)+qcf3*y(14)+qi2*y(15)+r*qar*par/temp)*y(2)
```

```
c
c ***************************************************************************
c
c ********** lower level population density rate equations ************
c
c level 4 population density
c
      ydot(3) = (9.0/24.0)*(1.0-yield)*pump
     1 + (sigma(1)*(y(1)-(7.0/9.0)*y(3))*y(7))/hnui
     2 + y(1)*a34
     3 + (relax(14)*y(4)+relax(13)*y(5)+relax(11)*y(6)
     4 - (relax(3)+relax(4)+relax(5))*y(3))
     5 * (r*par/temp+y(13)+y(14)+y(15)+y(16))
     5 + (9.0/24.0)*(qcf3i*y(13)+qcf3*y(14)+qi2*y(15)+r*qar*par/temp)
     6 * (y(1)+y(2)) - recf3*y(14)*y(3)
     7 - (dar*r*par/temp+dcf3i*y(13)+di2*y(15))*y(3)**2
c
c level 3 population density
c
      ydot(4) = (7.0/24.0)*(1.0-yield)*pump
     1 + (sigma(2)*(y(1)-y(4))*y(8))/hnui
     2 + (sigma(4)*(y(2)-(5.0/7.0)*y(4))*y(10))/hnui
     3 + y(1)*a33 + y(2)*a23
     4 + (relax(3)*y(3)+relax(12)*y(5)+relax(10)*y(6)
     5 - (relax(14)+relax(6)+relax(7))*y(4))
     5 * (r*par/temp+y(13)+y(14)+y(15)+y(16))
     6 + (7.0/24.0)*(qcf3i*y(13)+qcf3*y(14)+qi2*y(15)+r*qar*par/temp)
     6 * (y(1)+y(2)) - recf3*y(14)*y(4)
     7 - (dar*r*par/temp+dcf3i*y(13)+di2*y(15))*y(4)**2
c
c level 2 population density
c
      ydot(5) = (5.0/24.0)*(1.0-yield)*pump
     1 + (sigma(3)*(y(1)-(7.0/5.0)*y(5))*y(9))/hnui
     2 + (sigma(5)*(y(2)-y(5))*y(11))/hnui
     3 + y(1)*a32 + y(2)*a22
     4 + (relax(4)*y(3)+relax(6)*y(4)+relax(9)*y(6)
     5 - (relax(13)+relax(12)+relax(8))*y(5))
     5 * (r*par/temp+y(13)+y(14)+y(15)+y(16))
     6 + (5.0/24.0)*(qcf3i*y(13)+qcf3*y(14)+qi2*y(15)+r*qar*par/temp)
     6 * (y(1)+y(2)) - recf3*y(14)*y(5)
     7 - (dar*r*par/temp+dcf3i*y(13)+di2*y(15))*y(5)**2
c
c level 1 population density
c
      ydot(6) = (3.0/24.0)*(1.0-yield)*pump
```

```
     1 + (sigma(6)*(y(2)-(5.0/3.0)*y(6))*y(12))/hnui
     2 + y(2)*a21
     3 + (relax(5)*y(3)+relax(7)*y(4)+relax(8)*y(5)
     4 - (relax(11)+relax(10)+relax(9))*y(6))
     5 * (r*par/temp+y(13)+y(14)+y(15)+y(16))
     5 + (3.0/24.0)*(qcf3i*y(13)+qcf3*y(14)+qi2*y(15)+r*qar*par/temp)
     6 * (y(1)+y(2)) - recf3*y(14)*y(6)
     7 - (dar*r*par/temp+dcf3i*y(13)+di2*y(15))*y(6)**2
c
c ***********************************************************************
c
c ********** two-way circulating intensity rate equations ***********
c
c                3-4 transition
c
      ydot(7) = sigma(1)*(y(1)-(7.0/9.0)*y(3))*fill*y(7)
     1        - cavlos*y(7) + 2*sn34*(ganlen/cavlen)*y(1)
c
c                3-3 transition
c
      ydot(8) = sigma(2)*(y(1)-y(4))*fill*y(8)
     1        - cavlos*y(8) + 2*sn33*(ganlen/cavlen)*y(1)
c
c                3-2 transition
c
      ydot(9) = sigma(3)*(y(1)-(7.0/5.0)*y(5))*fill*y(9)
     1        - cavlos*y(9) + 2*sn32*(ganlen/cavlen)*y(1)
c
c                2-3 transition
c
      ydot(10) = sigma(4)*(y(2)-(5.0/7.0)*y(4))*fill*y(10)
     1         - cavlos*y(10) + 2*sn23*(ganlen/cavlen)*y(2)
c
c                2-2 transition
c
      ydot(11) = sigma(5)*(y(2)-y(5))*fill*y(11)
     1         - cavlos*y(11) + 2*sn22*(ganlen/cavlen)*y(2)
c
c                2-1 transition
c
      ydot(12) = sigma(6)*(y(2)-(5.0/3.0)*y(6))*fill*y(12)
     1         - cavlos*y(12) + 2*sn21*(ganlen/cavlen)*y(2)
c
c ***********************************************************************
c
c cf3i population density
```

```
c
      ydot(13) = recf3*y(14)*(y(3)+y(4)+y(5)+y(6)) - pump
c
c cf3 population density
c
      ydot(14) = pump - recf3*y(14)*(y(3)+y(4)+y(5)+y(6))
     1          - dc2f6*y(14)**2
c
c i2 population density
c
      ydot(15) = (dcf3i*y(13)+dar*r*par/temp+di2*y(15))
     1          *(y(3)+y(4)+y(5)+y(6))**2
c
c c2f6 population density
c
      ydot(16) = dc2f6*y(14)**2
c
c
c ***************************************************************************
c
      return
      end
c
c
c ***************************************************************************
c
c  dummy subroutine for jacobian array
c
      subroutine jex (neq, t, y, ml, mu, pd, nrpd)
      implicit real*8 (a-h,o-z)
      parameter(nsize = 16)
      real*8 t, y, pd
      dimension y(nsize), pd(nrpd,nsize)
      common /user/ cavlos,sn34,sn33,sn32,sn23,sn22,sn21,fill,hnui,
     1              pump,relax(14),sigma(6),yield,qcf3i,qcf3,qi2,r,
     2              qar,par,temp,a34,a33,a32,a23,a22,a21,ganlen,cavlen,
     3              recf3,dc2f6,di2,dcf3i,dar
c
c  jacobian matrix:
c
      pd(1,1) = - (sigma(1)*y(7))/hnui
     1          - (sigma(2)*y(8))/hnui
     2          - (sigma(3)*y(9))/hnui
     3          - (a34+a33+a32)
     4          - relax(2)*(y(3)+y(4)+y(5)+y(6))
     5          - (qcf3i*y(13)+qcf3*y(14)+qi2*y(15)+r*qar*par/temp)
```

```
      pd(1,2) = + relax(1)*(y(3)+y(4)+y(5)+y(6))
      pd(1,3) = (sigma(1)*(7.0/9.0)*y(7))/hnui
     1          + (relax(1)*y(2)-relax(2)*y(1))
      pd(1,4) = (sigma(2)*y(8))/hnui
     1          + (relax(1)*y(2)-relax(2)*y(1))
      pd(1,5) = (sigma(3)*(7.0/5.0)*y(9))/hnui
     1          + (relax(1)*y(2)-relax(2)*y(1))
      pd(1,6) = (relax(1)*y(2)-relax(2)*y(1))
      pd(1,7) = - sigma(1)*(y(1)-(7.0/9.0)*y(3))/hnui
      pd(1,8) = - sigma(2)*(y(1)-y(4))/hnui
      pd(1,9) = - sigma(3)*(y(1)-(7.0/5.0)*y(5))/hnui
      pd(1,10) = 0.0
      pd(1,11) = 0.0
      pd(1,12) = 0.0
      pd(1,13) = - qcf3i*y(1)
      pd(1,14) = - qcf3*y(1)
      pd(1,15) = - qi2*y(1)
      pd(1,16) = 0.0
c
      pd(2,1) = + relax(2)*(y(3)+y(4)+y(5)+y(6))
      pd(2,2) = - (sigma(4)*y(10))/hnui
     1          - (sigma(5)*y(11))/hnui
     2          - (sigma(6)*y(12))/hnui
     3          - (a23+a22+a21)
     4          - relax(1)*(y(3)+y(4)+y(5)+y(6))
     5          - (qcf3i*y(13)+qcf3*y(14)+qi2*y(15)+r*qar*par/temp)
      pd(2,3) = (relax(2)*y(1)-relax(1)*y(2))
      pd(2,4) = (sigma(4)*(5.0/7.0)*y(10))/hnui
     1          + (relax(2)*y(1)-relax(1)*y(2))
      pd(2,5) = (sigma(5)*y(11))/hnui
     1          + (relax(2)*y(1)-relax(1)*y(2))
      pd(2,6) = (sigma(6)*(5.0/3.0)*y(12))/hnui
     1          + (relax(2)*y(1)-relax(1)*y(2))
      pd(2,7) = 0.0
      pd(2,8) = 0.0
      pd(2,9) = 0.0
      pd(2,10) = - (sigma(4)*(y(2)-(5.0/7.0)*y(4)))/hnui
      pd(2,11) = - (sigma(5)*(y(2)-y(5)))/hnui
      pd(2,12) = - (sigma(6)*(y(2)-(5.0/3.0)*y(6)))/hnui
      pd(2,13) = - qcf3i*y(2)
      pd(2,14) = - qcf3*y(2)
      pd(2,15) = - qi2*y(2)
      pd(2,16) = 0.0
c
      pd(3,1) = + (sigma(1)*y(7))/hnui
     1          + a34
```

```
     2         + (9.0/24.0)*(qcf3i*y(13)+qcf3*y(14)+qi2*y(15)
     3         + r*qar*par/temp)
      pd(3,2) = + (9.0/24.0)*(qcf3i*y(13)+qcf3*y(14)+qi2*y(15)
     1         + r*qar*par/temp)
      pd(3,3) = - (sigma(1)*(7.0/9.0)*y(7))/hnui
     1         - (relax(3)+relax(4)+relax(5))
     5         * (r*par/temp+y(13)+y(14)+y(15)+y(16))
     2         - recf3*y(14)
     3         - (dar*r*par/temp+dcf3i*y(13)+di2*y(15))*y(3)*2.0
      pd(3,4) = relax(14)*(r*par/temp+y(13)+y(14)+y(15)+y(16))
      pd(3,5) = relax(13)*(r*par/temp+y(13)+y(14)+y(15)+y(16))
      pd(3,6) = relax(11)*(r*par/temp+y(13)+y(14)+y(15)+y(16))
      pd(3,7) = + (sigma(1)*(y(1)-(7.0/9.0)*y(3)))/hnui
      pd(3,8) = 0.0
      pd(3,9) = 0.0
      pd(3,10) = 0.0
      pd(3,11) = 0.0
      pd(3,12) = 0.0
      pd(3,13) = + (relax(14)*y(4)+relax(13)*y(5)+relax(11)*y(6)
     1         - (relax(3)+relax(4)+relax(5))*y(3))
     2         + (9.0/24.0)*qcf3i*(y(1)+y(2)) - dcf3i*y(3)**2
      pd(3,14) = + (relax(14)*y(4)+relax(13)*y(5)+relax(11)*y(6)
     1         - (relax(3)+relax(4)+relax(5))*y(3))
     2         + (9.0/24.0)*qcf3*(y(1)+y(2)) - recf3*y(3)
      pd(3,15) = + (relax(14)*y(4)+relax(13)*y(5)+relax(11)*y(6)
     1         - (relax(3)+relax(4)+relax(5))*y(3))
     2         + (9.0/24.0)*qi2*(y(1)+y(2)) - di2*y(3)**2
      pd(3,16) = + (relax(14)*y(4)+relax(13)*y(5)+relax(11)*y(6)
     1         - (relax(3)+relax(4)+relax(5))*y(3))
c
      pd(4,1) = + (sigma(2)*y(8))/hnui
     1         + a33
     2         + (7.0/24.0)*(qcf3i*y(13)+qcf3*y(14)+qi2*y(15)
     3         + r*qar*par/temp)
      pd(4,2) = + (sigma(4)*y(10))/hnui
     1         + a23
     2         + (7.0/24.0)*(qcf3i*y(13)+qcf3*y(14)+qi2*y(15)
     3         + r*qar*par/temp)
      pd(4,3) = relax(3)*(r*par/temp+y(13)+y(14)+y(15)+y(16))
      pd(4,4) = - (sigma(2)*y(8))/hnui
     1         - (sigma(4)*(5.0/7.0)*y(10))/hnui
     2         - (relax(14)+relax(6)+relax(7))
     5         * (r*par/temp+y(13)+y(14)+y(15)+y(16))
     2         - recf3*y(14)
     3         - (dar*r*par/temp+dcf3i*y(13)+di2*y(15))*y(4)*2.0
      pd(4,5) = relax(12)*(r*par/temp+y(13)+y(14)+y(15)+y(16))
```

```
      pd(4,6) = relax(10)*(r*par/temp+y(13)+y(14)+y(15)+y(16))
      pd(4,7) = 0.0
      pd(4,8) = + (sigma(2)*(y(1)-y(4)))/hnui
      pd(4,9) = 0.0
      pd(4,10) = + (sigma(4)*(y(2)-(5.0/7.0)*y(4)))/hnui
      pd(4,11) = 0.0
      pd(4,12) = 0.0
      pd(4,13) = + (relax(3)*y(3)+relax(12)*y(5)+relax(10)*y(6)
     1          - (relax(14)+relax(6)+relax(7))*y(4))
     2          + (7.0/24.0)*qcf3i*(y(1)+y(2)) - dcf3i*y(4)**2
      pd(4,14) = + (relax(3)*y(3)+relax(12)*y(5)+relax(10)*y(6)
     1          - (relax(14)+relax(6)+relax(7))*y(4))
     2          + (7.0/24.0)*qcf3*(y(1)+y(2)) - recf3*y(4)
      pd(4,15) = + (relax(3)*y(3)+relax(12)*y(5)+relax(10)*y(6)
     1          - (relax(14)+relax(6)+relax(7))*y(4))
     2          + (7.0/24.0)*qi2*(y(1)+y(2)) - di2*y(4)**2
      pd(4,16) = + (relax(3)*y(3)+relax(12)*y(5)+relax(10)*y(6)
     1          - (relax(14)+relax(6)+relax(7))*y(4))
c
      pd(5,1) = + (sigma(3)*y(9))/hnui
     1          + a32
     2          + (5.0/24.0)*(qcf3i*y(13)+qcf3*y(14)+qi2*y(15)
     3          + r*qar*par/temp)
      pd(5,2) = + (sigma(5)*y(11))/hnui
     1          + a22
     2          + (5.0/24.0)*(qcf3i*y(13)+qcf3*y(14)+qi2*y(15)
     3          + r*qar*par/temp)
      pd(5,3) = relax(4)*(r*par/temp+y(13)+y(14)+y(15)+y(16))
      pd(5,4) = relax(6)*(r*par/temp+y(13)+y(14)+y(15)+y(16))
      pd(5,5) = - (sigma(3)*(7.0/5.0)*y(9))/hnui
     1          - (sigma(5)*y(11))/hnui
     2          - (relax(13)+relax(12)+relax(8))
     5          * (r*par/temp+y(13)+y(14)+y(15)+y(16))
     2          - recf3*y(14)
     3          - (dar*r*par/temp+dcf3i*y(13)+di2*y(15))*y(5)*2.0
      pd(5,6) = relax(9)*(r*par/temp+y(13)+y(14)+y(15)+y(16))
      pd(5,7) = 0.0
      pd(5,8) = 0.0
      pd(5,9) = + (sigma(3)*(y(1)-(7.0/5.0)*y(5)))/hnui
      pd(5,10) = 0.0
      pd(5,11) = + (sigma(5)*(y(2)-y(5)))/hnui
      pd(5,12) = 0.0
      pd(5,13) = + (relax(4)*y(3)+relax(6)*y(4)+relax(9)*y(6)
     1          - (relax(13)+relax(12)+relax(8))*y(5))
     2          + (5.0/24.0)*qcf3i*(y(1)+y(2)) - dcf3i*y(5)**2
      pd(5,14) = + (relax(4)*y(3)+relax(6)*y(4)+relax(9)*y(6)
```

```
     1          - (relax(13)+relax(12)+relax(8))*y(5))
     2          + (5.0/24.0)*qcf3*(y(1)+y(2)) - recf3*y(5)
      pd(5,15) = + (relax(4)*y(3)+relax(6)*y(4)+relax(9)*y(6)
     1          - (relax(13)+relax(12)+relax(8))*y(5))
     2          + (5.0/24.0)*qi2*(y(1)+y(2)) - di2*y(5)**2
      pd(5,16) = + (relax(4)*y(3)+relax(6)*y(4)+relax(9)*y(6)
     1          - (relax(13)+relax(12)+relax(8))*y(5))
c
      pd(6,1) = + (3.0/24.0)*(qcf3i*y(13)+qcf3*y(14)+qi2*y(15)
     1          + r*qar*par/temp)
      pd(6,2) = + (sigma(6)*y(12))/hnui
     1          + a21
     2          + (3.0/24.0)*(qcf3i*y(13)+qcf3*y(14)+qi2*y(15)
     3          + r*qar*par/temp)
      pd(6,3) = relax(5)*(r*par/temp+y(13)+y(14)+y(15)+y(16))
      pd(6,4) = relax(7)*(r*par/temp+y(13)+y(14)+y(15)+y(16))
      pd(6,5) = relax(8)*(r*par/temp+y(13)+y(14)+y(15)+y(16))
      pd(6,6) = - (sigma(6)*(5.0/3.0)*y(12))/hnui
     1          - (relax(11)+relax(10)+relax(9))
     5          * (r*par/temp+y(13)+y(14)+y(15)+y(16))
     2          - recf3*y(14)
     3          - (dar*r*par/temp+dcf3i*y(13)+di2*y(15))*y(6)*2.0
      pd(6,7) = 0.0
      pd(6,8) = 0.0
      pd(6,9) = 0.0
      pd(6,10) = 0.0
      pd(6,11) = 0.0
      pd(6,12) = + (sigma(6)*(y(2)-(5.0/3.0)*y(6)))/hnui
      pd(6,13) = + (relax(5)*y(3)+relax(7)*y(4)+relax(8)*y(5)
     1          - (relax(11)+relax(10)+relax(9))*y(6))
     2          + (3.0/24.0)*qcf3i*(y(1)+y(2)) - dcf3i*y(6)**2
      pd(6,14) = + (relax(5)*y(3)+relax(7)*y(4)+relax(8)*y(5)
     1          - (relax(11)+relax(10)+relax(9))*y(6))
     2          + (3.0/24.0)*qcf3*(y(1)+y(2)) - recf3*y(6)
      pd(6,15) = + (relax(5)*y(3)+relax(7)*y(4)+relax(8)*y(5)
     1          - (relax(11)+relax(10)+relax(9))*y(6))
     2          + (3.0/24.0)*qi2*(y(1)+y(2)) - di2*y(6)**2
      pd(6,16) = + (relax(5)*y(3)+relax(7)*y(4)+relax(8)*y(5)
     1          - (relax(11)+relax(10)+relax(9))*y(6))
c
      pd(7,1) = sigma(1)*fill*y(7) + 2.0*sn34*(ganlen/cavlen)
      pd(7,2) = 0.0
      pd(7,3) = - sigma(1)*(7.0/9.0)*fill*y(7)
      pd(7,4) = 0.0
      pd(7,5) = 0.0
      pd(7,6) = 0.0
```

```
      pd(7,7) = sigma(1)*(y(1)-(7.0/9.0)*y(3))*fill - cavlos
      pd(7,8) = 0.0
      pd(7,9) = 0.0
      pd(7,10) = 0.0
      pd(7,11) = 0.0
      pd(7,12) = 0.0
      pd(7,13) = 0.0
      pd(7,14) = 0.0
      pd(7,15) = 0.0
      pd(7,16) = 0.0
c
      pd(8,1) = sigma(2)*fill*y(8) + 2.0*sn33*(ganlen/cavlen)
      pd(8,2) = 0.0
      pd(8,3) = 0.0
      pd(8,4) = - sigma(2)*fill*y(8)
      pd(8,5) = 0.0
      pd(8,6) = 0.0
      pd(8,7) = 0.0
      pd(8,8) = sigma(2)*(y(1)-y(4))*fill - cavlos
      pd(8,9) = 0.0
      pd(8,10) = 0.0
      pd(8,11) = 0.0
      pd(8,12) = 0.0
      pd(8,13) = 0.0
      pd(8,14) = 0.0
      pd(8,15) = 0.0
      pd(8,16) = 0.0
c
      pd(9,1) = sigma(3)*fill*y(9) + 2.0*sn32*(ganlen/cavlen)
      pd(9,2) = 0.0
      pd(9,3) = 0.0
      pd(9,4) = 0.0
      pd(9,5) = - sigma(3)*(7.0/5.0)*fill*y(9)
      pd(9,6) = 0.0
      pd(9,7) = 0.0
      pd(9,8) = 0.0
      pd(9,9) = sigma(3)*(y(1)-(7.0/5.0)*y(5))*fill - cavlos
      pd(9,10) = 0.0
      pd(9,11) = 0.0
      pd(9,12) = 0.0
      pd(9,13) = 0.0
      pd(9,14) = 0.0
      pd(9,15) = 0.0
      pd(9,16) = 0.0
c
      pd(10,1) = 0.0
```

```
      pd(10,2) = sigma(4)*fill*y(10) + 2.0*sn23*(ganlen/cavlen)
      pd(10,3) = 0.0
      pd(10,4) = - sigma(4)*(5.0/7.0)*fill*y(10)
      pd(10,5) = 0.0
      pd(10,6) = 0.0
      pd(10,7) = 0.0
      pd(10,8) = 0.0
      pd(10,9) = 0.0
      pd(10,10) = sigma(4)*(y(2)-(5.0/7.0)*y(4))*fill - cavlos
      pd(10,11) = 0.0
      pd(10,12) = 0.0
      pd(10,13) = 0.0
      pd(10,14) = 0.0
      pd(10,15) = 0.0
      pd(10,16) = 0.0
c
      pd(11,1) = 0.0
      pd(11,2) = sigma(5)*fill*y(11) + 2*sn22*(ganlen/cavlen)
      pd(11,3) = 0.0
      pd(11,4) = 0.0
      pd(11,5) = - sigma(5)*fill*y(11)
      pd(11,6) = 0.0
      pd(11,7) = 0.0
      pd(11,8) = 0.0
      pd(11,9) = 0.0
      pd(11,10) = 0.0
      pd(11,11) = sigma(5)*(y(2)-y(5))*fill - cavlos
      pd(11,12) = 0.0
      pd(11,13) = 0.0
      pd(11,14) = 0.0
      pd(11,15) = 0.0
      pd(11,16) = 0.0
c
      pd(12,1) = 0.0
      pd(12,2) = sigma(6)*fill*y(12) + 2.0*sn21*(ganlen/cavlen)
      pd(12,3) = 0.0
      pd(12,4) = 0.0
      pd(12,5) = 0.0
      pd(12,6) = - sigma(6)*(5.0/3.0)*fill*y(12)
      pd(12,7) = 0.0
      pd(12,8) = 0.0
      pd(12,9) = 0.0
      pd(12,10) = 0.0
      pd(12,11) = 0.0
      pd(12,12) = sigma(6)*(y(2)-(5.0/3.0)*y(6))*fill - cavlos
      pd(12,13) = 0.0
```

```
      pd(12,14) = 0.0
      pd(12,15) = 0.0
      pd(12,16) = 0.0
c
      pd(13,1) = 0.0
      pd(13,2) = 0.0
      pd(13,3) = recf3*y(14)
      pd(13,4) = recf3*y(14)
      pd(13,5) = recf3*y(14)
      pd(13,6) = recf3*y(14)
      pd(13,7) = 0.0
      pd(13,8) = 0.0
      pd(13,9) = 0.0
      pd(13,10) = 0.0
      pd(13,11) = 0.0
      pd(13,12) = 0.0
      pd(13,13) = 0.0
      pd(13,14) = recf3*(y(3)+y(4)+y(5)+y(6))
      pd(13,15) = 0.0
      pd(13,16) = 0.0
c
      pd(14,1) = 0.0
      pd(14,2) = 0.0
      pd(14,3) = - recf3*y(14)
      pd(14,4) = - recf3*y(14)
      pd(14,5) = - recf3*y(14)
      pd(14,6) = - recf3*y(14)
      pd(14,7) = 0.0
      pd(14,8) = 0.0
      pd(14,9) = 0.0
      pd(14,10) = 0.0
      pd(14,11) = 0.0
      pd(14,12) = 0.0
      pd(14,13) = 0.0
      pd(14,14) = - recf3*(y(3)+y(4)+y(5)+y(6)) - dc2f6*y(14)*2.0
      pd(14,15) = 0.0
      pd(14,16) = 0.0
c
      pd(15,1) = 0.0
      pd(15,2) = 0.0
      pd(15,3) = (dcf3i*y(13)+dar*r*par/temp+di2*y(15))
     1           *y(3)*(y(3)+y(4)+y(5)+y(6))*2.0
      pd(15,4) = (dcf3i*y(13)+dar*r*par/temp+di2*y(15))
     1           *y(4)*(y(3)+y(4)+y(5)+y(6))*2.0
      pd(15,5) = (dcf3i*y(13)+dar*r*par/temp+di2*y(15))
     1           *y(5)*(y(3)+y(4)+y(5)+y(6))*2.0
```

```
      pd(15,6) = (dcf3i*y(13)+dar*r*par/temp+di2*y(15))
     1          *y(6)*(y(3)+y(4)+y(5)+y(6))*2.0
      pd(15,7) = 0.0
      pd(15,8) = 0.0
      pd(15,9) = 0.0
      pd(15,10) = 0.0
      pd(15,11) = 0.0
      pd(15,12) = 0.0
      pd(15,13) = dcf3i*(y(3)+y(4)+y(5)+y(6))**2
      pd(15,14) = 0.0
      pd(15,15) = di2*(y(3)+y(4)+y(5)+y(6))**2
      pd(15,16) = 0.0
c
      pd(16,1) = 0.0
      pd(16,2) = 0.0
      pd(16,3) = 0.0
      pd(16,4) = 0.0
      pd(16,5) = 0.0
      pd(16,6) = 0.0
      pd(16,7) = 0.0
      pd(16,8) = 0.0
      pd(16,9) = 0.0
      pd(16,10) = 0.0
      pd(16,11) = 0.0
      pd(16,12) = 0.0
      pd(16,13) = 0.0
      pd(16,14) = dc2f6*y(14)*2.0
      pd(16,15) = 0.0
      pd(16,16) = 0.0
c
      return
      end
c
c ***************************************************************************
c
      subroutine erf(x,y,rim,re)
c
c     this program computes the error function for complex values of the
c     argument. it computes the function
c                exp(-z**2)*erfc(-i*z)
c     where z = x + i*y
c     if z = i*a - del, where a = sqrt(alog(2))*wlornz/wdopp
c     and del = 2*sqrt(alog2)*(nu - nu0)/wdopp, then re is the line
c     shape function
c
c
```

```
c ------------------------------------------------------------------
c
      integer capn,nu,n,np1
      real*8 x,y,re,rim
      real*8 h,h2,rlmbda,r1,r2,s1,s2,t1,t2,c,s
      logical b,sign
      cst=1.12837916709551
      sign=.false.
c
c ------------------------------------------------------------------
c
      if(x.lt.0.0) sign=.true.
c     x=abs(x)
      if(x.lt.0.0) x=0.0-x
      if(y.lt.4.29.and.x.lt.5.33) go to 100
      h=0.0
      capn = 0
      nu = 8
      go to 200
 100  s=(1.0-y/4.29)*sqrt(1.0-x*x/28.41)
      h=1.6*s
      h2=2.0*h
      capn=6.5+23*s
      rlmbda=h2**capn
      nu=9.5+21*s
 200  b=.false.
      if(h.eq.0.0.or.rlmbda.eq.0.0) b=.true.
 400  r1 = 0.0
      r2 = 0.0
      s1 = 0.0
      s2 = 0.0
      nup1=nu+1
      do 600 nn=1,nup1
      n=nu+1-nn
      np1=n+1
      t1=y+h+np1*r1
      t2=x-np1*r2
      c=.5/(t1*t1+t2*t2)
      r1=c*t1
      r2=c*t2
      if(h.gt.0.0.and.n.le.capn) go to 500
      go to 600
 500  t1=rlmbda+s1
      s1=r1*t1-r2*s2
      s2=r2*t1+r1*s2
      rlmbda=rlmbda/h2
```

```
600  continue
     if(b) go to 700
     rim=cst*s2
     re=cst*s1
     go to 800
700  rim=cst*r2
     re=cst*r1
800  if(y.eq.0.0) re=exp(-x*x)
     if(sign) rim=-rim
     return
     end
```

Pulsed I* 16 Equation Model I/O Parameters

gain length =	2.800 cm.
cavity length =	16.000 cm.
uv pump energy =	0.175 Joules
i* yield =	90.000 %
pump pulse width =	0.180E-07 secs fwhm
output mirror reflectivity =	0.964 %
internal loss =	0.000 %
iodide pressure =	60.000 torr
argon pressure =	0.000 torr
upper level relaxation rate constant =	1.50E-09 cc/s
lower level relaxation rate constant =	0.40E-09 cc/s
window transmission =	1.000
scattering losses =	0.000
excimer energy deposited in gain region =	3.48E-02 Joules
extracted energy =	3.21E-03 Joules
cavity build-up time =	3.38E+02 nsec
maximum small signal gain =	2.94E-03 /cm

no. steps = 10094 no. f-s = 12873 no. j-s = 1860

Table B-1 Text Output from I.f

The following codes produce plots in the form of CGM files using the NCAR

Graphics library. The first code listed is pulse.f which plots I* laser intensity from the data file produced by the previous code. An example of the output is plotted in Figure B-1 just after the code listing. The second listing is dens.f which plots out the number density in each of the hyperfine levels from the data file. An example of this is seen in Figure B-2. The third listing is ssg.f which plots out the small signal gain from the data file. An example plot follows in Figure B-3.

```
c
c     implicit real*8 (a-h,o-z)
      parameter(isize = 1500,jsize = 25,nsize = 2,lsize = 6)
      real datar(isize,jsize)
      real x(jsize)
      common /user/ scale2
C
C Define the data arrays and the dash-pattern array.
C
      REAL XDRA(isize),YDRA(isize,nsize)
      CHARACTER*28 DSHP(nsize)
C
C Declare the type of the dash-pattern-name generator.
C
      CHARACTER*16 AGDSHN
c
c This opens the data files:
c
      open(unit=8,file='data',form='unformatted',status='old')
c
c This reads the data array from a binary file:
c
      do 300 iout=1,isize
        do 200 jout=1,jsize
          read(8) datar(iout,jout)
 200    continue
 300  continue
C
C Initialize GKS.
C
      CALL OPNGKS
c
c set scale for I* pulse
c
      scale2 = 0.3
```

```
C
C Fill the data arrays and the dash pattern array.
C
      do 101 iout=1,isize
        XDRA(iout)=1.e9*datar(iout,1)
        YDRA(iout,1)=1.e-6*datar(iout,19)
        YDRA(iout,2)=1.e-4*datar(iout,2)*scale2
  101 continue
C
      do 103 jout=1,nsize
        write (DSHP(jout),1001) jout
  103 continue
C
C Turn on windowing.
C
      CALL AGSETI ('WINDOWING.',1)
C
C Move the edges of the curve window (grid).
C
      CALL AGSETF ('GRID/LEFT.'  ,.10)
      CALL AGSETF ('GRID/RIGHT.' ,.90)
      CALL AGSETF ('GRID/BOTTOM.',.10)
      CALL AGSETF ('GRID/TOP.'   ,.85)
C
C Set the x and y minimum and maximum.
C
      CALL AGSETF ('X/MINIMUM.',   0.)
      CALL AGSETF ('X/MAXIMUM.',1500.)
      CALL AGSETF ('Y/MINIMUM.',  -.2)
      CALL AGSETF ('Y/MAXIMUM.',   2.)
C
C Set left axis parameters.
C
      CALL AGSETI ('LEFT/MAJOR/TYPE.',1)
      CALL AGSETF ('LEFT/MAJOR/BASE.',0.2)
      CALL AGSETI ('LEFT/MINOR/SPACING.',4)
C
C Set right axis parameters.
C
      CALL AGSETI ('RIGHT/FUNCTION.',1)
      CALL AGSETF ('RIGHT/MAJOR/BASE.',5.)
      CALL AGSETI ('RIGHT/MINOR/SPACING.',4)
      CALL AGSETF ('RIGHT/NUMERIC/TYPE.',1.E36)
C
C Set bottom axis parameters.
C
```

```
      CALL AGSETI ('BOTTOM/MAJOR/TYPE.',1)
      CALL AGSETF ('BOTTOM/MAJOR/BASE.',100.)
      CALL AGSETI ('BOTTOM/MINOR/SPACING.',3)
C
C Set up the dash patterns to be used.
C
      CALL AGSETI ('DASH/SELECTOR.',nsize)
      CALL AGSETI ('DASH/LENGTH.',28)
      DO 104 I=1,nsize
        CALL AGSETC (AGDSHN(I),DSHP(I))
  104 CONTINUE
C
C Set up the left label.
C
      CALL AGSETC ('LABEL/NAME.','L')
      CALL AGSETI ('LINE/NUMBER.',100)
      CALL AGSETC ('LINE/TEXT.','Excimer Pulse Energy (MW)$')
C
C Set up the right label.
C
      CALL AGSETC ('LABEL/NAME.','R')
      CALL AGSETI ('LINE/NUMBER.',-100)
      CALL AGSETC ('LINE/TEXT.',
     +             'Iodine Pulse Energy (kW)$')
C
C Set up the bottom labels.
C
      CALL AGSETC ('LABEL/NAME.','B')
      CALL AGSETI ('LINE/NUMBER.',-100)
      CALL AGSETC ('LINE/TEXT.','Time (ns)$')
C
C Set up the top label.
C
      CALL AGSETC ('LABEL/NAME.','T')
      CALL AGSETI ('LINE/NUMBER.',80)
      CALL AGSETC ('LINE/TEXT.',
     +             '1. Excimer  2. Iodine$')
      CALL AGSETI ('LINE/NUMBER.',90)
      CALL AGSETC ('LINE/TEXT.',' $')
      CALL AGSETI ('LINE/NUMBER.',100)
      CALL AGSETC ('LINE/TEXT.',
     +             'I* Laser Pulse$')
C
C Draw a boundary around the edge of the plotter frame.
C
      CALL BNDARY
```

```
C
C Draw the graph, using EZMXY.
C
      CALL EZMXY (XDRA,YDRA,isize,nsize,isize,CHAR(0))
C
C Close GKS.
C
      CALL CLSGKS
C
      STOP
C
C Format for encode above.
C
 1001 FORMAT ('$$$$$$$$$$$$$$$$$$$$$$$$$$$''',I1,'''')
C
      END
      SUBROUTINE AGUTOL (IAXS,FUNS,IDMA,VINP,VOTP)
      common /user/ scale2
C
C Mapping for the right axis.
C
      IF (FUNS.EQ.1.) THEN
        IF (IDMA.GT.0) VOTP=10.*VINP/scale2
        IF (IDMA.LT.0) VOTP=scale2*VINP/10.
C
C Mapping for the top axis.
C
      ELSE IF (FUNS.EQ.2.) THEN
        IF (IDMA.GT.0) VOTP=70.136*VINP
        IF (IDMA.LT.0) VOTP=VINP/70.136
C
C Default (identity) mapping.
C
      ELSE
        VOTP=VINP
      END IF
C
C Done.
C
      RETURN
C
      END
      SUBROUTINE BNDARY
C
C Routine to draw the plotter-frame edge.
C
```

```
CALL PLOTIT (    0,    0,0)
CALL PLOTIT (32767,    0,1)
CALL PLOTIT (32767,32767,1)
CALL PLOTIT (    0,32767,1)
CALL PLOTIT (    0,    0,1)
RETURN
END
```

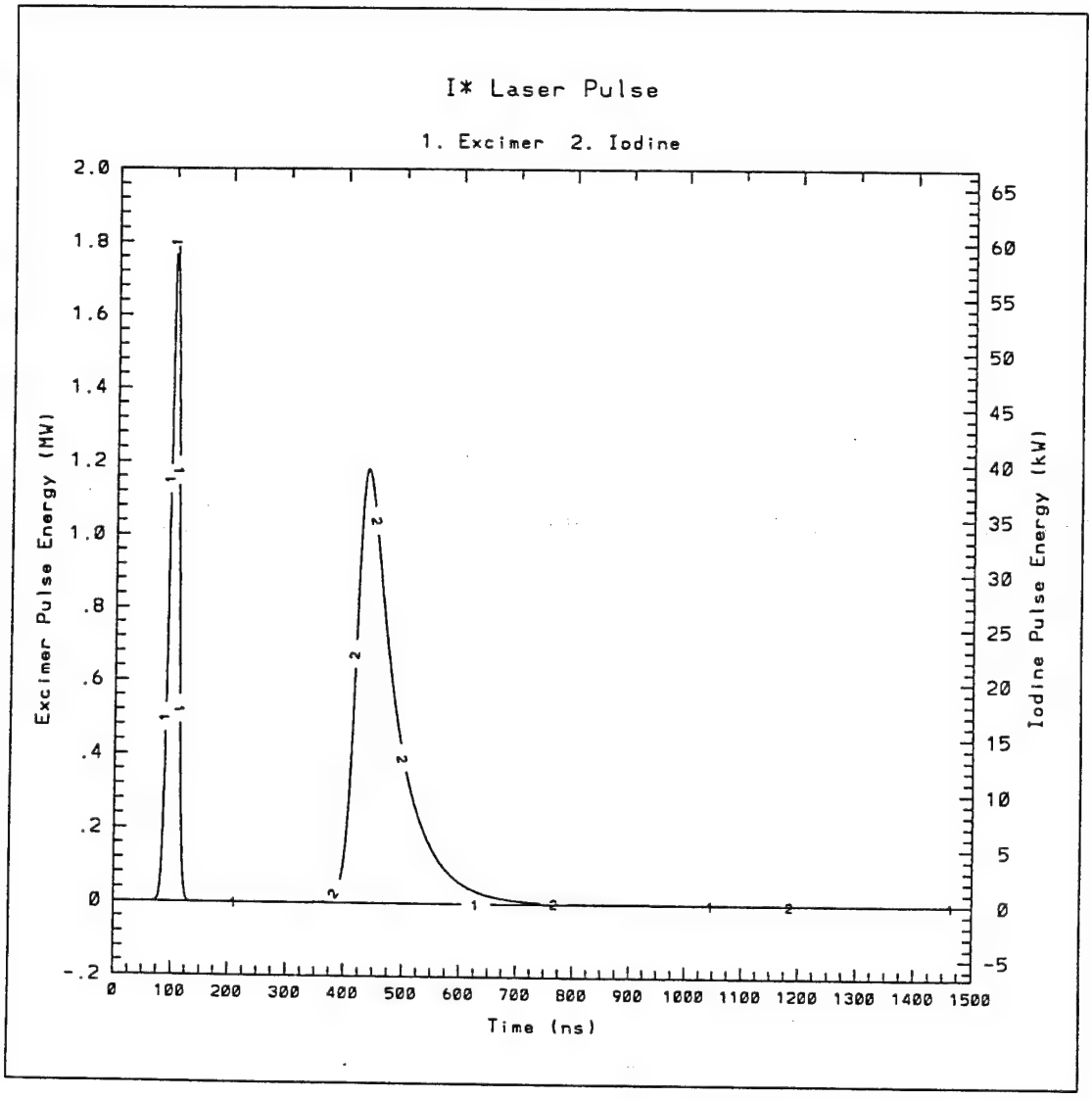

Figure B-1 Output from pulse.f

```
c
      implicit real*8 (a-h,o-z)
      parameter(isize = 1500,jsize = 25,nsize = 6,lsize = 6)
      real datar(isize,jsize)
      real x(jsize)
C
C Define the data arrays and the dash-pattern array.
C
      REAL XDRA(isize),YDRA(isize,nsize)
      CHARACTER*28 DSHP(nsize)
C
C Declare the type of the dash-pattern-name generator.
C
      CHARACTER*16 AGDSHN
c
c This opens the data files:
c
      open(unit=8,file='data',form='unformatted',status='old')
c
c This reads the data array from a binary file:
c
      do 300 iout=1,isize
        do 200 jout=1,jsize
          read(8) datar(iout,jout)
  200   continue
  300 continue
C
C Initialize GKS.
C
      CALL OPNGKS
C
C Fill the data arrays and the dash pattern array.
C
      do 101 iout=1,isize
        XDRA(iout)=1.e9*datar(iout,1)
        do 102 jout=1,nsize
          YDRA(iout,jout)=datar(iout,2+jout)
  102   continue
  101 continue
C
      write (DSHP(1),1001)
      write (DSHP(2),1002)
      write (DSHP(3),1003)
      write (DSHP(4),1004)
      write (DSHP(5),1005)
      write (DSHP(6),1006)
```

```
C
C Turn on windowing.
C
      CALL AGSETI ('WINDOWING.',1)
C
C Move the edges of the curve window (grid).
C
      CALL AGSETF ('GRID/LEFT.'  ,.10)
      CALL AGSETF ('GRID/RIGHT.' ,.90)
      CALL AGSETF ('GRID/BOTTOM.',.10)
      CALL AGSETF ('GRID/TOP.'   ,.85)
C
C Set the x and y minimum and maximum.
C
      CALL AGSETF ('X/MINIMUM.',  0.)
      CALL AGSETF ('X/MAXIMUM.',1500.)
C
C Set left axis parameters.
C
      CALL AGSETI ('LEFT/MAJOR/TYPE.',1)
      CALL AGSETF ('LEFT/MAJOR/BASE.',1.e+15)
      CALL AGSETI ('LEFT/MINOR/SPACING.',4)
C
C Set right axis parameters.
C
      CALL AGSETI ('RIGHT/MINOR/SPACING.',4)
C
C Set bottom axis parameters.
C
      CALL AGSETI ('BOTTOM/MAJOR/TYPE.',1)
      CALL AGSETF ('BOTTOM/MAJOR/BASE.',100.)
      CALL AGSETI ('BOTTOM/MINOR/SPACING.',3)
C
C Set top axis parameters.
C
      CALL AGSETI ('TOP/MINOR/SPACING.',4)
C
C Set up the dash patterns to be used.
C
      CALL AGSETI ('DASH/SELECTOR.',nsize)
      CALL AGSETI ('DASH/LENGTH.',28)
      DO 104 I=1,nsize
        CALL AGSETC (AGDSHN(I),DSHP(I))
  104 CONTINUE
C
C Set up the left label.
```

```
C
      CALL AGSETC ('LABEL/NAME.','L')
      CALL AGSETI ('LINE/NUMBER.',100)
      CALL AGSETC ('LINE/TEXT.','Iodine Atoms (#/cc)$')
C
C Set up the right label.
C
      CALL AGSETC ('LABEL/NAME.','R')
      CALL AGSETI ('LINE/NUMBER.',-100)
      CALL AGSETC ('LINE/TEXT.',
     +             '    $')
C
C Set up the bottom labels.
C
      CALL AGSETC ('LABEL/NAME.','B')
      CALL AGSETI ('LINE/NUMBER.',-100)
      CALL AGSETC ('LINE/TEXT.','Time (ns)$')
C
C Set up the top label.
C
      CALL AGSETC ('LABEL/NAME.','T')
      CALL AGSETI ('LINE/NUMBER.',80)
      CALL AGSETC ('LINE/TEXT.',
     +             '    $')
      CALL AGSETI ('LINE/NUMBER.',90)
      CALL AGSETC ('LINE/TEXT.',' $')
      CALL AGSETI ('LINE/NUMBER.',100)
      CALL AGSETC ('LINE/TEXT.',
     +             'I* Laser Population Densities$')
C
C Draw a boundary around the edge of the plotter frame.
C
      CALL BNDARY
C
C Draw the graph, using EZMXY.
C
      CALL EZMXY (XDRA,YDRA,isize,nsize,isize,CHAR(0))
C
C Close GKS.
C
      CALL CLSGKS
C
      STOP
C
C Format for encode above.
C
```

```
 1001 FORMAT ('$$$$$$$$$$$$$$$$$$$$$$$''','I3*','''')
 1002 FORMAT ('$$$$$$$$$$$$$$$$$$$$$$$''','I2*','''')
 1003 FORMAT ('$$$$$$$$$$$$$$$$$$$$$$$''','I4g','''')
 1004 FORMAT ('$$$$$$$$$$$$$$$$$$$$$$$''','I3g','''')
 1005 FORMAT ('$$$$$$$$$$$$$$$$$$$$$$$''','I2g','''')
 1006 FORMAT ('$$$$$$$$$$$$$$$$$$$$$$$''','I1g','''')
C
      END
      SUBROUTINE AGUTOL (IAXS,FUNS,IDMA,VINP,VOTP)
C
C Mapping for the right axis.
C
      IF (FUNS.EQ.1.) THEN
        IF (IDMA.GT.0) VOTP=ALOG10(20.-VINP)
        IF (IDMA.LT.0) VOTP=20.-10.**VINP
C
C Mapping for the top axis.
C
      ELSE IF (FUNS.EQ.2.) THEN
        IF (IDMA.GT.0) VOTP=70.136*VINP
        IF (IDMA.LT.0) VOTP=VINP/70.136
C
C Default (identity) mapping.
C
      ELSE
        VOTP=VINP
      END IF
C
C Done.
C
      RETURN
C
      END
      SUBROUTINE BNDARY
C
C Routine to draw the plotter-frame edge.
C
      CALL PLOTIT (    0,    0,0)
      CALL PLOTIT (32767,    0,1)
      CALL PLOTIT (32767,32767,1)
      CALL PLOTIT (    0,32767,1)
      CALL PLOTIT (    0,    0,1)
      RETURN
      END
```

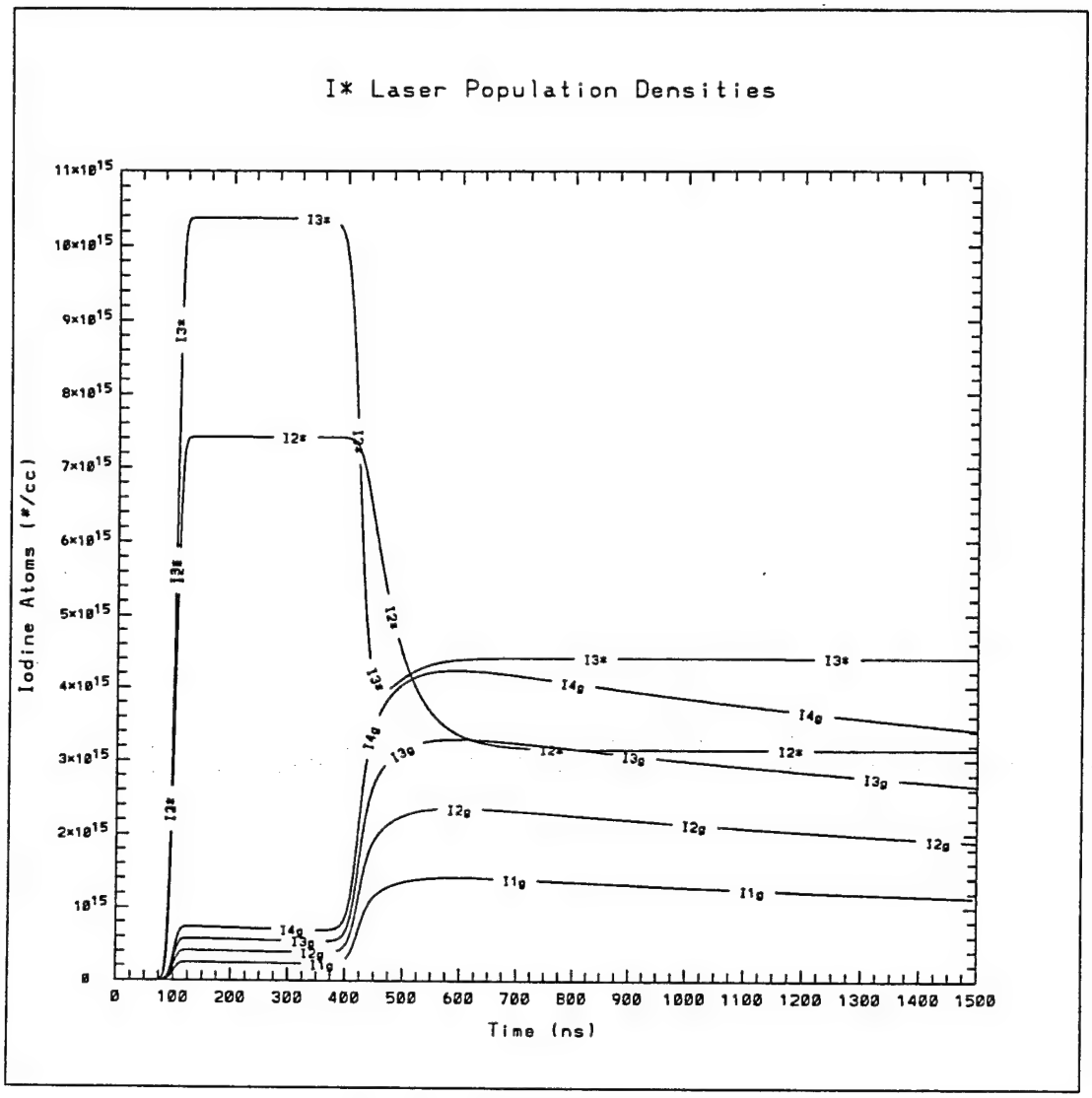

Figure B-2 Output from dens.f

```
c
      implicit real*8 (a-h,o-z)
      parameter(isize = 1500,jsize = 25,nsize = 6)
      real datar(isize,jsize)
      real x(jsize)
C
```

```
C Define the data arrays and the dash-pattern array.
C
      REAL XDRA(isize),YDRA(isize,nsize)
      CHARACTER*28 DSHP(nsize)
C
C Declare the type of the dash-pattern-name generator.
C
      CHARACTER*16 AGDSHN
c
c This opens the data files:
c
      open(unit=8,file='data',form='unformatted',status='old')
c
c This reads the data array from a binary file:
c
      do 300 iout=1,isize
        do 200 jout=1,jsize
          read(8) datar(iout,jout)
  200   continue
  300 continue
C
C Initialize GKS.
C
      CALL OPNGKS
C
C Fill the data arrays and the dash pattern array.
C
      do 101 iout=1,isize
        XDRA(iout)=1.e9*datar(iout,1)
        do 102 jout=1,nsize
          YDRA(iout,jout)=datar(iout,19+jout)
  102   continue
  101 continue
C
      write (DSHP(1),1001)
      write (DSHP(2),1002)
      write (DSHP(3),1003)
      write (DSHP(4),1004)
      write (DSHP(5),1005)
      write (DSHP(6),1006)
C
C Turn on windowing.
C
      CALL AGSETI ('WINDOWING.',1)
C
C Move the edges of the curve window (grid).
```

```
C
      CALL AGSETF ('GRID/LEFT.' ,.10)
      CALL AGSETF ('GRID/RIGHT.' ,.90)
      CALL AGSETF ('GRID/BOTTOM.',.10)
      CALL AGSETF ('GRID/TOP.'   ,.85)
C
C Set the x and y minimum and maximum.
C
      CALL AGSETF ('X/MINIMUM.',   0.)
      CALL AGSETF ('X/MAXIMUM.',1500.)
      CALL AGSETF ('Y/MINIMUM.',   0.)
      CALL AGSETF ('Y/MAXIMUM.',   .04)
C
C Set left axis parameters.
C
      CALL AGSETI ('LEFT/MAJOR/TYPE.',1)
      CALL AGSETF ('LEFT/MAJOR/BASE.',.005)
      CALL AGSETI ('LEFT/MINOR/SPACING.',4)
C
C Set right axis parameters.
C
      CALL AGSETI ('RIGHT/MINOR/SPACING.',4)
C
C Set bottom axis parameters.
C
      CALL AGSETI ('BOTTOM/MAJOR/TYPE.',1)
      CALL AGSETF ('BOTTOM/MAJOR/BASE.',100.)
      CALL AGSETI ('BOTTOM/MINOR/SPACING.',3)
C
C Set top axis parameters.
C
      CALL AGSETI ('TOP/MINOR/SPACING.',4)
C
C Set up the dash patterns to be used.
C
      CALL AGSETI ('DASH/SELECTOR.',nsize)
      CALL AGSETI ('DASH/LENGTH.',28)
      DO 104 I=1,nsize
        CALL AGSETC (AGDSHN(I),DSHP(I))
  104 CONTINUE
C
C Set up the left label.
C
      CALL AGSETC ('LABEL/NAME.','L')
      CALL AGSETI ('LINE/NUMBER.',100)
      CALL AGSETC ('LINE/TEXT.','Gain (1/cm)$')
```

```
C
C Set up the right label.
C
      CALL AGSETC ('LABEL/NAME.','R')
      CALL AGSETI ('LINE/NUMBER.',-100)
      CALL AGSETC ('LINE/TEXT.',
     +            '    $')
C
C Set up the bottom labels.
C
      CALL AGSETC ('LABEL/NAME.','B')
      CALL AGSETI ('LINE/NUMBER.',-100)
      CALL AGSETC ('LINE/TEXT.','Time (ns)$')
C
C Set up the top label.
C
      CALL AGSETC ('LABEL/NAME.','T')
      CALL AGSETI ('LINE/NUMBER.',80)
      CALL AGSETC ('LINE/TEXT.',
     +            '   $')
      CALL AGSETI ('LINE/NUMBER.',90)
      CALL AGSETC ('LINE/TEXT.',' $')
      CALL AGSETI ('LINE/NUMBER.',100)
      CALL AGSETC ('LINE/TEXT.',
     +            'I* Laser Gain$')
C
C Draw a boundary around the edge of the plotter frame.
C
      CALL BNDARY
C
C Draw the graph, using EZMXY.
C
      CALL EZMXY (XDRA,YDRA,isize,nsize,isize,CHAR(0))
C
C Close GKS.
C
      CALL CLSGKS
C
      STOP
C
C Format for encode above.
C
 1001 FORMAT ('$$$$$$$$$$$$$$$$$$$$$$$''','3-4',''')
 1002 FORMAT ('$$$$$$$$$$$$$$$$$$$$$$$''','3-3',''')
 1003 FORMAT ('$$$$$$$$$$$$$$$$$$$$$$$''','3-2',''')
 1004 FORMAT ('$$$$$$$$$$$$$$$$$$$$$$$''','2-3',''')
```

```
 1005 FORMAT ('$$$$$$$$$$$$$$$$$$$$$$$''','2-2','''')
 1006 FORMAT ('$$$$$$$$$$$$$$$$$$$$$$$''','2-1','''')
C
      END
      SUBROUTINE AGUTOL (IAXS,FUNS,IDMA,VINP,VOTP)
C
C Mapping for the right axis.
C
      IF (FUNS.EQ.1.) THEN
        IF (IDMA.GT.0) VOTP=ALOG10(20.-VINP)
        IF (IDMA.LT.0) VOTP=20.-10.**VINP
C
C Mapping for the top axis.
C
      ELSE IF (FUNS.EQ.2.) THEN
        IF (IDMA.GT.0) VOTP=70.136*VINP
        IF (IDMA.LT.0) VOTP=VINP/70.136
C
C Default (identity) mapping.
C
      ELSE
        VOTP=VINP
      END IF
C
C Done.
C
      RETURN
C
      END
      SUBROUTINE BNDARY
C
C Routine to draw the plotter-frame edge.
C
      CALL PLOTIT (    0,    0,0)
      CALL PLOTIT (32767,    0,1)
      CALL PLOTIT (32767,32767,1)
      CALL PLOTIT (    0,32767,1)
      CALL PLOTIT (    0,    0,1)
      RETURN
      END
```

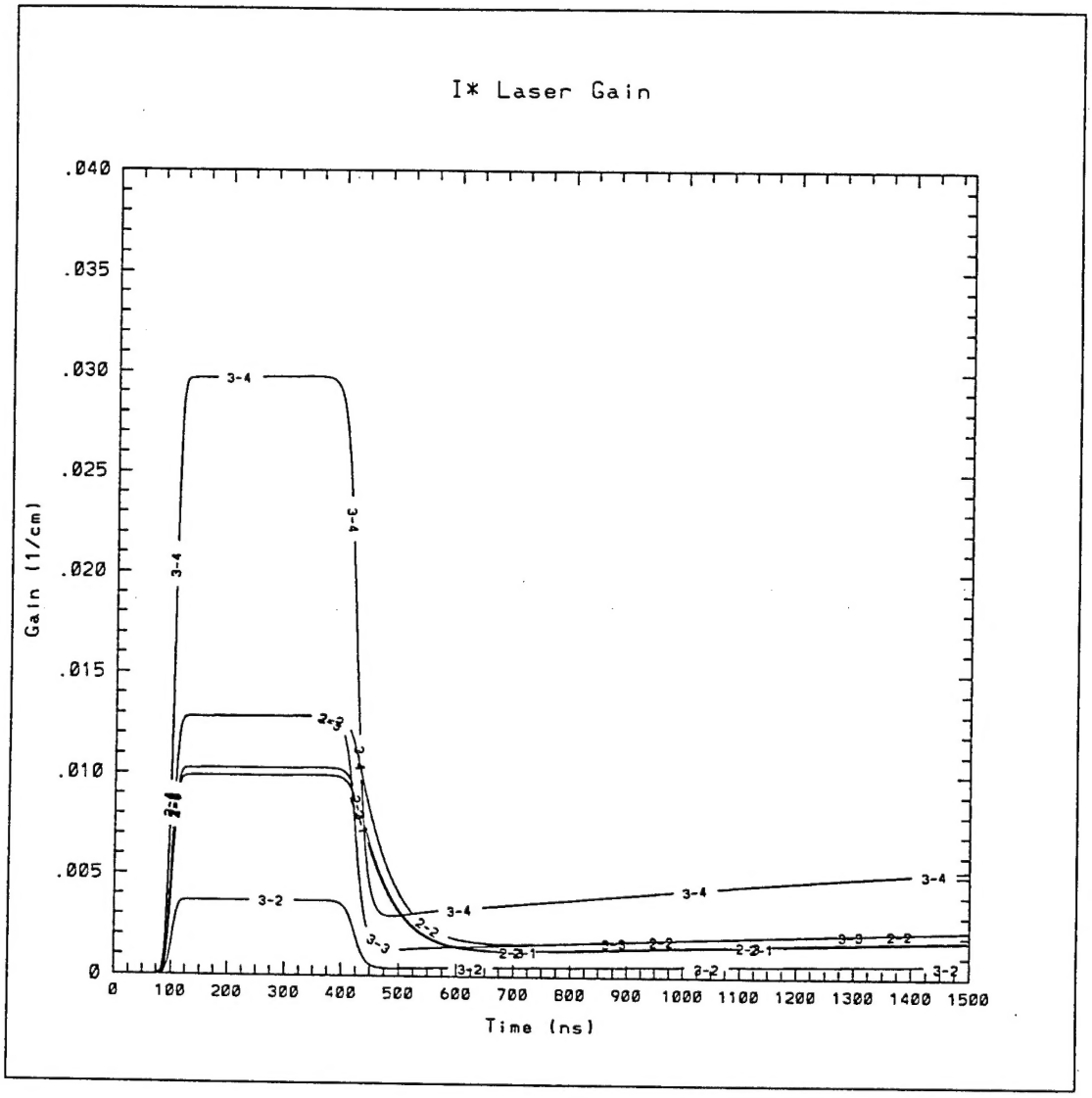

Figure B-3 Output from ssg.f